MULTISCALE INVESTIGATION OF ALTERNATIVE CEMENTITIOUS MATERIAL SYSTEMS

A Dissertation
Presented to
The Academic Faculty

by

Prasanth Alapati

In Partial Fulfillment
of the Requirements for the Degree
Doctor of Philosophy in the
School of Civil and Environmental Engineering

Georgia Institute of Technology
August 2020

MULTISCALE INVESTIGATION OF ALTERNATIVE CEMENTITIOUS MATERIAL SYSTEMS

Approved by:

Dr. Kimberly E. Kurtis, Advisor
School of Civil and Environmental Engineering
Georgia Institute of Technology

Dr. Preet Singh
School of Materials Science and Engineering
Georgia Institute of Technology

Dr. Lawrence F. Kahn
School of Civil and Environmental Engineering
Georgia Institute of Technology

Dr. Maria C. Garci Juenger
Civil, Architectural and Environmental Engineering
The University of Texas at Austin

Dr. T. Russell Gentry
School of Civil and Environmental Engineering
Georgia Institute of Technology

Date Approved: October 25, 2019

ACKNOWLEDGMENTS

I express immense pleasure to thank my advisor Dr. Kimberly E. Kurtis: thank you for your guidance and relentless effort to bring the best in me over the past five years and for providing me access to all the required sophisticated facilities to carry out this research work. My sincere thanks to my committee members Dr. Maria C. Garci Juenger, Dr. Preet Singh , Dr. Lawrence F. Kahn, and Dr. T. Russell Gentry for their valuable suggestions, technical inputs, and comments on this thesis work.

The relentless help and support of all the laboratory managers, especially Jeremy Mitchell, Eric Woods, and David Tavakoli throughout my entire project, are appreciated.

I would like to take this opportunity to acknowledge the financial support from the Federal Highway Administration (FHWA) under grant number DRFH61-14-H-00003 and Spanos fellowship.

I would like to thank my collaborators Dr. Lisa E. Burris, Dr. Tyler Ley, Dr. Neal Berke, Dr. Robert D. Moser, and Richard C. Meininger, and my research assistants – Theotim Paul, Molly Canet, Krissia Ortiz, Rebecca Tien, Xinyi Zhang, and Colleen Thompson. This research would not have been completed without their help, support, and thoughtful discussions.

I thank my amazing group of past and present colleagues from Georgia tech Dr. Mehdi Rashidi, Dr. Behnaz Zaribaf, Dr. Natalia Cardelino, Qingxu (Bill) Jin, Dr. Ahmad Shalan, Dr. Elizabeth Nadelman, Dr. Sasha Walker, Dr. Álvaro Paul, Dr. Bradley Dolphyn, Scotty Smith, Cole Spencer, Daniel Benkeser, Dr. Francesca Lolli, Leonidas Emmenegger, Renee

Rios, Aaron Miller, and Ogulcan Canbek for their support, conversations, technical inputs and fun full potlucks.

I would also like to thank my friends Jacob Sebastian, Neelakandan Ramalingam, Parth Desai, Phanisri Pradeep Pratapa, Satya Sarvani Malladi, Trilochan Rambhatla, and Vaidheeswara Sharma Ganesan; and my cousin family (Aswani and Praveen Ravela) who made my stay in Atlanta a memorable one.

Most importantly, I would like to thank my parents (Dr. Tilak A. V. N. and Mrs. Padmaja A.), my brother (Dr. Susanth A.), and the rest of my family, for their continuous guidance and support in all the ways they were able to do. I am grateful to the Almighty for keeping me in touch with the utmost caring and loving people, who stood by my side in every difficult situation.

Prasanth Alapati

TABLE OF CONTENTS

LIST OF TABLES

LIST OF FIGURES

LIST OF ABBREVIATIONS AND SYMBOLS

Abbreviations

AA	Activated Aluminosilicate
ACM	Alternative Cementing Materials
ACI	American Concrete Institute
AMBT	Accelerated Mortar Bar Test
ASR	Alkali-Silica Reaction
ASTM	Refers to ASTM International (formerly American Society for Testing and Materials) standards
CAC	Calcium Aluminate Cement
CSA	Calcium SulfoAluminate Cement
CPT	Concrete Prism Test
FA	Fly Ash
MPC	Magnesium Phosphate Cement
GDOT	Georgia Department of Transportation
OPC	Ordinary Portland Cement

Cement chemistry notations

A	Aluminum oxide (Al_2O_3)
C	Calcium oxide (CaO)
$\overline{C}$	Carbon dioxide (CO_2)
F	Ferric oxide (Fe_2O_3)
H	Water (H_2O)
K	Potassium oxide (K_2O)
M	Magnesium oxide (MgO)
N	Sodium oxide (Na_2O)
P	Phosphorus pentoxide (P_2O_5)
S	Silicon dioxide (SiO_2)
$\overline{S}$	Sulfur trioxide (SO_3)

SI* (MODERN METRIC) CONVERSION FACTORS

APPROXIMATE CONVERSIONS TO SI UNITS

Symbol	When You Know	Multiply By	To Find	Symbol
		LENGTH		
in	inches	25.4	millimeters	mm
ft	feet	0.305	meters	m
yd	yards	0.914	meters	m
mi	miles	1.61	kilometers	km
		AREA		
in^2	square inches	645.2	square millimeters	mm^2
ft^2	square feet	0.093	square meters	m^2
yd^2	square yard	0.836	square meters	m^2
ac	acres	0.405	hectares	ha
mi^2	square miles	2.59	square kilometers	km^2
		VOLUME		
fl oz	fluid ounces	29.57	milliliters	mL
gal	gallons	3.785	liters	L
ft^3	cubic feet	0.028	cubic meters	m^3
yd^3	cubic yards	0.765	cubic meters	m^3
		NOTE: volumes greater than 1000 L shall be shown in m^3		
		MASS		
oz	ounces	28.35	grams	g
lb	pounds	0.454	kilograms	kg
T	short tons (2000 lb)	0.907	megagrams (or "metric ton")	Mg (or "t")
		TEMPERATURE (exact degrees)		
°F	Fahrenheit	5 (F-32)/9 or (F-32)/1.8	Celsius	°C
		ILLUMINATION		
fc	foot-candles	10.76	lux	lx
fl	foot-Lamberts	3.426	candela/m^2	cd/m^2
		FORCE and PRESSURE or STRESS		
lbf	poundforce	4.45	newtons	N
lbf/in^2	poundforce per square inch	6.89	kilopascals	kPa

APPROXIMATE CONVERSIONS FROM SI UNITS

Symbol	When You Know	Multiply By	To Find	Symbol
		LENGTH		
mm	millimeters	0.039	inches	in
m	meters	3.28	feet	ft
m	meters	1.09	yards	yd
km	kilometers	0.621	miles	mi
		AREA		
mm^2	square millimeters	0.0016	square inches	in^2
m^2	square meters	10.764	square feet	ft^2
m^2	square meters	1.195	square yards	yd^2
ha	hectares	2.47	acres	ac
km^2	square kilometers	0.386	square miles	mi^2
		VOLUME		
mL	milliliters	0.034	fluid ounces	fl oz
L	liters	0.264	gallons	gal
m^3	cubic meters	35.314	cubic feet	ft^3
m^3	cubic meters	1.307	cubic yards	yd^3
		MASS		
g	grams	0.035	ounces	oz
kg	kilograms	2.202	pounds	lb
Mg (or "t")	megagrams (or "metric ton")	1.103	short tons (2000 lb)	T
		TEMPERATURE (exact degrees)		
°C	Celsius	1.8C+32	Fahrenheit	°F
		ILLUMINATION		
lx	lux	0.0929	foot-candles	fc
cd/m^2	candela/m^2	0.2919	foot-Lamberts	fl
		FORCE and PRESSURE or STRESS		
N	newtons	0.225	poundforce	lbf
kPa	kilopascals	0.145	poundforce per square inch	lbf/in^2

*SI is the symbol for the International System of Units. Appropriate rounding should be made to comply with Section 4 of ASTM E380.
(Revised March 2003)

SUMMARY

The necessity and the universality of concrete infrastructure prompt innovation in addressing the global challenge of meeting societal needs in the most sustainable and economical ways possible. Increasing the use of non-portland cements or "alternative cementitious materials" (ACMs) is of growing interest due to their unique properties and to their potential to reduce the environmental footprint of concrete. The unique properties of ACMs may vary by material, but include rapid setting, rapid strength development, higher ultimate strength, improved dimensional stability, and increased durability in aggressive environments. The increased strength and increased durability further contribute to enhanced service life which can help offset initially higher material costs, and also to enhanced sustainability.

In the past, most ACMs were primarily used in limited specialty applications, and some of them have been shown in lab-scale studies to be feasible for the partial or full replacement of traditional portland cements used in concrete. However, there is a limited understanding of the scalability of construction with these material systems, their long-term performance, and durability in a range of environments, and their structural response when subjected to transportation-relevant loading conditions. This thesis presents the results from the comprehensive investigation of the applications of these commercially available ACMs in durable and sustainable transportation infrastructure, which include the early-age and long-term material properties as well as multi-scale durability investigations.

A novel multi-scale approach was proposed to design concrete mixtures with these commercial ACMs to meet both the prescriptive requirements and the performance targets.

The multi-approach involves (i) using multiple advanced material characterization techniques to understand how these commercially blends hydrate, (ii) changing their fresh properties to meet the prescriptive requirements without adversely affecting their long-term material properties to meet the performance targets. New test methods and protocols also involving multi-scale material characterization were proposed to gauge the long-term performance of these ACMs against wide range of exposure conditions. These new test methods were designed, relying as much as possible on existing test methods for traditional portland systems, to facilitate rapid adoption of the ACM formulations. From this, guidance for the lab-scale investigation and guidance for the ACM selection and mixture design for use in transportation infrastructure, primarily in the aspects investigated in this thesis, are provided.

Successful concrete mixtures were developed by using a combination of isothermal calorimetry, x-ray diffraction, set time assessments, and flow tests to link cement characteristics, admixture type, and dosage to early-age behavior. For all ACMs, except for one calcium aluminate cement and one magnesium phosphate cement, concretes were designed that met both the early age requirements for the set time and slump, at w/c of 0.40 or less, and later age requirements for mechanical properties. Even though commercially available polycarboxylate based superplasticizers and citric acid based set modifiers are known to perform well with calcium sulfoaluminate (CSA) based systems, it was found out that CSA cements containing high iron content have compatibility issues with those admixtures.

A new test method for measuring formation factor in both the low resistive and highly resistive systems that is easy to perform and that does not require pore solution extraction

or even prior knowledge of pore solution composition and its resistivity is developed; was used to understand permeability and interconnectivity in the ACM systems at varied w/b. Understanding permeability and interconnectivity in ACM mixtures are essential for durability assessment in these systems. New insights were provided on the chemical sulfate attack mechanisms in ACM systems. (C,N)-A-S-H type gel was found to be forming on the outside exposed surface in all the ettringite based systems investigated in this thesis, and it is found to be one of the primary reason for the superior resistance of these systems in resistance external sulfate attack. A new accelerated cylinder mortar test method was developed to assess the alkali-silica reaction (ASR) in ACM systems without the need for alkali boosting and also addressing the leaching issues found the current ASTM C 1293 accelerated test method. This new test method can be used as a complementary test method for the ASTM C1293 test, or it can be used as a standalone test method upon further validation. Using the combination of these two test methods, it was found out that most of the ACMs investigated in this thesis offer excellent resistance to alkali-silica reaction. It was also found that portlandite and alkali content played an important roll in resisting ASR compared to the permeability of these systems. Accelerated carbonation studies were performed on both OPC and ACM systems at various exposure levels (0.04%, 1%, 7%, and 14%). Out of the accelerated CO2 exposure levels tested in this chapter, both 7% and 15% exposure levels were found to be aggressive in all the OPC and ACM mixtures, except in one calcium aluminate system. Even the 1% exposure level found to be aggressive in activated aluminosilicate systems and two of the CSA systems investigated in this thesis. However, accelerated carbonation at 1% or higher CO_2 exposure levels underestimated the carbonation in calcium aluminate cements having higher amounts of CAH_{10} compared to

the atmospheric CO_2 level. Therefore, selection of CO2 exposure levels, to accurately test the ACM systems for carbonation in accelerated conditions, can be made only after taking their sensitivity towards CO_2 exposure level into account.

1 INTRODUCTION

1.1 Project description

Cement, which accounts for nearly 20 percent by weight of concrete, is a manufactured material, unlike the other components of concrete. The cement industry emits around 800 lbs. of carbon dioxide (CO_2) for every 1000 lbs. of cement it produces, making it one of the two largest producers of industrial CO_2. The ubiquity and the necessity of concrete infrastructure prompt innovation in addressing the global challenge of meeting societal needs in the most sustainable and economical ways possible. Increasing the use of non-portland cements or "alternative cementitious materials" (ACMs) is of increasing interest due both to their potential to reduce the "environmental footprint" of concrete and their unique properties. The unique properties of ACMs may vary by material but include rapid setting, rapid strength development, higher ultimate strength, improved dimensional stability, and increased durability in aggressive environments. The increased strength (and the resulting potential for decreased materials usage) and increased durability further contribute to enhanced sustainability and can help offset initially higher materials costs.

In the past, most ACMs have primarily been used in specialty applications, such as repairing defects or rapid replacement of damaged pavement sections and creating joints for precast panel road replacements. Of the myriad of commercially available ACMs, chemically-activated aluminosilicates (AA) (including geopolymer concrete), calcium sulfoaluminate (CSA) cements, calcium aluminate cements (CAC), phosphate-based cements (e.g., magnesium phosphate cements, MPC), and novel (e.g., high belite; blended with A…….CMs) portland cement formulations have been shown in lab-scale studies to

be feasible for the partial or full replacement of traditional portland cements (OPC) used in concrete. However, there is a limited understanding of the scalability of construction with these material systems, their long-term performance, and durability in a range of environments, and their structural response when subjected to transportation-relevant loading conditions. The goal of this research is to investigate the early-age and long-term material properties as well as complete multi-scale durability investigations. From this, guidance for ACM selection and mixture design for use in transportation infrastructure, including highway structures and rigid pavements, will be provided.

1.2 Motivation and Background

Two primary motivations for expanded use of ACMs include their potential to contribute to sustainable construction and their potential to provide a longer service life in a range of aggressive environments. Many ACMs – a term used here which includes clinkered, calcined, and unclinkered binding materials (ACI ITG-10R-18) - often can be produced with lower carbon dioxide (CO_2) emissions relative to portland cement manufacture. For example, manufacturing CSA and CAC cement clinker can result in around 30% and 15% reduction in CO_2 emissions, respectively [1]. The reduction in CO_2 emissions derives from the reduced amount of calcium carbonate feedstock and lower temperatures during clinkering. When blending clinker with other mineral phases, such as in CSA or ternal blends of CAC, OPC, and calcium sulfate (CACT), further reductions in embodied CO_2 can be realized due to clinker dilution. Other ACM formulations, like geopolymers or other activated aluminosilicates, do not require calcination. As a result, the embodied CO_2 in these systems can be quite variable, even among ACM classes, since embodied CO_2 for these mixtures is primarily a function of the activating solution used and can vary

considerably based on type and quantity of aluminosilicate precursor(s). Figure 1 gives an overview of potential CO_2 reductions for ACM cements, calculated based on the cement compositions (by phase) used in this study [1]. The relative uncertainty in the production methods for the AA and MPC materials examined requires that the values determined for those formulations be viewed in that context.

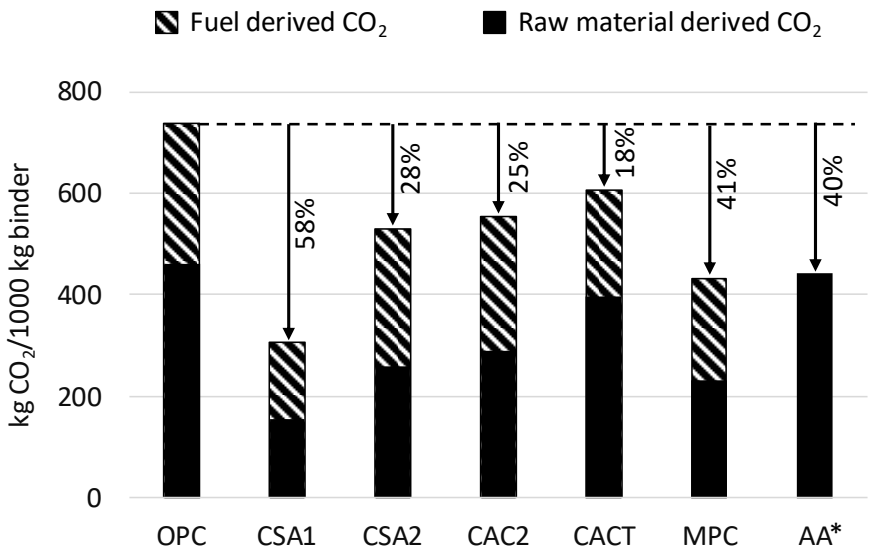

Fig. 1 Calculated potential reductions in embodied carbon dioxide in ACMs examined in this study, based upon phase composition. *For class C fly ash (precursor for AA system), does not include CO_2 emissions from chemical activators. Figure recreated from unpublished work (credit: Lisa E. Burris) and forthcoming Federal Highway Administration technical report [2].

ACMs also have been used in applications where their unique properties such as high early strength development, high later age strengths, low shrinkage, and superior durability are of value. For example, activated aluminosilicate materials are known for their thermal stability and fire resistance, and MPCs exhibit rapid set and high early strength [3]. Whereas CAC systems are known for their superior resistance to acid and sulfate attack and mechanical abrasion [4], some CSA systems have been associated for their higher resistance to freeze-thaw attack and other external chemical attacks like sulfate attack [5]

and improved dimensional stability [5,6]. However, despite the potential advantages of ACMs, an AASHTO survey [1] conducted at the outset of the project in 2014, revealed that only about half the states responding reported having experience using these materials. Concerns about the long-term performance of ACM concrete was the most commonly cited concern preventing broader use of these materials in transportation infrastructure.

1.3 Research objective

The primary objective of this research is to facilitate the rapid adoption of the ACM formulations in sustainable transportation infrastructure by comprehensively investigating the applications of these novel ACMs, which includes early-age, long-term material properties, and a multi-scale durability investigation. The specific goals of this research are as follows:

- To identify commercially available ACMs across a wide variety of formulations that are viable for developing mixtures that could be batched with conventional equipment. This would provide a greater potential for more rapid upscaling compared to lab-produced materials and materials that would require specialized manufacturing and batching requirements.
- To identify prescriptive and performance requirements that meet existing standards and specifications, and to design mixtures with ACMs that meet these requirements.
- To establish dimensional stability, multi-scale durability and other performance testing protocols, relying as much as possible on existing standardized test methods, and using these testing protocols to benchmark the performance of the ACM mixtures against traditional portland cement (OPC) mixtures.

1.4 Research approach

To minimize capital investment, it is desirable to use conventional concrete proportioning, mixing methods, and construction techniques for ACM concrete. To compare among ACMs, and to benchmark against the OPC performance, a combination of prescriptive and performance metrics was used. The metrics used were based on input from the federal highway administration (FHWA) exploratory advanced research program (contract: DTFH61-15-A-0001) advisory board, composed of transportation and construction professionals. The prescriptive requirements for the ACM concrete included a water-to-cement (or solids) ratio of 0.40 or less, at least 765 lbs. cement per cubic yard (454 kg/m^3) of concrete, and use of a ¾-inch (19 mm) maximum size coarse aggregate meeting ASTM C33 #67 gradation. The performance requirements included a set time of 1 hour or more, at least 3-inch (76 mm) slump 60 minutes after mixing, 7-day and 28-day compressive strength of at least 3500 psi (24 MPa) and 5000 psi (35 MPa) respectively, and a 28-day modulus of rupture of at least 700 psi (4.8 MPa).

The performance was benchmarked against OPC concrete meeting these criteria. ACM concrete not achieving these prescriptive and performance requirements were not included in further investigation. However, to future-proof the research work, some of the detailed investigations were also carried on the ACMs that did not pass the initial screening phase. The research was executed in two phases: (1) an initial screening phase that included mixture proportioning, early-age and hardened properties, and assessments of basic transport properties of all ACMs and (2) a more detailed investigation of downselected ACMs that assessed their durability, dimensional stability, and other performance

characteristics that are relevant to realistic operational environments. The specific research approach for phase 1 include:

Part 1. Detailed understanding of the hydration mechanisms and microstructure evolution in the mixtures developed with commercially available ACM formulations and comparing it to that of OPC mixture. These include understanding the effects of w/b, chemical admixtures (both set modifiers and water reducers), and mixing action on both early-age properties and later age properties. Vicat test, mini-slump test on cement paste, and flow tests on cement mortar will be used to understand the workability of ACM mixtures. Whereas several characterization techniques including isothermal calorimetry, in-situ x-ray diffraction, thermo gravimetric analysis, and scanning electron microscopy coupled with energy-dispersive x-ray analysis will be used to understand the hydration kinetics and microstructure evolution of these mixtures.

Part 2. Detailed understanding of early age and later age properties from part 1 will be used to design and develop OPC and ACM concrete mixtures that meet both the prescriptive and performance requirements.

Part 3. Assessment of basic transport properties of ACM mixtures developed in part 2 and comparing them to each other and to that of OPC mixtures.

The research approach for phase 2 includes a detailed assessment of following properties of ACM mixtures and comparing them to each other and to that of OPC mixtures:

- Transport properties of ACM mixtures at varied w/b using water sorption tests and formation factor measurements.

- Dimensional stability of ACM mixtures using autogenous tests.
- Resistance to external sulfate attack. A modified test method based on constant pH accelerated sulfate exposure test [6] coupled with several microstructure characterization techniques were used to understand the effects of sulfate exposure on binder composition and its integrity.
- Resistance to physical sulfate salt attack. Testing was performed on cement mortar cubes subjected to thermal loading to induce cyclic crystallization pressure on submerged mortar cubes [7,8].
- Resistance to alkali exposure. One modified length expansion test based on ASTM 1260 test procedure was used to understand the performance of ACM binders in severe alkali exposure.
- Resistance to alkali-silica reaction. Two modified length expansion tests based on ASTM 1260 and 1293 tests followed by detailed petrographic examination were used to understand the performance of ACM binders in resisting alkali-silica reaction of embedded reactive aggregates.
- Effects of carbonation on binder and pore solution composition. Several accelerated carbonation tests at different carbon dioxide (CO_2) exposure levels were conducted to understand its effects on mechanical properties, porosity, and pore solution pH of ACM mixtures. Electrochemical tests were also performed to understand the effects of carbonation on the passivity of embedded reinforcements.

Based on the research outcomes from the two phases, a detailed performance matrix is developed comparing the ACM mixtures to each other and to the corresponding OPC mixtures.

1.5 Thesis organization

This thesis is organized into 14 chapters. Chapter 1 is the introduction section of this thesis providing details on the project description, thesis objectives, and research approach. Chapter 2 provides background on the composition and reactions of the ACM systems. Information on the materials investigated in this thesis, including their physical and chemical properties, are provided in chapter 3.

Chapters 4 to 8 provide the results and the relevant discussions and conclusions from phase 1 of the research. The detailed investigation of the reaction mechanisms and microstructure evolution of the materials considered in this thesis are provided in chapter 4. Chapters 5 and 6 provide results from the in-depth investigation of the effects of admixtures and w/b on early-age properties, including hydration kinetics and workability, and the extent of hydration at later ages. Chapter 7 discusses the concrete mixture design and their fresh properties, whereas the later age mechanical characteristics of these concrete mixtures are provided in chapter 8.

The results from phase 2 of the research are discussed in chapters 8 to 13. Chapter 8 also discusses the dimensional stability of the ACM mixtures compared to that of OPC. The effect of binder composition and w/b on the transport properties of ACM and OPC mixtures are discussed in detail in chapter 9. In chapter 10, detailed investigation of the effects of external chemical sulfate exposure on the ACM and OPC mixtures is provided. The effects of alkali exposure on the ACM and OPC mixtures and the effects of binder composition in resisting the alkali-silica reaction of embedded reactive aggregates are discussed in chapter

11. Chapter 12 provides in-depth investigation of the effects of CO_2 exposure on the binder composition, pore solution pH, and embedded reinforcement in ACM and OPC mixtures.

Conclusions and recommendations are provided in chapter 13, and references in chapter 14.

2 BACKGROUND ON ACMS

Like OPC, CSA and CAC are typically produced through clinkering, although their compositions vary from OPC. Activated aluminosilicate systems, a broad term that encompasses geopolymers [9], are typically unclinkered. Here, the composition and reactions of these systems are briefly reviewed, with an emphasis on those factors relevant to aspects discussed in the later sections of this thesis.

2.1 Ordinary portland cement (OPC)

The main phases present in a typical anhydrous portland cement are C_3S, C_2S, C_3A, C_4AF, and $C\overline{S}H_x$. The dissolution and reaction of these phases with water results in the primary hydration products (calcium silicate hydrate, ettringite, monosulfate, calcium hydroxide) as shown in the SEM-EDS micrograph (Fig. 2) of a Type I/II portland cement hydrated for 56 days with 0.45 w/b. The calcium silicate hydrates (C-S-H) are the main strength-giving component, whereas the calcium hydroxide (portlandite), along with the oxides of sodium and potassium are responsible for the alkalinity of portland cement systems. Concrete alkalinity helps to maintain the steel reinforcement in a passive state, limiting the corrosion rate. Also, C-S-H and monosulfate (AFm) phases, along with anhydrous C_3A, can bind chlorides [10–13], thereby potentially significantly reducing the concentration of free chlorides at the rebar interface, limiting corrosion.

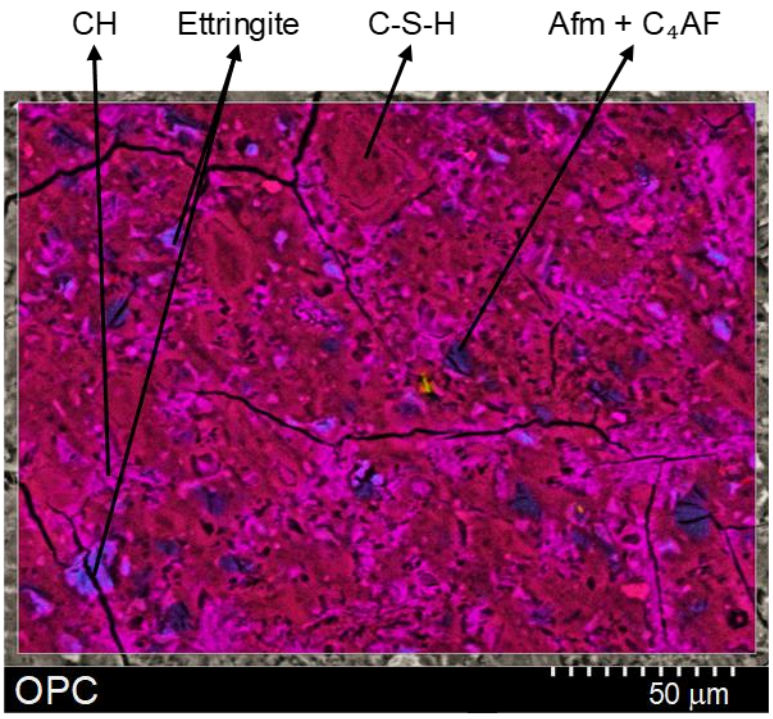

Fig. 2 SEM-EDS micrograph of hydrated cement paste made with an ASTM C150 Type I/II OPC cement at 56 days, with w/b of 0.45.

2.2 Calcium sulfoaluminate cement (CSA)

The main phases present in a typical CSA cement are $C\overline{S}$ (anhydrite, or form of calcium sulfate) and $C_4A_3\overline{S}$ (Ye'elimite) [14]. The possible hydration reactions/products depend on the relative amount of calcium sulfate to Ye'elimite present in the cement and the amount of portlandite formed with hydration. If there is sufficient sulfate present in the cement, reactions (i) and (ii) in Equation 1 occur, forming ettringite as the main hydration product, as well as aluminum hydroxide. Whereas reaction (iii) in Equation 1 will be dominant if there is insufficient sulfate present in the cement, leading to the formation of monosulfate instead of ettringite [15,16]. With CSA cements also containing the C_2S phase, a fourth reaction (iv) in Equation 1 is also possible if there is excess calcium hydroxide present along with excess amounts of calcium sulfate, potentially forming expansive ettringite [17].

Equation 1

$$C_4A_3\overline{S} + 2C\overline{S} + 38H \rightarrow Ettringite + 4AH_3 \quad \text{(i)}$$

$$3CA + 3C\overline{S} + 38H \rightarrow Ettringite + 2AH_3 \quad \text{(ii)}$$

$$3C_4A_3\overline{S} + 18H \rightarrow monosulfate + 2AH_3 \quad \text{(iii)}$$

$$C_4A_3\overline{S} + 8C\overline{S} + 6CH + 90H \rightarrow 3\,Ettringite \quad \text{(iv)}$$

Ettringite and C-S-H (formed in CSA binders containing C_2S or other reactive siliceous phases) are the main hydration products for CSA cement. With no or low amounts of C_3S present in typical CSA cements and since the C-S-H is formed from the C_2S reaction, the amount of portlandite formed is low compared to traditional portland cement systems. Also, the portlandite formed early can be consumed to form the ettringite. Therefore, most of the alkalinity in CSA systems derives from the presence of the alkalis, sodium (Na) and potassium (K) in the pore solution – leading to in general lower pH and pH buffering capacity compared to portland systems. These differences in pH, as well as in the hydration productions and their concentrations, can lead to considerably different carbonation and corrosion mechanisms. Fig. 3 shows the SEM-EDS micrograph of a hydrated CSA belite cement produced at 0.45 w/b. As shown in the micrograph, the hydrated matrix is primarily composed of ettringite.

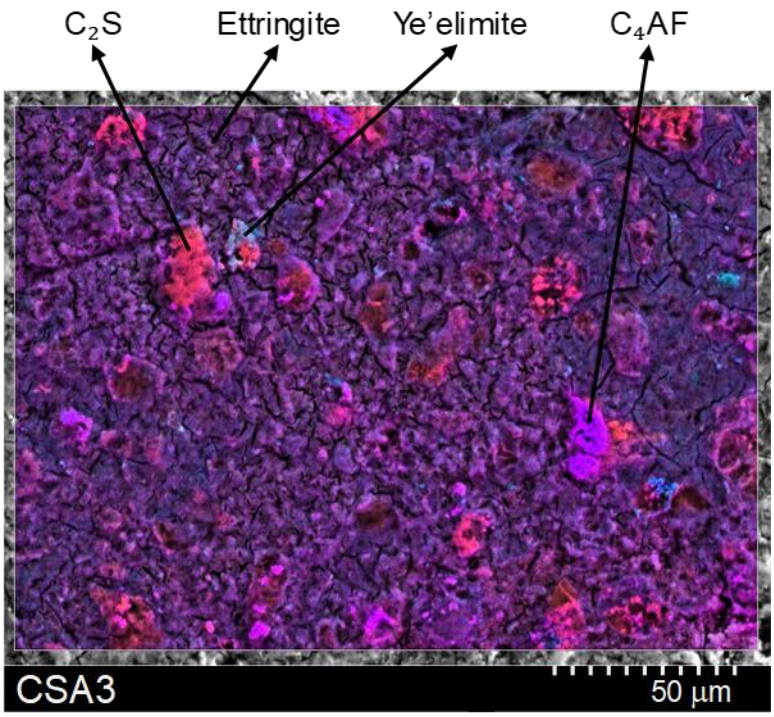

Fig. 3 SEM-EDS micrograph of hydrated cement paste made with a CSA cement at 56 days, with w/b of 0.45.

2.3 Calcium aluminate cement (CAC)

CA, C_3A, and C_4AF are the main phases (sometimes the only phases) present in calcium aluminate cement (CAC). Some CACs may also contain siliceous phases such as C_2S and C_2AS. The nature of hydration products formed on reaction with water greatly depends on the temperature during hydration. At lower temperatures below 15 ºC, CAH_{10} forms [reaction (i) in Equation 2], with C_2AH_8 and C_3AH_6 [reaction (ii) and (iii) in Equation 3] being the dominant hydration product at intermediate (15 to 70 ºC) and higher (> 70 ºC) hydration temperatures respectively. C_3AH_6 is the most stable product. Over time, the unstable lower density CAH_{10} and C_2AH_8 phases convert to more dense C_3AH_6, leading to increased porosity and a significant reduction in strength [4,18,19]. Also, the $C_{12}A_7$ phase reacts faster compared to the CA phase and primarily hydrates according to reaction (iv) at

room temperature. Fig. 4 shows the SEM-EDS micrograph of a 56-day hydrated CAC mixture produced at 0.45 w/b and cured at 23 ºC. the hydrated matrix is primarily C_2AH_8, CAH_{10}, and AH_3 phases. A significant amount of C3AH6 phase is not formed since it is cured at 23 ºC and it is only at 56 days of age.

Equation 2

$$6CA+60H \rightarrow CAH_{10} \quad \text{(i)}$$

$$6CA+60H \rightarrow 3C_2AH_8+3AH_3+27H \quad \text{(ii)}$$

$$6CA+60H \rightarrow 2C_3AH_6+4AH_3+36H \quad \text{(iii)}$$

$$C_{12}A_7+60H \rightarrow 6C_2AH_8+AH_3 \quad \text{(iv)}$$

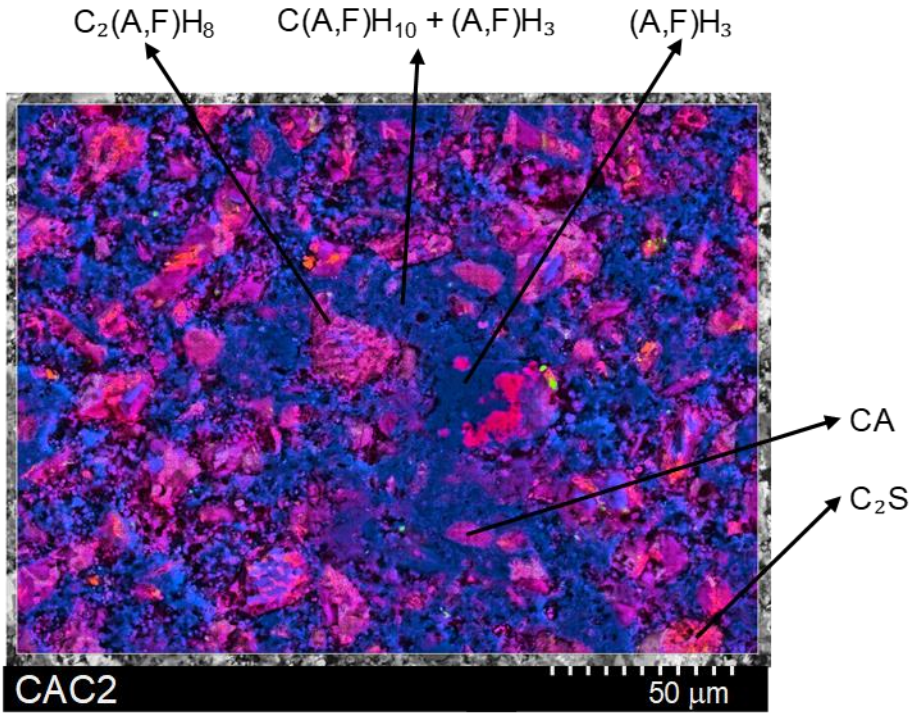

Fig. 4 SEM-EDS micrograph of hydrated cement paste made with a CAC cement at 56 days, with w/b of 0.45.

Like CSA cement, no C_3S phase is present in the CAC, and if C_2S is present, the C-S-H is formed from its reaction, resulting in lower amounts of portlandite in the hydrated matrix. Thus, a lower pH buffering capacity may be expected in CAC systems compared to the traditional portland cement. The anhydrous calcium aluminate phases present in CAC can bind chlorides from the pore solution, forming Friedel's salt (C-A-H-$CaCl_2$). However, Friedel's salt is known to partially dissolve over time to calcium aluminate hydrate phases (e.g., hydrogarnet), which releases chloride ions into the pore solution. Also, Friedel's salt carbonates rapidly compared to other hydrogarnet phases present in CAC mixtures, again leading to the release of bound Cl ions into the pore solution [20–22].

2.4 OPC – CAC – Calcium sulfate blends

In order to minimize the effects of conversion and offset the high costs of CAC, $OPC - CAC - C\bar{S}$ ternary blended cements, consisting of a large proportion of portland cement with significant additions of calcium aluminates and calcium sulfates, are becoming increasingly common [23]. When mixed with water, both the C_3A and CA present in the ternary blend hydrate to form ettringite (Equation 3 (i)) and monosulfate (Equation 3 (ii)) after the depletion of the system's calcium sulfate [24]. Additionally, calcium silicate phases present in the OPC fraction of the blend will produce C-S-H and CH phases similar to normal OPC hydration processes. In mixtures containing calcium carbonate, monocarbonate and hemicarbonate phases can also form as shown in Equation 3 (iii) and (iv), leading to consumption of CH [25]. The SEM-EDS micrograph of a hydrated CACT mixture (Fig. 5) shows a blend of multiple hydrated phases that are a combination of commonly observed phases in both OPC and CSA mixtures.

Equation 3

$$3CA + 3C\overline{S}H_x + (38 - 3x)H \rightarrow \textit{Ettringite} + 2AH_3 \quad \text{(i)}$$

$$\textit{Ettringite} + 6CA + 16H \rightarrow \textit{monosulfate} + 4AH_3 \quad \text{(ii)}$$

$$AH_3 + 3CH + C\overline{C} + 5H \rightarrow \textit{monocarbonate} \quad \text{(iii)}$$

$$2AH_3 + 7CH + C\overline{C} + 11H \rightarrow \textit{2.hemicarbonate} \quad \text{(iv)}$$

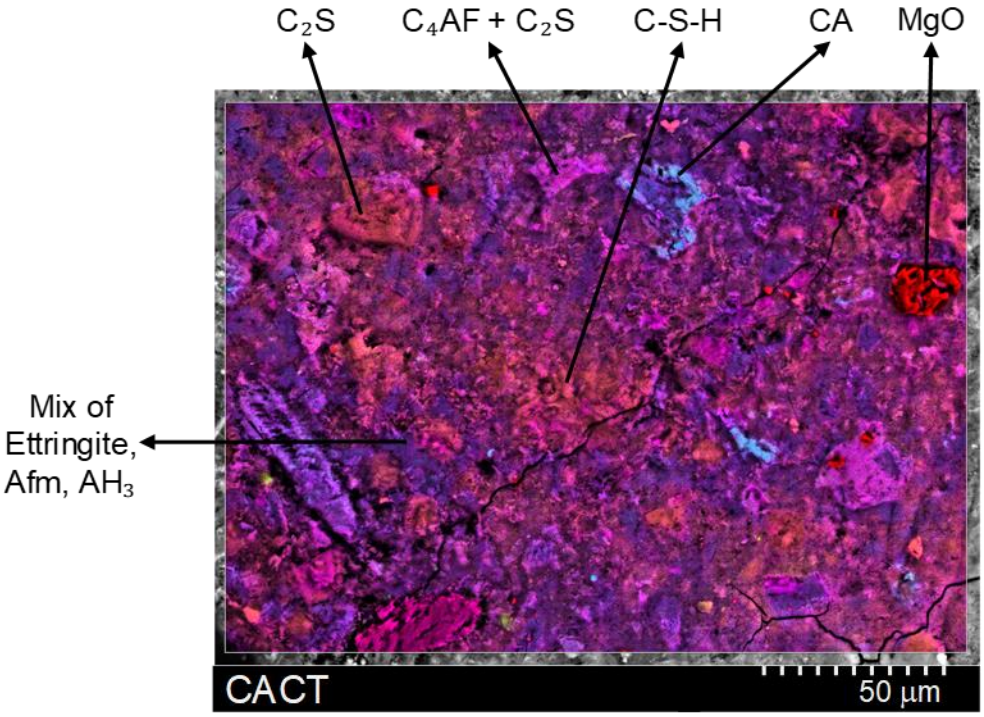

Fig. 5 SEM-EDS micrograph of hydrated cement paste made with an *OPC-CAC-Calcium sulfate* blended cement at 56 days, with w/c of 0.45.

2.5 Activated aluminosilicate binders (AA)

The products formed in AA systems greatly depend on the type of precursor material and the ratio of amorphous silica and alumina to alkalis in the activator solution. In a calcium-rich precursor, such as blast furnace slag and Class C fly ash, the main hydration products

include C-A-S-H type gel, N-A-S-H type gel, as well C-S-H gel and some minor phases such as ettringite, AFm phases and stratlingite [26–28]. However, in systems with low calcium precursors such as Class F fly ash, N-A-S-H type gel is the dominant hydration product. The SEM-EDS micrograph of an activated Class C fly ash with non alkaline activator (Fig. 6) shows both the C-N-A-S-H and N-A-S-H gel around the fly ash particles. Alkalies from the precursor material buffer the pore solution pH in AA systems with non alkaline activators.

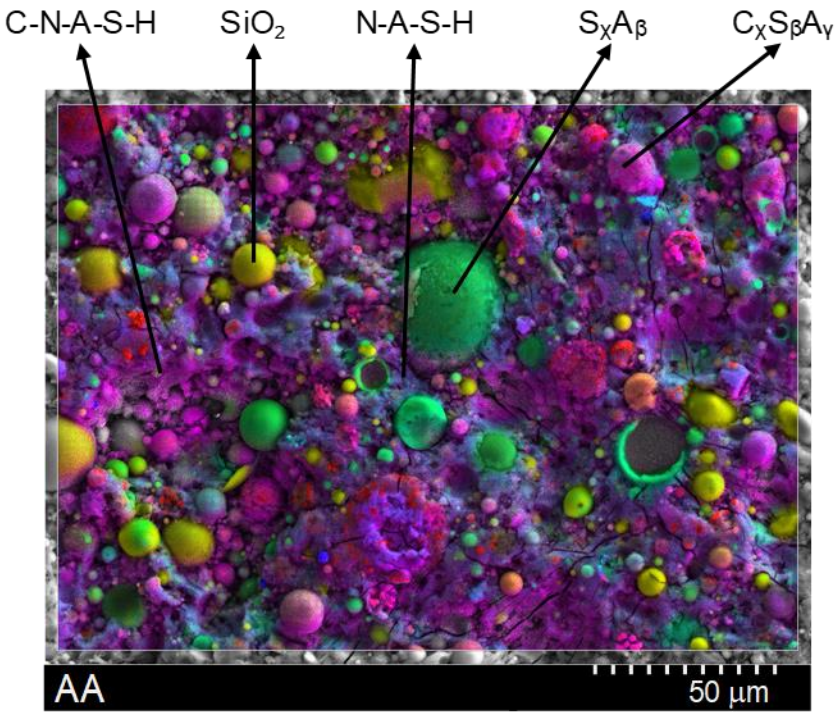

Fig. 6 SEM-EDS micrograph of an activated cement paste made with an AA binder at 56 days, with w/c of 0.25.

2.6 Magnesium phosphate cements (MPC)

Magnesium phosphate cements, which sometimes referred to as chemically bonded ceramics, are primarily composed of MgO and P_2O_5 phases. Multiple formulations of MPC

exists mainly with varying phosphate sources such as KH_2PO_4, $NH_4H_2PO_4$, and NaH_2PO_4. Of these, the formulations involving KH_2PO_4 are found to be effective in producing mixtures which doesn't produce too much heat while setting [29–32]. KH_2PO_4 has low solubility compared to the other two phosphate phases. Equation 4 shows the reaction mechanism involving the formation of K-struvite ($KMgPO_4.6H_2O$) form the hydration of MgO and KH_2PO_4. Often inert fillers such as wollastonite (CS) are blended with the cement to increase the setting time by diluting the reaction phase and also improving the durability of the mixtures [29,33]. Fig. 7 shows the SEM-EDS of hydrated MPC mixtures produced at 0.30 w/b. The micrograph shows K-struvite as the main hydration product.

Equation 4

$$MgO + KH_2PO_4 + 4H \rightarrow KMgPO_4.6H_2O$$

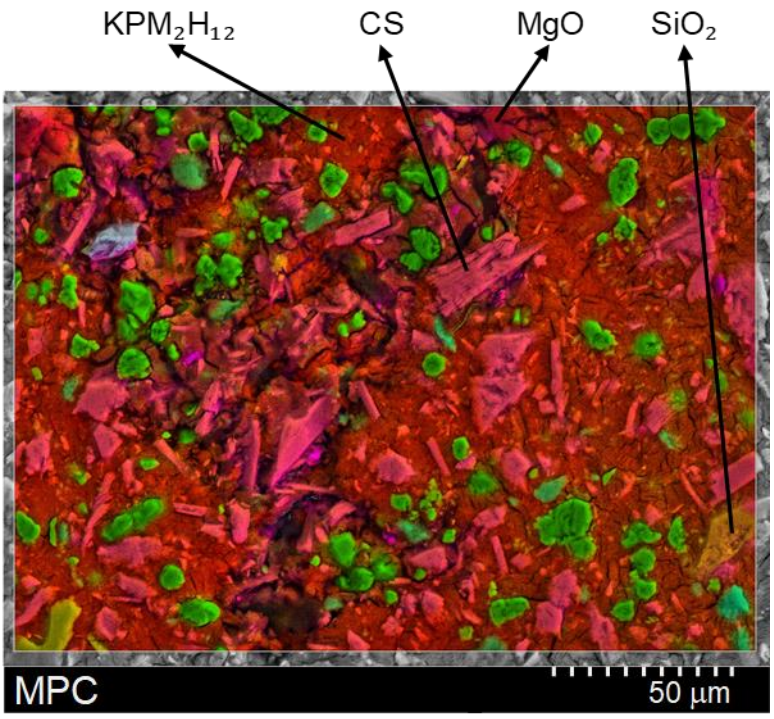

Fig. 7 SEM-EDS micrograph of hydrated cement paste made with an MPC cement at 56 days, with w/c of 0.30.

3 MATERIALS

The following nine commercially available ACMs were evaluated and benchmarked against ASTM C150 Type I/II portland cement (OPC):

- Two calcium aluminate cements (CAC1 and CAC2).
- One ternary blend of calcium aluminate, portland cement, and calcium sulfate (CACT).
- Four calcium sulfoaluminate belite cements, including one with polymer (P) modification (CSA1, CSA2, CSA2P, and CSA3).
- One activated aluminosilicate binder system (AA) consisting of ASTM C618 Class C fly ash and a proprietary two-part activator solution (most likely a combination of carboxylate-based citrate or lactate activator and a retarder); and
- One magnesium phosphate cement (MPC).

Fig. 8 shows the particle size distribution of all the ACMs compared to OPC. Specific gravity, specific surface area (SSA), and normal consistency (determined according to ASTM standard C187-11) of all the binders are shown in Table 1. The fineness of all the 3 CSAs and AA is significantly higher compared to OPC and other ACMs. Both the CAC2 and the ternary blend (CACT) have lower fineness compared to OPC and all other ACMs. The oxide composition of all the ACMs and OPC determined from μXRF is shown in Table 2. The phase composition of OPC and ACMs is shown in Table 3. For OPC and all other ACMs (except AA and MPC), the phase composition was estimated from quantitative XRD using Rietveld refinement procedure. Fig. 9 shows the SEM-EDS micrographs of

OPC and ACMs (except AA and MPC). These micrographs corroborate the phase compositions shown in Table 3. For MPC, the phase composition was estimated from the oxide composition based on the qualitative understanding of phase composition from the SEM-EDS technique. The SEM-EDS micrographs of MPC cement are shown in Fig. 10. Whereas for AA, SEM-EDS technique was employed (shown in Fig. 11) to quantify the phase composition [34], due to the significant presence of amorphous content. Each of the ACMs examined has a lower CaO content than OPC, as related to the lower limestone content in their feedstock and associated for savings in carbon dioxide emissions. These cements have different phase composition, which leads to different reaction mechanisms, reaction rates, products, and microstructure than OPC. An overview of the ACM reactions with water, or in the case of AA with a chemical activator solution, is discussed in detail in section 2 and section 4.

Fig. 12 shows the initial and final setting times of the paste mixes made with OPC and ACMs determined at their normal consistency according to the procedure given in section 5.1.1. Both CAC1 and CAC2 mixtures have higher initial and final setting compared to OPC past mixture. Whereas CACT, CSA1, CSA2, CSA2P, and MPC past mixtures have both initial and final setting times less than 60 minutes and significantly lower compared to that of OPC. In order to achieve the initial setting time of at least 60 minutes, a 99% pure grade anhydrous citric acid was used to retard the setting time in CACT and all the CSA binders [35–38], and a 99% pure boric acid was used to retard the setting time in MPC [29,39–41] mixes (refer to section 6.3 for more details). Two commercially available high range water reducers/ plasticizers – admix1 (ADVA 195 from *gcp applied technologies*)

and admix2 (CHRYSO AL 810 from *CHRYSO group*) were used to achieve the desired workability in ACM and OPC mixtures (refer to section 6.3 and chapter 7 for more details).

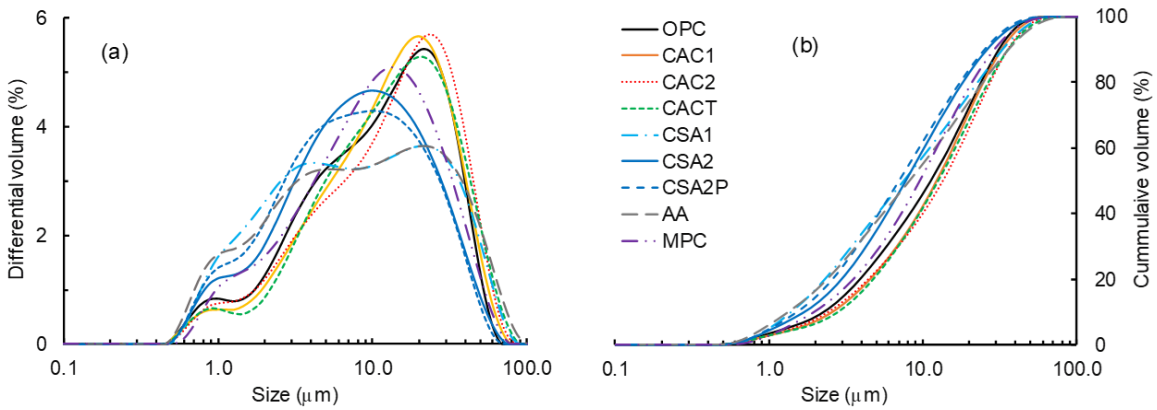

Fig. 8 Particle size (a) differential volume, and (b) cumulative volume of ACMs compared to OPC.

Table 1 Specific gravity (SG), specific surface area (SSA), D-values (D10, D50, D90), and normal consistency (NC) of ACMs compared to OPC.

Cement	OPC	CAC1	CAC2	CACT	CSA1	CSA2	CSA2P	CSA3	AA	MPC
SG	3.05	3.13	2.97	2.91	2.81	2.81	2.81	2.99	2.58	2.77
SSA (m^2/kg)	333.3	291.5	306.4	302.7	501.3	453.2	492.6	350.2	550.7	398.2
D10 (µm)	2.58	2.95	2.77	3.2	1.59	1.93	1.73	2.35	1.52	2.23
D50 (µm)	12.8	14	15.3	14.3	8.59	8.8	7.96	12.8	9.3	10.9
D90 (µm)	35.4	37.4	40.6	40.8	37.9	29.7	28.6	36.4	41	33.1
NC*	0.25	0.325	0.285	0.27	0.31	0.31	0.31	0.30	–	0.21

*w/b ratio determined according to ASTM C187-11

Table 2 Oxide composition of ACMs compared to OPC.

Oxide	OPC	CAC1	CAC2	CACT	CSA1	CSA2	CSA2P	CSA3	AA	MPC
SiO_2	17.39	4.54	5.50	14.95	8.96	13.97	14.21	13.20	35.56	21.70
Al_2O_3	4.87	38.70	45.16	12.03	20.44	14.70	15.40	18.10	18.80	2.35
Fe_2O3	4.71	15.89	6.90	2.66	1.57	1.04	0.92	6.60	6.19	0.21
CaO	65.15	36.72	37.68	55.15	44.91	49.63	49.94	48.30	24.49	16.60
MgO	1.40	0.54	0.22	2.57	1.65	1.54	1.43	1.50	5.66	23.82
P_2O_5	0.13	0.12	0.09	0.14	0.19	0.11	0.10	0.06	0.94	17.61
SO_3	2.51	0.13	0.07	7.72	18.87	13.80	13.92	7.50	2.33	0.15
K_2O	0.48	0.19	0.26	0.83	0.38	0.68	0.62	0.70	0.50	12.10
Na_2O	0.46	0.06	0.00	0.28	0.10	0.13	0.13	0.10	1.77	0.11
TiO_2	0.39	1.87	2.11	0.51	0.47	0.71	0.65	0.93	1.45	0.10
Mn_2O_3	0.11	0.19	0.02	0.16	0.08	0.02	0.02	0.08	0.03	0.02
SrO	0.15	0.02	0.04	0.21	0.08	0.20	0.16	0.10	0.41	0.00
ZnO	0.03	0.01	0.00	0.11	0.05	0.01	0.02	0.00	0.01	0.00
Cr_2O_3	0.09	0.13	0.09	0.07	0.05	0.05	0.05	0.04	0.05	0.03
CO_2[#]	0.57	0.90	0.24	1.61	0.50	1.43	0.49	0.38	0.08	0.45
LOI*	1.56	0.00	1.62	1.00	1.70	1.99	1.94	2.41	1.73	4.74

[*]excluding CO_2; [#]determined using TGA technique; Source: Robert Moser, U.S. Army Engineer Research and Development Center, Vicksburg, MS.

Table 3 Phase composition of ACMs compared to OPC.

Phase	OPC	CAC1	CAC2	CACT	CSA1	CSA2	CSA2P	CSA3	AA*	MPC[#]
C_3S	65.2	0.0	0.0	40.8	0.0	0.0	0.0	0.0	0.0	0.0
C_2S	14.0	10.7	12.2	22.7	28.1	41.1	45.2	36.9	0.0	0.0
CS	0.0	0.0	0.0	0.0	0.0	0.0	0.0	0.0	0.0	33.2
CA	0.0	55.3	56.9	15	0.0	0.0	0.0	0.0	0.0	0.0
$C_{12}A_7$	0.0	10.2	1.4	0.0	0.0	1.6	1.1	0.5	0.0	0.0
C_3A	2.1	18.4	12.3	0.5	0.0	0.0	0.0	0.0	0.0	0.0
C_4AF	15.1	0.9	0.0	11.1	1.4	1.9	1.2	17.5	0.0	0.0
$CaCO_3$	1.7	0.2	0.0	0.7	1.8	3.9	1.3	0.7	0.0	1.0
$C\bar{S}$	1.6	0.0	0.0	9.1	24.5	15.3	13.8	11.5	3.3	0.0
$C\bar{S}H_{0.5}$	0.1	0.0	0.0	0.0	2.1	2.9	2.7	0.1	0.0	0.0
$C\bar{S}H_2$	0.0	0.0	0.0	0.0	0.0	0.0	0.0	0.1	0.0	0.0
$C_4A_3\bar{S}$	0.0	0.0	0.0	0.0	40.7	32.9	33.8	32.2	0.0	0.0
C_2AS	0.0	2.1	16.2	0.0	0.0	0.0	0.0	0.0	0.0	0.0
SiO_2	0.0	0.0	0.0	0.1	0.2	0.4	0.9	0.5	5.0	3.1
MgO	0.2	0.0	0.0	0.0	0.0	0.0	0.0	0.0	0.0	23.8
Fe_2O_3	0.0	2.2	1.0	0.0	0.0	0.0	0.0	0.0	0.0	0.21
M_2S	0.0	0.0	0.0	0.0	1.2	0.0	0.0	0.0	0.0	0.0
KH_2PO_4	0.0	0.0	0.0	0.0	0.0	0.0	0.0	0.0	0.0	33.8
A_xS_y	0.0	0.0	0.0	0.0	0.0	0.0	0.0	0.0	5.4	3.7
C_xS_y	0.0	0.0	0.0	0.0	0.0	0.0	0.0	0.0	7.3	0.0
$C_xA_yS_z$	0.0	0.0	0.0	0.0	0.0	0.0	0.0	0.0	75.7	0.0
other	0.0	0.0	0.0	0.0	0.0	0.0	0.0	0.0	3.2	1.1

*estimated based on the quantitative understanding of phase composition from the SEM-EDS technique shown in Fig. 11; [#]estimated from oxide composition based on the qualitative understanding of phase composition from SEM-EDS technique.

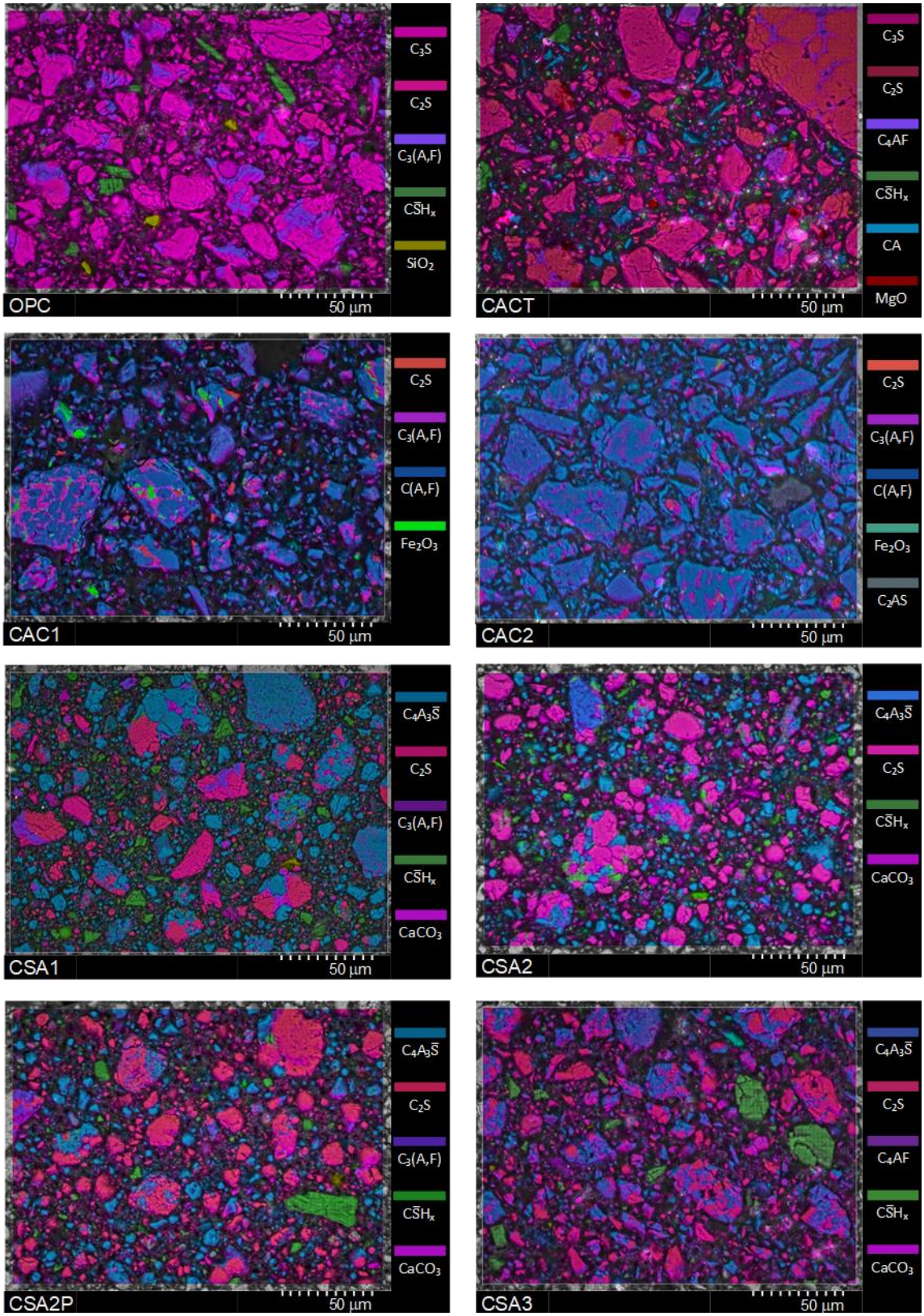

Fig. 9 SEM-EDS micrographs of OPC, CACT, CAC1, CAC2, CSA1, CSA2, CSA2P, and CSA3 cements.

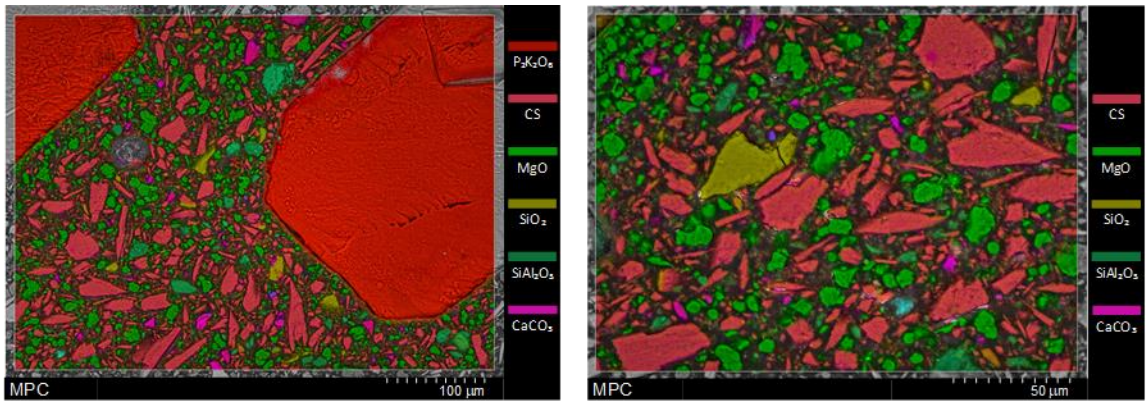

Fig. 10 SEM-EDS micrographs of MPC cement.

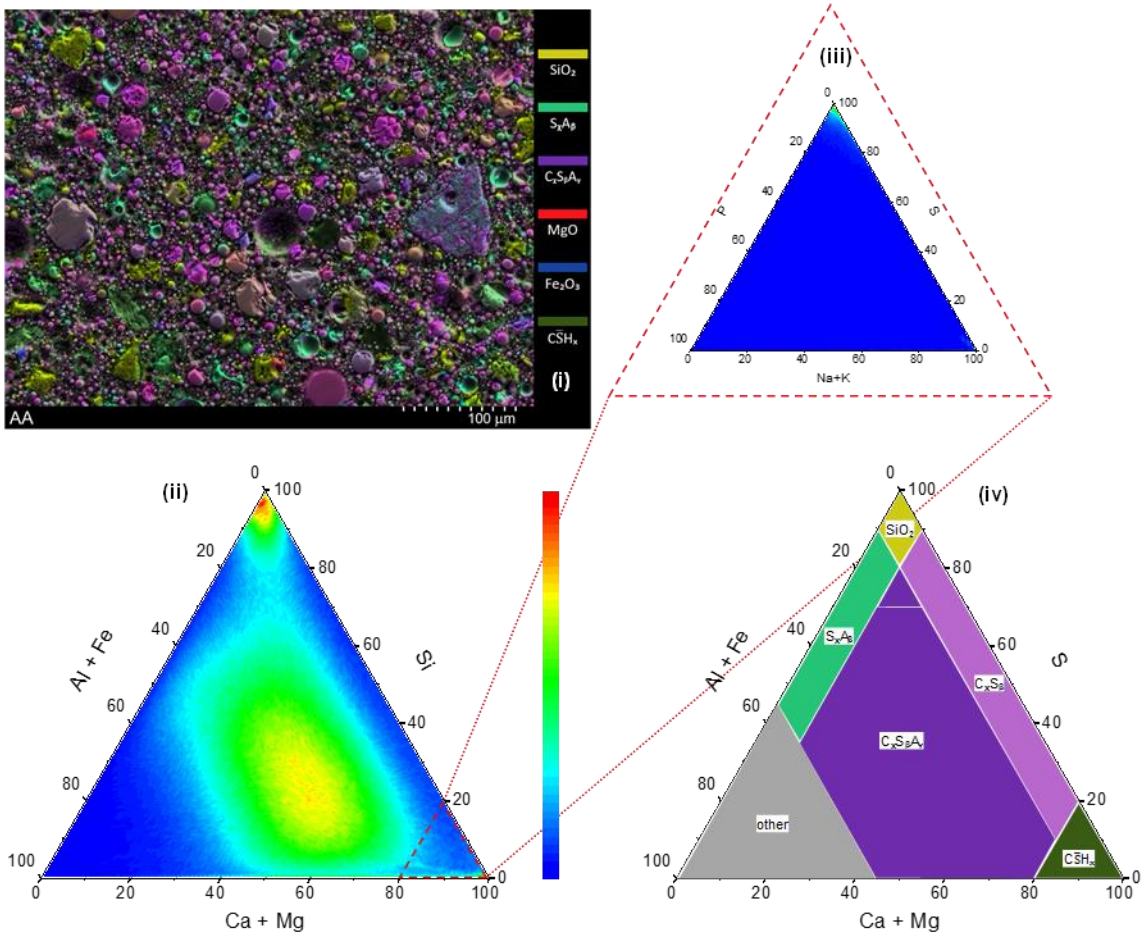

Fig. 11 (i) SEM-EDS micrograph of Class C fly ash used as a precursor for AA mixtures. (ii) Ternary frequency plot of atomic percentage of (Ca+Mg), Si, (Al+Fe). (iii) Ternary frequency plot of atomic percentage of (Na+K), S, P in the dotted triangular region of ternary frequency diagram shown in (ii). (iv) Segmentation into phases based on the ternary frequency plot shown in (ii).

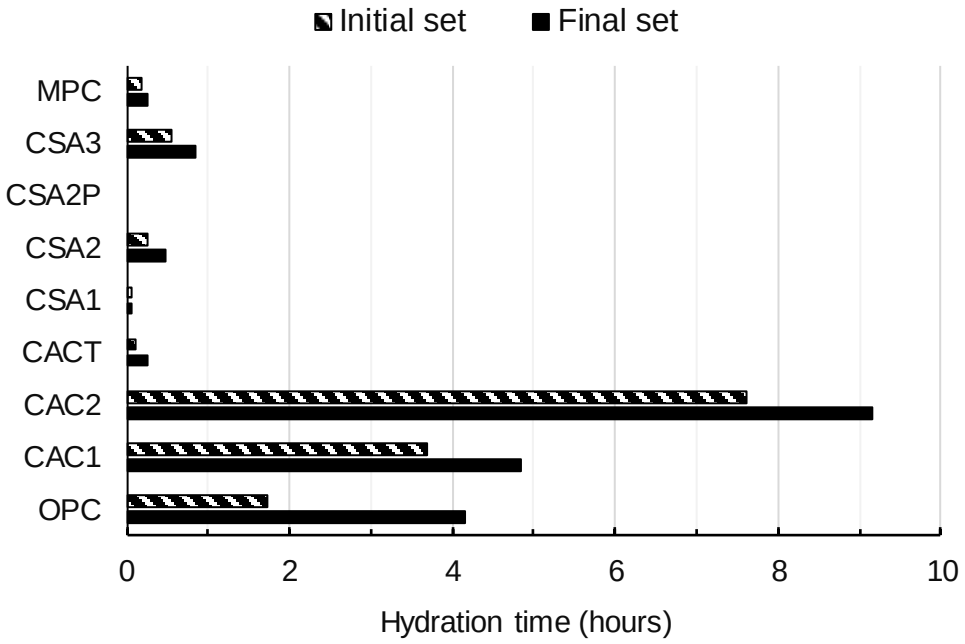

Fig. 12 Vicat setting times of cement pastes made with ACMs at normal consistency compared to that of OPC.

4 REACTION MECHANISMS

This chapter validates and compares the hydration mechanisms in the commercially available ACM formulations with that of lab-produced ACM materials researched in the literature. Isothermal calorimetry tests were also performed to understand the effects of mixing actions in these ACM mixtures, which is required to develop successful concrete mixtures (chapter 7) to meet the set prescriptive requirements and performance target (section 1.4) with the understanding of admixture interactions on cement pastes alone (chapter 5 and 6).

4.1 Methods

4.1.1 Thermogravimetric Analysis (TGA)

A Hitachi simultaneous thermogravimetric analyzer STA7300 was used to carry out the thermogravimetric measurements. TGA was carried out on powdered cement paste samples prepared according to mixture proportions shown in Table 4 and cured at 23 ºC in sealed bags. Prior to performing TGA, the paste samples were ground and sieved to a particle size of less than 300 microns, and the free water was removed using a solvent exchange procedure [42]. 5 g of powdered sample was mixed in 50 ml of isopropyl alcohol, and the suspension rests for 15 min. Then, the suspension is filtered using Büchner funnel and a vacuum pump for 5 min, and later, it is washed with 10 ml of diethylene ether for 1 min, during which the vacuum pump is turned off. The resulting suspension is again filtered under vacuum for five more minutes, or until the suspension is dry, whichever is longer.

The dried sample is further ground and approximately 20 mg of the sample with the particle size less than 74 microns is taken in an open 70 μl platinum crucible and dried in TG at 25 ºC under a constant stream of Nitrogen (N_2) gas for 15 min, or until the constant mass, whichever is longer. Later the temperature is increased to 40 ºC and held constant for 5 min. Then, the sample is heated from 40 to 1000 ºC, at a rate of 10 ºC/min, and the data is recorded at a rate of 120 data points per minute. During measurement, N_2 is used as a protective gas with a flow rate of 100 mL/min.

4.1.2 Isothermal calorimetry

Isothermal calorimetry was also performed on cement pastes mixed in a high shear mixer and planetary mixer (ASTM C305-14), and cement mortars, also mixed in a planetary mixer (ASTM C305-14) to understand the effects of mixing action on hydration kinetics. The mix proportions for both cement pastes and mortars are given in Table 5. The dosages of set modifiers/activators were chosen such that the corresponding concrete mixtures had a working time of at least 1 hour (refer to section 5 and 7 for more details). Crushed granitic river sand (Lambert Sand and Gravel, Shorter, Alabama) with gradation conforming to ASTM C33 specification was used in making mortar mixtures. Immediately after mixing, approximately 5g of paste mixtures are loaded into HDPE ampules of volume 20 ml, and then loaded into an isothermal calorimeter (8 channel TAM Air by Thermometric) at 23 ºC. The heat evolution of the sample was measured at a rate of 6 data points per minute.

Table 4 Cement paste mixture proportions.

Cement	w/b	Set modifier/ activators (by weight of cement)
OPC	0.40	–
CAC1	0.40	–
CAC2	0.40	–
CACT	0.40	Citric acid – 1.5%
CSA1	0.40	Citric acid – 2.0%
CSA2	0.40	Citric acid – 0.5%
CSA3	0.40	Citric acid – 0.75%
AA	0.20	Activator 1 – 2.47%, activator 2 – 2.21%
MPC	0.30	Boric acid – 14%

Table 5 Cement paste and mortar mixture proportions.

Cement	w/b	Sand/cement	Set modifier/ activators (by weight of cement)
OPC	0.40	2	–
CAC2	0.40	2	–
CACT	0.40	2	Citric acid – 1.5%
CSA1	0.40	2	Citric acid – 2.0%
CSA2	0.40	2	Citric acid – 0.5%
CSA3	0.40	2	Citric acid – 0.75%
AA	0.25	2	Activator 1 – 2.47%, activator 2 – 2.21%
MPC	0.30	2	Boric acid – 14%

4.2 Results and Discussion

4.2.1 Evolution of hydration products/ microstructure

The thermogravimetric analysis results for OPC and ACM mixtures at 56 days of hydration are shown in Fig. 13 (i to ix). Fig. 14 shows the evolution of bound water in OPC and ACM mixtures over time. For the OPC mixtures, the hydration products include C-S-H,

portlandite, ettringite, and monosulfate phases, as expected [43–45]. At 9 hours of hydration, the hydration products in OPC primarily included ettringite, portlandite, and C-S-H – as evident by DTG data in Fig. 13 (i) and SEM micrographs in Fig. 17 (i). The total bound water in OPC mixtures at 9 h and 56 d of hydration is about 11.2% and 24.6%. The standard error for the bound water measurements is less than 1% of the measured bound water value (more details in appendix section A.2.2). About 46% of the hydration (compared to 56 days) has happened within the first 9 hours of hydration times. Also, out of 40% mix water added to the cement, about 15.4% of it did not participate in hydration, which can result in significant porosity.

In CACT mixtures, the hydration products include primarily ettringite, followed by hemicarboaluminate, monocarboaluminate, AH_3, C-S-H, and portlandite [23–25]. The SEM micrographs in Fig. 17 (iii) and DTG in Fig. 13 (ii) show ettringite as the hydration product at 24 h of hydration. The total bound water at 8 h, 24 h, and 56 d of hydration are about 5.6, 6.7, and 33% by weight of cement. No significant change is observed in the bound water during the first 8 to 24 hours of hydration period, which suggests either significant retardation or significant latent period in CACT mixtures during the initial 24 hours. Also, only about 20% of the hydration has happened during the first 24 hours of hydration compared to OPC mixtures, where 46% of the hydration happened even in the first 9 hours of hydration. However, at the end of the 56 days, only about 7% of the added mix water did not contribute to hydration.

Even though CACT contains significantly higher amounts of siliceous phases (40.8% C_3S and 22.7% C_2S), the amount of portlandite formed in the CACT system is significantly low

compared to OPC. This suggests the formed portlandite is being consumed back in the ettringite reaction [17,25].

The hydration products in CAC1 mixtures are CAH_{10}, C_2AH_8, C_3AH_6, and AH_3, formed from the hydration of calcium aluminate phases, and also C_2ASH_8 formed from the hydration of calcium aluminate and siliceous phases – evident by the DTG peaks in Fig. 13 (v) [4,18,19]. After about 12 hours of hydration, C_2AH_8 and AH_3 are the primary reaction products formed – likely due to the higher amount of $C_{12}A_7$ phase in the cement. With time more of CAH_{10} and C_3AH_6 phases started to appear, and a significant reduction in the C_2AH_8 is observed. The amount of bound water after 12, 35 hours, and 56 days of hydration is about 23%, 27, and 31%, respectively. This suggests CAC1 cements hydrate faster quicker strength development. At the end of 56 days of hydration, about 9% of the mix water did not contribute to hydration.

Similar to the CAC1 mixtures, the hydration of CAC2 mixtures also resulted in the formation of CAH_{10}, C_2AH_8, C_2ASH_8, C_3AH_6, and AH_3 phases [4,18,19]. However, the hydration in CAC2 mixtures significant amounts of CAH_{10} phase compared to the C_2AH_8 phase. This is because CAC2 cement has a significantly lower amount of $C_{12}A_7$ phase compared to CAC1 cement. The SEM micrographs in Fig. 17 (ii) show C-A-H crystals growing on cement grain. . The amount of bound water after 13, 35 hours, and 56 days of hydration is about 23.5%, 25%, and 31%, respectively. Even though the amount of bound water at each of these hydration times is similar to that of CAC1 mixtures, it doesn't necessarily relate to a similar degree of reaction. The primary reaction product in CAC2 cement is CAH_{10}, which has a higher amount of bound water compared to C_2AH_8, the primary reaction product in CAC1 mixtures. So CAC2 has slow rate of hydration compared

to CAC1 cements, which is expected since CAC2 cement has a lower amount of $C_{12}A_7$ phase.

Conversion is a key issue in CAC mixtures. Fig. 15 and Fig. 16 shows the TGA and XRD of both CAC1 and CAC2 mixtures produced at 0.45 w/b and at 56 days of hydration compared to the CAC1 and CAC2 mixture that is completely converted. Conversion is accelerated in these mixtures by producing at higher w/b (0.45) and exposing them to 60 ºC and 100% RH for an additional 56 days. With the conversion, there is a significant decrease in CAH_{10}, C_2AH_8 phases, and an increase in C_3AH_6 and AH_3. Also, the amount of bound water decreased by about 20% - most of which would lead to a significant increase in porosity [22].

In both the CSA1 and CSA2 mixtures (Fig. 13 [v] and [vi]), the main hydration product is ettringite, followed by AFm and AH_3 phases [15,16,46–49]. There was no portlandite present in the hydrated CSA1 and CSA2 systems, suggesting either the portlandite formed initially is completely consumed back through the reactions to form ettringite, or that the anhydrous C_2S phase did not undergo significant hydration because of the limited availability of water at the later ages associated with this reaction. The limited availability of mix water for C_2S hydration can be due to the huge water demand required for the reactions involving ettringite formation – which are significantly faster compared to that of C_2S hydration. The SEM micrographs in Fig. 18 (i) and (ii) show ettringite crystals growing on top of cement grains after 6.5 h and 4 h of hydration in CSA1 and CSA2 mixtures, respectively. Out of 40% mix water added in the CSA1 and CSA2 mixtures, about 36.4% and 33.7% of it contributed to hydration, respectively. So about 3.4% and

6.3% of mix water (by weight of cement) did not contribute to hydration in CSA1 and CSA2 mixtures, respectively.

Similar to CSA1 and CSA2 mixtures, ettringite is the main hydration product in CSA3 mixtures, and it is the dominant reaction product forming until 5 days (120 h) of hydration time – as evident by the DTG graph shown in Fig. 13 (vii). The SEM micrograph in Fig. 18 (iii) of CSA3 mixtures at 120 h of hydration also show a significant amount of ettringite crystals growing on top of the cement grains. At a later stage of hydration (from 6 days onwards), monosulfate, C_2ASH_8, and AH_3 are also formed [25]. CSA3 has a significant amount of C_4AF phase compared to the other CSA cements, which was mainly responsible for the formation of monosulfate phase.

In the AA mixture, the main hydration products are N-A-S-H gel and C-A-S-H (or C-S-H) gel. Portlandite, ettringite, and C_2ASH_8 phases are present in minor quantities (shown in Fig. 13 [viii]**)**. The presence of calcium-containing products is expected in this AA system because it is based upon a Class C (or calcium-rich) fly ash. The SEM micrographs of AA mixtures at 18 hours of hydration (Fig. 19) showed hydration products of different morphologies growing on top of the spherical fly ash particles.

K-Struvite is the main reaction product formed in the MPC mixtures [29–32]. The SEM micrographs in Fig. 20 show struvite crystals are growing out of the potassium phosphate phase in MPC mixtures. The amount of bound water at 9, 24 hours, and 56 days is about 14.2%, 17.8%, and 23.7%, respectively. So about 60% of the total hydration compared to 56 days has occurred in about 9 hours of hydration. Out of 30% mix water added to MPC mixtures, about 6.3% (by wt. of cement) of it did not participate in the hydration at 56 days.

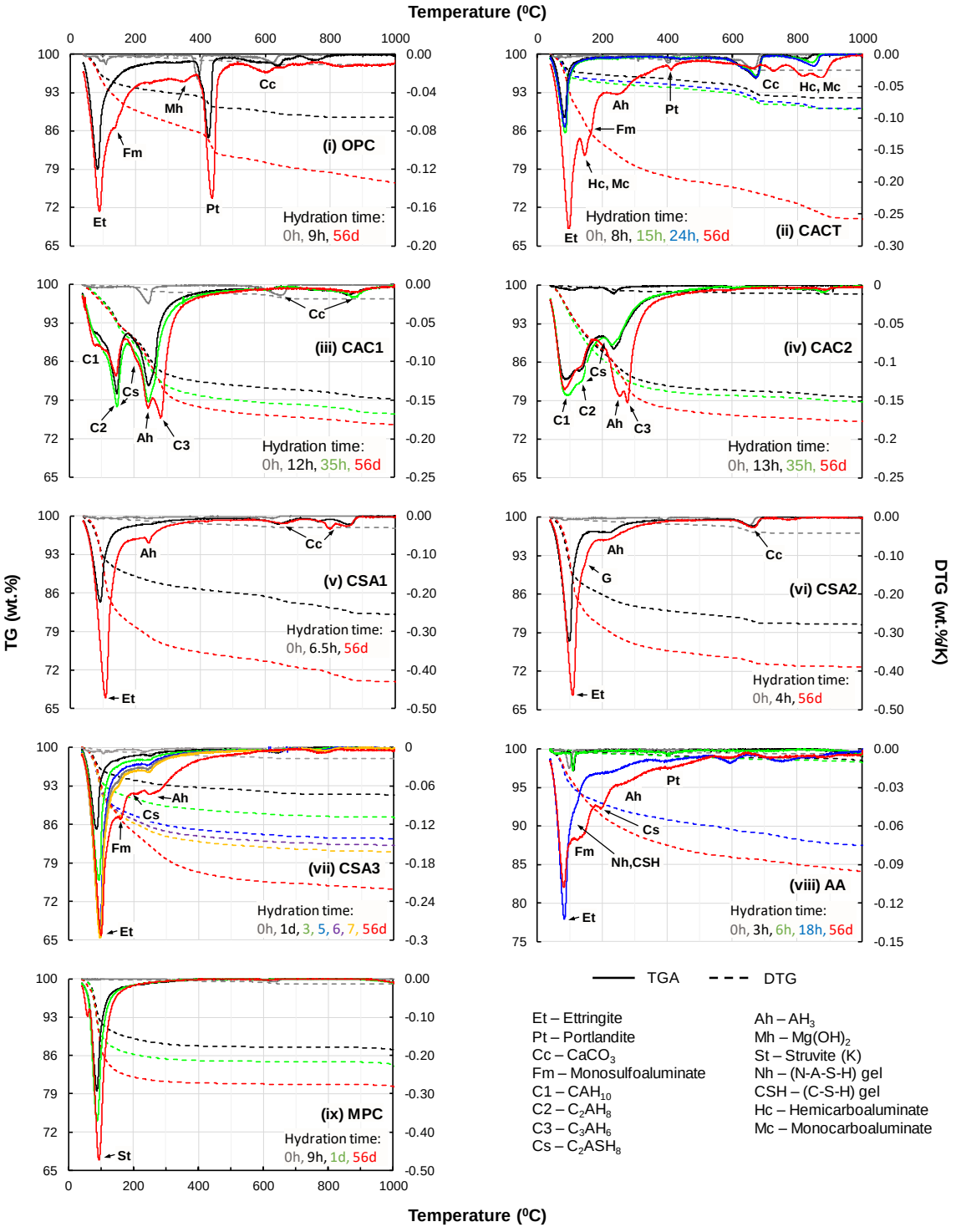

Fig. 13. TGA of cement pastes made with ACMs at different hydration times compared to that of OPC.

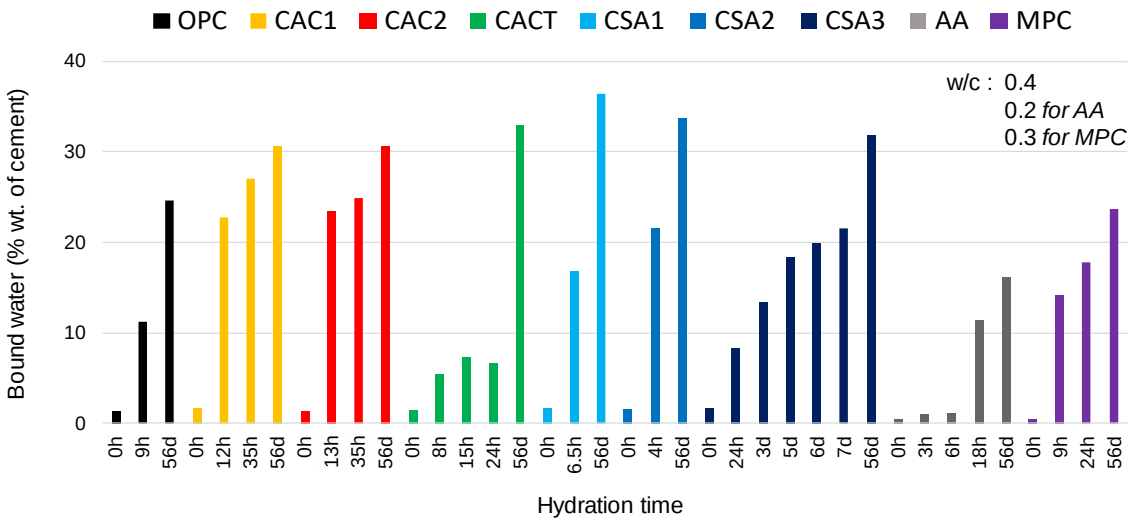

Fig. 14. Bound water in cement pastes made with ACMs at different hydration times compared to that of OPC.

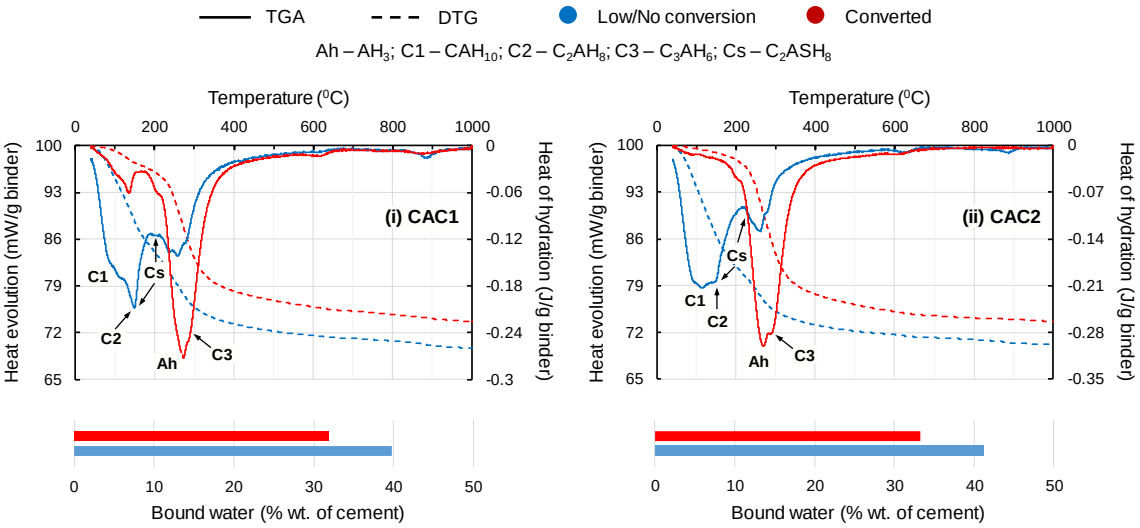

Fig. 15. TGA and bound water of cement pastes made with (i) CAC1 and (ii) CAC2, showing conversion.

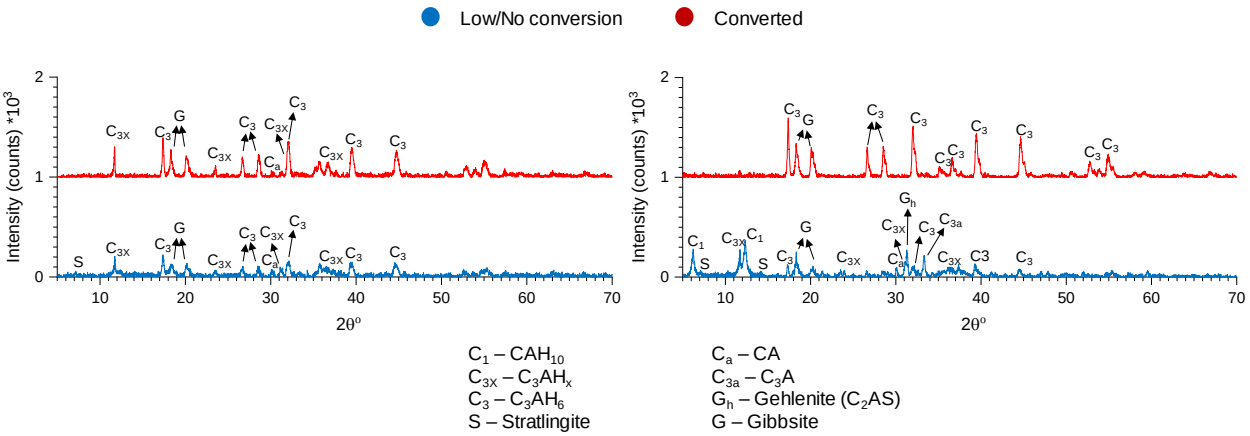

Fig. 16. XRD of cement pastes made with (i) CAC1 and (ii) CAC2, showing conversion.

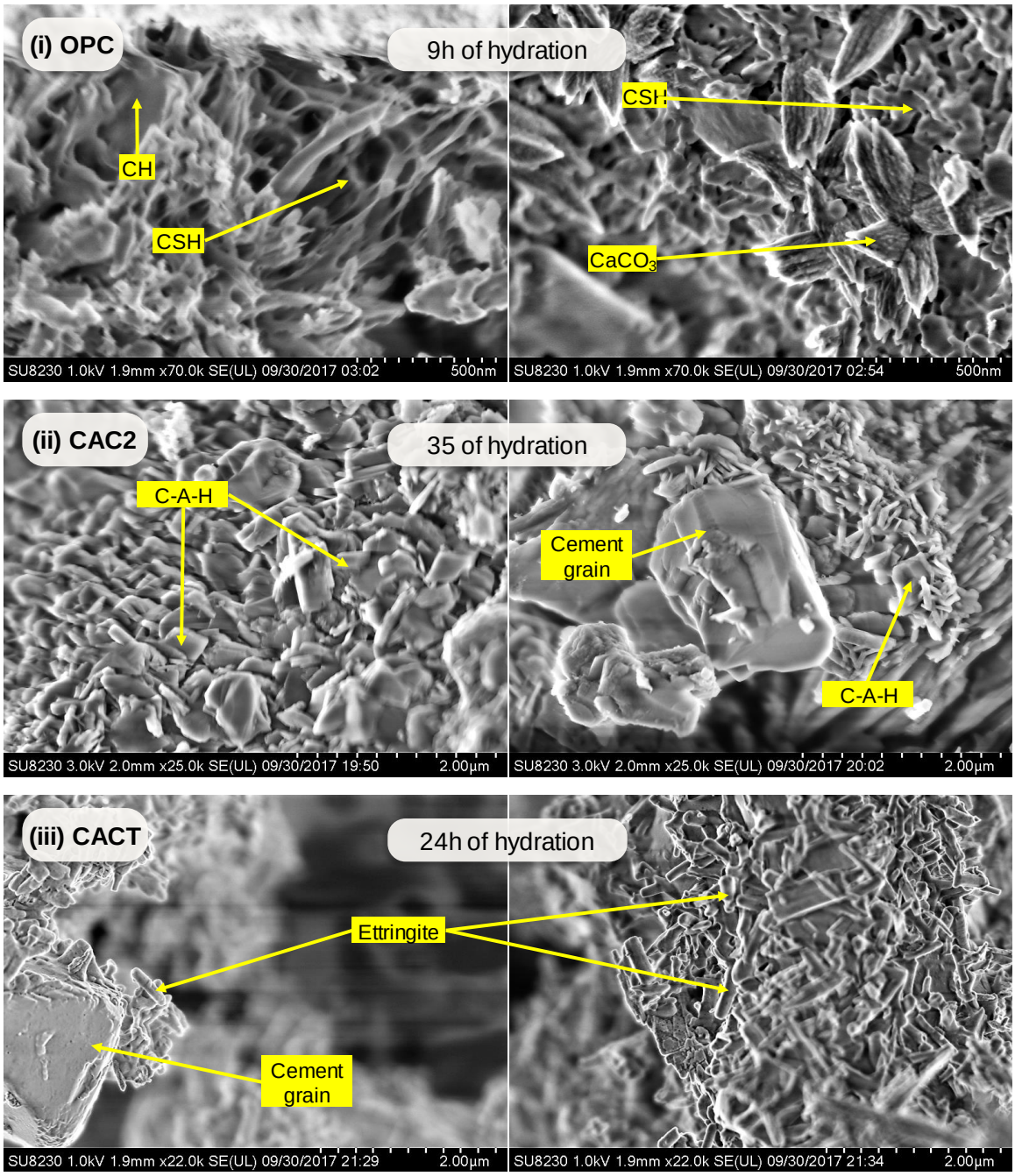

Fig. 17. SEM micrographs of (i) OPC, (ii) CAC2, and (iii) CACT cement pastes after 9, 35, and 24 hours of hydration, respectively.

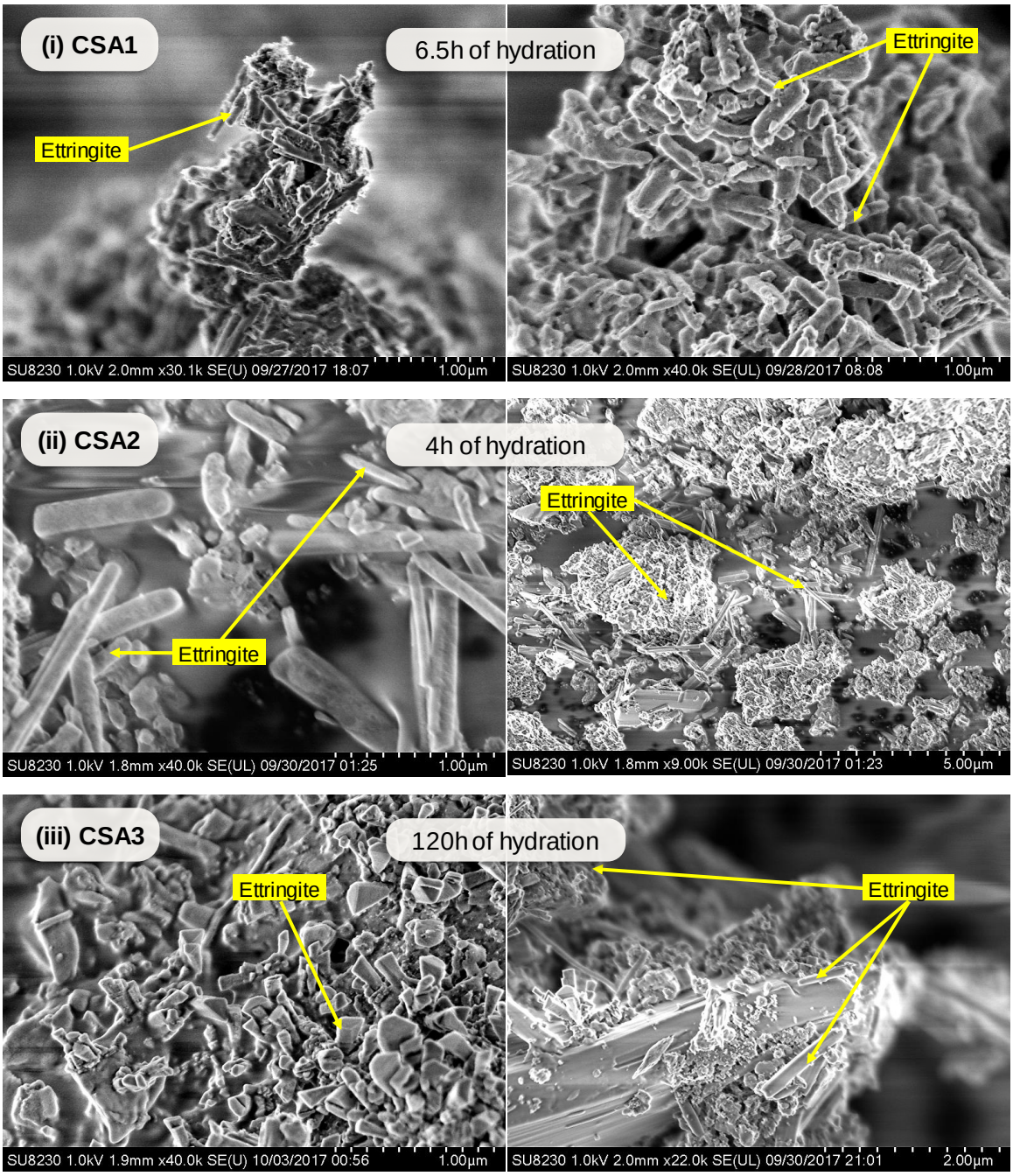

Fig. 18. SEM micrographs of (i) CSA1, (ii) CSA2, and (iii) CSA3 cement pastes after 6.5, 4, and 120 hours of hydration, respectively.

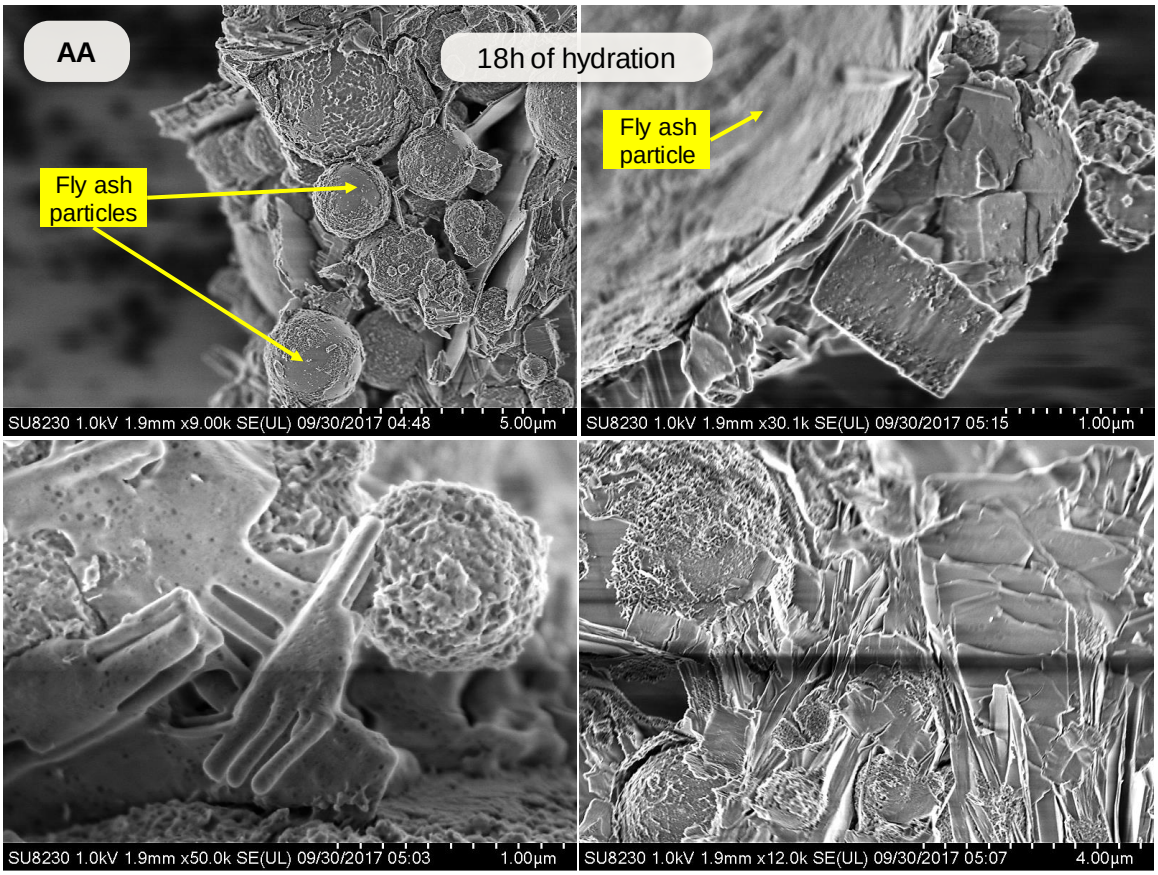

Fig. 19. SEM micrographs of AA cement pastes after 18 hours of hydration, showing platelet and comb-shaped reaction products around the fly ash grains.

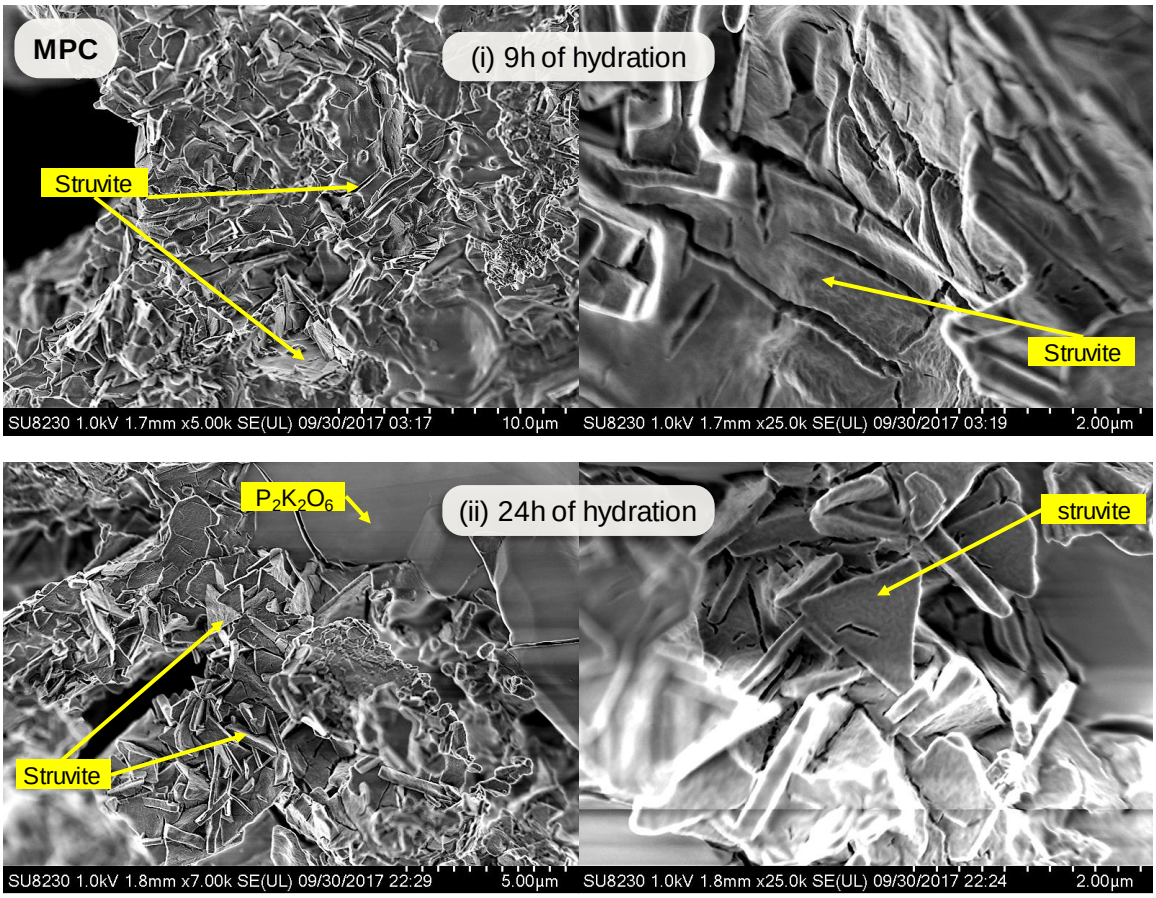

Fig. 20. SEM micrographs of MPC cement pastes after (i) 9 hours, and (ii) 24 hours of hydration.

4.2.2 Early age reaction kinetics – Effects of mixing action

Fig. 21 shows the heat evolution and heat of hydration of cement pastes with different methods of mixing, normalized to binder content in the mixtures. Calorimetry was performed on cement paste with a high-shear mixer, cement paste with a planetary mixer, and cement mortar with a planetary mixer. For all the mixtures, the cement paste with a high-shear mixer had the highest total heat of hydration (per gram of binder) at 18 hours. For AA, the cement paste with a high-shear mixer and the cement mortar with a planetary mixer had similar heats of hydration, but the cement paste mixed with a planetary mixer had a significantly lower heat of hydration. In CAC2 mixtures, the early age hydration is

accelerated significantly in cement mortar mixtures mixed with a planetary mixer compared to cement paste mixtures mixed in either planetary or high shear mixer. This trend was evident up to about 10h of age and is particularly notable when comparing it to OPC. Mixing in a planetary mixer or high shear mixer produced less significant effects on CAC hydration. The CAC2 mixtures had significant higher mini-slump compared to other mixtures (6.2.3), due to which it is possible that the mixing action by the high-shear mixer wasn't able to provide good shear to the mix compared to what is provided by the sand grains while mixing mortars in a planetary mixer. However, the total heat of hydration at 18 hours is higher in cement pastes compared to cement mortar. In all other ACM mixture, similar to OPC mixtures, mixing pastes in high-shear mixer accelerated the hydration compared to the paste mixtures or mortar mixtures mixed in planetary mixer. Also, in CACT and CSA2 mixtures, the acceleration in hydration provided by high-shear mixing action is significantly higher compared to others – as evident by the total heat of hydration at 18 hours.

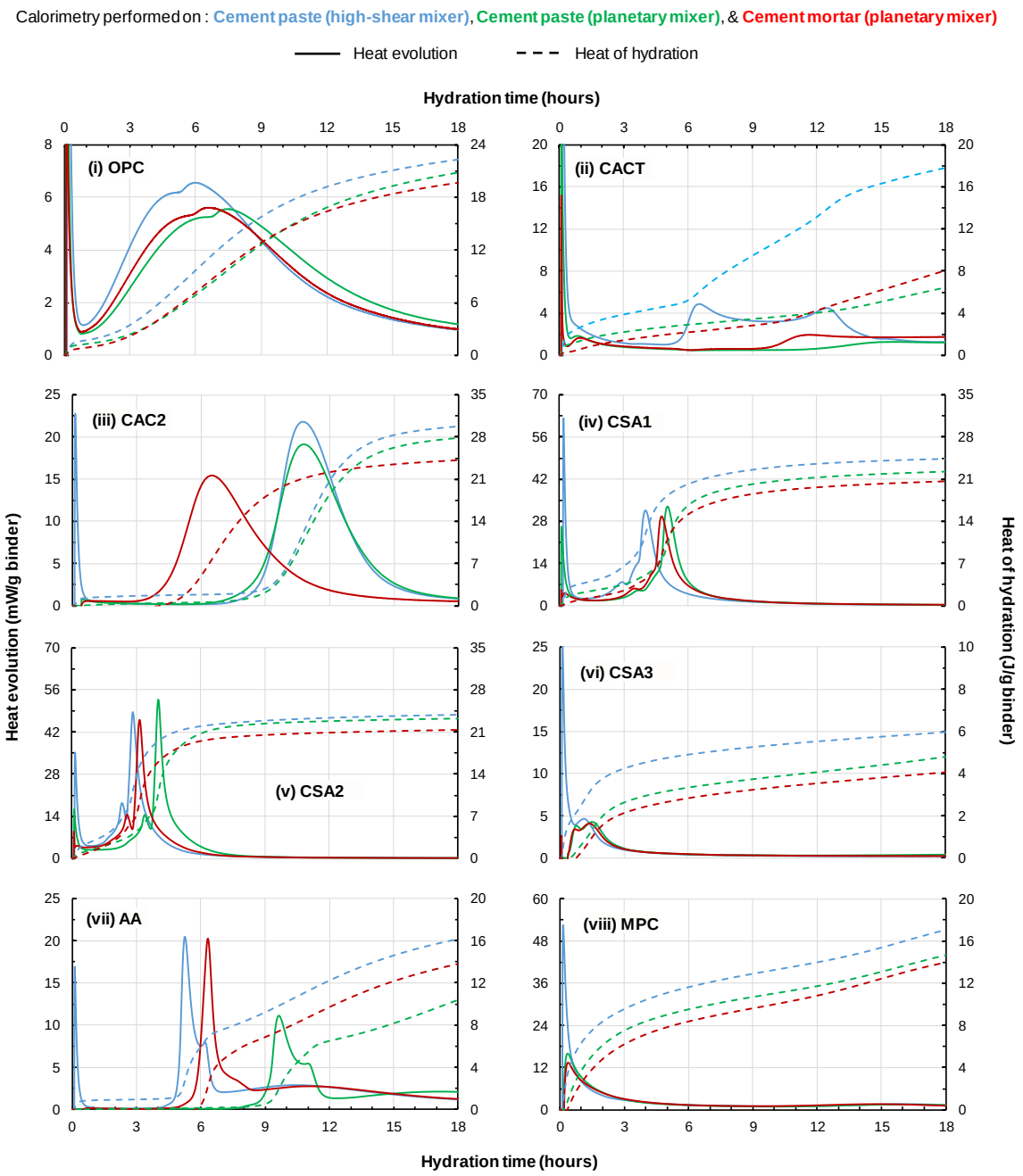

Fig. 21 Effect of mixing action on heat evolution and heat of hydration of cement pastes made with OPC and ACM mixtures at w/c of 0.4 (0.25 for AA and 0.30 for MPC). Note: Heat evolution and heat of hydration are normalized to the cement content in the mixtures.

4.3 Summary

- In CACT mixtures, the hydration products include primarily ettringite, followed by hemicarboaluminate, monocarboaluminate, AH_3, C-S-H, and portlandite. Whereas it is primarily ettringite and AH_3 in CSA1, CSA2, and CSA3 mixtures. CSA3 mixtures also had significant amounts of monosulfate and C_2ASH_8 phases after 56 days of hydration. The hydration products formed in these commercial blends is similar to the hydration products in the lab-produced materials explored by other researchers.

- Hydrated CAC1 mixtures are primarily composed of C_2AH_8, C_3AH_6, and AH_3 phases. CAH_{10} and C_2ASH_8 are also formed in addition to those phases. CAC2 mixtures are primarily composed of CAH_{10}, C_3AH_6, and AH_3 phases, followed by the C_2AH_8 phase. The higher amount of $C_{12}A_7$ phase in CAC1 cement compared to CAC2 cement is responsible for the higher amount of C_2AH_8 phase compared to the CAH_{10} phase.

- Both CACT and CSA3 mixtures had a slower hydration rate during the initial 24 hours of hydration compared to OPC and other ACM mixtures – which could lead to slower strength development in these mixtures at an early age (refer to chapter 5 for more details).

- In OPC, CACT, CSA1, CSA2, CSA3, AA, and MPC mixtures, the mixing action provided by the high-shear mixer accelerated the hydration even when compared to mortar mixtures mixed in a planetary mixer. Whereas in CAC2 mixtures, the early age hydration is accelerated significantly in cement mortar mixtures mixed

with a planetary mixer compared to the cement paste mixtures mixed in planetary mixer or even high-shear mixer. So identifying the dosages of admixture for CAC2 systems based on the cement paste mixtures alone may not be adequate for the corresponding concrete mixtures.

5 EFFECT OF SET MODIFIERS ON EARLY AGE PROPERTIES

This chapter examines the influence of set retarders and their dosages on setting time and hydration kinetics in ACM formulations. The primary goal of this chapter is to identify a suitable dosage of set modifier to achieve an initial setting time greater than 60 minutes (section 1.4) without adversely affecting the later age properties of ACM mixtures. Isothermal calorimetry tests were used to understand the effect of set retarder dosages on cement pastes made with ACM mixtures. In-situ XRD measurements were also made on cement pastes to understand, in detail, the effects of retarder dosage on early age hydration kinetics and the formation of reaction products/phases.

5.1 Methods

5.1.1 Vicat test

The initial and final setting times are determined on cement paste mixtures made with CACT, CSA1, CSA2, CSA3, and MPC at their normal consistency (last row in Table 1) with different dosages of set retarder according to the test procedure given in ASTM C191-13. Citric acid was used as a retarder for CACT, CSA1, CSA2, and CSA3 mixtures [35–38]. Whereas boric acid was used to retard MPC mixtures [29,30,39–41]. The mixture proportions are given in Table 6 and are machine mixed in a planetary mixer (ASTM C305-14).

Table 6 Cement paste mixture proportions to understand the influence of set modifiers and their dosages on setting time and reaction kinetics.

Cement	w/b at (NC)	Set modifier (by weight of cement)
CACT	0.27	Citric acid (0%, 0.5%, 1.0%, 1.5%, 2%)
CSA1	0.31	Citric acid (0%, 0.5%, 1.0%, 1.5%, 2%)
CSA2	0.31	Citric acid (0%, 0.5%, 0.75%, 1.0%, 1.5%)
CSA3	0.31	Citric acid (0%, 0.25%, 0.5%, 0.75%, 1%)
MPC	0.21	Boric acid (0%, 6%, 14%)

5.1.2 Isothermal calorimetry

Isothermal calorimetry was performed on hydrating cement pastes for the mixture proportions given in Table 6, and the mixtures were mixed in planetary mixer according to ASTM C305–14. Immediately after mixing, the mixtures were loaded into the calorimeter, and the heat evolution was measured according to the procedure listed in section 4.1.2.

5.1.3 Insitu x-ray diffraction (XRD)

Insitu XRD was performed on hydrating cement paste samples. Immediately after mixing (according to the procedure listed in section 5.1.2), the pastes were loaded into the sample holder with an opening diameter of 27 mm and the exposed sample surface is covered with a low-permeability thin film made of polyethylene terephthalate (i.e., PET or ‘Mylar’) of thickness 6 μm to prevent evaporation of mix water and carbonation of mix water and hydrated paste. A PANalytical Empyrean diffractometer with Bragg–Brentano HD X-ray mirror and goniometer radius of 240 mm was used for data collection. The sample was incident with CuKα X-rays generated using Empyrean Cu LFF HR X-ray tube at 45 kV

and 40 mA operating conditions. Soller slits of 0.04 rad and the fixed Mask, anti-scatter, and divergence slits of 10 mm, ½ º, and ⅛ º were used in the incident beam path. In the diffracted beam path, a fixed anti-scatter slit of 7.5 mm and soller slits of 0.04 rad were used. A PIXcel3D-Medipix3 1x1 area detector with an active length of 3.347 º was used for data acquisition. Data was collected over an angular range of 7 º to 70 º with a step size and counting time of 0.013 º and 16.32 s, respectively, resulting in a total measurement time of approximately 6 min. Phase identification was carried out using PANalytical X' Pert High Score plus v4.5 using PDF-4+ 2017 material identification database by International Center for Diffraction Data.

5.2 Results and Discussion

5.2.1 Effects of set modifiers on initial and final setting time

The influence of citric acid retarder on setting time and heat of hydration within the first 3 hours of CACT, CSA1, CSA2, and CSA3 paste mixtures are shown in Fig. 22. These mixtures are prepared at their normal consistency. In general, the heat of hydration decreased with the addition of citric acid, and the time to set increased, but the amount of delay in set time varied across mixtures with different binders and dosages of retarder.

In CACT mixtures, with the addition of citric acid even at 0.5%, significant retardation in the time of start of the acceleratory period and increase in initial setting time by about 30 minutes can be observed. With a further increase in dosage to 1.5%, the initial setting time increased to about 80 minutes, and the final setting time increased to about 150 minutes. However, with further increase in dosage to 2%, a regression in delay in initial setting time is observed, with no change is the final set.

In CSA1 mixtures, the retardation by citric acid is less effective compared to the CACT mixtures. At 0.5% dosage of citric acid, an increase in the initial set by only a few minutes (about 10 min) is observed. With a further increase in dosage to 2%, the initial and the final setting time increased to about 32 and 135 minutes, respectively. However, in CSA2 mixtures, the retardation by citric acid is significantly effective compared to both the CACT and CSA1 mixtures. With only 0.5% citric acid dosage, the initial and final setting time increased by more than 50 and 90 minutes, to about 67 and 125 minutes, respectively. With a further increase in dosage, no significant change is observed in heat of hydration and the initial setting time is observed; however, the final set time continued to increase.

At 0.5% citric acid dosage, no significant change in an initial set time is observed in CSA3 mixtures. However, the final set time increased by more than 60 minutes – as evident by the retardation observed in the heat of hydration. With a further increase in dosage to 0.75%, significant retardation in the heat of hydration is observed, and the initial and final setting times increased to about 61 and 120 minutes, respectively. Further increase in setting time is also observed with an increase in dosage to 2.0%.

With the citric acid dosage of 1.5%, 0.5%, and 0.75%, an initial setting time greater than 60 minutes and a final setting greater than 120 minutes was achieved in CACT, CSA2, and CSA3 mixtures, respectively. In CSA1 mixtures, even at 2% citric acid dosage, the initial setting time increased to only about 30 minutes; however, the final setting time is higher than 120 minutes. With a combination of 2% citric acid dosage and a plasticizer, an initial set time greater than 60 minutes was achieved in the CSA1 concrete mixtures and was discussed in detail in chapters 6 and 7.

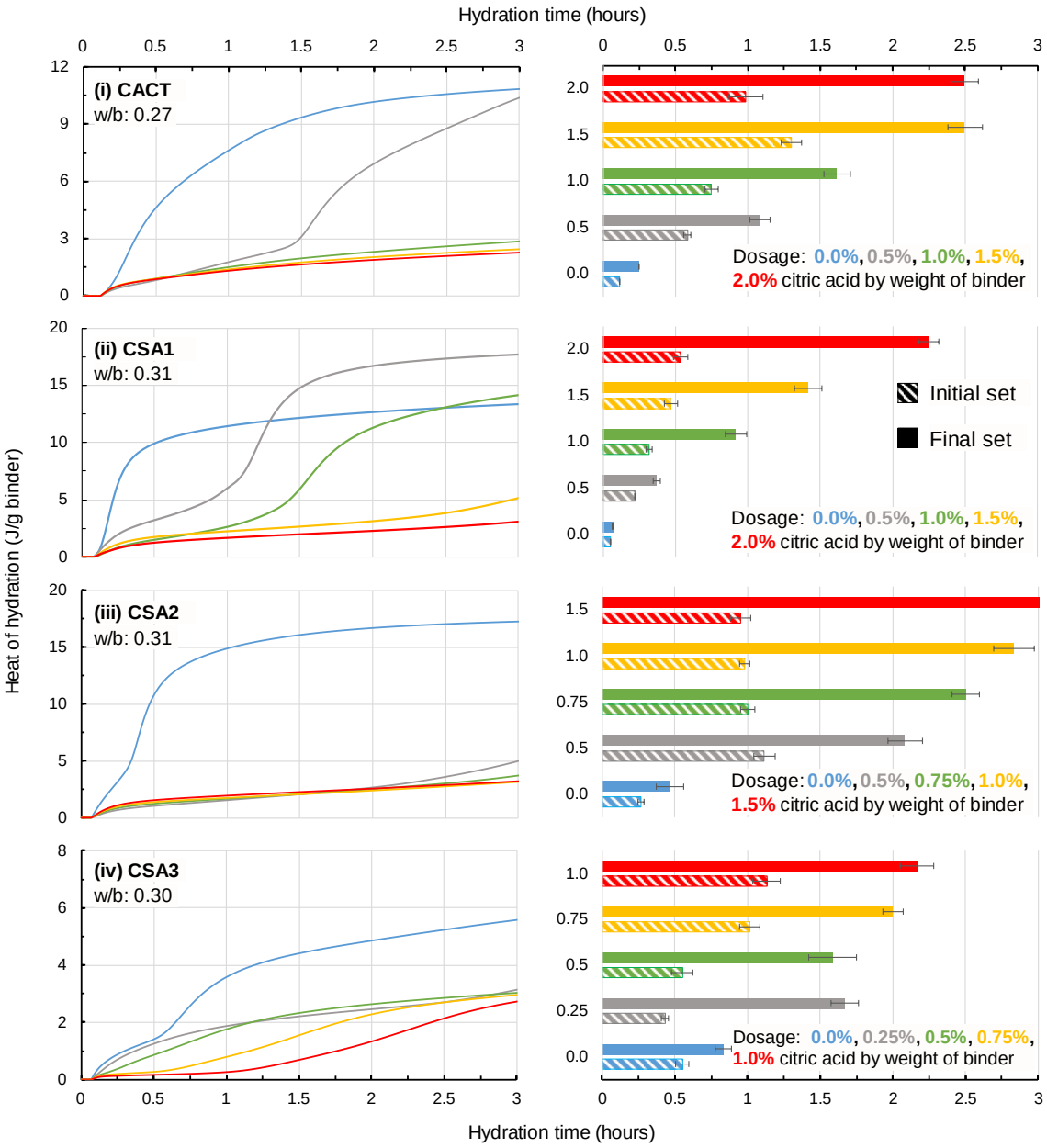

Fig. 22. Influence of set modifier (citric acid) dosage on early heat of hydration (left) and Vicat setting times (right) of cement pastes made with (i) CACT, (ii) CSA1, (iii) CSA2, and (iv) CSA3 at normal consistency.

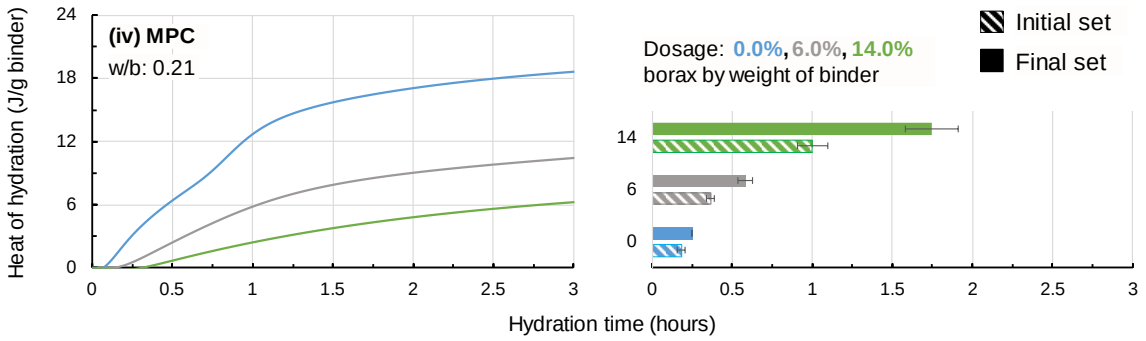

Fig. 23. Influence of set modifier (boric acid) dosage on early age heat of hydration (left) and Vicat setting times (right) of cement pastes made with MPC at normal consistency.

5.2.2 Effect of set modifiers on early age hydration kinetics

Fig. 24 shows the influence of citric acid dosage on the heat evolution, the heat of hydration, and phase development in CACT mixtures. With the addition of citric acid, a deceleration and broadening in both the primary and the secondary peak is observed. Fig. 24 [iii] and Fig. 24 [iv] provides the XRD pattern (for every 60 min - up to 24hrs) of hydrating CACT cement paste with 0% and 1.5% citric acid dosage. The XRD patterns show that ettringite is the main hydration product, and there is no presence of CH phase even after 24 hours of hydration. Fig. 24 (ii) shows the normalized XRD peak intensities of ettringite compared to the heat evolution of CACT cement paste with hydration. At 0% citric acid dosage, a significant amount of ettringite is formed within the first 2 hours of hydration, and no significant increase in ettringite XRD peak is observed thereafter – correlating well with the heat evolution peak. With addition of 1.5% citric acid, the evolution of ettringite peak is retarded, similar to the heat evolution, and continues to evolve throughout the initial 18-hour hydration period examined. Fig. 24 (v) shows the heat of hydration of CACT mixtures with 0% and 1.5% citric acid dosage during the initial 10 days of hydration. While the addition of citric acid delayed the heat of hydration and

formation of ettringite initially, after about 22 hours of hydration, the total heat of hydration in mixtures with citric acid surpassed that of the one with no citric acid dosage. However, addition of citric acid can significantly delay the hydration of phase associated with OPC component in the CACT mixtures [25]. This can lead to significant retardation in strength development at early ages.

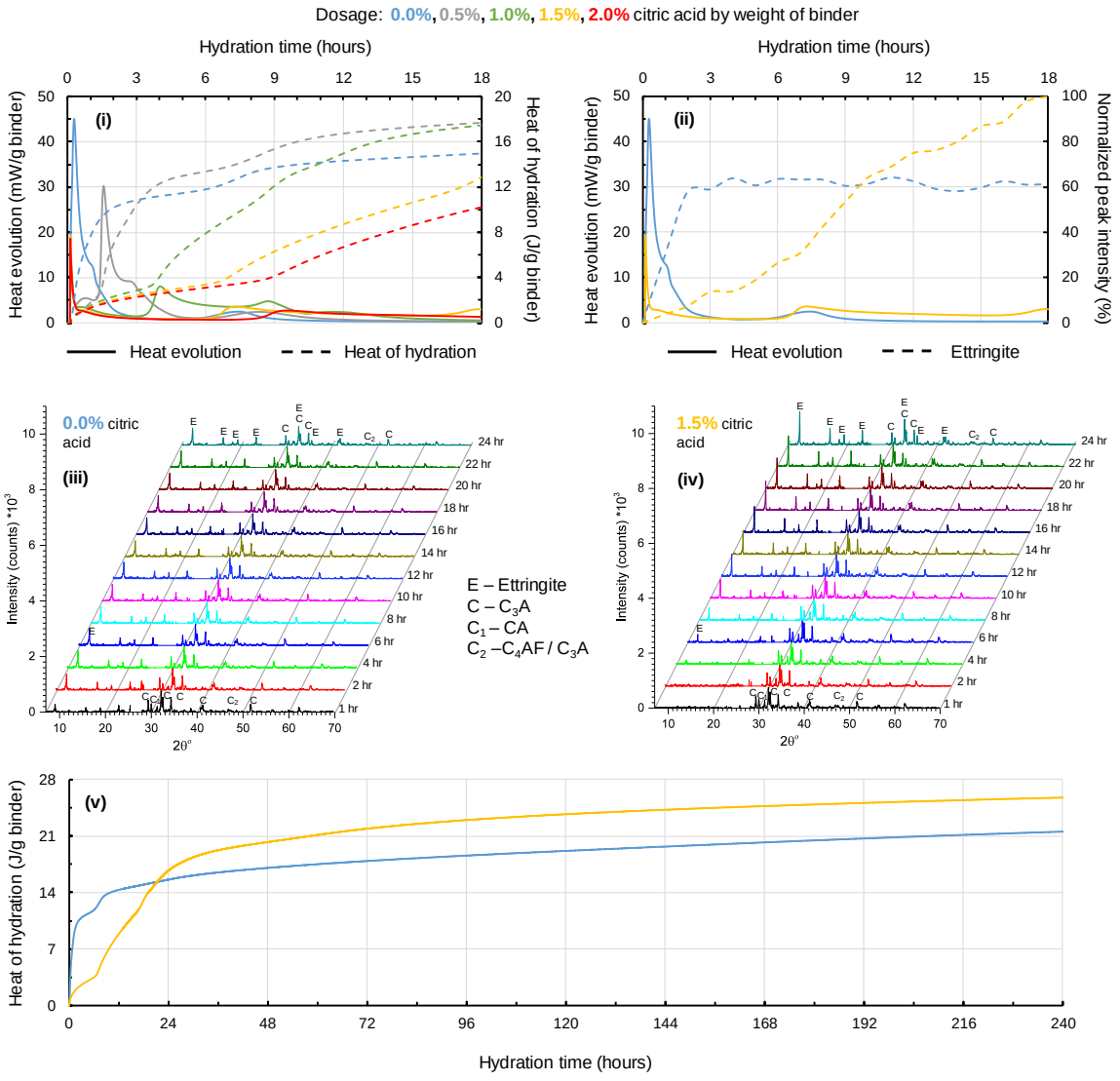

Fig. 24. Influence of set modifier dosage on heat evolution, heat of hydration, and phase development in cement pastes made with CACT at normal consistency.

Fig. 25 shows the influence of citric acid dosage on heat evolution, the heat of hydration, and phase development in CSA1 mixtures. With the addition of citric acid, a deceleration and broadening in the primary peak are observed. Fig. 25 [iii] and Fig. 25 [iv] provides the XRD pattern (for every 60 min - up to 24hrs) of hydrating CSA1 cement paste with 0% and 2% citric acid dosage. The XRD patterns show that ettringite is the main hydration product. Fig. 25 (ii) shows the normalized XRD peak intensities of ettringite compared to the heat evolution of CSA1 cement mixtures with hydration. At 0% citric acid dosage, a significant amount of ettringite is formed within the first 2 hours of hydration, and no significant increase in ettringite XRD peak is observed thereafter – correlating well with the heat evolution peak. With the addition of 2% citric acid, the evolution of the ettringite peak is retarded significantly until about 4.5 hours, similar to the heat evolution, and formed at a significant rate from about 4.5 hours to 7 hours of hydration. After about 7 hours of hydration, no significant change is observed in the peak intensity of ettringite until the initial 18-hour hydration period examined. Fig. 25 (v) shows the heat of hydration of CSA1 mixtures with 0% and 2% citric acid dosage during the initial 10 days of hydration. While the addition of citric acid delayed the heat of hydration and formation of ettringite initially, after about 6 hours of hydration, the total heat of hydration in mixtures with citric acid surpassed that of the one with no citric acid dosage. However, after 24 hours of hydration, the heat evolution in mixtures with citric acid is significantly lower than the mixtures without citric acid. So, after about 9 hours of hydration, the total heat of hydration in mixture without a citric acid surpassed the mixtures with citric acid.

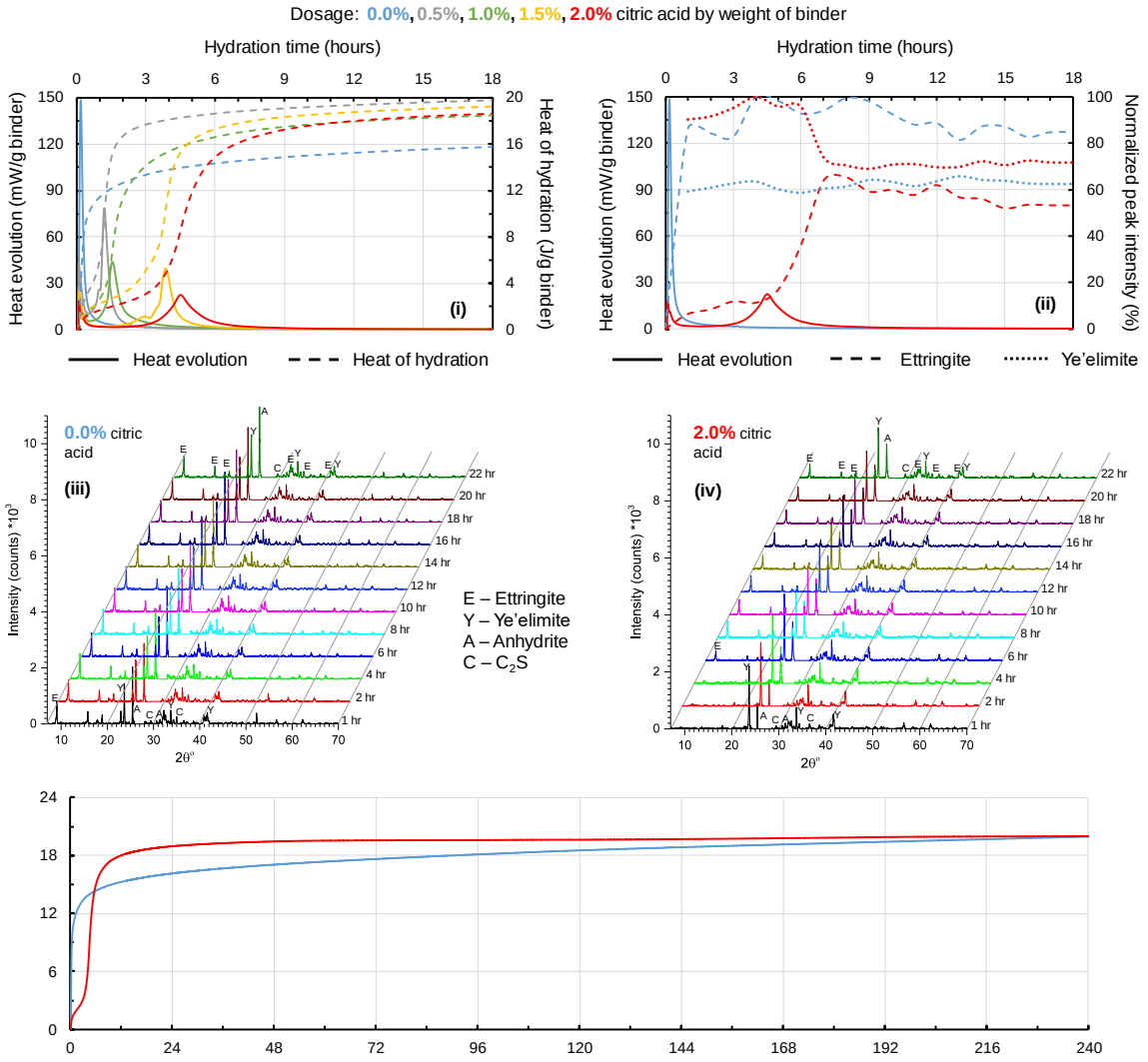

Fig. 25. Influence of set modifier dosage on heat evolution, heat of hydration, and phase development in cement pastes made with CSA1 at normal consistency.

Fig. 26 shows the influence of citric acid dosage on heat evolution, the heat of hydration, and phase development in CSA2 mixtures. Just like the CACT and CSA1 mixtures, the main hydration product in CSA2 is ettringite. With the addition of citric acid, a deceleration and broadening in both the initial smaller peak and the secondary bigger peak was observed. Fig. 26 [iii] and Fig. 26 [iv] provides the XRD pattern (for every 60 min - up to 24hrs) of hydrating CSA2 cement paste with 0% and 0.5% citric acid dosage. The XRD

patterns show that ettringite is the main hydration product. Fig. 26 (ii) shows the normalized XRD peak intensities of ettringite compared to the heat evolution of CSA2 cement paste with hydration. At 0% citric acid dosage, a significant amount of ettringite is formed within the first 1 hours of hydration, and no significant increase in ettringite XRD peak is observed thereafter – correlating well with the heat evolution peak. With addition of 0.5% citric acid, the evolution of the ettringite peak is retarded significantly until about 3 hours, similar to the heat evolution, and formed at significant rate from about 3 hours to 6 hours of hydration. Fig. 26 (v) shows the heat of hydration of CSA2 mixtures with 0% and 0.5% citric acid dosage during the initial 10 days of hydration. While the addition of citric acid delayed the heat of hydration and formation of ettringite initially, after about 5.5 hours of hydration, the total heat of hydration in mixtures with citric acid surpassed that of the one with no citric acid dosage.

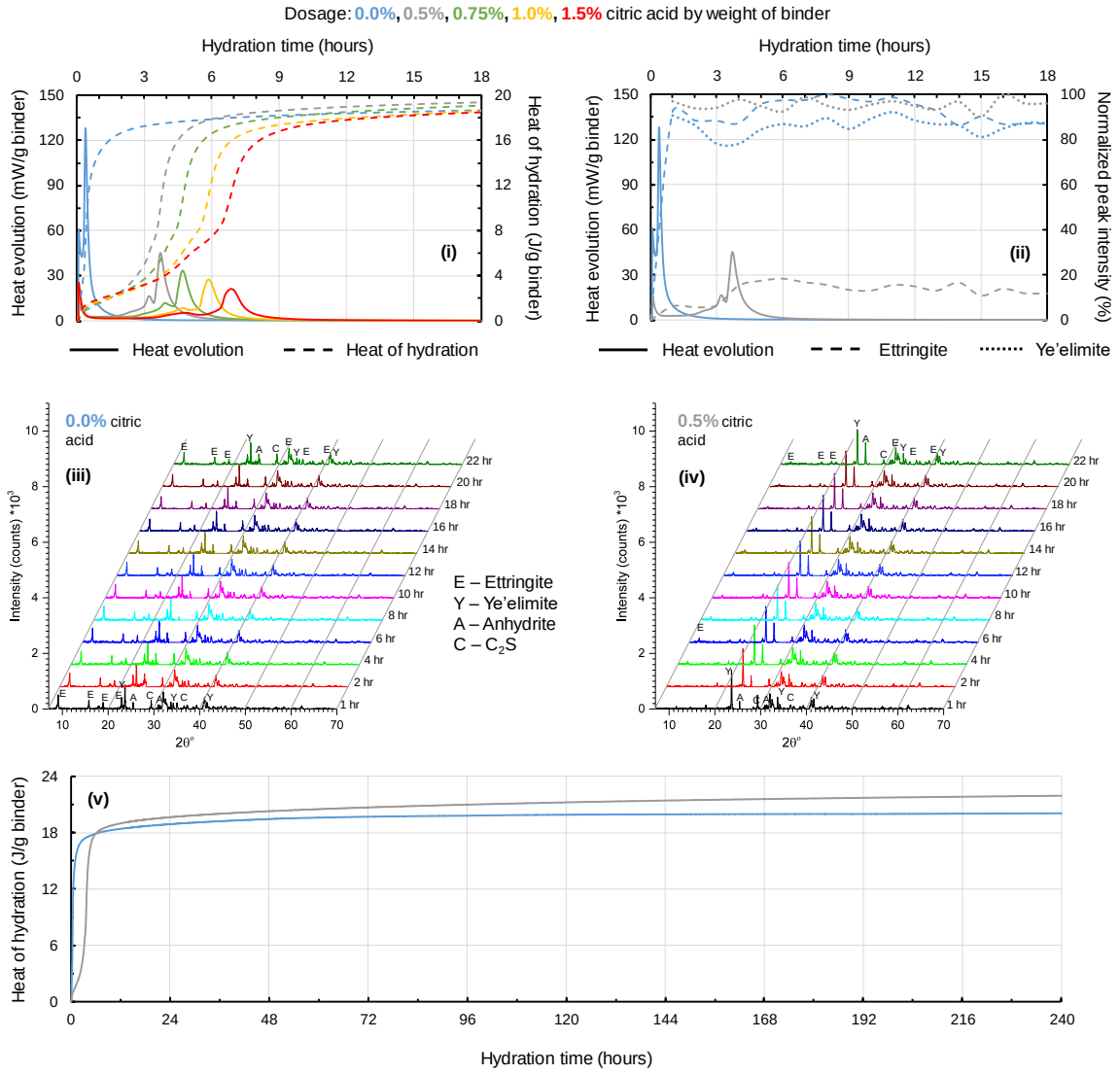

Fig. 26. Influence of set modifier dosage on heat evolution, heat of hydration, and phase development in cement pastes made with CSA2 at normal consistency.

The influence of citric acid dosage on heat evolution, heat of hydration, and phase development in CSA3 mixtures is shown in Fig. 27. Just like the CACT, CSA1, and CSA2 mixtures, the main hydration product in CSA3 mixtures is ettringite. With the addition of citric acid, a deceleration and broadening in both the primary and the secondary peaks were observed. Furthermore, the time delay between the primary and the secondary peaks also increased significantly with the addition of citric acid. Fig. 27 [iii] and Fig. 27 [iv] provides

the XRD pattern (for every 60 min - up to 24hrs) of hydrating CSA3 cement paste with 0% and 0.75% citric acid dosage. The XRD patterns show that ettringite is the main hydration product. Fig. 27 (ii) shows the normalized XRD peak intensities of ettringite compared to the heat evolution of CSA2 cement paste with hydration. At 0% citric acid dosage, a significant amount of ettringite is formed during the initial 3 of hydration, and no significant increase in ettringite XRD peak is observed thereafter until 9 hours of hydration – correlating well with the heat evolution peak. After about 9 hours of hydration, the ettringite continued to form again at a faster rate, coinciding with the second peak observed in the heat evolution curve. With the addition of 0.75% citric acid, the evolution of the ettringite peak is retarded by only about 1 hour, similar to the heat evolution, and continued to evolve throughout the initial 18 hours of hydration. Fig. 27 (v) shows the heat of hydration of CSA3 mixtures with 0% and 0.75% citric acid dosage during the initial 10 days of hydration. The addition of citric acid delayed the secondary peak significantly, and the total heat of hydration after 10 days of hydration is about 10% lower in mixtures with 0.75% citric acid compared to mixtures without citric acid.

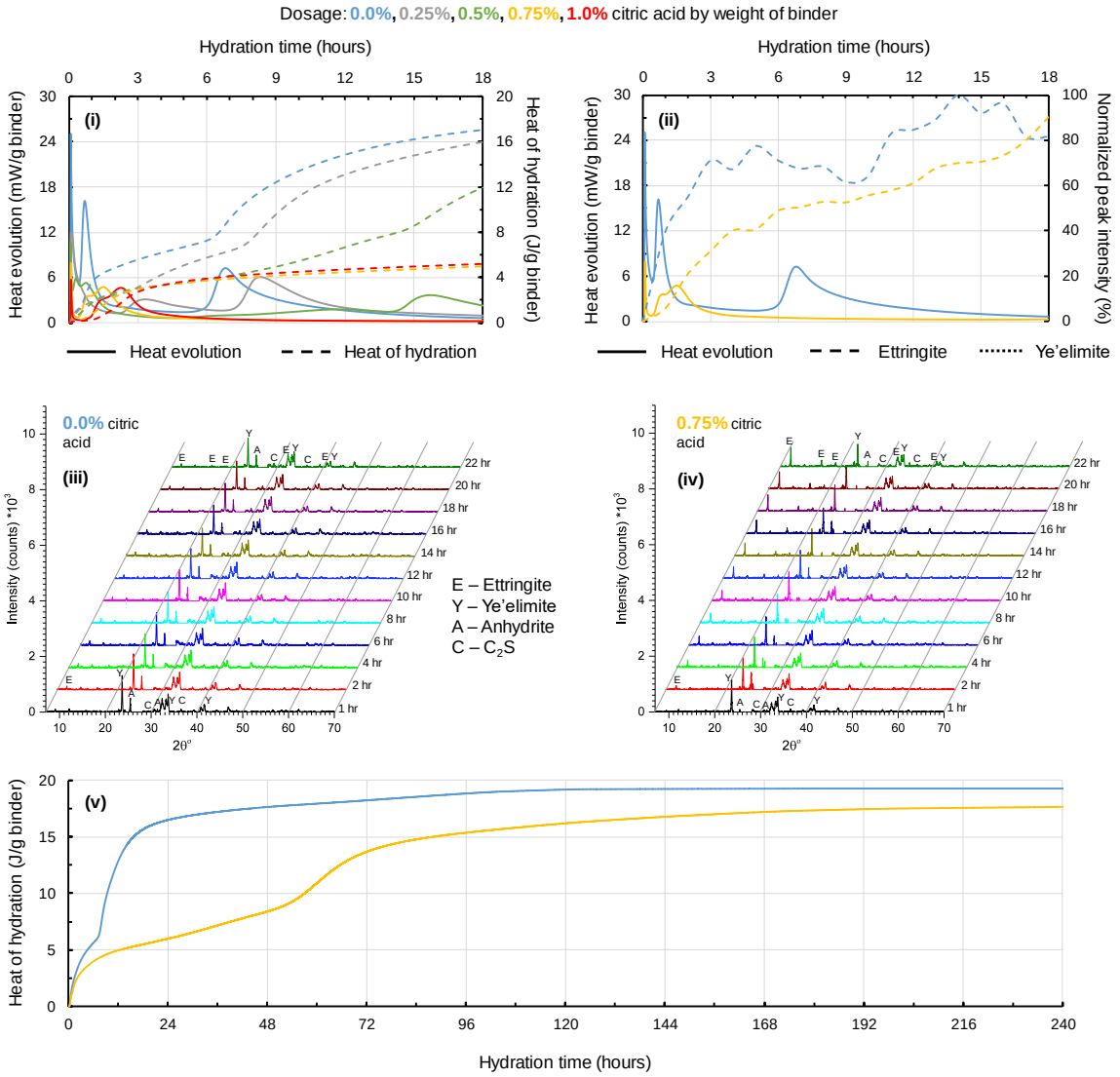

Fig. 27. Influence of set modifier dosage on heat evolution, heat of hydration, and phase development in cement pastes made with CSA3 at normal consistency.

Citric acid is known to retard or accelerate (in some cases) the dissolution and formation of phases in multiple ways: 1) It can form complexes with dissolved Ca ions in the pore solution, lowering their availability to participate in hydration [50–53]. However, this mechanism is found to be weak, and may not significantly contribute to the retardation [53]. 2) Citric acid can delay the hydration by getting adsorbed on the cement grains and forming a protective layer, thereby preventing their dissolution [37,53–55]. 3) It can

prevent or retard the nucleation and growth of ettringite crystals in the pore solution [56]. 4) Citric acid is also known to accelerate the dissolution of some phases that especially contain higher amount of ferrites in them (such as C_4AF). This is because citric acid forms complexes with Fe^{3+}, there by accelerating the growth of dissolution of those phases [57].

CSA1 binder has higher fineness (Table 1) and higher amount of ye'elimite phase (Table 2) in them compared to CSA2 and CSA3 binders – which implies total higher surface area of ye'elimite grains in CSA1. So, a higher amount of citric acid is required to get adsorbed on these ye'elimite grains to slow down their dissolution in CSA1 mixtures (2% by weight of cement compared to 0.5% and 1.5% in CSA2 and CSA3 mixtures). However, even though CSA3 binders are coarser compared to CSA2, and have similar amounts of ye'elimite in them, a higher dosage of citric acid was required to achieve 1 hour setting time compared to CSA2 mixtures. CSA3 binders have significantly higher amount of ferrous, there by higher amount of C_4AF in them compared to CSA2 and CSA1 binders (Table 2 and Table 3). These higher amounts of Fe in the cement could have also led to partial replacement of Al with Fe in the ye'elimite phase. So, this could have led to competing acceleration (for C_4AF and ye'elimite containing Fe) and deceleration (for ye'elimite phases containing only Al instead of Fe) in the dissolution of phases in the clinker. So, a higher dosage of citric acid was required in CSA3 mixtures to achieve sufficient set times. However, since higher amounts of citric acid was used, this led to significant deceleration in the hydration (evident by the time delay in the occurrence of second peak in Fig. 27) at later stages.

Fig. 28 shows the influence of boric acid dosage on heat evolution, the heat of hydration, and phase development in MPC mixtures. With the addition of boric acid, a significant

reduction in the initial peak, and a significant deceleration in the secondary peak was observed. Fig. 28 [iii] and Fig. 28 [iv] provides the XRD pattern (for every 60 min - up to 24hrs) of hydrating MPC mixtures with 0% and 14% boric acid dosage. The XRD patterns show that potassium struvite is the main hydration product. Fig. 28 (ii) shows the normalized XRD peak intensities of K-struvite compared to the heat evolution of MPC cement paste with hydration. At 0% boric acid dosage, a significant amount of K-struvite is formed within the first 4 hours of hydration and it continued to form during the rest of the hydration period – correlating well with the heat evolution peak. With an addition of 14% boric acid, the evolution of the K-struvite peak got suppressed significantly during the initial 18-hour hydration. The exact mechanism in which boric acid retards the hydration in MPC is not fully understood [29,58]. However, addition of boric acid in MPC systems is believed to retard the precipitation of hydration products significantly [39,58], and it doesn't form any complexes with the hydration products [58]. So even though a significant amount of boric acid is added to the MPC mixtures (14% by weight of cement), no change in the composition of hydration products was observed [59]. Fig. 28 (v) shows the heat of hydration of MPC mixtures with 0% and 14% boric acid dosage during the initial 10 days of hydration. The addition of boric acid significantly delayed the heat of hydration significantly during the initial 24-hour period. However, at 10 days of hydration, the total heat of hydration in mixtures with boric acid is only about 7% lower compared to the mixtures without boric acid dosage. Addition of boric acid at higher dosages is reported to significantly reduce the volume of open pores, thereby leading to increase in mechanical properties [39,40]. So even though addition of boric acid retarded the early age hydration

(longer than 10 days), the mechanical properties at later ages are expected to be better compared to the mixtures without boric acid.

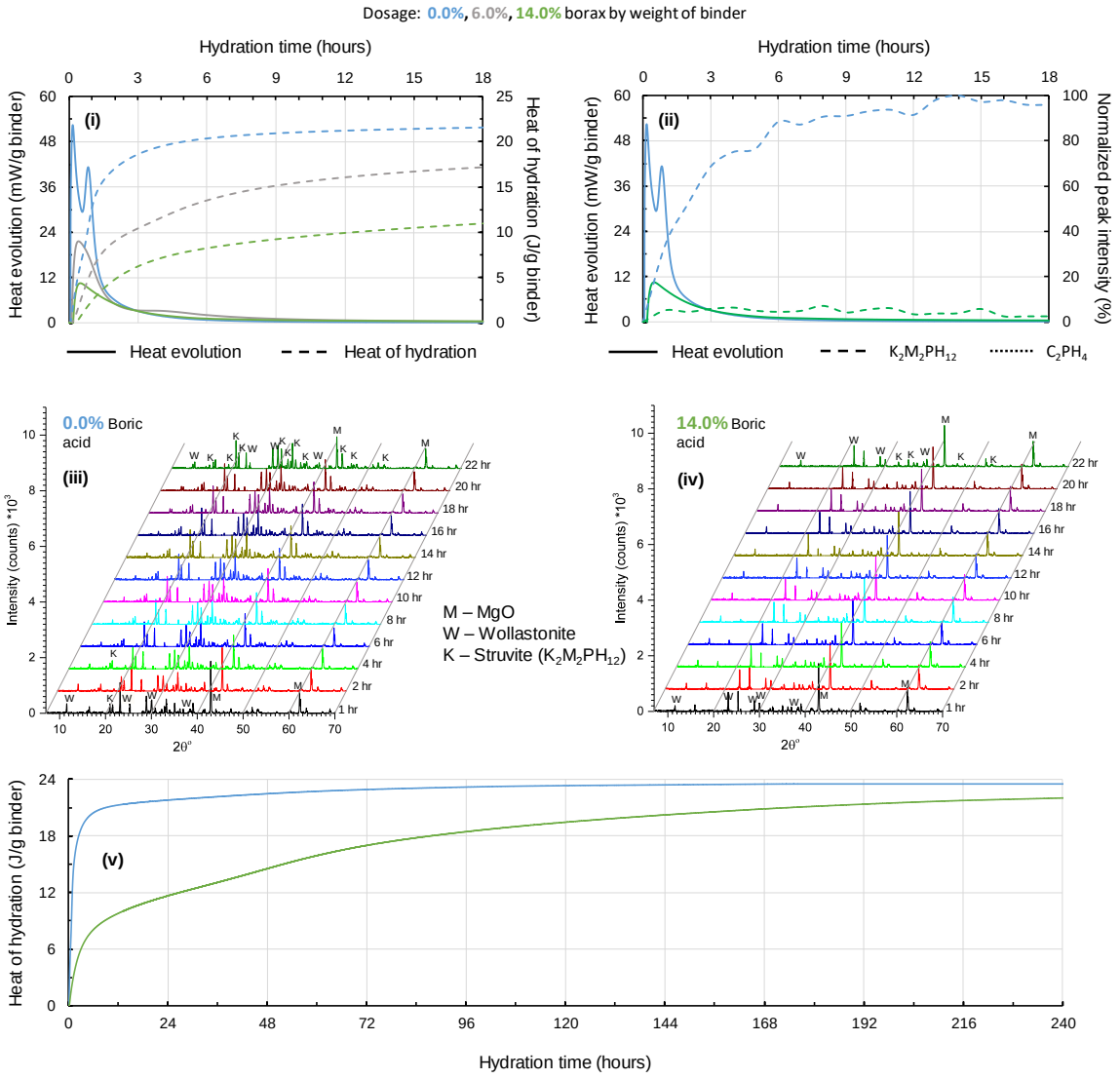

Fig. 28. Influence of set modifier dosage on heat evolution, heat of hydration, and phase development in cement pastes made with MPC at normal consistency.

5.3 Conclusions

- A suitable dosage of set retarders was identified to achieve an initial setting time greater than 60 minutes in all the mixtures investigated in this chapter (except CSA1).

- With the citric acid dosage of 1.5%, 0.5%, and 0.75%, an initial setting time greater than 60 minutes and a final setting greater than 120 minutes was achieved in CACT, CSA2, and CSA3 mixtures, respectively.

- In CSA1 mixtures, even at 2% citric acid dosage, the initial setting time increased to only about 30 minutes; however, the final setting time is higher than 120 minutes. With a combination of 2% citric acid dosage and a plasticizer, an initial set time greater than 60 minutes was achieved in the CSA1 concrete mixtures and was discussed in detail in chapters 6 and 7.

- In CACT, CSA1, and CSA2 mixture, while the addition of citric acid delayed the heat of hydration and formation of ettringite initially, its retardation effects got nullified after about 22, 9, and 5.5 hours of hydration, respectively, whereafter which the total heat of hydration in mixtures with citric acid surpassed that of the one without citric acid dosage.

- In CSA3 mixtures, the addition of citric acid delayed the secondary peak significantly, and the total heat of hydration after 10 days of hydration is still about 10% lower in mixtures with 0.75% citric acid compared to mixtures without citric acid. This could lead to lower strength development in these mixtures containing

citric acid. The higher content of Fe in the CSA3 clinker is believed to be the reason for having to use a higher citric acid dosage that retarded the reaction even at later ages. More work needs to be performed to understand the influence of citric acid in CSA cements containing high Fe content.

- Boric acid dosage of 14% by weight of binder is required to achieve an initial setting time greater than 60 minutes in MPC mixtures. While such high levels of boric acid addition in MPC mixtures successfully retarded the mixtures initially, its retardation effects continued even until about 10 days of hydration, where the total heat of hydration with retarder dosage is about 7 lower compared to the mixtures without retarder dosage. This could lead to lower strength development in these mixtures as well. However, the addition of boric acid at higher dosages is believed to reduce the pore volume of mixtures, leading to better mechanical properties at later ages [39]. Also, the usage of boric acid at higher levels did not have any influence on the composition of the hydration products.

6 EFFECT OF PLASTICIZERS AND W/B ON EARLY AND LATER AGE PROPERTIES

This chapter examines the influence of plasticizer and their dosages, and w/b (in case of AA and MPC) on both the hydration kinetics and flow characteristics in OPC and ACM formulations. A commercially available PCE based superplasticizer (admix1 [commercial name - ADVA 195 from gcp applied technologies]) was used to increase workability in OPC and ettringite based ACM mixtures [60–64]. Whereas, a commercially available plasticizer (admix2 [commercial name - CHRYSO AL 810 from CHRYSO group]) that is specifically designed for high alumina cements was used to increase workability in CAC mixtures (based on cement manufacturer recommendation). Even though significant research has been performed recently on the compatibility of PCE admixtures with CSA systems, none of the prior research looked at the compatibility between the set retarders (citric acid) and plasticizers (PCE) in CSA mixtures.

Isothermal calorimetry tests were used to understand the effect of HRWR dosage on cement pastes made with ACM and OPC mixtures. TGA measurements were also made on cement pastes to understand, in detail, the effects of plasticizer dosage on hydration kinetics and the formation of reaction products/phases at both early age and later age. Mini-slump and flow tests were performed to understand the influence of plasticizers (w/b in case of AA and MPC mixtures) on compatibility with plasticizers and flow characteristics of the OPC and ACM mixtures, respectively.

6.1 Introduction

6.1.1 Mini-slump test

The mini-slump test method can be used to measure the consistency of cement paste, which can be used to evaluate the influence of plasticizers on the workability of cement pastes. Consistency is related to the measured area of the pat formed when the mini slum test is conducted using the mini-slump cone. The loss in consistency (or slump loss) with hydration time can be measured by performing the test at different time intervals. Many flow properties of concrete depend on the cement paste component of the mix [65]. The mini-slump test on cement paste mixes is performed using a small sample size. Therefore, it is rapid and requires less effort and materials than the conventional slump test method on concrete mixes. As the mini-slump is conducted on cement pastes, it is more sensitive than the slump test method on concrete mixes. Because of the sensitivity of this test, it is possible to identify separate effects (like the effect of water reducers on mix stiffening) that are not easily differentiated with concrete mix slump data [65]. The dosages determined by the mini-slump are often less than those required for comparable slump and water reductions with concrete mixes. However, according to Kantro D.L [65], there is a correlation between the mini-slump on cement paste to that of slump on the concrete mix. Many researchers have used mini-slump to measure the influences of various admixtures (water reducers, air entraining admixtures, etc.) on workability [66–70]

6.2 Methods

6.2.1 Isothermal calorimetry

Isothermal calorimetry was performed on hydrating cement pastes for the mixture proportions given in Table 7 and were mixed in high shear mixer according to ASTM C305-14. Immediately after mixing, the mixtures were loaded into the calorimeter, and the heat evolution was measured according to the procedure listed in section 4.1.2.

Table 7 Cement paste mixture proportions to understand the influence of HRWR and w/b on reaction kinetics.

Cement	w/b	Set modifier (by weight of cement)	High range water reducer (ml/kg of cement)
OPC	0.4	-	Admix1 (0, 0.5, 1.0, 2.0, 3.0, 4.0)
CAC1	0.4	-	Admix2 (0, 0.5, 1.0, 2.0, 3.0)
CAC2	0.4	-	Admix2 (0, 0.4, 0.8, 1.0, 2.0, 3.0)
CACT	0.4	Citric acid – 1.5%	Admix1 (0, 0.5, 1.0, 2.0, 3.0, 4.0)
CSA1	0.4	Citric acid – 2.0%	Admix1 (0, 0.5, 1.0, 2.0, 3.0, 4.0)
CSA2	0.4	Citric acid – 0.5%	Admix1 (0, 0.5, 1.0, 2.0, 3.0, 4.0)
CSA3	0.4	Citric acid – 0.75%	Admix1 (0, 0.5, 1.0, 2.0, 3.0, 4.0)
AA	0.20, 0.233, 0.25, 0.30	activator 1 - 2.47% activator 2 – 2.21%	-
MPC	0.25, 0.25, 0.30, 0.35, 0.40	Boric acid – 14%	-

6.2.2 Thermogravimetric analysis (TGA)

A Hitachi simultaneous thermogravimetric analyzer STA7300 was used to carry out the thermogravimetric measurements. TGA was carried out on powdered cement paste samples prepared according to the procedure detailed in section 6.2.1 and cured at 23 ºC in sealed bags. Prior to performing TGA, the paste samples were ground and sieved to a

particle size of less than 300 microns, and the free water was removed using a solvent exchange procedure [42]. 5 g of powdered sample was mixed in 50 ml of isopropyl alcohol, and the suspension rests for 15 min. Then, the suspension is filtered using Büchner funnel and a vacuum pump for 5 min, and later, it is washed with 10 ml of diethylene ether for 1 min, during which the vacuum pump is turned off. The resulting suspension is again filtered under vacuum for five more minutes, or until the suspension is dry, whichever is longer.

The dried sample is further ground and approximately 20 mg of the sample with the particle size less than 74 microns is taken in an open 70 µl platinum crucible and dried in TG at 25 ºC under a constant stream of Nitrogen (N_2) gas for 15 min, or until the constant mass, whichever is longer. Later the temperature is increased to 40 ºC and held constant for 5 min. Then, the sample is heated from 40 to 1000 ºC, at a rate of 10 ºC/min, and the data is recorded at a rate of 120 data points per minute. During measurement, N_2 is used as a protective gas with a flow rate of 100 mL/min.

6.2.3 Mini-slump test (or miniature slump test)

The mini-slump cone [71] (shown in Fig. 29) used in this research has the top and base diameters of 19 and 38 mm, respectively. The height of the cone is 57 mm. The cement paste mixtures were prepared according to the proportions given in Table 8 and were mixed in high shear mixer according to ASTM C305-14. Immediately after mixing, the slump cone is filled with cement paste and compacted using the flat edge of a spatula for 15 times. The excess paste is stroked off using the flat edge of a spatula. Then the cone is lifted vertically in 3 seconds. The diameter of the resulting pat is measured in two perpendicular directions, and the average of the two diameters is used to calculate the pat area. If the paste

is too stiff for consolidation in the cone, the bottom diameter of the cone (38 mm) is used in determining the pat area. The test is repeated at 30, 60, and 90 minutes of hydration time. Prior to loading the mixtures in the mini-slump cone at these measurement intervals, the paste is mixed in a high shear mixer at 10,000 rpm for 60 seconds.

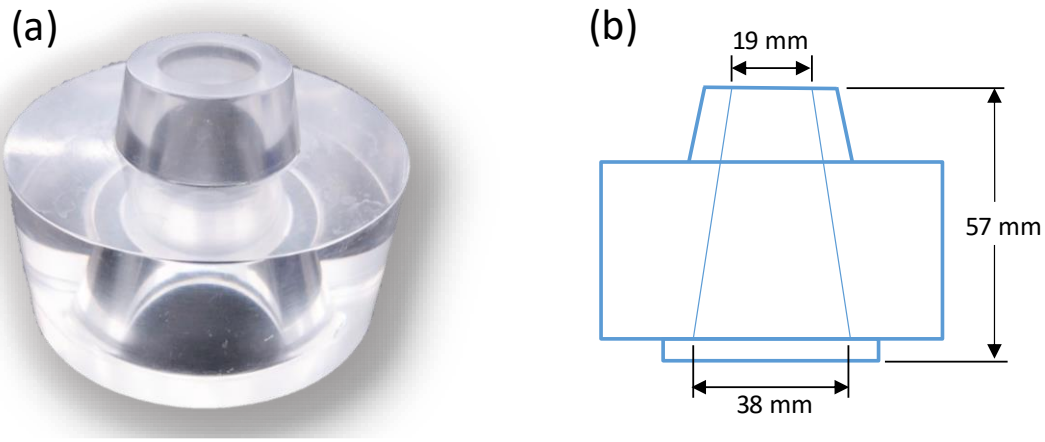

Fig. 29 (a) Picture and (b) sketch of the mini-slump cone used. Based on the recommendations provided by Kantro D.L [71]**.**

Table 8 Cement paste mixture proportions to understand the influence of plasticizer (HRWR) on the pat area in a mini-slump test.

Cement	w/b	Set modifier (by weight of cement)	High range water reducer (ml/kg of cement)
OPC	0.4	-	Admix1 (0, 0.5, 1.0, 2.0, 3.0, 4.0)
CAC2	0.4	-	Admix2 (0, 0.4, 0.8, 1.0, 2.0, 3.0)
CACT	0.4	Citric acid – 1.5%	Admix1 (0, 0.5, 1.0, 2.0, 3.0, 4.0)
CSA1	0.4	Citric acid – 2.0%	Admix1 (0, 0.5, 1.0, 2.0, 3.0, 4.0)
CSA2	0.4	Citric acid – 0.5%	Admix1 (0, 0.5, 1.0, 2.0, 3.0, 4.0)
CSA3	0.4	Citric acid – 0.75%	Admix1 (0, 0.5, 1.0, 2.0, 3.0, 4.0)

6.2.4 Flow test

The flow of cement mortars made with OPC and ACM mixtures were determined according to ASTM C1437-13 at 4, 30, 60, and 90 minutes of hydration. All the mortar mixtures were machine mixed in a planetary mixer (ASTM C305-14) according to the mixture proportions given in Table 9 and Table 10. Crushed granitic river sand (Lambert Sand and Gravel, Shorter, Alabama) with gradation conforming to ASTM C33 specification was used in making all the mortar mixtures.

Table 9 Cement mortar mixture proportions to understand the influence of plasticizer (HRWR) on the flow of cement mortar.

Cement	w/b	Set modifier (by weight of cement)	High range water reducer (ml/kg of cement)	Sand content (kg per kg cement)
OPC	0.4	-	Admix1 (0, 0.5, 1.0, 2.0, 3.0, 4.0)	2.000
CAC2	0.4	-	Admix2 (0, 0.4, 0.8, 1.0, 2.0, 3.0)	1.977
CACT	0.4	Citric acid – 1.5%	Admix1 (0, 0.5, 1.0, 2.0, 3.0, 4.0)	1959
CSA1	0.4	Citric acid – 2.0%	Admix1 (0, 0.5, 1.0, 2.0, 3.0, 4.0)	1.926
CSA2	0.4	Citric acid – 0.5%	Admix1 (0, 0.5, 1.0, 2.0, 3.0, 4.0)	1.926
CSA3	0.4	Citric acid – 0.75%	Admix1 (0, 0.5, 1.0, 2.0, 3.0, 4.0)	1.983

Table 10 Cement mortar mixture proportions to understand the influence of w/b on the flow of cement mortar.

Cement	w/b	Set modifier (by weight of cement)	Sand content (kg per kg cement)
AA	0.20, 0.233, 0.25, 0.30	activator 1 - 2.47% activator 2 – 2.21%	1.843
MPC	0.25, 0.25, 0.30, 0.35, 0.40	Boric acid – 14%	1.888

6.3 Results and Discussion

6.3.1 Effects of plasticizers on early age hydration kinetics and extent of hydration at later ages

Fig. 30 (i) shows the heat evolution and heat of hydration in the OPC mixture at varied dosages of admix1. Even though the addition of admix1 retarded the hydration initially, the total heat of hydration in mixtures with admix1 surpassed the mixtures without admix1 within 10 hours of hydration. The TGA of the OPC cement paste with 0 and 4 ml/kg dosage of admix1 at 9 hours and 56 days of hydration is shown in Fig. 30 (ii) and (iii), respectively. At 9 hours of hydration, a slight reduction in the amount of ettringite and portlandite in the mixtures with admix1 can be observed. The bound water (Fig. 38) in OPC mixtures with admix1 at 9 hours of hydration is about 9.6%, and it is about 11.2% in mixtures without admix1 – showing about 14% retardation in hydration. However, at 56 days of hydration, the amount of ettringite and portlandite is higher in mixtures with admix1. The bound water in the OPC mixtures with admix1 at 56 days of hydration is about 26.4%, and it is about 24.6% in mixtures without admix1 – showing an increase in total hydration by about 7% with admix1 dosage. The initial retardation provided a greater amount of dissolution of cement grains, which contributed to increased hydration at later ages.

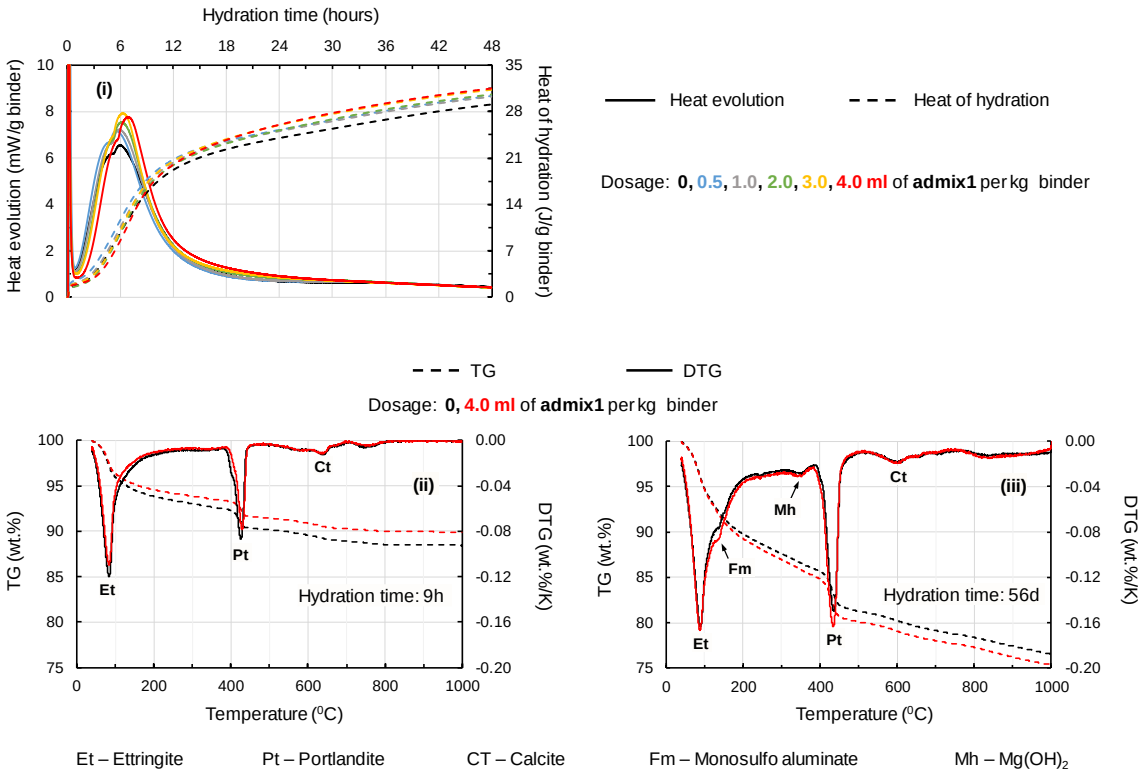

Fig. 30 Influence of admix1 at different dosages on (i) heat evolution and heat of hydration, (ii) and (iii) phase development in cement pastes made with OPC.

Fig. 31 (i) shows the influence of admix2 addition and its dosages on the heat evolution and heat of hydration in CAC1 mixtures. Unlike OPC mixtures with admix1 dosage, the addition of admix2 significantly retarded the hydration. At an admix2 dosage of 3 ml/kg binder, the primary peak in heat evolution got retarded by more than 20 hours. The primary heat evolution peak corresponds to the formation of C_2AH_8 and C_2AH_{8-x} phases, as shown in Fig. 32 (i). These two phases are the main hydration products in CAC1 cement (section 4.2.1). The TGA of the CAC1 cement paste with 0 and 3 ml/kg dosage of admix2 at 12 hours and 56 days of hydration is shown in Fig. 31 (ii) and (iii), respectively. At 12 hours of hydration, a significant reduction in the amount of CAH_{10}, C_2AH_8, AH_3, and C_3AH_6 phases in the mixtures with admix2 can be observed. The bound water (Fig. 41) in CAC1 mixtures with admix2 at 12 hours of hydration is about 4.8%, and it is about 22.8% in

mixtures without admix2 – showing about 79% retardation in hydration. The bound water in CAC1 mixtures with admix2 at 56 days of hydration is about 29.8%, and it is about 30.6% in mixtures without admix2 – showing about a 3% retardation with admix2 dosage. However, the mixtures with admix2 at 56 days of hydration had more amount of converted C_3AH_6 phase compared to the CAH_{10} phase – which implies the usage of admix2 accelerated the conversion process in the CAC1 mixtures with only about 3% less bound water. The significant early retardation in the mixtures with admix2 dosage provided more moisture to the already hydrated unconverted phases, thereby accelerating the conversion in them.

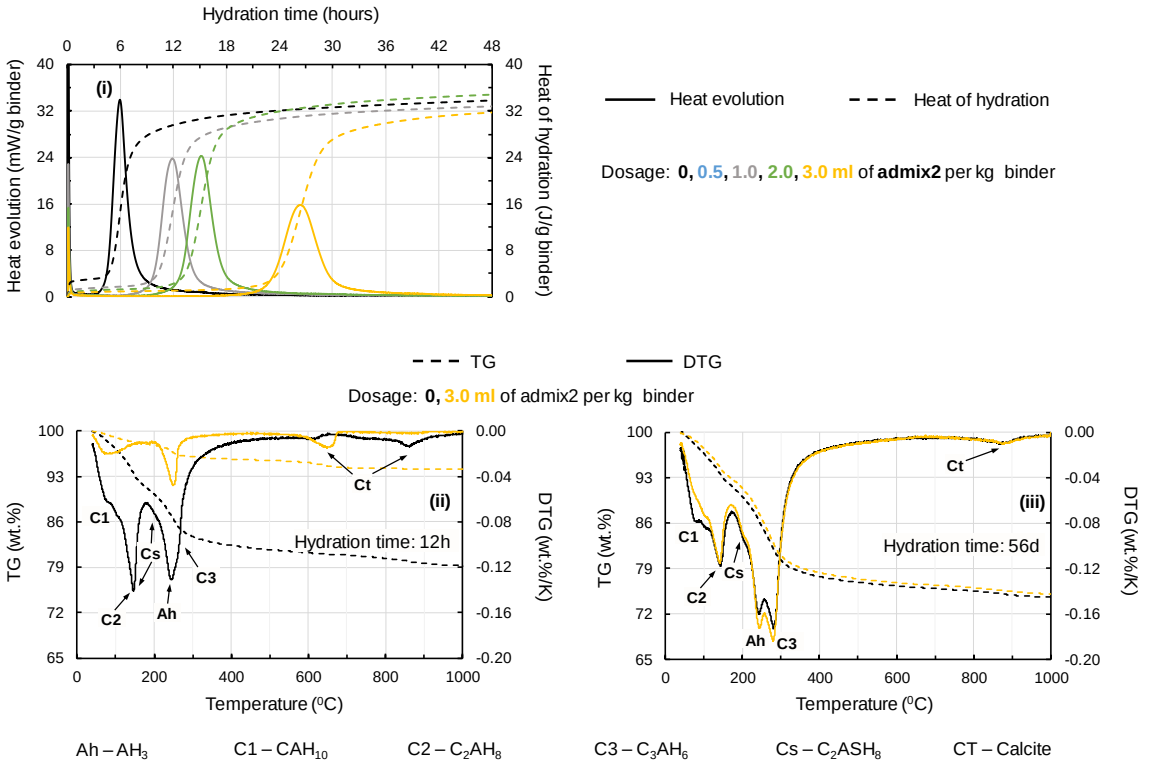

Fig. 31 Influence of admix2 at different dosages on (i) heat evolution and heat of hydration, (ii) and (iii) phase development in cement pastes made with CAC1.

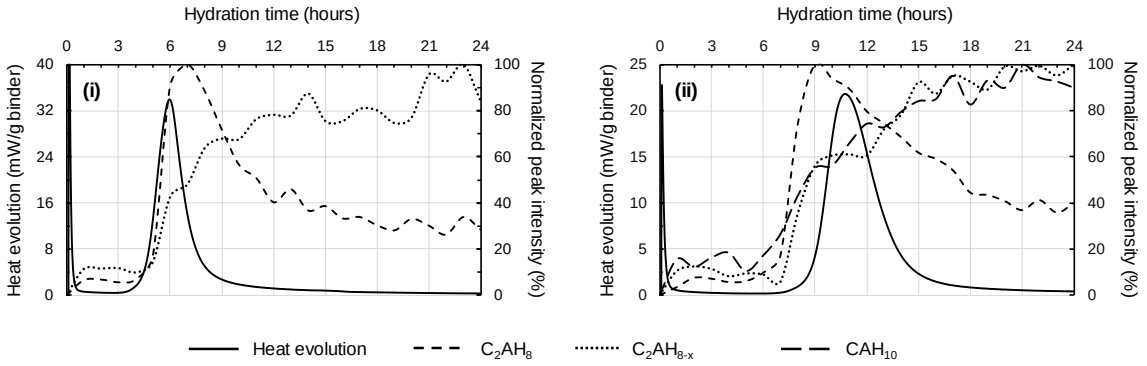

Fig. 32 Comparing early age heat evolution with phase development in cement pastes made with (i) CAC1 and (ii) CAC2.

The influence of admix2 addition and its dosages on the heat evolution and heat of hydration in CAC2 mixtures is shown in Fig. 33. Similar to the CAC1 mixtures, addition of admix2 significantly retarded the hydration- however, the amount of retardation is lower compared to the CAC1 mixtures. At an admix2 dosage of 3 ml/kg binder, the primary peak in heat evolution got retarded by about 8 hours compared to about 20 hours in CAC1 mixtures. The primary heat evolution peak corresponds to the formation of mainly C_2AH_8 and C_2AH_{8-x} phases, as shown in Fig. 32 (i). The CAH_{10} phase started to crystallize early compared to the onset of the main heat evolution peak. These phases are also the main hydration products in CAC2 mixtures (section 4.2.1). The TGA of the CAC2 cement paste with 0 and 3 ml/kg dosage of admix2 at 13 hours and 56 days of hydration is shown in Fig. 33 (ii) and (iii), respectively. At 13 hours of hydration, the amount of CAH_{10} phase is slightly higher in the mixtures with admix2 compared to the mixtures without admix2. However, the amount of C_2AH_8 and AH_3 phases is significantly lower. The bound water (Fig. 41) in CAC2 mixtures with admix2 at 13 hours of hydration is about 21.8%, and it is about 23.5% in mixtures without admix2 – showing only about 7% retardation in hydration. The bound water in CAC2 mixtures with admix2 at 56 days of hydration is about 29.3%,

and it is about 30.7% in mixtures without admix2 – showing about 5% with admix2 dosage. And unlike the CAC1 mixtures, the CAC2 mixture with admix2 at 56 days of hydration had more amount of unconverted CAH_{10} phase compared to the converted C_3AH_6 phase – likely due to the significant lower retardation in the CAC2 mixtures with admix2 compared to the CAC1 mixtures.

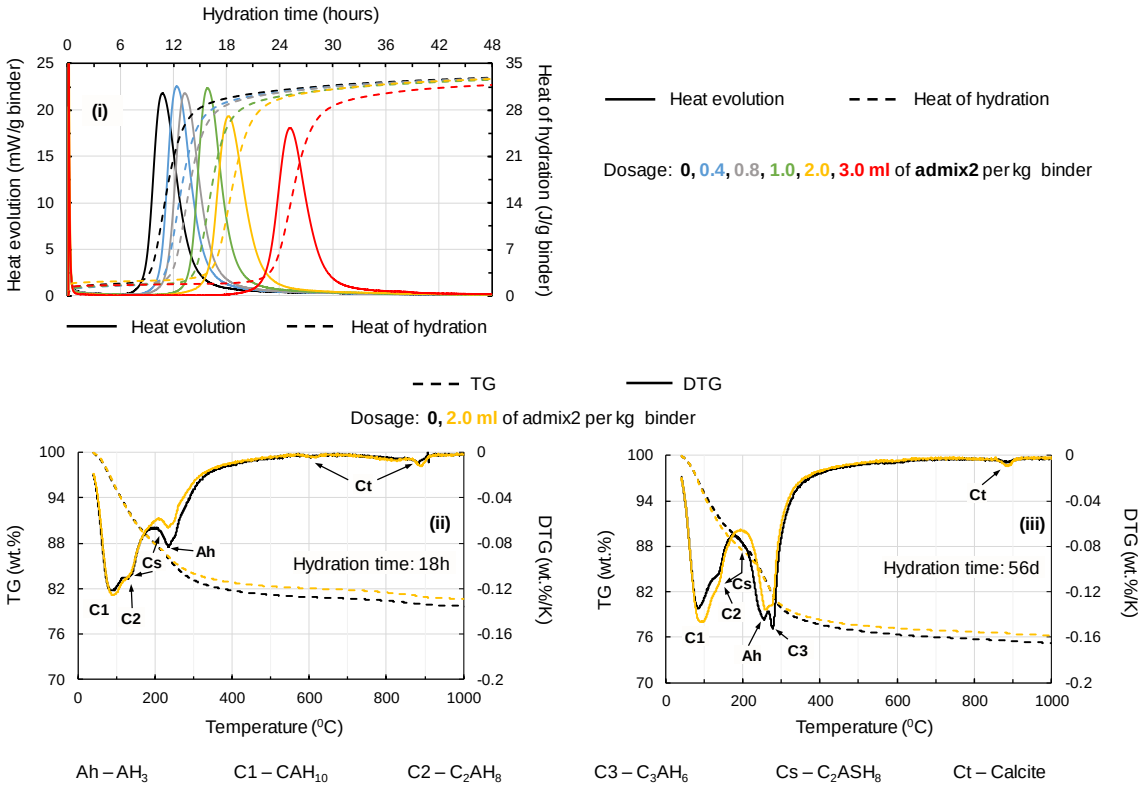

Fig. 33 Influence of admix2 at different dosages on (i) heat evolution and heat of hydration, (ii) and (iii) phase development in cement pastes made with CAC2.

Fig. 34 (i) shows the heat evolution and heat of hydration in the CACT mixtures at varied dosages of admix1. Similar to OPC mixtures, the addition of admix1 retarded the hydration initially. However, the total heat of hydration in mixtures with admix1 surpassed the mixtures without admix1 [60–64] at only about 36 hours of hydration, compared to 10 hours of hydration in OPC mixtures. The TGA of the CACT cement paste with 0 and 4

ml/kg dosage of admix1 at 9 hours and 56 days of hydration is shown in Fig. 34 (ii) and (iii), respectively. At 15 hours of hydration, a slight reduction in the ettringite content in the mixtures with admix1 can be observed. The bound water (Fig. 38) in CACT mixtures with admix1 at 9 hours of hydration is about 6.3%, and it is about 7.3% in mixtures without admix1 – showing about 14% retardation in hydration. However, at 56 days of hydration, the amount of ettringite, hemicarboaluminate, and monocarboaluminate is higher in mixtures with admix1. The bound water in the CACT mixtures with admix1 at 56 days of hydration is about 32.8%, and it is about 33.0% in mixtures without admix1 – showing no significant change in the total hydration with admix1 dosage.

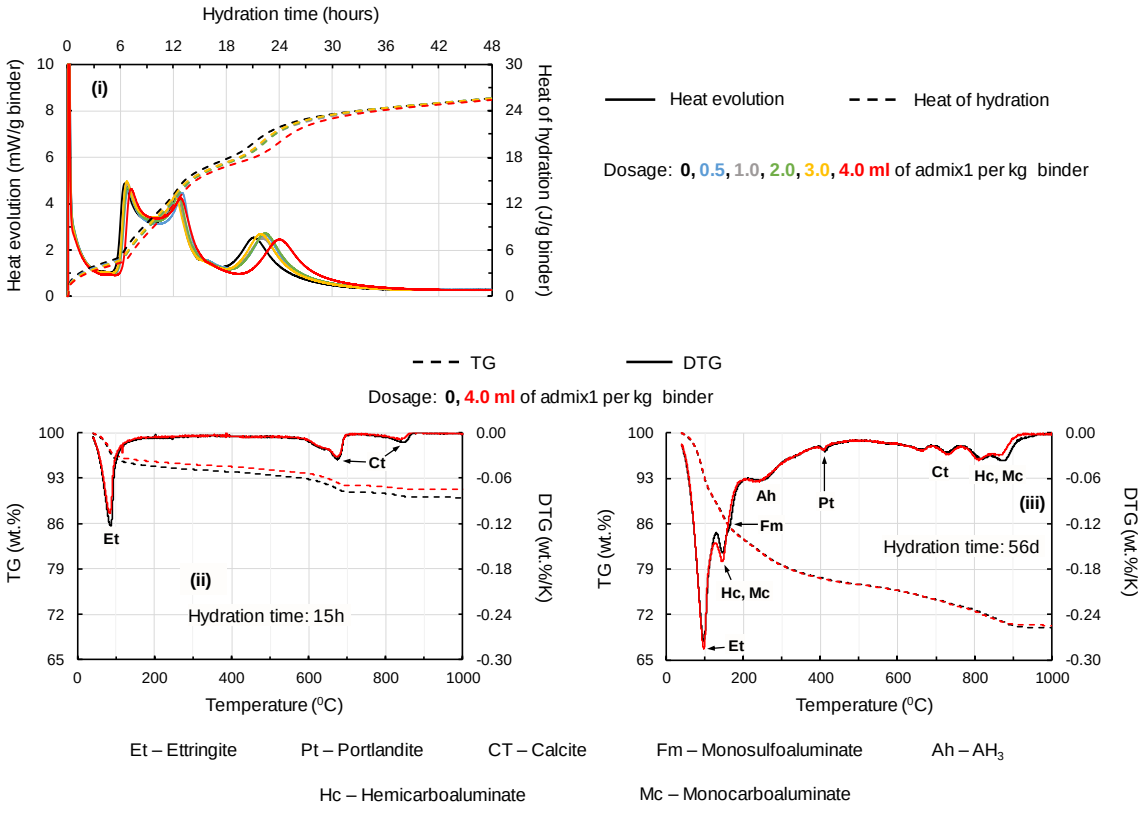

Fig. 34 Influence of admix1 at different dosages on (i) heat evolution and heat of hydration, (ii) and (iii) phase development in cement pastes made with CACT.

Fig. 35 (i) shows the heat evolution and heat of hydration in the CSA1 mixtures at varied dosages of admix1. Unlike OPC and CACT mixtures, the addition of admix1 accelerated the primary heat evolution peak by about 1 hour. However, the total heat of hydration in mixtures with admix1 during the initial 2 hours of hydration is significantly lower compared to the mixtures without admix1. At about 2 hours, the total heat of hydration in mixtures with 4 ml/kg admix1 dosage surpassed the mixtures without admix1 dosage. But at about 5 hours of hydration time, the crossover happened again, from after which the mixtures without admix1 dosage had a higher amount of heat of hydration compared to the mixtures with admix dosage. The TGA of the CSA1 cement paste with 0 and 4 ml/kg dosage of admix1 at 6.5 hours and 56 days of hydration is shown in Fig. 35 (ii) and (iii), respectively. At 6.5 hours of hydration, the amount of ettringite content in the mixtures with admix1 is higher compared to the mixtures without admix1 dosage. The bound water (Fig. 38) in CSA1 mixtures with admix1 at 6.5 hours of hydration is about 17.2%, and it is about 16.9% in mixtures without admix1 – showing about 2% acceleration in hydration. However, at 56 days of hydration, the amount of ettringite is significantly lower in mixtures with admix1. The bound water in the CSA1 mixtures with admix1 at 56 days of hydration is about 34%, and it is about 36.4% in mixtures without admix1 – showing about 7% retardation in total hydration with admix1 dosage. The initial acceleration observed with admix1 addition might be responsible for the reduction in the total hydration at 56 days – the opposite of the dissolution effect observed in OPC and CACT mixtures. This contradicts the prior research on CSA systems containing PCEs [60–64] – it could be because a set retarder was not used in conjunction with the PCEs in those CSA systems.

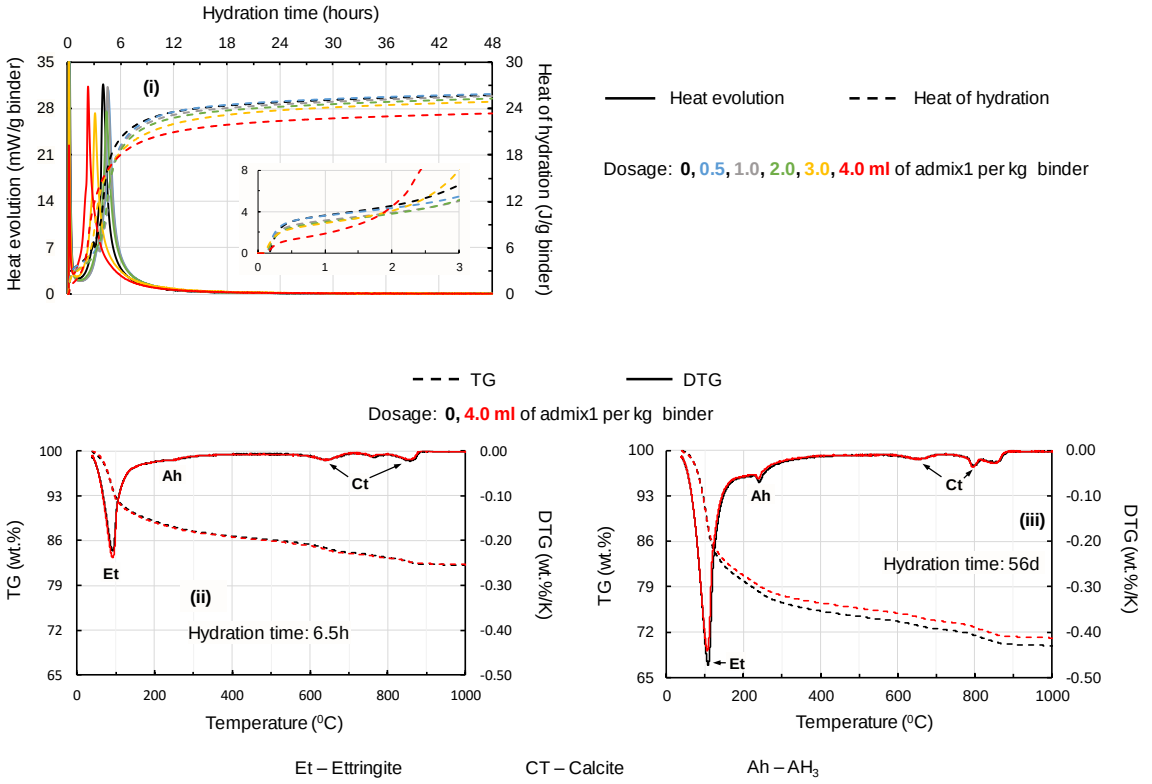

Fig. 35 Influence of admix1 at different dosages on (i) heat evolution and heat of hydration, (ii) and (iii) phase development in cement pastes made with CSA1.

Fig. 36 (i) shows the heat evolution and heat of hydration in the CSA2 mixtures at varied dosages of admix1. Unlike OPC, CACT, and CSA1 mixtures, no significant effect is observed on the heat evolution in CSA2 mixtures with the addition of admix1. The TGA of the CSA2 cement paste with 0 and 4 ml/kg dosage of admix1 at 6.5 hours and 56 days of hydration is shown in Fig. 36 (ii) and (iii), respectively. At 4 hours of hydration, the amount of ettringite content in the mixtures with admix1 is higher compared to the mixtures without admix1 dosage. The bound water (Fig. 38) in CSA1 mixtures with admix1 at 6.5 hours and 56 days of hydration is about 12% and 2% higher compared to the mixtures without admix1, respectively. Overall, no significant effect is observed in CSA2 mixtures with the addition of admix1.

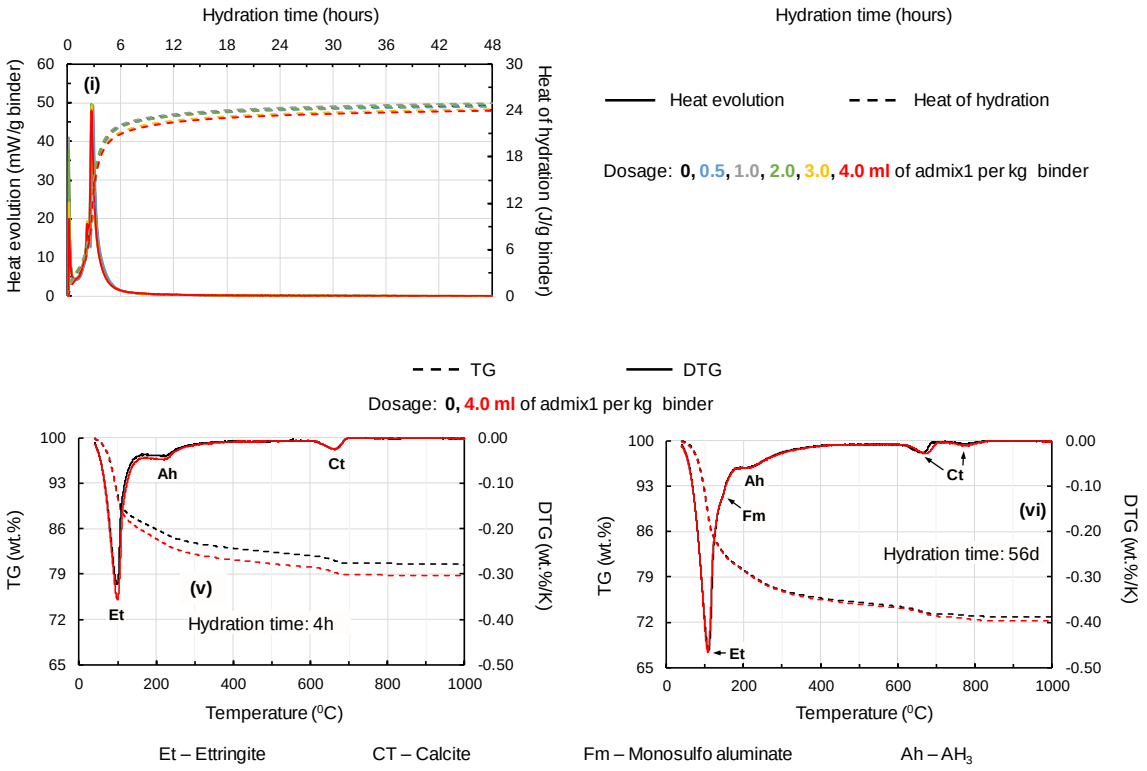

Fig. 36 Influence of admix1 at different dosages on (i) heat evolution and heat of hydration, (ii) and (iii) phase development in cement pastes made with CSA2.

Fig. 37 (i) shows the heat evolution and heat of hydration in the CSA3 mixtures at varied dosages of admix1. With the addition of admix1 dosage in the CSA3 mixtures, no significant difference is observed in the heat evolution until about 24 hours of hydration. But after 24 hours, significant retardation is observed in the heat evolution in the mixtures. At 4 ml/kg dosage of admix1, the retardation in the primary heat evolution peak is more than 24 hours. At 48 hours of hydration, the total heat of hydration with admix1 dosage is about 40% lesser compared to the mixtures without admix1 dosage. After about 144 hours of hydration, the heat of hydration in the mixtures with 4ml/kg admix1 dosage surpassed the mixtures without admix2 dosage. Winnefeld [60] reported strong retardation with the addition of PCEs in CSA systems containing anhydrite compared to the CSA systems

containing gypsum. Also, the mixtures containing a lower amount of anhydrite experienced higher retardation compared to mixtures with higher amount of anhydrite. CSA3 binder does not contain gypsum, whereas gypsum is present in both the CSA1 and CSA2 binders. Also, CSA3 binders have a lower amount of anhydrite when compared to CSA1 and CSA2 binders. This lower amount of gypsum and anhydrite, in addition to the significant retardation observed with citric acid in CSA3 mixtures, could be the reasons for significant further retardation observed with the addition of admix1.

The TGA of the CSA3 cement paste with 0 and 4 ml/kg dosage of admix1 at 120 hours and 56 days of hydration is shown in Fig. 37 (ii) and (iii), respectively. At 120 hours of hydration, a slight reduction in the amount of ettringite and AH_3 phases in the mixtures with admix1 can be observed. The bound water (Fig. 38) in CSA3 mixtures with admix1 at 120 hours of hydration is about 16.9%, and it is about 18.3% in mixtures without admix1 – showing about 8% retardation in hydration. However, at 56 days of hydration, the amount of ettringite is higher in mixtures with admix1. The bound water in the CSA3 mixtures with admix1 at 56 days of hydration is about 32.4%, and it is about 31.8% in mixtures without admix1 – showing an increase in total hydration by only about 2% with admix1 dosage. The initial retardation provided a greater amount of dissolution of cement grains, which could have contributed to increased hydration at later ages.

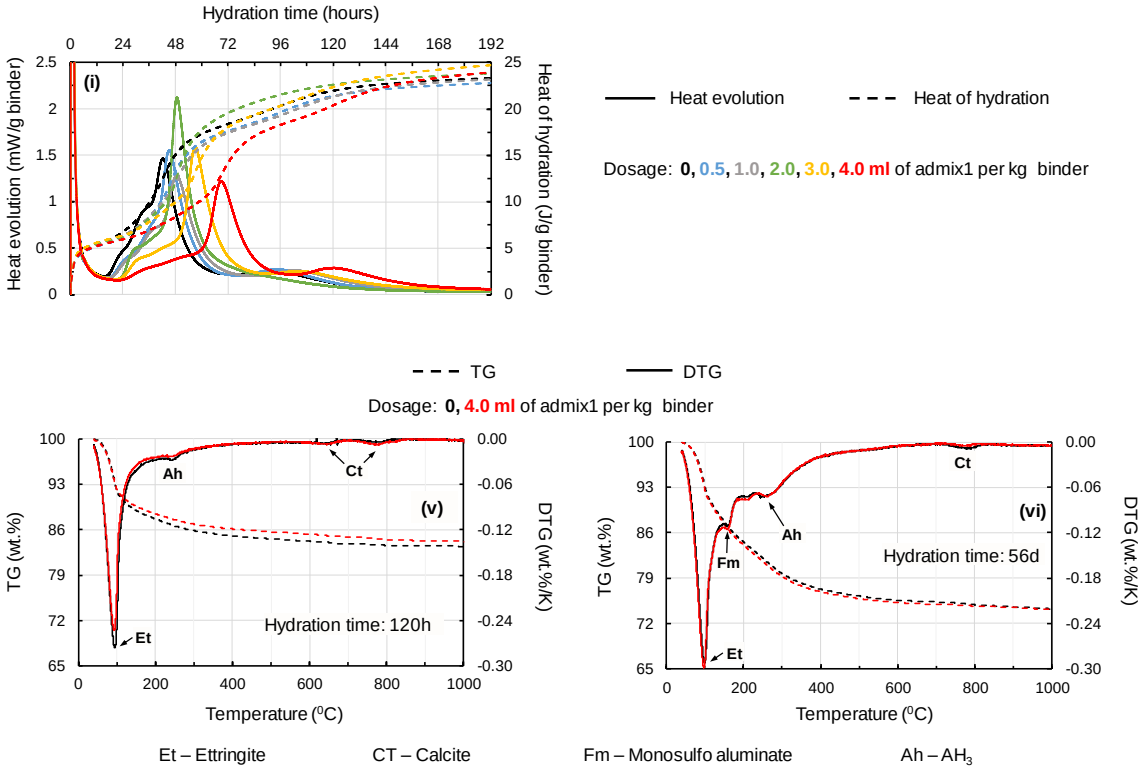

Fig. 37 Influence of admix1 at different dosages on (i) heat evolution and heat of hydration, (ii) and (iii) phase development in cement pastes made with CSA3.

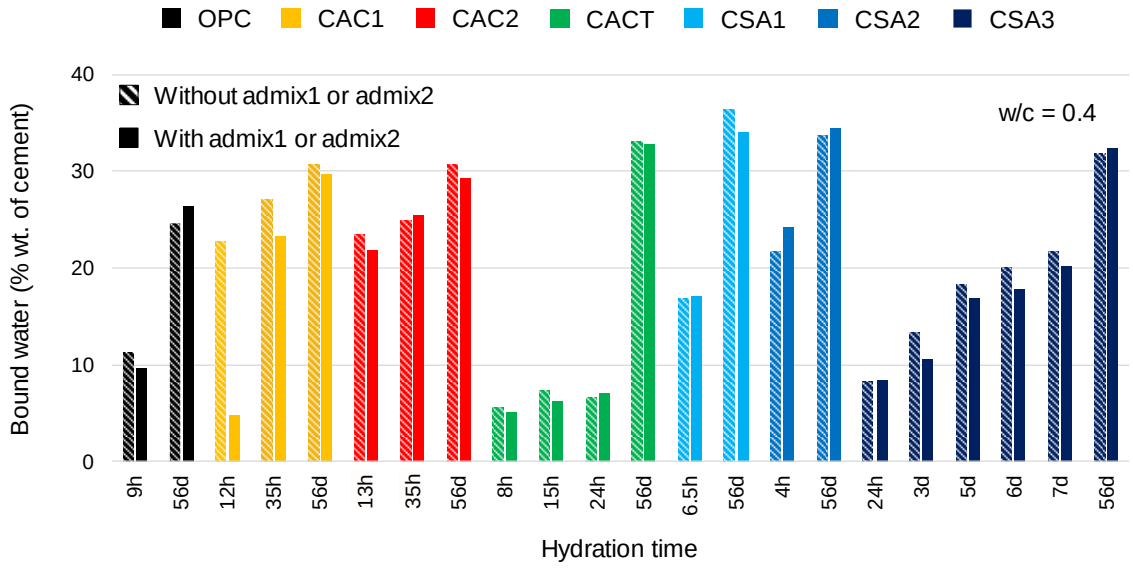

Fig. 38 Effect of plasticizers on bound water in cement pastes made with ACMs at different hydration times compared to that of OPC.

6.3.2 Effect of admixtures on mini-slump of cement pastes

The mini-slump parameters (area of a pat) of OPC and ACM paste mixtures versus hydration time at varying dosages of plasticizers are shown in Fig. 39. In OPC mixtures, with increase in admix1 dosage from 0 to 3 ml/kg of cement, the area of the pat increased significantly [72–74]. After further increase in dosage to 4 ml/kg, the mini-slump increased at 4 min of hydration, but later dropped significantly compared to the mixture with 3 ml/kg dosage. The CACT mixtures, even without admix1 dosage, have significantly higher mini-slump compared to the OPC mixtures with admix1 dosage. With addition of 1 ml/kg of admix1 in CACT mixtures did not significantly change the mini-slump in these mixtures – likely because of already high mini-slump in those mixtures without any admix1 dosage. In CSA1 mixtures, no significant change in observed in mini-slump with addition of admix1 at dosage lower than 2 ml/kg. At dosage of 3 and 4 ml/kg, a significant increase in mini-slump is observed until 30 minutes of hydration [60,63]. However, the mini-slump significantly dropped even at those higher dosages of admix1. Also, at those higher dosages, the mini-slump increased with hydration time for up to 30 minutes and decreased from 30 to 60 minutes. This could be due to the multiple mixing cycles on the cement paste, or the admix1 might need some time to disperse the cement and water apart. Unlike CSA1 mixtures, CSA2 mixtures showed significant improvement in mini-slump even at lower dosages of amix1, and the mini-slump achieved in these mixtures was higher than that of CSA1 mixtures at 4 and 15 minutes of hydration. However, the slump retention capability was significantly lower in CSA2 mixtures when compared to CSA1 mixtures – especially at higher dosages of admix1. Similar to CACT mixtures, the CSA3 mixtures also had significantly higher mini-slump even without admix1 dosage compared to OPC and other

ACM mixtures with admix1 dosage. So, no additional mini-slump measurements were performed on these mixtures with admix1 dosage. The mini-slump in CAC2 mixtures, even without admix2 dosage, increased with hydration time. This could be due to the higher setting time in these mixtures, coupled with the multiple mixing cycles that might have freed the trapped water between the cement grains. The mini-slump improved with increase in admix2 dosages, achieving mini slumps higher than OPC and other ACM mixtures.

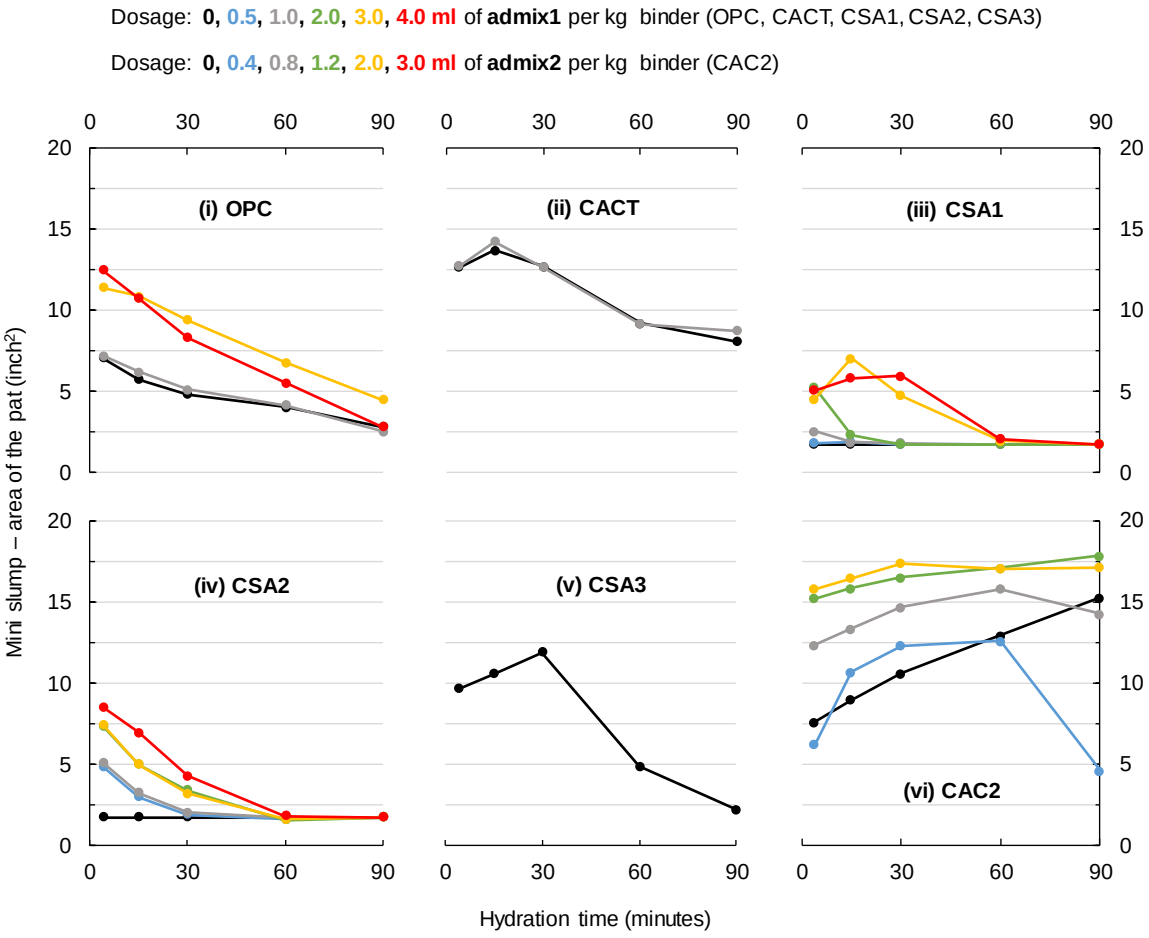

Fig. 39 Influence of admixtures at different dosages on mini-slump area of cement pastes made with ACMs at w/c of 0.4.

6.3.3 Effects of admixtures on flow on cement mortars

The flow diameter of OPC, CACT, CSA1, CSA2, CSA3, and CAC2 mortar mixtures at varied dosages of plasticizers and hydration times is shown in Fig. 40. With an increase in the admix1 dosage in OPC mixture, the flow diameter increased significantly and provided flow retention up to 90 minutes of hydration. Whereas in the CACT mixture, the increase in flow diameter with increase is admix1 dosage is not as significant as compared to the OPC mixtures – likely due to the already high flow diameter (compared to OPC and other ACMs) in CACT mixture without any admix1 addition. CSA1 mixtures also exhibited higher flow compared to OPC mixtures without admix1 dosage. But the rate of reduction in flow with hydration time is higher in CSA1 mixtures compared to both the OPC and CACT mixtures. An increase in the admix1 dosage resulted in an increase in flow in CSA1 mixtures. But the magnitude of increase in flow diameter with dosage is not as high as compared to that of OPC mixtures or even CACT mixtures. In CSA2 mixtures, an increase in the admix1 dosage resulted in an increase in flow diameter and better flow retention, even up to 90 min of hydration. However, the increase in flow diameter with dosage is not as high as compared to that of OPC mixtures, but it is significantly higher compared to the CACT and CSA1 mixtures. Compared to CACT and CSA1 mixtures, CSA3 mixtures had significant increase in flow with admix1 dosage. But the flow dropped significantly between 60 to 90 minutes of hydration. As discussed in section 5.2.1 and 6.3.1, the CSA3 mixtures with 0.75% citric acid dosage had about 60 minutes of initial setting time, and also the addition of admix1 did not result in any retardation during the initial 24 hours of hydration. This could be the reason for the significant reduction in flow after 60 minutes of hydration. Overall, all the OPC and ACM mixtures (except CAC2) showed significant

improvement in flow characteristics in cement mortars (Fig. 40) compared to mini-slump area (Fig. 39) on corresponding cement pastes. This is because all these mixtures experienced accelerated hydration at early age when mixed as cement pastes in high shear mixer compared to when mixed as cement mortars in planetary mixer. In CAC2 mixtures, addition of admix2 did not improve the flow of mortar mixtures both at early age and up to 90 minutes of hydration – even though the dosage of admix2 resulted in significant increase in the mini-slump of cement pastes made with CAC2. As discussed in section 4.2.2, the CAC2 mixtures experienced significant acceleration in hydration when mixed with sand in planetary mixer compared to mixing just as cement paste in high shear mixer. This could be the reason for not seeing improved performance in the flow of cement mortars with admix2.

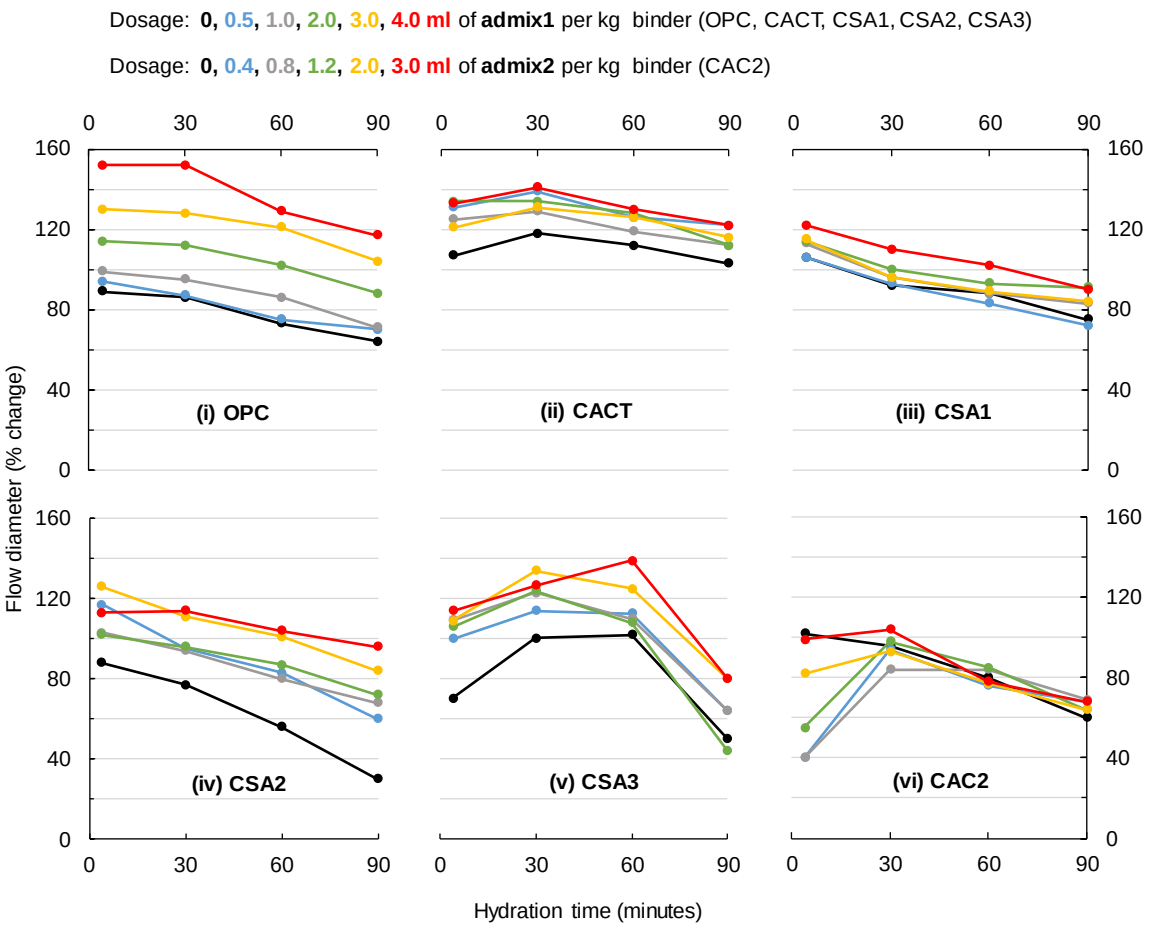

Fig. 40 Influence of admixtures at different dosages on the flow of cement mortars made with ACMs at w/c of 0.4.

6.3.4 Effects of w/b on flow on cement mortars made with AA and MPC

Fig. 41 shows the flow diameter of mortar mixtures made with AA and MPC at different w/b and hydration times. An increase in w/b ratio from 0.2 to 0.3 provided a significant increase in the flow of AA mixtures, even up to 90 minutes of hydration. In MPC mixtures, an increase in w/b also resulted in increase in flow diameter until 60 minutes of hydration, but the flow reduced significantly between 60 to 90 minutes of hydration at all the w/b examined.

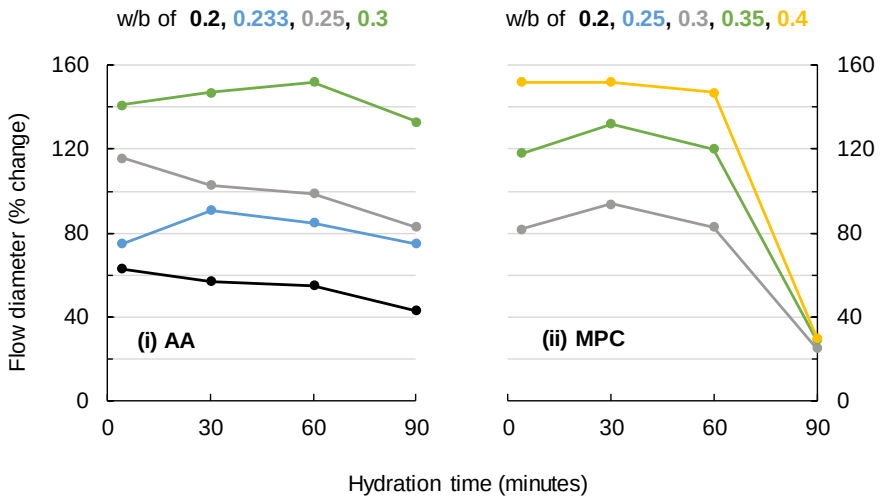

Fig. 41 Influence of w/b on the flow of cement mortars made with AA and MPC.

6.4 Conclusions and Recommendations

- Admixture dosages determined on cement pastes (for OPC and all ACM mixtures except CAC mixtures) mixed in a high shear mixer will lead to over conservative estimates compared to what is required in cement mortars and concrete mixtures.
- The addition of plasticizer (admix1) did not significantly affect the heat evolution of the cement pastes made with OPC, CACT, and CSA2. In CSA1 mixtures, the addition of admix1 significantly accelerated the main hydration peak. However, retardation is observed in all these 4 mixtures with the addition of admix1 during the initial 2 hours of hydration. This could contribute to increased setting time and workability during that early age period.
- No retardation in heat evolution is observed during the initial 24 hours of hydration in CSA3 mixtures with the addition of admix1. However, significant retardation is observed in the hydration between 1 and 6 days of hydration time. This could lead to a significant slower strength development in these mixtures. More research needs

to be performed on the interaction of the combination of PCEs and citric acid on high Fe CSA systems.

- In CAC1 and CAC2, the addition of admix2 significantly delayed the reaction. However, no significant change is observed in the amount of hydration products after about 13 hours of hydration period in the CAC2 mixtures.
- With an appropriate dosage of superplasticizers, a desirable flow even after 60 minutes of hydration can be achieved with ACM and OPC mixtures (except CAC2). Whereas, for mixtures made with AA, using higher w/b can significantly improve the flow characteristics – even for up to 90 minutes of hydration.
- Admix1 can be used to increase the flow of mixtures with OPC, CACT, CSA1, CSA2, and CSA3. However, the effectiveness of the admix1 varied across binders. Admix1 was most effective in increasing the flow in OPC mixtures followed by CSA2 and CSA3 mixtures. Both the CACT and CSA1 mixtures already had higher flow without any admix2 dosage. So, the effectiveness of admix2 is lower in these two mixtures compared to OPC, CSA2, and CSA3 mixtures. Admix2 also improved the flow retention capability in both the CSA2 (up to 90 min of hydration) and CSA3 mixtures (only up to 60 minutes of hydration).
- Admix2 was not effective in increasing the flow in cement mortar mixtures made with CAC2, even though it is found to be significantly effective in paste mixtures.

7 DEVELOPING CONCRETE MIXTURES WITH ALTERNATIVE CEMENTITIOUS MATERIALS

Because many ACMs experience rapid hydration and early set, it was necessary to identify suitable retarding admixtures and dosages, particularly for CACT, CSA1, CSA2, CSA3, and MPC mixtures. For others, high range water-reducing admixtures (HWRA) were needed to achieve necessary workability. A 99% pure grade anhydrous citric acid [22] was used to retard the setting times of CACT, CSA1, CSA2, CSA2P, and CSA3 cements. A polycarboxylate-based high range water reducer (admix1) conforming to both ASTM C494 (Type A & F) and ASTM C1017 (Type I) specifications were used to achieve desirable slumps in OPC, CACT, CSA1, CSA2, and CSA2P mixtures. A specialized plasticizer (admix1), which also acts as a set retarder, was used in CAC2 mixtures. For CAC1, another specialized plasticizer (admix3) instead of admix2 was used, since the CAC1 mixtures produced with admix2 showed significant bleeding and segregation during the initial 30 minutes of hydration. Admixture selections were based upon manufacturer recommendations. The set modifier (and activator, for the AA) dosages were chosen so that the corresponding concrete mixtures had a workable window of at least 60 min and a slump of at least 3 inches after 60 minutes of the addition of water.

The successful concrete mixtures were developed by using a combination of isothermal calorimetry, x-ray diffraction, set time assessments, and mini-slump tests to link cement characteristics, admixture type, and dosage to early-age behavior. For all ACMs, except for CAC1 and MPC, concretes were designed that met the early age requirements for the set time and slump, at w/c of 0.40 or less. Despite investigations of admixture type and

dosing rate, a workable CAC1 mix was not produced. For MPC, an increase in w/c was necessary to achieve an adequate slump. This resulted in a concrete mixture that did not meet strength criteria.

Crushed granitic river sand (Lambert Sand and Gravel, Shorter, Alabama) with gradation conforming to ASTM C33 specification and crushed granitic gneiss coarse aggregates (Vulcan Materials Company Lithia Springs, Georgia) conforming to ASTM C33 #67 gradation were used in making all concrete mixtures given in Table 4. In the mixing of AA, the activator was added to the water. The sand content was adjusted to account for the differences in the specific gravity of all the ACMs compared to OPC, to have the same mass of binder in all the concrete mixtures. The concrete mixtures were machine-mixed in the concrete drum of capacity 0.255 m^3 (9 ft^3) according to ASTM C192-14 at w/b of 0.40 (AA at 0.205 w/b as per manufacturer recommendations). In all the concrete mixtures, the water dosage was adjusted to account for the absorption of aggregates. A summary of the resulting mix designs for cements that met target performance (except CAC1 and MPC) is given in Table 11, and the corresponding concrete slumps achieved after 10 and 60 minutes of hydration times are shown in Table 12.

Table 11 Concrete mixture proportions.

Cement	w/b	Admixtures/ activators (by weight of cement)	Cement (kg/m^3)	Water (kg/m^3)	Sand (kg/m^3)	#67 aggregate (kg/m^3)
OPC	0.40	Admix1 - 3.5 ml/kg	454	189	703	1056
CAC1	0.40	Admix3 – 0.4%	454	189	713	1056
CAC2	0.40	Admix2 - 1.6 ml/kg	454	189	693	1056
CACT	0.40	citric acid – 1.5%, HRWR1 - 3.5 ml/kg	454	189	674	1056
CSA1	0.40	citric acid - 2%, HRWR1 – 3.0 ml/kg	454	189	656	1056
CSA2	0.40	citric acid – 0.5%, HRWR1 - 0.5 ml/kg	454	189	656	1056
AA	0.205	activator 1 - 2.27%, activator 2 – 1.78%	488	109	811	1056
MPC	0.2	boric acid – 14%	533	115	660	1056
	0.25		533	141	590	1056

Table 12 Slump of ACM and OPC concrete mixtures at 10 and 60 minutes of hydration time.

Binder	w/b	HRWR dosage (ml/kg)	Hydration time (min)	Concrete slump (inches)
OPC	0.4	3.5	10	8.5
			60	5.0
CAC1	0.4	1.6	10	0.8
			20 and 60	0.0
CAC2	0.4	1.6	10	8.5
			60	6.0
CACT	0.4	3.5	10	9.0
			60	6.5
CSA1	0.4	3.0	10	6.2
			60	6.5
CSA2	0.4	0.5	10	7.5
			60	4.5
AA	0.205	NA	10	4.5
			60	3.0
MPC	0.2	NA	10	1.0
	0.25		10	9.0

Fig. 42 Montage of concrete slumps made with ACMs compared to OPC. All the concrete mixes (except CAC1 and MPC) have slumps greater than 3 inches even after 60 minutes of addition of water.

7.1 Conclusions

The successful concrete mixtures were developed by using a combination of isothermal calorimetry, x-ray diffraction, set time assessments, and mini-slump tests to link cement characteristics, admixture type, and dosage to early-age behavior. For all ACMs, except for CAC1 and MPC, concretes were designed that met the early age requirements for the set time and slump, at w/c of 0.40 or less.

8 MECHANICAL AND HARDENED PROPERTIES

This chapter examines the mechanical and hardened properties of ACM mixtures compared to that of OPC mixtures. The shrinkage and cracking behavior of the ACMs have not been adequately examined and must be better understood and able to be controlled before alternative binder concretes can be effectively used in the field. With the reduction in fluid transport throughout the hardened media, the binder will begin to self-desiccate, with removal of water from the pores leading to increases in capillary pressures. Water will be removed from larger pores first, with the generated pressures inversely correlated with pore size. As the pressures increase, the section will contract, and autogenous shrinkage will occur. Autogenous shrinkage is based on many factors, including the rate and magnitude of chemical shrinkage after the paste reaches final set, the development of mechanical properties in the hardened binder, and the pore sizes and distribution of pores throughout the binder [75].

8.1 Methods

8.1.1 Autogenous Shrinkage Testing

The autogenous shrinkage of ACM mortar samples was measured according to ASTM C1698. All the mortar mixtures were mixed at w/b of 0.4 (AA at 0.25 w/b, MPC at 0.3 w/b), and sand/cement of 2.0 according to the mixture proportions given in Table 13. Crushed granitic river sand (Lambert Sand and Gravel, Shorter, Alabama) with gradation conforming to ASTM C33 specification was used in making mortar mixtures. The sand content was adjusted to account for the differences in the specific gravities of cements, and

the water dosage was also adjusted to account for the sand absorption and water content of admixtures. All the mortar samples were mixed in a Hobart mixer, according to ASTM C305. After mixing, the corrugated tubes were filled and sealed completely according to the guidelines provided in the ASTM 1698, and were cured at 23^0C during the entire testing period. The length measurements were made on 4 replicate samples at the time of the final setting (shown in Table 14 and determined using Vicat needle of diameter 2mm) and ages of 1, 2, 3, 7, 14, 28, and 56 days of hydration. The autogenous shrinkage strains were calculated with reference to the initial length measurements made at the final setting time.

Table 13 Mortar mixture proportions for autogenous shrinkage testing.

Cement	w/b	Admixtures/ activators (by weight of cement)	Cement (kg)	Water (kg)	Sand (kg)
OPC	0.40	HRWR1 – 2.0 ml/kg	1	0.408	2.000
CACT	0.40	citric acid – 1.5%	1	0.408	1.959
CAC2	0.40	HRWR2 – 2.0 ml/kg	1	0.408	1.977
CSA1	0.40	citric acid - 2%, HRWR1 – 4.0 ml/kg	1	0.408	1.926
CSA2	0.40	citric acid – 0.5%, HRWR1 – 4.0 ml/kg	1	0.408	1.926
CSA2P	0.40	citric acid – 0.5%, HRWR1 - 4.0 ml/kg	1	0.408	1.926
CSA3	0.40	citric acid – 0.75%, HRWR1 - 0.5 ml/kg	1	0.408	1.983
AA	0.25	activator 1 - 2.47%, activator 2 – 2.21%	1	0.257	1.843
MPC	0.3	Boric acid – 14%,	1	0.308	1.888

Table 14 Final setting times (in minutes) of mortar mixtures.

OPC	CACT	CAC2	CSA1	CSA2	CSA2P	CSA3	AA	MPC
255	390	1080	95	180	160	120	1080	140

8.1.2 Compressive strength

Compressive strength was measured on 3 concrete cylinders of dimensions 3 in x 6 in, which are cured at 23 ºC and 100% RH. The measurements were made at the age of 1, 2, 3, 7, 14, 21, 28, and 56 days.

8.1.3 Modulus of elasticity and poisons ratio

The static modulus of elasticity and poisons ratio were determined on 3 6 in x 12 in concrete cylinders according to ASTM C469-14. The cylinders were cured at 23 ºC and 100% RH, and the tests were performed at the age of 28 days.

8.1.4 Flexural strength (modulus of rupture)

Flexural strength was measured on 3 unreinforced concrete beams of dimensions 6 in x 6 in x 21 in that are cured at 23 ºC and 100% RH. The beams were tested in simply supported third-point loading configuration according to ASTM C78-10 at the age of 3, 7, and 28 days.

8.2 Results and discussion

8.2.1 Autogenous shrinkage of ACMs and OPC

Fig. 43 shows the development of autogenous shrinkage in the OPC and ACM mixtures over 56 days of hydration, while Fig. 44 shows the change in shrinkage for each mixture relative to the OPC. The CSA1, CSA2, CAC2, and AA mixtures generated significantly less total autogenous shrinkage at both 7 and 28 days, compared to the OPC mixture, while the CACT and CSA2P mixtures had equal or greater total autogenous shrinkage. Polymer

addition in CSA2P mixtures might have been the reason for higher shrinkage observed in these mixtures. With hydration in these mixtures, the amount of free water in the capillary porosity reduces, which causes the polymers to polymerize and precipitate in the pores – which can lead to higher shrinkage. Since all the autogenous shrinkage measurements were made from the final setting time, it might be the reason for lower shrinkage values observed in the case of CSA2, CAC2, and AA. Most of the shrinkage for these three cements occurred before the final set and thus is best captured during chemical shrinkage measurements (especially for CSA2 and CAC2) rather than autogenous shrinkage measurements [76]. Additionally, most of the shrinkage developed by the CSA2, CAC2, and AA mixtures was developed during the first 48 hours of measurements, with only small increases continuing over the subsequent 54 days. Increases in shrinkage occurred over a much longer period for the CACT mixture and were likely a result of continued hydration of the calcium silicates present in large proportion in that mixture as the continuing changes in the CACT mixture were similar to those occurring in the OPC mixture (section 4.2.1). Regression of shrinkage appeared to occur in the CAC2 sample at about 28 days of hydration and was believed to indicate the start of conversion in that sample. Conversion results in release of water (Fig. 16) that can lead to regression in shrinkage. CSA3 mixtures showed increasing expansion for about 14 days of hydration and was constant for the remainder of the test period. MPC mixtures exhibited shrinkage until 3 days of hydration and continued to expand significantly thereafter until 14 days of hydration and stayed constant for the remainder of the test period.

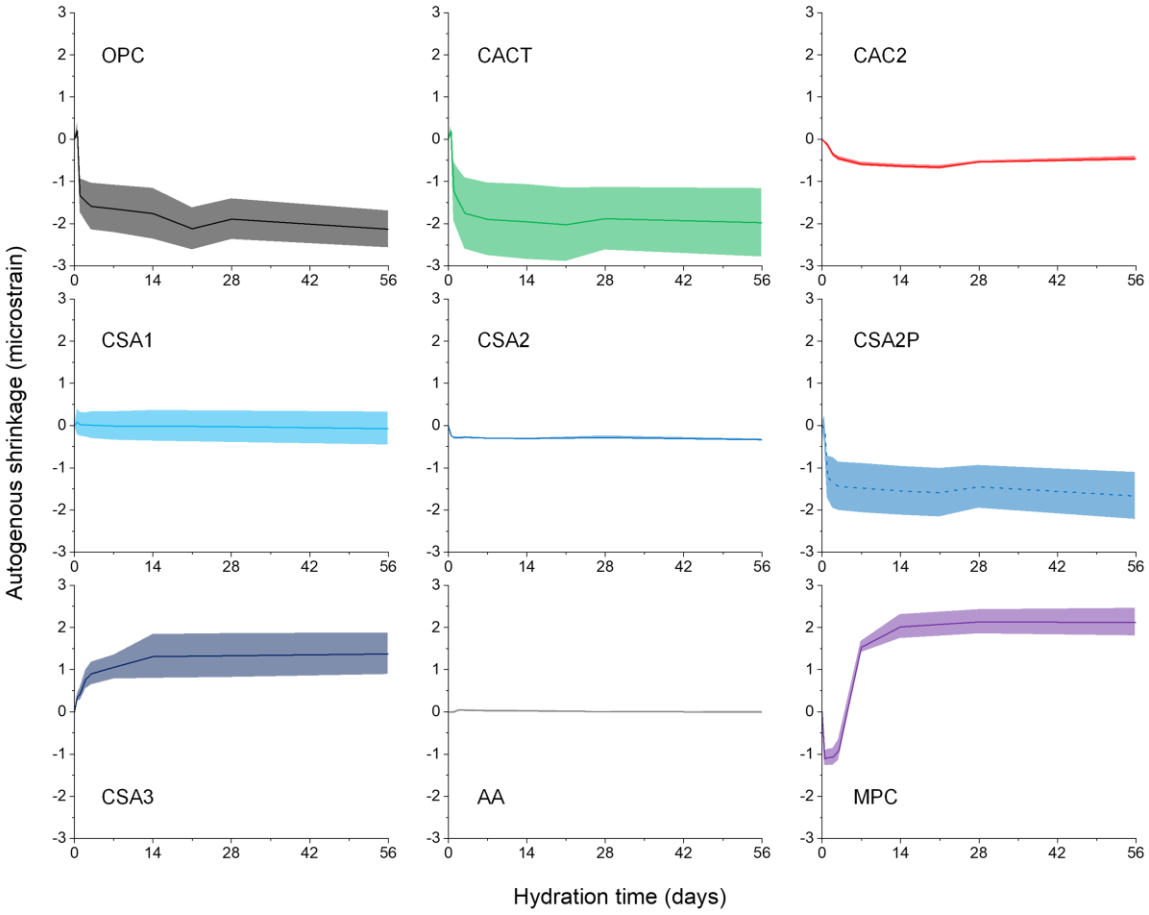

Fig. 43 Autogenous shrinkage of ACM mortar samples over 56 days of hydration.

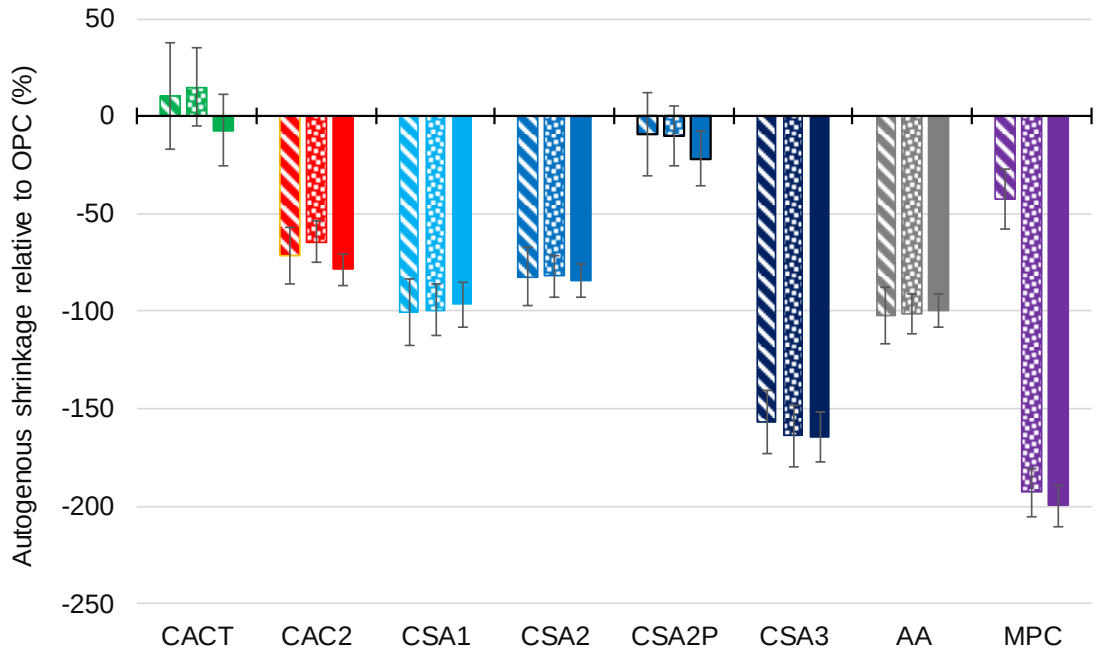

Fig. 44 Relative autogenous shrinkage of the ACM mortar samples compared to that of OPC at 3, 7, and 56 days of hydration.

8.2.2 Mechanical Properties

Fig. 45, Fig. 46, and Fig. 47 shows the concrete compressive strength development over 56 days, flexural strength (modulus of rupture or MOR) development over 28 days, and 28-day elastic modulus and Poisson's ratio, respectively. The ACMs examined – CAC2, CACT, CSA1, and CSA2 – met the performance requirements set (i.e., 7-day strength of 3500psi; 28-day strength of 5000psi; 28-day MOR of 700psi). Even though AA concrete mixers met the 7 and 28-day strength requirements, its 28-day MOR was lower than 700psi. CSA3 mixtures did not meet both the 7-day compressive strength and 28-day MOR requirements. The rates of strength development and the ultimate strength, both in compression and flexure, varied considerably among the ACMs, with CAC2 achieving the highest strengths. However, caution should be taken with CAC2 due to significant strength loss due to conversion, as is beginning to be evident by the slight reduction in strength from

28 to 56 days in CAC2 shown in Fig. 45. CAC2, CSA1, and CSA2 mixtures developed significantly higher strength compared to OPC and other ACM mixtures. These three mixtures even surpassed the 28-day strength requirement after 1 day of hydration. CAC2 and CSA1 mixtures also had higher MOR compared to OPC mixtures at 28 days of hydration. NO significant difference is observed in elastic modulus and Poisson's ratio in ACM mixtures compared to the OPC mixtures after 28 days of hydration.

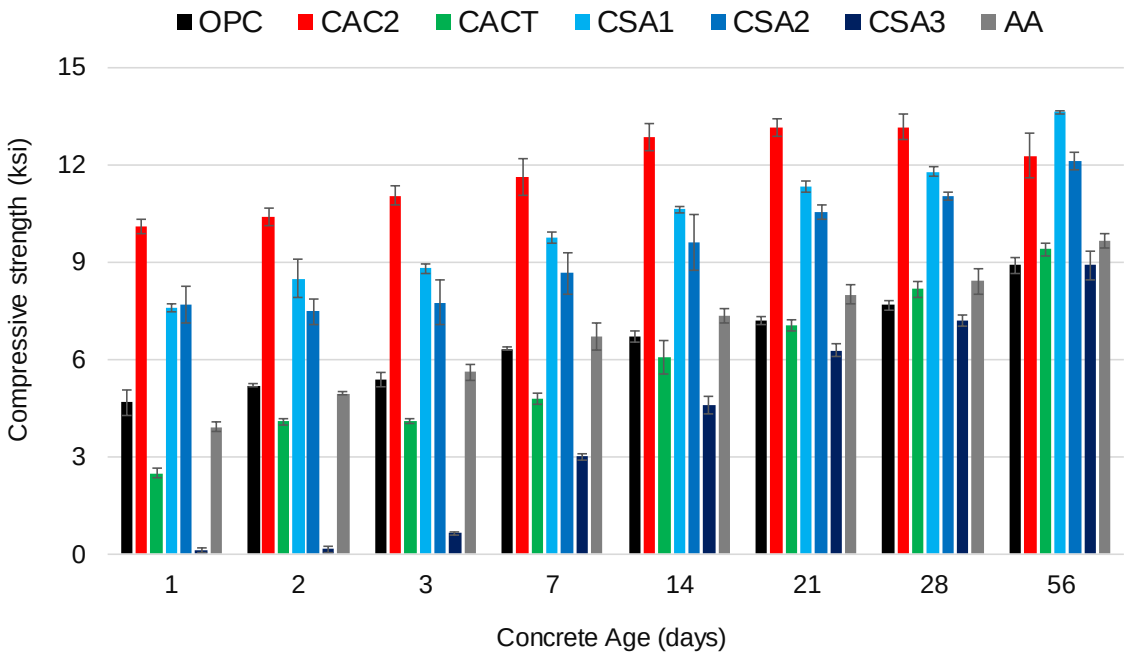

Fig. 45 Compressive strength of ACM and OPC concrete mixtures at different hydration times.

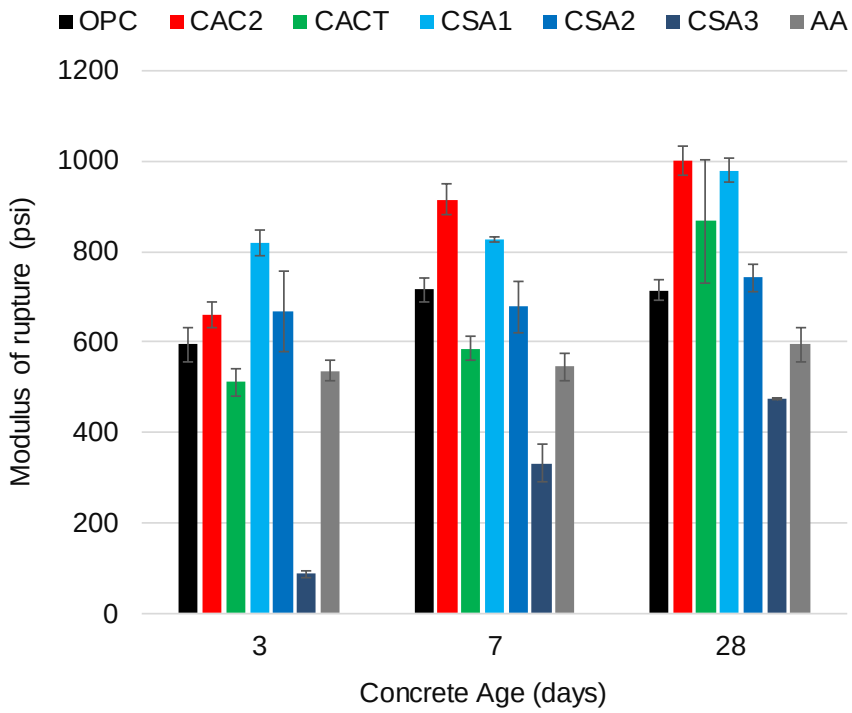

Fig. 46 Flexural strength of ACM and OPC concrete mixtures at different hydration times.

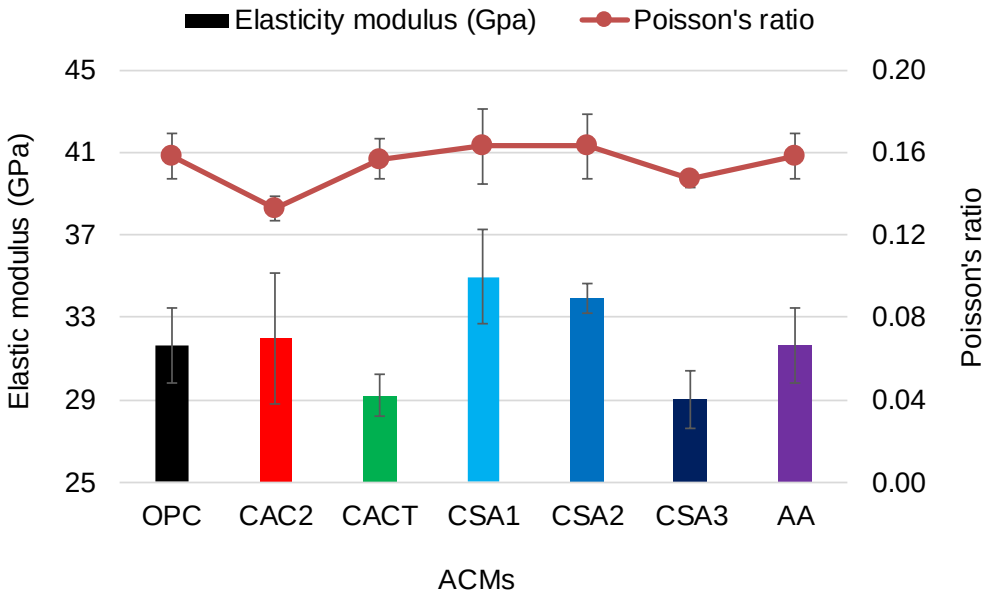

Fig. 47 Modulus of elasticity and poisons ratio of ACM and OPC concrete mixtures at 28 days of hydration time.

8.3 Conclusions and Recommendations

Based on the evaluation performed in this chapter, the following conclusion are made:

- CAC2, CSA1, CSA2, and AA mixtures showed significant lower autogenous shrinkage compared to OPC and other ACM mixtures. Whereas both CSA3 and MPC mixtures exhibited significant expansion. CACT and CSA2P mixtures exhibited significant shrinkage compared to other ACM mixtures but were similar to that of OPC mixtures.

- CACT, CAC2, CSA1, CSA2, and AA mixtures along with the OPC mixtures met the 7-days and the 28-day compressive strength requirements, whereas only OPC, CACT, CAC2, CSA1, and CSA2 mixtures met the 28-day MOR requirement. CSA3 mixtures did not meet both the 7-day compressive strength and 28-day MOR requirements.

- No significant difference is observed in both the elastic modulus and the Poisson's ratio in ACM mixtures compared to that of OPC mixtures.

9 TRANSPORT PROPERTIES

Water sorptivity tests were performed on ACM mortar mixtures at varied w/b to understand its influence on porosity and transport in ACM systems compared to that of OPC. Formation factor measurements were also made over mortar mixtures at varied w/b to understand the effects of w/b and binder composition on permeability and interconnectivity of the system. The range of w/b examined for each ACM was based upon fresh properties, bounding against segregation and stiffness. By examining a range of w/b, the sorptivity tests and formation factor measurements can be used to benchmark the performance of different ACM mixture proportions against OPC.

The current testing protocol for formation factor measurements involves measuring the concrete resistivity and also the pore solution resistivity [77–79]. The pore solution resistivity is determined by either one of the following three approaches [80]: 1) assuming a constant value based on the wide range of binders used in the USA, 2) estimating the pore solution resistivity based on the binder chemistry [81], and 3) experimentally measuring the resistivity on the expressed pore solution. Out of these three approaches, the third approach is the most accurate method for portland cements. ACM systems have a wide range of cement chemistry that are different from portland systems. Also, no virtual models exist to date to predict the pore solution chemistry of ACM systems based on their binder chemistry. The extraction of pore solution can be tedious and may not be reliable, especially for systems that have higher resistivity. Using other pore solution extraction methods such as ex-situ leaching and in-situ leaching methods are found to be not reliable for even portland systems [82–84]. So, neither of the above three approaches can be reliable

in measuring the pore solution resistivity of a wide range of ACM systems. So a new test method (section 9.1.2) is proposed to measure the formation factor in both the OPC and ACM systems. This test method is similar to the formation factor measurement approach used for testing geological rocks, where the rocks are saturated with a known high molar solution (usually ionic brine solution) [85]. Since the resistivity of the filling solution is already known, a simple test to measure the electrical resistivity of the saturated rock is sufficient to calculate the formation factor in those systems. However, the cement-based OPC and ACM systems already possess some pore solution in them, which can change the resistivity of the filling solution. This issue can be avoided by vacuum drying the samples before saturating them with an overwhelming low resistive solution (such as 1N NaOH).

9.1 Methods

9.1.1 Water sorption

The initial and secondary water sorptivity rates were determined on cement mortar discs, averaged from two test specimens. The cylinders of 3 inches (76.2 mm) diameter and 6 inches (152.4 mm) height are cast according to mix proportions given in Table 15 and cured at 23 ºC and 100% RH for 28 days. A standard ASTM 20-30 test sand from Humboldt Mfg. Co. conforming to ASTM C778 specification was used in making all the mortar mixtures. After curing, the cylindrical mortar samples were cut into discs of 3 inches (76 mm) in diameter and thickness of 1.5 inches (38.1 mm) using a wet tile saw. Later, the mortar discs were further cured for an additional 28 days at 55% RH, and epoxy coated on all sides except one end of the flat surface. After the epoxy coat dried, the uncoated side of the sample was exposed to water with 1 to 2 mm of the sample immersed. The uptake of

water is measured by weighing the specimens at intervals of 30 min, 60 min, every hour until 6 hours to determine initial sorption rate; and once a day up to 7 days to determine secondary sorption rate. The sorption rate ($mm/s^{0.5}$) is measured using the slope of the line that is the best fit to water absorption plotted against the square root of time ($s^{0.5}$), according to ASTM C1585-13.

Table 15 Cement mortar mixture proportions for water sorptivity and formation factor tests.

Cement	w/b	Admixtures (by weight of cement)	Cement (units)	Water (units)	Sand (units)
OPC	X = (0.4, 0.45, 0.485)	-	100	100*X	275
CACT	X = (0.35, 0.4, 0.45, 0.485)	Citric acid – 1.5%	100	100*X	271
CAC2	X = (0.4, 0.45, 0.485, 0.55)	-	100	100*X	273
CSA1	X = (0.4, 0.45, 0.485, 0.55, 0.60)	Citric acid – 2.0%	100	100*X	268
CSA2	X = (0.35, 0.4, 0.45, 0.485)	Citric acid – 0.5%	100	100*X	268
CSA2P	X = (0.35, 0.4, 0.45, 0.485)	Citric acid – 0.5%	100	100*X	268
CSA3	X = (0.35, 0.4, 0.45, 0.485, 0.55)	Citric acid – 0.5%	100	100*X	273
AA	X = (0.21, 0.233, 0.25, 0.30, 0.35, 0.40, 0.45)	Activator 1 – 2.47% Activator 2 – 2.21%	100	100*X	259
MPC	X = (0.25, 0.30, 0.35, 0.40, 0.45)	Boric acid – 14%	100	100*X	264

9.1.2 Formation factor

The formation factor was measured on cement mortar discs, averaged from two test specimens. The cylinders of 3 inches (76.2 mm) diameter and 6 inches (152.4 mm) height are cast according to mix proportions given in Table 15 and cured at 23 ºC and 100% RH for 28 days. Then they were cut into discs of 3 inches (76 mm) in diameter and thickness of 1.5 inches (38.1 mm) using a wet tile saw. Later, the mortar discs were further cured for an additional 28 days at 23 ºC and 55% RH. After curing, the mortar discs were dried in

vacuum for 2 hours, purged with dry N_2 gas, and the initial weight (W_1) was taken. Immediately after taking the initial weight measurement, the samples were saturated with 1N NaOH solution (except for MPC — which was saturated with 1N KCl solution) according to the vacuum conditioning procedure adapted from ASTM 1202-19 (section 9). After conditioning, the weight of the saturated mortar disc (W_2) and its bulk electrical resistivity was measured. The bulk resistivity was measured according to the test setup shown in Fig. 48. Formation factor (F) of the mixture was determined according to Equation 5 [86], where the bulk resistivity of the saturated solution (1N KCl solution for MPC, 1N NaOH solution for the rest) was determined using the concentration of ions present in solution according to the method given in Snyder et al. [87]. The total porosity was measured according to Equation 6. The formation factor is plotted against total porosity in log-log plot (Fig. 49) to verify if the relationship between formation factor and total porosity follows Archie's law [88] in heterogenous mixtures [89,90] according to Equation 7, where F is formation factor, Φ is total porosity, m is pore geometry exponent, and A is pore geometry (tortuosity) factor.

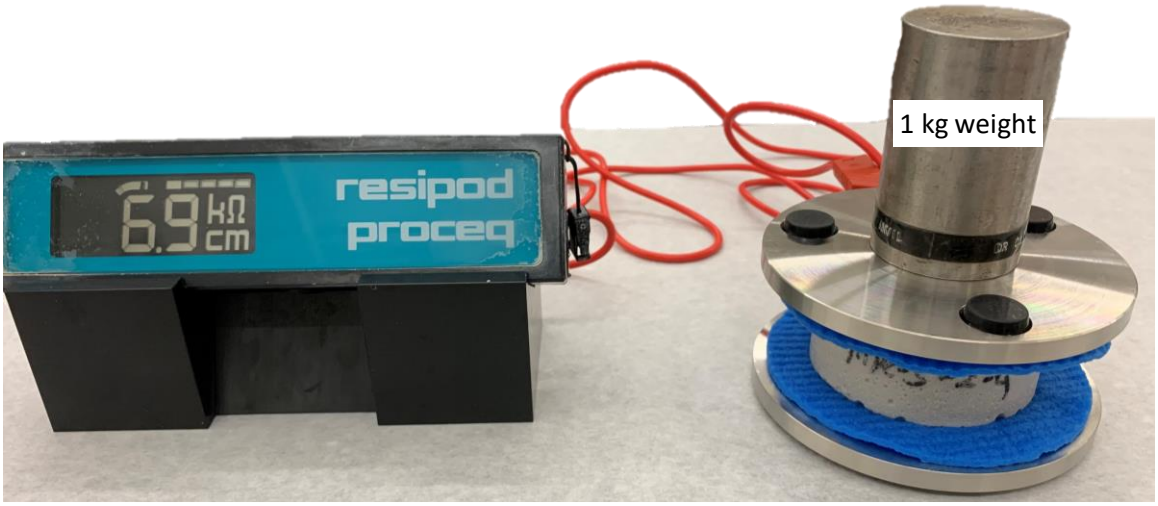

Fig. 48 Test setup for measuring the bulk electrical resistivity of saturated specimens.

Equation 5

$$Formation\ factor\ (F) = \frac{Bulk\ resistivity\ of\ cement\ mortar\ disc}{Bulk\ resistivity\ of\ the\ solution\ used\ for\ saturation}$$

Equation 6

$$Total\ porosity\ (\Phi) = \frac{100 \times (W_2 - W_1)}{(density\ of\ saturated\ solution) \times (volume\ of\ mortar\ disc)}$$

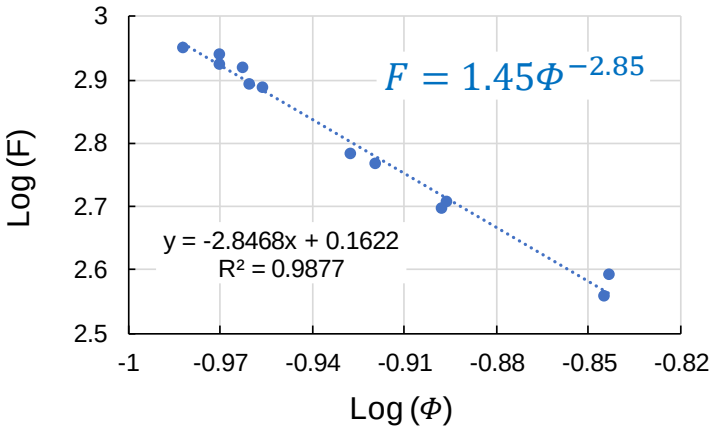

Fig. 49 Formation factors versus total porosity at varied w/b.

Equation 7

$$F = A \times \Phi^{-m}$$

9.2 Results and Discussion

9.2.1 Water sorption

Fig. 50 shows the initial and secondary sorption rate of ACM mortar mixtures at varied w/b compared to OPC mixtures at w/b of 0.40, 0.45, and 0.485. The total amount of water sorption after 7 days of exposure is given in Fig. 51. First, for the OPC, as expected, with increasing w/b, an increase in initial and secondary sorption rates and an increase in total water sorption was observed due to an increase in porosity and pore structure interconnectivity [91]. At w/b of 0.485, a reduction in secondary sorption rate was observed – likely due to the significantly higher initial sorption. The initial and secondary sorption rates can be related to the penetration of foreign substances, especially in relatively dry and partially saturated concrete, where the external substances (such as Cl ions) permeate into

the system along with water. So, higher initial sorption rates with lower secondary sorption rate could imply higher penetration rates of external substances with shallow penetration depths (e.g., due to capillary suction), whereas higher initial and secondary sorption rates imply higher penetration rates with higher penetration depths [92].

In CACT mixtures, the initial sorption rate significantly increased with an increase in w/b from 0.35 to 0.45, and slightly decreased with further increase in w/b to 0.485. The secondary sorption rate also increased with an increase in w/b from 0.35 to 0.40 but decreased with further increase in w/b to 0.485. At a w/b between 0.40 and 0.485, the initial sorption rate in CACT is at least three times that of corresponding w/b in OPC – suggesting significantly higher interconnectivity in the porosity in CACT mixtures compared to OPC at this w/b. The secondary sorption rate is also higher in CACT mixtures at w/b of 0.40 and 0.45 compared to that of OPC. However, the secondary sorption rate at 0.485 is similar to that of OPC. Even at w/b of 0.40 and 0.45, the initial and secondary sorption rates in CACT were significantly higher compared to that of OPC at w/b of 0.485. Also, the total water sorption at 7 days is higher in CACT at w/b greater than or equal to 0.40 compared to OPC at 0.485. However, at w/b of 0.35, the initial and secondary sorption rates, as well as the total sorption is significantly lower in CACT mixtures compared to that of OPC at 0.4 w/b.

In CAC2 mixtures, the initial sorption rate increased with an increase in w/b from 0.40 to 0.45. But it decreased with an increase in w/b from 0.45 to 0.485, and significantly increased with further increase in w/b to 0.55. The decrease in the initial sorption rate between w/b of 0.45 and 0.485 could be due to the increase in initial dispersion of cement grains leading to a greater extent of hydration. However, the secondary sorption rate decreased with an increase in w/b from 0.40 to 0.55. All the CAC2 mixtures at w/b greater

or equal to 0.45 have higher or similar initial sorption rates to that of OPC mixture at 0.485, and the secondary sorption rates are significantly higher even at w/b of 0.40 compared to OPC at both 0.40 and 0.485 – resulting in higher total sorption (after 7 days) at 0.40 compared to OPC at 0.40. The total sorption for CAC2 mixtures at w/b 0.45 is even higher than the OPC mixtures at 0.485 w/b. Overall the CAC2 mixtures have significantly higher water sorption compared to the corresponding OPC mixtures – suggesting significantly greater interconnectivity in the porosity in CAC2 mixtures compared to OPC mixtures.

The initial and secondary sorption rates increased with an increase in w/b in CSA1 mixtures. The initial sorption rates in CSA1 mixtures are either lower or similar to the corresponding OPC mixtures at the same w/b. Also, even the initial sorption rate in CSA1 mixtures at w/b of 0.6 is lower compared to OPC mixtures at 0.485 w/b. However, the secondary sorption rates are either similar or significantly higher compared to OPC mixtures at corresponding w/b ratios. The total water sorption at every w/b (except at 0.45) is also higher in CSA1 mixtures compared to the OPC mixtures.

In CSA2 mixtures, like CACT, the initial sorption rates increased with an increase in w/b from 0.40 to 0.485, whereas the secondary sorption rates decreased with an increase in w/b. At a w/b of 0.40, 0.45, and 0.485, the initial sorption rate in the CSA2 mixtures are significantly higher compared to that of OPC at the corresponding w/b – again suggesting greater interconnectivity in the porosity in CSA2 mixtures (like CACT) compared to OPC. The CSA2 mixture also had a higher initial sorption rate even at w/b of 0.45 compared to OPC at 0.485, but the secondary sorption rate at all the w/b investigated in this paper (except 0.35) was either similar or lower compared to OPC at both 0.40 and 0.45. Overall, the total sorption in CSA2 mixtures is also significantly higher compared to that of OPC

mixtures at corresponding w/b. The total sorption in the CSA2 mixture at w/b of 0.35 is even higher compared to OPC mixtures at w/b of 0.4.

CSA2P mixtures showed significant improvement in sorption rates compared to CSA2 mixtures – likely due to polymer addition. The initial sorption rates in CSA2P mixtures at w/b of 0.40, 0.45, and 0.485 are significantly lower compared to the corresponding OPC mixtures. The secondary sorption rate and the total water sorption at w/b of 0.4 is also significantly lower (at least 3 times lower) compared to that of OPC mixtures. However, at w/b of 0.45 and 0.485, the secondary sorption rates and the total water sorption are higher in CSA2P mixtures compared to that of OPC mixtures.

The initial sorption rates in CSA3 mixtures increased with an increase in w/b from 0.35 to 0.40 but continuously decreased with further increase in w/b to 0.55. However, the secondary sorption rates remained constant with w/b. The initial sorption rates in CSA3 mixtures are significantly higher compared to that of OPC mixtures at w/b of 0.40 and 0.45. Whereas it is similar to OPC at w/b of 0.485. However, the secondary sorption rates are lower compared to that of OPC at w/b of 0.40 and 0.45. Overall the total water sorption in CSA3 mixtures at w/b between 0.40 and 0.55 is significantly higher compared to OPC mixture even at w/b of 0.485, and the total sorption at w/b of 0.35 in CSA3 is similar to OPC at 0.45 w/b – suggesting greater interconnectivity in the porosity in CSA3 mixtures (like CACT and CSA2) compared to OPC mixtures.

In AA mortar mixtures, since the amount of water required for hydration is significantly lower compared to OPC and other ACMs evaluated in this paper, the w/b was limited to 0.35 (to prevent bleeding and segregation). However, the data corresponding to the AA

mixture at w/b of 0.40 and 0.45 are still shown. These mixtures experienced heavy bleeding during curing – so no efforts were made in explaining the data corresponding to these two w/b. The initial sorption rates in AA mixtures did not change significantly with an increase in w/b from 0.233 to 0.35. However, the secondary sorption rates decreased with an increase in w/b from 0.233 to 0.25 but increased significantly thereafter. At w/b ratios between 0.233 and 0.35, all the AA mixtures had higher initial sorption rates and total water sorption compared to OPC mixture at w/b of 0.40 and lower compared to the OPC mixtures at 0.485 w/b.

Similar to AA mixtures, the MPC mixtures also experienced bleeding at higher w/b – but only at 0.45 w/b. The initial sorption rates increased with an increase in w/b from 0.25 to 0.40 in MPC mixtures. The secondary sorption rates also increased with an increase in w/b from 0.25 to 0.30 but decreased significantly thereafter with further increase in w/b to 0.40. The initial sorption rates in MPC at w/b of 0.25 and 0.30 are significantly lower compared to that of OPC mixtures at 0.40, and were either similar or higher in MPC mixture at w/b to 0.35 and 0.40 compared to OPC mixtures at 0.485 w/b. The total water sorption in MPC mixtures at w/b of 0.25 and 0.30 is lower compared to OPC mixtures at 0.45. However, at w/b of 0.35 and 0.40, the total sorption in MPC mixtures is similar or higher compared to OPC mixtures at 0.485 w/b.

Overall, all the ACM mixtures (except CSA2P, AA, and MPC) had higher total sorption compared to OPC at the same w/b of 0.40, 0.45, and 0.485. The CSA1 mixture at 0.45 w/b had slightly lower total sorption compared to OPC at the same w/b. At w/b less than or equal to 0.485, the CACT mixtures exhibited higher differences in initial sorption rates with changes in w/b compared to OPC and other ACM mixtures – suggesting CACT

mixtures are more sensitive to changes in w/b with initial sorption rate compared to other ACMs investigated here. CSA2P mixtures exhibited higher sensitivity to w/b with the secondary sorption rates as well as the total water sorption.

In order to design mixtures with similar sorption compared to OPC at 0.40, the w/b in all the ACM mixtures (except CSA2P) should be less than 0.40. The CSA2P mixture at 0.4 w/b has significantly lower sorption compared to that of OPC. In the AA mixture, the total sorption w/b should be further lower than 0.233 and 0.30. Whereas in MPC it should be lower than 0.30.

9.2.2 Formation factor

Fig. 52, Fig. 53, and Fig. 54 shows the total porosity, formation factor, and interconnectivity in OPC and ACM mixtures at varied w/b, respectively. In OPC mixtures, as expected, the formation factor reduces with an increase in the w/b ratio. At 0.4 w/b, the formation factor in OPC mixtures is about 820, and it dropped to about 470 at 0.485 w/b.

Similar to OPC, the formation factor also reduced in CACT mixtures with an increase in w/b. However, the formation factors were significantly lower compared to the corresponding OPC mixtures. At w/b of 0.35, the formation factor in CACT mixtures is lower than the OPC mixtures at 0.485 w/b – even though the total porosity in CACT mixtures at 0.35 w/b is lower than OPC mixtures at 0.485 w/b. Overall this resulted in significantly greater interconnectivity in the porosity in CACT mixtures compared to the OPC mixtures.

In CAC2 mixtures, no trend in the formation factor and total porosity is observed with an increase in w/b. This could be due to conversion that is continuously happening in CAC2 mixtures, and the rate of which depends on multiple factors such as w/b, hydration, etc. Overall, the total porosity in the CAC2 mixtures between w/b of 0.40 to 0.55 is similar to OPC mixtures at 0.485 w/b. And the formation factor in CAC2 mixtures at these w/b is significantly lower compared to OPC mixtures even at 0.485 w/b. The formation factor in CAC2 mixtures is also lower in CAC2 mixtures compared to CACT mixtures, but only at w/b of 0.40 and 0.45. Similar to the CACT mixtures, the CAC2 mixtures also have significantly higher interconnectivity in pore structure compared to the OPC mixtures.

Similar to OPC and CACT mixtures, the formation factor in CSA1 mixtures increased, and the total porosity decreased with an increase in w/b. At w/b of 0.40 and 0.45, the formation in CSA1 mixtures is significantly higher (about 60% higher) compared to OPC mixture at corresponding w/b. However, at w/b of 0.485, the formation in CSA1 mixtures is similar to that of OPC mixtures at 0.485 w/b. This resulted in significantly lower interconnectivity in the CSA1 mixtures compared to the OPC mixtures, especially at w/b lower than 0.485.

In CSA2 mixtures, the formation factor also increased, and the total porosity also decreased with an increase in w/b. Compared to OPC mixtures, the total porosity is higher, and the formation is lower in CSA2 mixtures at the corresponding w/b. The formation factor in CSA2 mixture at w/b of 0.35 is even lower compared to OPC mixtures at w/b of 0.40 – suggests higher interconnectivity in CSA2 mixtures compared to OPC and CSA1 mixtures.

In CSA2P mixtures, the formation factor at w/b to 0.40 is about 4150 and is about 5 times and 3 times higher compared to OPC and CSA1 mixtures at the same w/b. However, with

further increase in w/b to 0.45, the formation factor dropped to about 235, significantly lower compared to both the OPC and CSA1 mixtures. The significantly higher formation factor and lower interconnectivity at 0.40 are due to the polymer addition, and the significant drop in formation with an increase in w/b to 0.45 suggests that the polymer addition is only effective at lower w/b. At higher w/b of 0.45 and 0.485, the polymer addition only showed modest improvements in formation factor compared to the CSA2 mixtures at the corresponding w/b. At w/b of 0.35, the formation factor in CSA2P mixtures is significantly lower compared to the mixture at w/b of 0.40. The CSA2P mixtures experienced heavy compaction issues at w/b of 0.35 – which could be the reason for the lower formation factor.

In CSA3 mixtures, the formation factor also increased, and the total porosity decreased with an increase in w/b. The total porosity in CSA3 mixtures was significantly higher, and the formation factor was significantly lower compared to the corresponding OPC mixtures – which resulted in overall significantly higher interconnectivity in the porosity of CSA3 mixtures compared to the OPC mixtures.

In the AA mixtures, the total porosity increased with an increase in w/b from 0.210 to 0.233, even though the formation was essentially constant. This suggests the extra porosity created was dispersed around the matrix with no increase in interconnectivity between them. With further increase in w/b from 0.233 to 0.300, the total porosity and the formation factor was essentially constant – which suggests all the extra mix water added is participating is hydration. But further research is required to validate this hypothesis. The formation factor in AA mixtures in w/b between 0.210 and 0.300 is similar to that of OPC

mixtures at 0.40 w/b, and the interconnectivity in w/b between 0.233 and 0.300 in the AA mixtures is lower compared to the OPC mixtures at 0.40 w/b.

The total porosity increased in MPC mixtures with an increase in w/b, and it is significantly higher compared to that of OPC and other ACM mixtures. Whereas the formation factor remained constant with an increase in w/b, and they were significantly lower compared to OPC mixtures. This resulted in significantly higher interconnectivity in MPC mixtures, even at w/b of 0.25, compared to OPC mixtures, even at w/b of 0.485.

Overall, CSA1 and AA mixtures had either lower or similar interconnectivity of pore structure compared to the OPC mixtures. CSA2P mixtures also had significantly lower interconnectivity, but only at w/b of 0.40. CSA2 mixtures had higher interconnectivity compared to OPC mixtures, but not significantly higher. Whereas CACT, CAC2, CSA3, and MPC mixtures have significantly higher interconnectivity compared to the OPC and the other ACM mixtures.

Fig. 55 shows the relationship between the formation factor and the total porosity plotted in log-log scale for OPC and ACM mixtures at varied w/b. A linear relationship exists between formation factor in log-log scale for all the OPC and ACM mixtures except CAC2 mixtures. As discussed earlier, the CACs mixtures undergo conversion, which changes the porosity and may also influence the interconnectivity and the shape of the pore structure. In both CSA3 and AA mixtures, a bilinear relation is observed in the w/b examined in this chapter. This suggests a change in the pore structure parameters in both these mixtures at lower w/b (w/b < 0.40 in CSA3 and w/b < 0.233 in AA mixtures).

Fig. 56 shows the relationship between the formation factor and the total porosity plotted in log-log scale for ACM mixtures at varied w/b compared to OPC mixtures at 0.40 and 0.485 w/b. Only the mixtures that have lower porosity than OPC mixtures at w/b of 0.40 have higher formation factor compared to the OPC mixtures at 0.40 w/b. Similarly, all the ACM mixture that has higher porosity compared to the OPC mixtures at 0.485 w/b have formation factors lower than OPC at w/b of 0.485. However, between the porosity ranges of OPC mixtures at 0.40 and 0.485 w/b, all the ACM mixtures except AA mixtures have lower formation factors compared to that of OPC mixtures at 0.485 w/b.

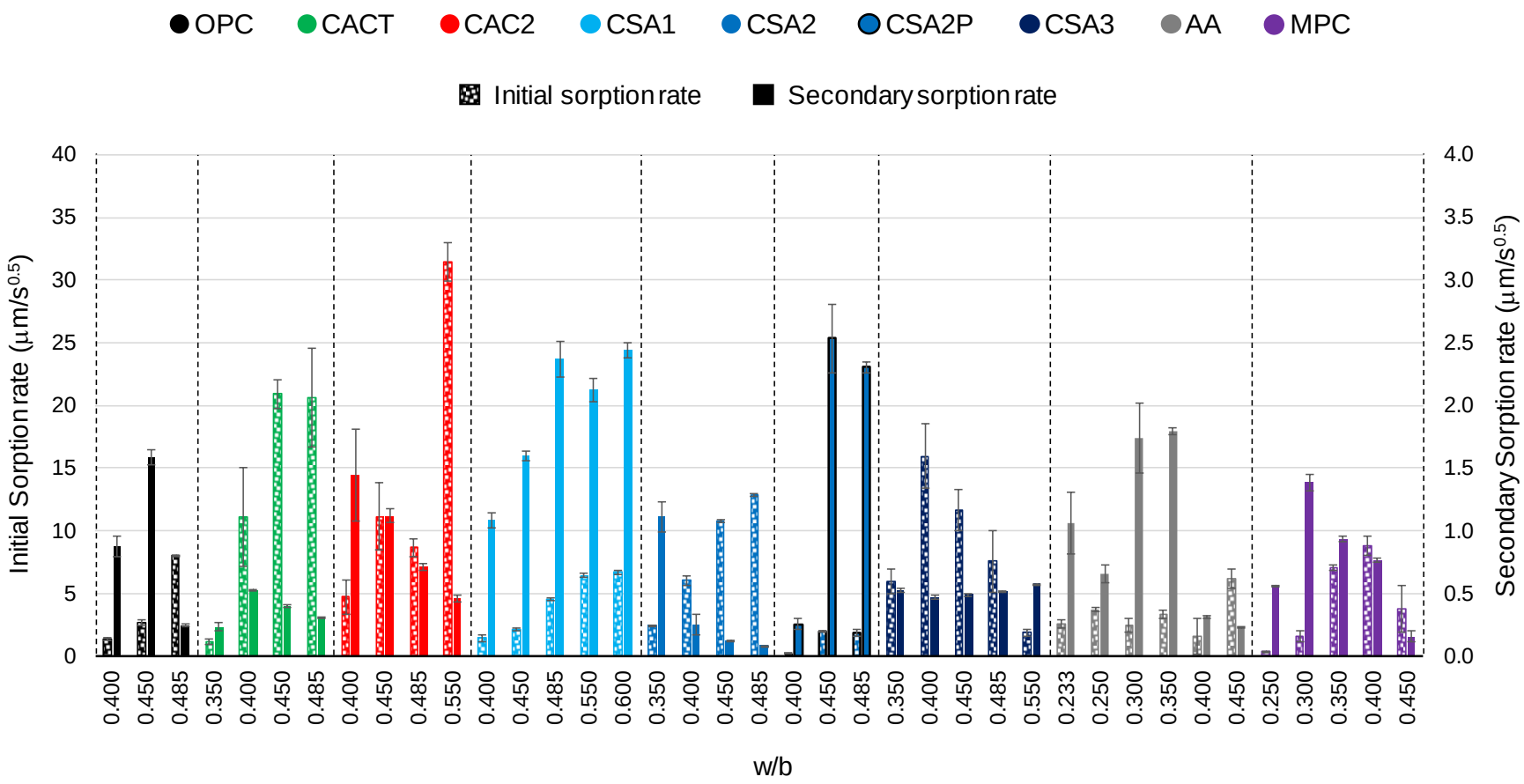

Fig. 50 Initial and secondary water sorption of ACM mixtures at varied w/b compared to OPC mixture at w/b of 0.4 (25.4 µm = 10^{-3} inches).

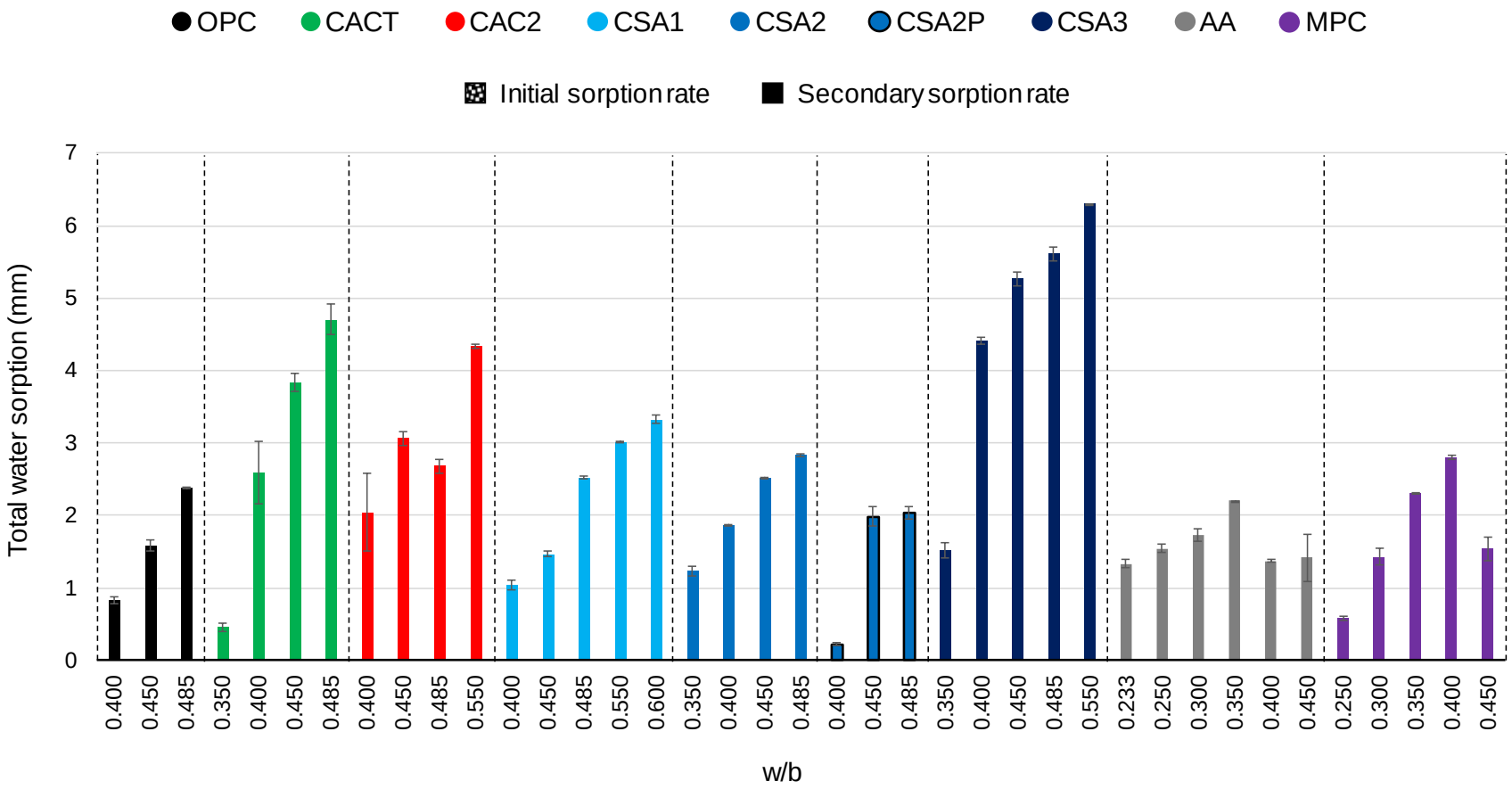

Fig. 51 Total water sorption of ACM mixtures at varied w/b compared to OPC mixture at w/b of 0.4.

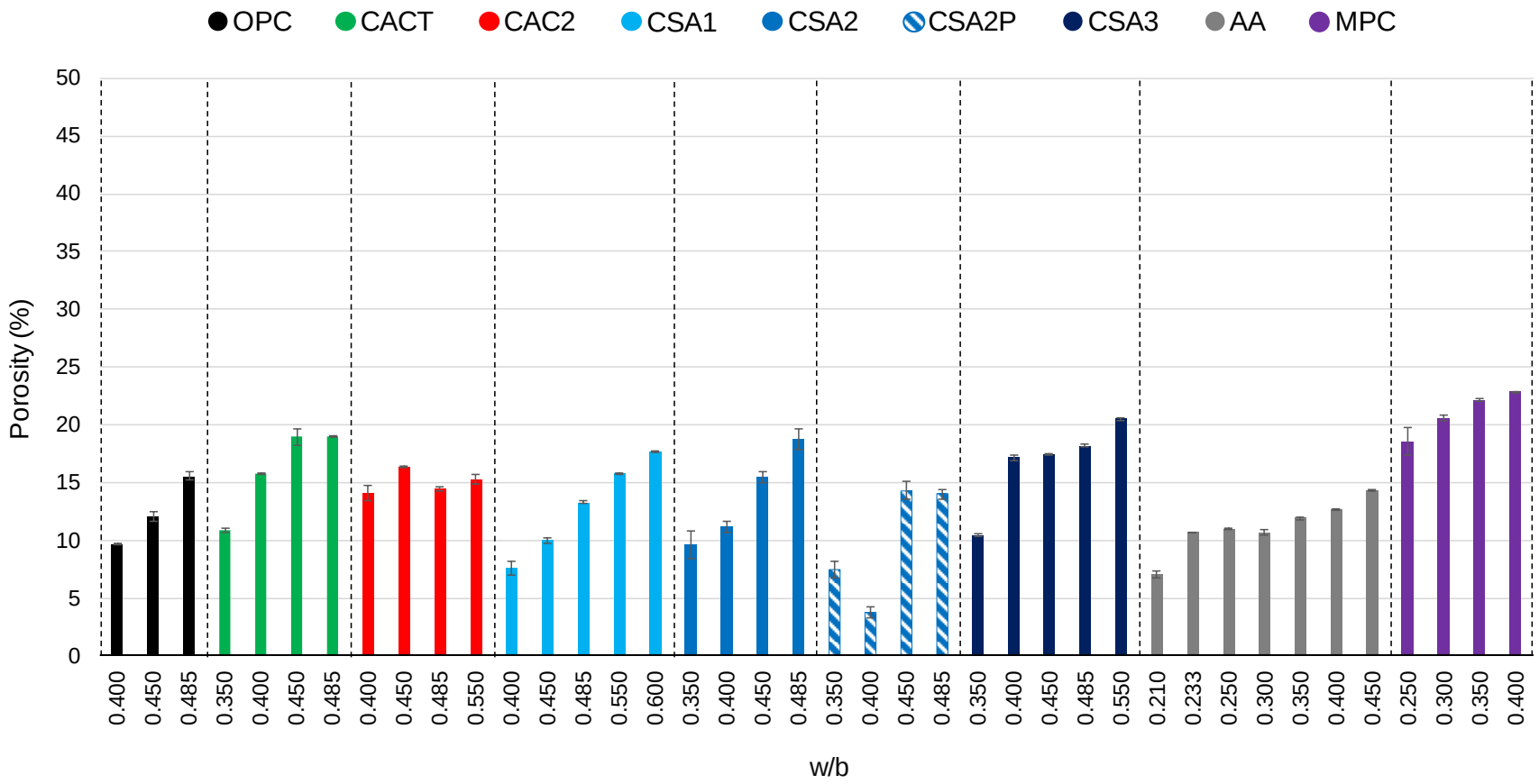

Fig. 52 Total porosity in ACM mortar mixtures compared to that of OPC at varied w/b.

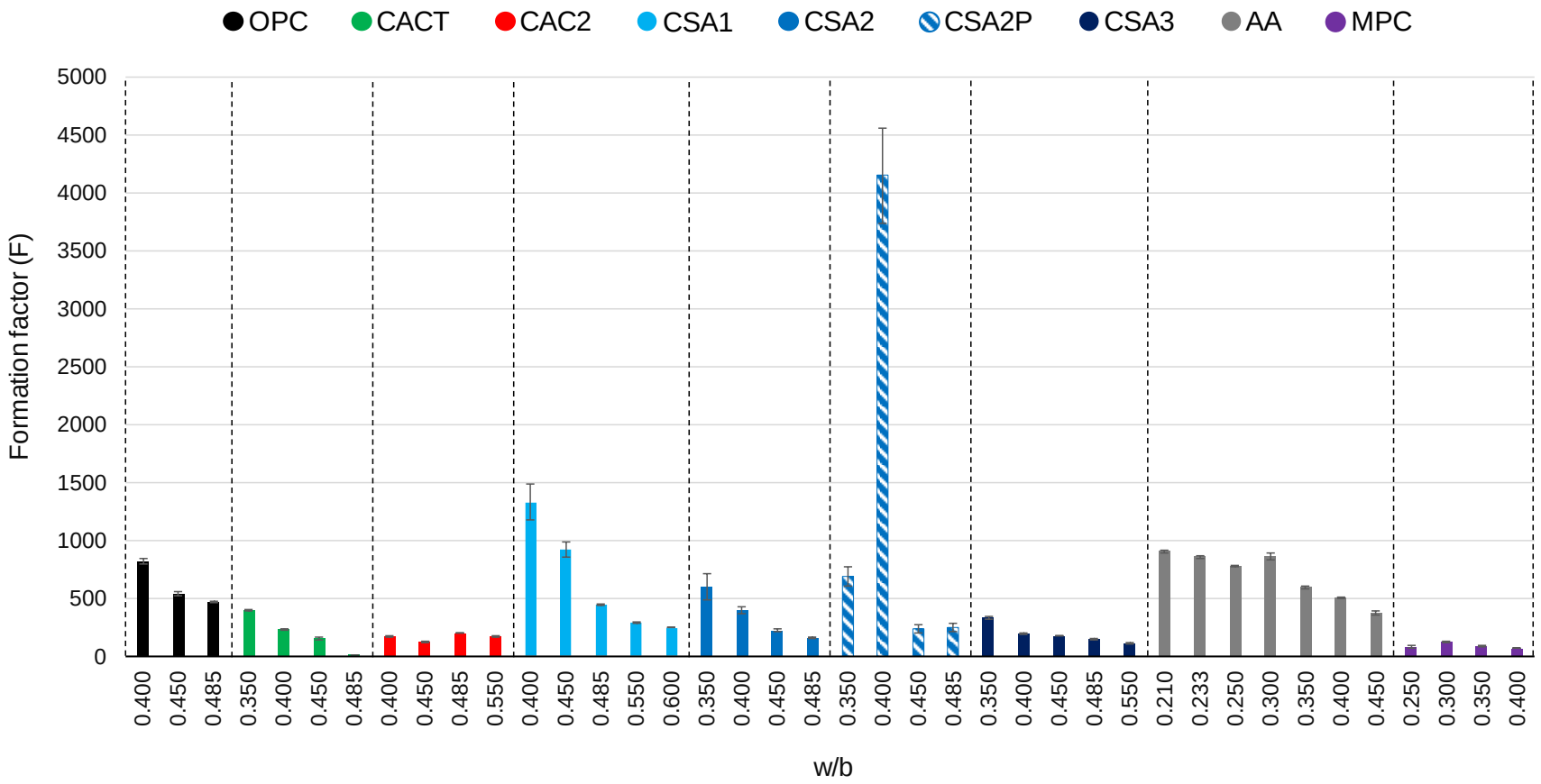

Fig. 53 The formation factor in ACM mortar mixtures compared to that of OPC at varied w/b.

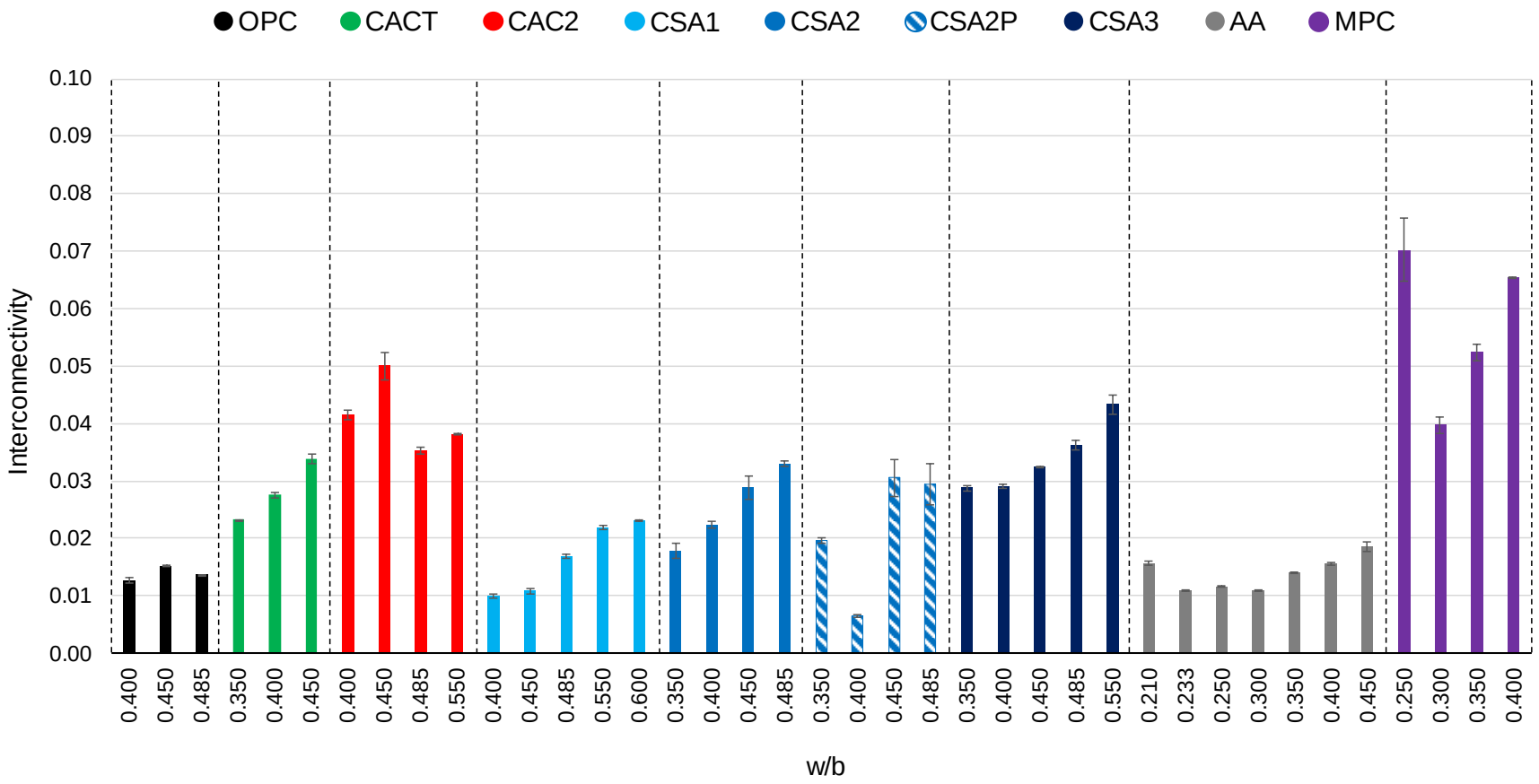

Fig. 54 Interconnectivity in ACM mortar mixtures compared to that of OPC at varied w/b. Note: the interconnectivity of CACT mixtures at 0.485 w/b is 0.536, and is not shown in the graph since it is significantly higher (at least 7.5 times higher) compared to others.

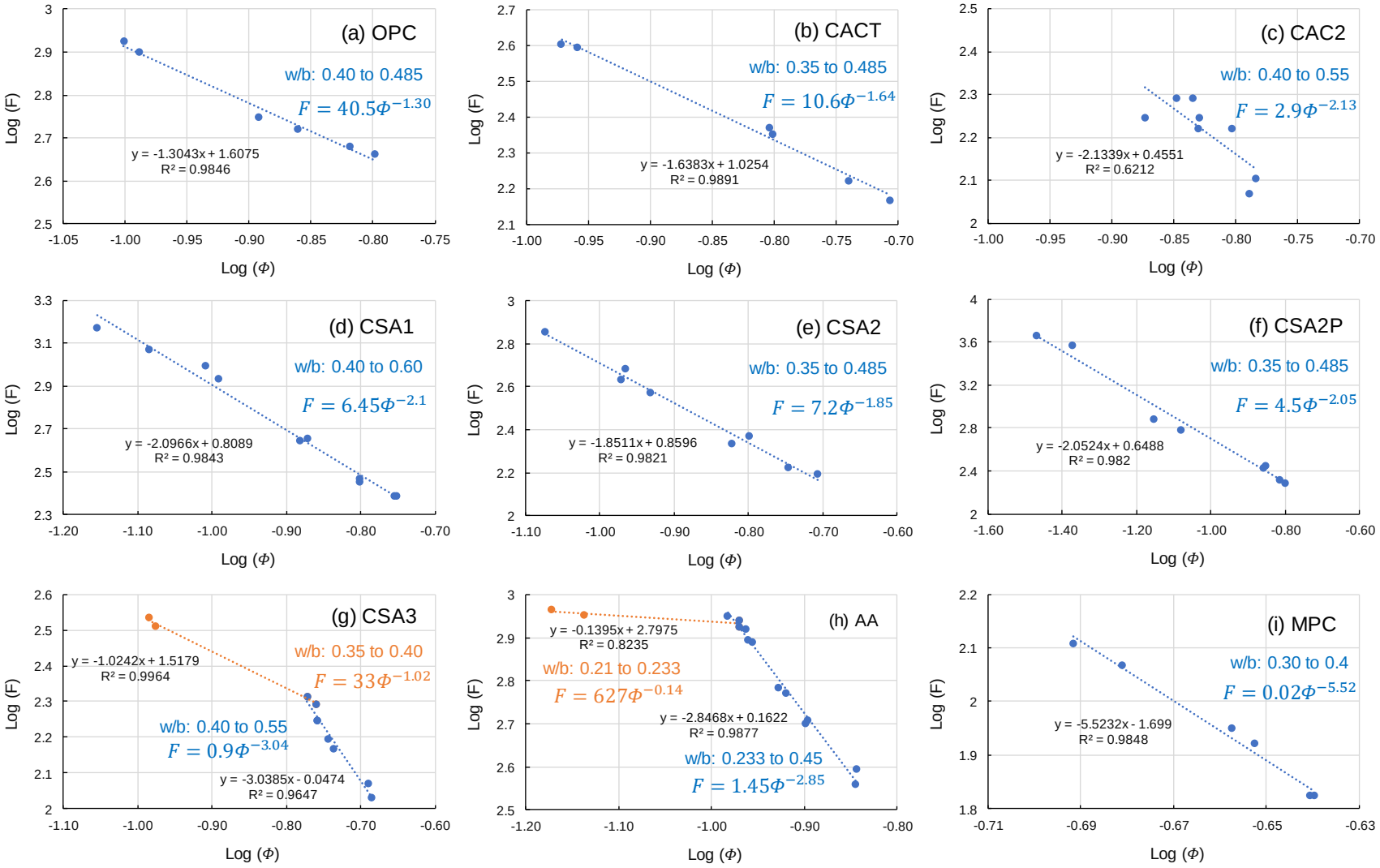

Fig. 55 Formation factor (F) versus total porosity (Φ) in ACM and OPC mortar mixtures at varied w/b.

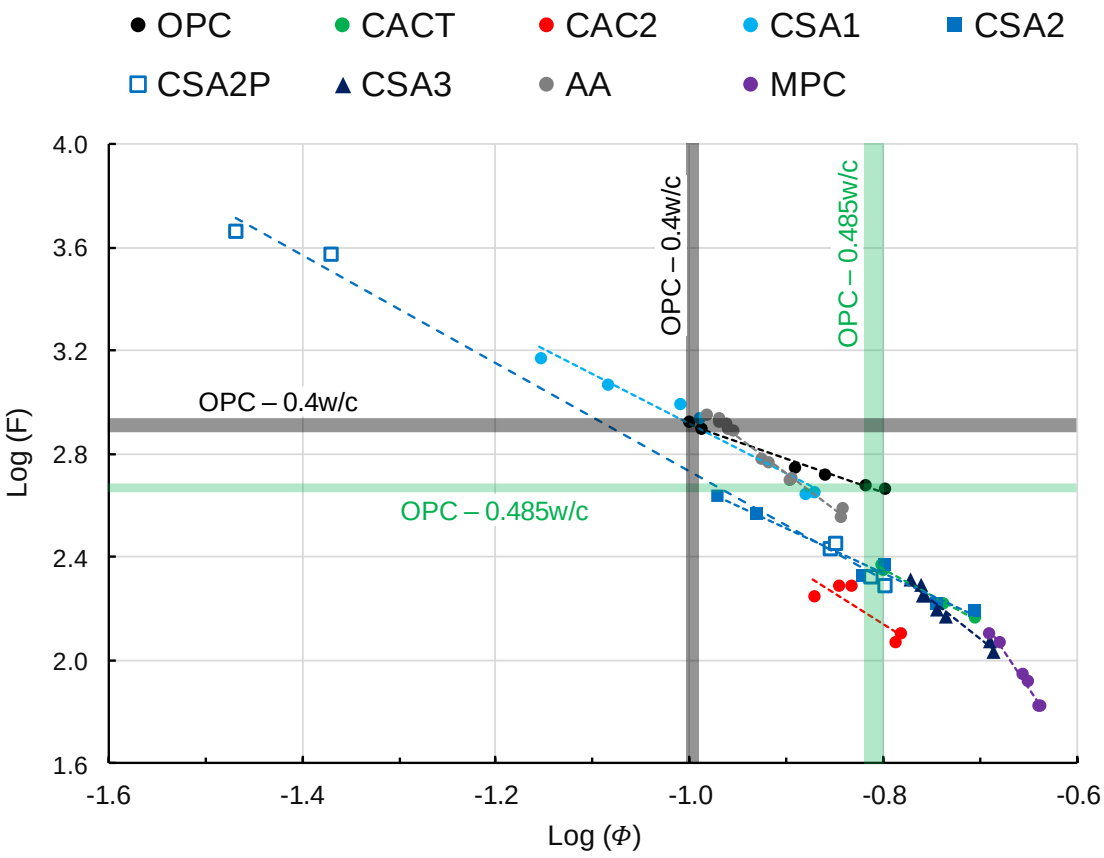

Fig. 56 Formation factor (F) versus total porosity (Φ) in ACM mortar mixtures compared to that of OPC at varied w/b.

9.3 Conclusions and Recommendations

A new test method was proposed and used to measure the formation factor in OPC and ACM mixtures. Water sorptivity, total porosity, and formation factor measurements performed in this study at a range of w/b were used to evaluate the performance of commercially available ACMs and their sensitivity towards w/b in resisting ingress of foreign substances. Analyzed together, this series of tests has led to the following conclusions:

- The influence of w/b on sorptivity (as influenced by porosity and pore structure) varied with different binder systems, with CACT being the most sensitive to variations in w/b

of all. At w/b less than or equal to 0.485, the CACT mixtures exhibited higher differences in initial sorption rates with changes in w/b compared to OPC and other ACM mixtures investigated in this chapter.

- All the ACM mixtures (except CSA2P, AA, and MPC) had higher total sorption compared to OPC at the same w/b of 0.40, 0.45, and 0.485. The CSA1 mixture at 0.45 w/b had slightly lower total sorption compared to OPC at the same w/b. CSA2P mixtures exhibited higher sensitivity to w/b with the secondary sorption rates as well as the total water sorption.
- The total sorption is significantly higher in CAC, CACT, and CSA mixtures. The AA mixtures had significantly lower sorption compared to OPC and other ACMs but were also produced at lower w/b (per manufacturer recommendations and due to their different reaction chemistry).
- To design mixtures with similar or lower sorption compared to OPC at 0.40, the w/b in all the ACM mixtures (except CSA2P) should be less than 0.40. The CSA2P mixture at 0.4 w/b has significantly lower sorption compared to that of OPC. In the AA mixture, the w/b should be further lower than 0.233 and 0.30. Whereas in MPC it should be lower than 0.30.
- Overall, CSA1 and AA mixtures had either lower or similar interconnectivity of pore structure compared to the OPC mixtures. CSA2P mixtures also had significantly lower interconnectivity, but only at w/b of 0.40. CSA2 mixtures had higher interconnectivity compared to OPC mixtures, but not significantly higher. Whereas CACT, CAC2, CSA3, and MPC mixtures have significantly higher interconnectivity compared to the OPC and the other ACM mixtures.

- A linear relationship exists between formation factor and porosity in a log-log scale for all the OPC and ACM mixtures except CAC2 mixtures. In both CSA3 and AA mixtures, a bilinear relation is observed in the w/b examined in this chapter. This suggests a change in the pore structure parameters in both these mixtures at lower w/b ($w/b < 0.40$ in CSA3 and $w/b < 0.233$ in AA mixtures).
- More research is needed to validate the proposed test method for measuring formation factor, such as a comparative study of relating formation factor measured with this new test method with apparent chloride diffusion coefficient measurements on a wide range of ACM and OPC mixtures.

10 RESISTANCE TO CHEMICAL SULFATE ATTACK

Chemical sulfate attack is a vital durability parameter as it often results in significant cracking, decomposition, and spalling of concrete structures that get exposed to sulfates from seawater, brackish water, groundwater, industrial and agricultural effluents, and coastal soils. When exposed to an aggressive sulfate environment, the resistance of a system depends primarily on its binder composition and the permeability of the system. Many of the ACM mixtures investigated in this thesis have different cement chemistry, which leads to different hydration products and microstructure, and in turn, can affect the way these materials react to external sulfate sources compared to traditional portland systems. Understanding the long-term durability performance of the ACM systems towards sulfate exposure is essential in designing 'green' alternatives to traditional portland cements for intended service lives. This chapter verifies and provides new insights into the sulfate attack mechanisms in commercially available CSA, CAC, AA, and MPC cements and evaluates its implications on phase composition, mechanical properties, and binder integrity in these systems against one traditional OPC system.

10.1 Background

10.1.1 Chemical sulfate attack in portland cements (OPC)

In traditional portland cements, once sulfate ions ingress into the concrete, the form of the sulfate attack, and therefore the effects of the attack, depends upon the amounts of monosulfate hydrate, calcium aluminate hydrate, unhydrated C_3A, and portlandite in the

cement paste. Primarily, three forms of sulfate attack are known to exist for portland systems [93–97]:

- Formation of expansive ettringite due to the reaction with monosulfate hydrate, calcium aluminate hydrate, and/or unhydrated C_3A.
- Formation of gypsum due to the reaction of external sulfates with CH. This results in expansion and also decrease in pore solution alkalinity and destabilization of C-S-H structure.
- Conversion of CH and C-S-H into magnesium hydroxide and magnesium silicate hydrate when the attacking solution contains magnesium ions, for example magnesium sulfate.

Portland cements containing higher amounts of C_4AF and lower amounts of C_3A are known to perform better to sulfate attack [96], especially when the formation of expansive ettringite was the driving mechanism for degradation.

10.1.2 Chemical sulfate attack in calcium sulfo-aluminate cement (CSA)

CSA cements have either low or no C_3S phase present in them, and if any CSH is formed, it is from the hydration of C_2S reaction. So, the amount of portlandite formed is low compared to traditional portland cement systems. Also, the portlandite can be consumed back in the reaction forming just the ettringite. Since the amount of portlandite present in the CSA system is significantly lower than the traditional portland systems, the sulfate attack mechanisms in CSA systems can be different. Conflicting results are found in the literature with respect to the resistance of CSA systems towards external sulfate exposure. Some researchers suggest CSA systems are unaffected to sulfate exposure [98–100], while

other researchers suggests they are not resistant to sulfate exposure [6,101]. The ettringite phase in the CSA systems can decompose to gypsum when the exposure environment pH drops below 10.7 to 11.5 [102–104] and can lead to a significant reduction in the strength of the matrix. However, CSA systems are known to be less permeable, which may improve their resistance towards sulfate attack. Furthermore, in CSA systems containing a lower amount of sulfates, the external sulfate exposure can contribute to further hydration – which can result in either reduction in permeability due to increased hydration or significant cracking due to the excessive formation of expansive ettringite [101]. With ettringite being the main hydration product and strength-giving component (rather than CSH), the long-term stability of these CSA systems towards sulfate exposure is a concern[105,106].

10.1.3 Chemical sulfate attack in calcium aluminate cements (CAC)

Calcium aluminate cements are generally known to be resistant to chemical sulfate attack when produced at lower w/c (insert citation) since they do not have CH or monosulfate hydrate or C_3A phases in a significant amount to cause expansion. However, when CACs are produced at higher w/c, it increases the permeability of the system and accelerates conversion, which makes them susceptible to sulfate attack. CAC systems produced at low w/c ratio have good sulfate resisting properties [107–110] due to low permeability of unconverted concrete and due to the inert behavior of the CAH_{10} phase towards reaction with sulfate. However, sulfate attack will occur in CAC systems that are made at higher w/c and that are converted because the C_3AH_6 phase readily reacts with sulfates to form ettringite. The converted CAC systems will also have increased permeability and free water, which can mobilize the sulfate ions into the system from outside exposure [108,111].

The inert behavior of the CAH_{10} phase towards sulfate attack is due to higher amounts of AH_3 phase that can get released upon reaction with sulfate and prevent a further reaction, as shown in Equation 8 (i). Whereas the C_3AH_6 phase upon reaction with sulfate produces a significantly lower amount of AH_3 (Equation 8 [ii]) compared to the CAH_{10} phase, making it more reactive with sulfates compared to the CAH_{10} phase.

Equation 8

$$6\mathrm{CAH}_{10} + 3SO_4^{2-} \rightarrow \mathrm{Ettringite} + 5\mathrm{AH}_3 + 14\mathrm{H} \quad \text{(i)}$$

$$2\mathrm{C}_3\mathrm{AH}_6 + 3SO_4^{2-} + 27\mathrm{H} \rightarrow \mathrm{Ettringite} + \mathrm{AH}_3 \quad \text{(ii)}$$

10.1.4 Chemical sulfate attack in activated aluminosilicate binder (AA)

Significant research has been performed to understand the performance of alkali-activated systems against sulfate attack [112–119]. Their research showed that alkali-activated materials exhibited superior resistance to sodium sulfate solution with little to no conversion to sulfate bearing phases (ettringite or monosulfate) are observed. However, most of the alkali-activated systems, especially the ones made with Ca-rich precursor, showed significant degradation when exposed to magnesium sulfates. The presence of magnesium led to significant decalcification of Ca-rich C-N-A-S-H gels to Mg-silicate gels, causing precipitation of gypsum and degradation of the binder system. No research has been performed to understand the non-alkaline based activated aluminosilicate systems, especially the ones with Ca-rich precursors. These systems have low pH and can lead to significant decalcification of Ca-rich C-N-A-S-H when exposed to constant pH

sodium sulfate solution and can lead to precipitation of gypsum, and thereby further decomposition of the binder.

10.1.5 Chemical sulfate attack in magnesium phosphate cements (MPC)

Very little research has been done to understand the sulfate resistance of MPC systems. Jun et al. tested the sulfate resistance OPC systems coated with MPC and found out that MPC overlays showed excellent protection in resisting sulfate attack [120,121]. The ammonia-based struvite phase in the MPC overlay reacted with the sulfate ions and formed stable new complex ($NaMg_3(OH)_2(CO_3)_2SO_4 \cdot 6H_2O$) that has low density, thereby filling the gaps in the porous MPC structure and offering good resistance to permeating sulfate ions. However, more research is required to further validate this mechanism in MPC systems, especially in systems containing K-struvite rather than the ammonia-based struvite tested in the literature.

10.1.6 Current testing methods for sulfate exposure

The current two ASTM test methods for accelerating testing of sulfate resistance of hydraulic cements (ASTM C 1012 and ASTM C 452) were often criticized by many researchers [122–130] for not adequately predicting the field performance. Due to continuous immersions of test specimens in a relatively low volume of sodium sulfate solution (the ratio of the volume of exposure solution to the volume of test specimens is about 10), the pH of the attacking solution can rapidly change from neutral (around 7) to basic (around 12) and the concentration of sulfates can decrease. This is due to the leaching of alkalis from test specimens into the sulfate exposure solution. The reaction mechanisms of sulfate attack can also change when the concentration of sulfates in the exposure solution

changes [104,131]. At low sulfate concentration (<1000 ppm), ettringite is the primary phase that crystallizes. Whereas at high sulfate concentrations (>8000 ppm), gypsum is the main product that crystallizes. So, the softening-spalling damage induced due to the gypsum formation and decalcification of the C-S-H phase is not induced in either of these two ASTM test methods. These two test methods were primarily designed to assess the ability of binder systems to resist expansion due to ettringite formation, even though the sulfate attack damage in the field was usually found out to be manifesting in the form of loss of strength and adhesion [6,132].

Kurtis et al. proposed an accelerated test method [6] to assess the resistance of both portland and non-portland binder systems towards external sulfate attack. This test method addresses the criticism surrounding the existing two ASTM test methods by maintaining constant pH and constant sulfate concentration in the exposure solution, and by using the change is compressive strength as a damage indicator. In this test method, cement paste cubes of 0.5 inch at w/b ratio of 0.5 were made and cured at 50 °C prior to testing them for 9 weeks of sulfate exposure. However, there are still three issues that need to be addressed with this test method before adopting it for testing broader ACM systems: 1) some of the binders tested in this chapter are found to bleed significantly at w/b of 0.5, 2) the impact of heated curing is not fully understood in these ACM mixtures, and 3) compression testing alone may not detect the surface damage that can be caused due to decalcification of C-S-H gel. So a new accelerated constant pH sulfate exposure test based on the accelerated test method proposed by Kurtis et al. was developed by addressing these three issues and is discussed in detail in section 10.2.

10.2 Methods – constant pH sulfate exposure test

Cement paste samples were used to test for changes in microstructure and compressive strength with exposure to sodium sulfate solution. Cement paste cubes of 0.5 inch (12.7 mm) were cast according to the mixture proportions given in Table 16 and cured at 23 °C and 100% RH for at least 56 days (rather than heat curing at 50 °C). The paste mixtures were mixed in a high shear mixer according to ASTM C1738-14 at w/c of 0.45 (0.25 for AA and 0.30 for MPC). The set modifier/ activator dosages were chosen so that the corresponding concrete mixes had a workable window of at least 60 min. After curing, cement paste cubes were immersed in a circulating bath of 4% (by weight) sodium sulfate solution (test setup is shown in Fig. 57). A pH controller, which doses 1N H_2SO_4, was used to maintain the solution pH constant at 7 - to minimize the effects of CH leaching into the exposure solution and maintain constant sulfate ion concentration in the solution over exposure time. Compressive strength was measured on 7 replicates before the exposure and after 2, 5, 10, and 20 weeks of exposure. Change in compressive strength with respect to the initial strength, along with the visual observation of the type of damage and microstructural characterization were used as an indicator to assess the resistance of the ACM mixtures to chemical sulfate attack. The visual damage rating is done according to Table 17. Microstructure characterization (section 10.2.1) was also done to understand the sulfate attack mechanism of both OPC and ACM mixtures in detail.

Table 16 Cement paste mixture proportions.

Cement	w/b	Set modifier/ activators (by weight of cement)
OPC	0.45	–
CAC1	0.45	–
CAC2	0.45	–
CACT	0.45	Citric acid – 1.5%
CSA1	0.45	Citric acid – 2.0%
CSA2	0.45	Citric acid – 0.5%
CSA2P	0.45	Citric acid – 0.5%
AA	0.25	Activator 1 - 2.47%, Activator 2 - 2.21%
MPC	0.30	Boric acid – 14%

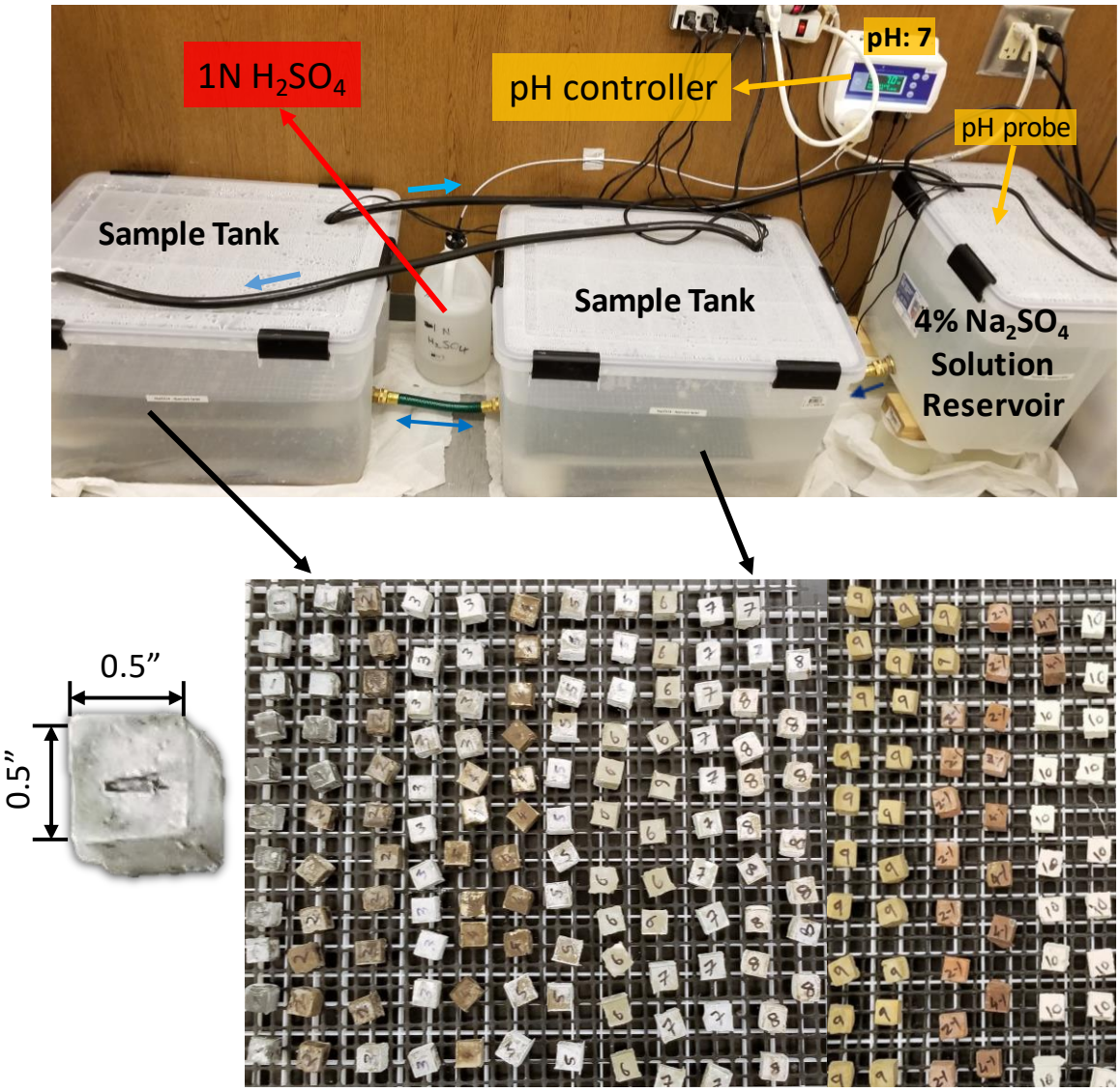

Fig. 57 Schematic of test setup and specimens used for accelerated sulfate testing.

Table 17 Visual damage rating for degradation due to chemical sulfate attack

Damage type (from visual observation)			Visual Rating
Surface spalling	**Corner damage**	**Internal cracking**	
None to low	None to low	None to low	**0**
Medium	None to low	None to low	**1**
Heavy	None to low	None to low	**2**
Heavy	Significant	None to low	**3**
None to Heavy	Significant	Significant	**4**

10.2.1 Microstructure Analysis

Microstructure analysis was carried out on both powdered and epoxy mounted cement paste samples. Prior to testing microstructure by TGA and XRD, the paste samples, both exposed and unexposed, were ground and sieved to a particle size less than 300 microns, and the free water was removed using solvent exchange procedure [42]. 5 g of powdered sample was mixed in 50 ml of isopropyl alcohol, and the suspension rests for 15 min. Then, the suspension is filtered using Büchner funnel and a vacuum pump for 5 min, and later, it is washed with 10 ml of diethylene ether for 1 min, during which the vacuum pump is turned off. The resulting suspension is again filtered under vacuum for five more minutes, or until the suspension is dry, whichever is longer. The dried sample is sealed in a small sealed plastic bag and stored in an airtight container.

10.2.1.1 Thermogravimetric Analysis (TGA)

A Hitachi simultaneous thermogravimetric analyzer STA7300 was used to carry out the thermogravimetric measurements. After the solvent exchange, the sample is further ground to a particle size of less than 74 microns. Approximately 20 mg of the ground sample is taken in an open 70 μl platinum crucible and further dried in TG at 25 ºC under a constant

stream of Nitrogen (N_2) gas for 15 min, or until the constant mass, whichever is longer. Later the temperature is increased to 40 ºC and held constant for 5 min. Then, the sample was heated from 40 to 1000 ºC, at a rate of 10 ºC/min, and the data is recorded at a rate of 120 data points per minute. During measurement, N_2 was used as a protective gas with a flow rate of 100 Cc/min.

10.2.1.2 X-ray Diffraction (XRD)

A PANalytical Empyrean diffractometer with a Bragg–Brentano HD X-ray mirror and a goniometer radius of 240 mm was used for data collection. The sample was incident with CuKα X-rays generated using Empyrean Cu LFF HR X-ray tube at 45 kV and 40 mA operating conditions. Soller slits of 0.04 rad and the fixed Mask, anti-scatter, and divergence slits of 4 mm, 1 º, and ¼ º were used in the incident beam path. In the diffracted beam path, a fixed anti-scatter slit of 7.5 mm and soller slits of 0.04 rad were used. A PIXcel3D-Medipix3 1x1 area detector with an active length of 3.347 º was used for data acquisition. Data was collected over an angular range of 5 º to 70 º with a step size and counting time of 0.013 º and 16.32 s, respectively, resulting in a total measurement time of less than 7 min.

The powdered and ground samples with particle dimension less than 74 microns were backloaded into the sample holder with an opening diameter of 17 mm. Phase identification was carried out using PANalytical X' Pert High Score plus v4.5 using PDF-4+ 2018 material identification database by International Center for Diffraction Data.

10.2.1.3 Scanning Electron Microscopy with Energy Dispersive X-ray Spectroscopy (SEM-EDS)

A Zeiss Ultra 60 FE-SEM coupled with Oxford Instruments X-Max N50 EDS detector was used for SEM-EDS imaging. Prior to imaging, the cement paste cubes were embedded in high viscous epoxy resin and split into two halves using a diamond saw with isopropanol as coolant. Later, one half of the epoxy mounted sample is further embedded in low viscous epoxy resin under vacuum, cured, and polished gradually down to 0.25 μm fineness with isopropanol as coolant. The polished samples were coated with a thin layer of conductive carbon on the polished surface and imaged under SEM at 1×10^{-3} Pa vacuum. The microscope was operated at 20 kV accelerating voltage with 120 μm aperture size. The field of view was 520 μm × 390 μm, and the pixel size was 0.254 × 0.254 μm — leading to an image resolution of 2048 × 1536. The EDS scanning was performed with 100 μs dwell time and dead time less than 10%. A total of 10 frames were collected at each spot, with a total acquisition time of about 1 hour. The X-rays hitting the EDS detector were pre-calibrated using external elemental standards with purity greater than 99.5% for quantitative estimation of composition. The scanned secondary electron image was overlaid with false-color compositional maps obtained by EDS scanning to facilitate identification and distinction of different phases present in these material systems.

10.3 Results and Discussion

10.3.1 Constant pH sulfate exposure test

Fig. 58 shows the change in compressive strength of OPC and ACM mixtures with exposure to sulfate solution, and Table 18 shows the visual damage rating after 5, 10, and 20 weeks of exposure. The microstructure characterization of the OPC and ACM cement paste mixtures is shown in Fig. 64 to Fig. 86. OPC mixture lost about 35% of its strength

with 5 weeks of exposure but exhibited some strengthening thereafter. The loss in strength after 20 weeks of exposure is about 22%. However, upon visual observation at 20 weeks of exposure (Fig. 59), there is significant softening and heavy spalling on all the 6 surfaces of the paste cube. Fig. 64 shows the TGA and XRD of OPC cement paste at different sulfate exposure age. With exposure, there is an increase in the amount of ettringite due to continued hydration with water and sulfates from exposure solution at the early exposure period (5 weeks of exposure). However, at later exposure periods, the amount of ettringite reduced – probably due to the decomposition of ettringite to gypsum [102–104]. The amount of portlandite reduced with exposure age due to leaching and due to reaction with sulfates from exposure solution, which led to the formation of a significant amount of gypsum as evident by the reduction in portlandite and increase in gypsum peaks in both TGA and XRD plots. Fig. 65 shows the SEM-EDS micrographs of OPC cement paste at 20 weeks of exposure. Heavy cracking due to decalcified C-S-H and significant crystallization of gypsum can be observed within the 500 μm layer at the edge, as shown in Fig. 65 (i). The crystallization of gypsum instead of ettringite in the outer layer is due to the lower pH of the exposure solution, which is maintained at 7. Decalcification of C-S-H and the crystallization of gypsum in the outer layer resulted in significant surface softening and heavy spalling as observed in Fig. 59.

CAC1 mixtures exhibited a significant loss in strength even at 2 weeks of exposure, with about 40% loss in strength at 2 weeks and until 10 weeks of exposure, and about 60% loss in strength after 20 weeks of exposure. Visual observation of the paste cubes at 20 weeks of exposure (Fig. 60) showed significant spalling, corner damage, and heaving cracking due to expansion. XRD and TGA of CAC1 cement paste cubes are shown in Fig. 66, and

SEM-EDS micrographs are shown in Fig. 67. The higher amount of $C_{12}A_7$ phase in the CAC1 cement resulted in a significant amount of C_2AH_8 phase compared to CAH_{10} and C_3AH_6 phases with hydration. With exposure, there is a significant reduction in C_2AH_8 phase and increase in AH_3 and ettringite phases. This is as expected since the exposure solution facilitates conversion to C_3AH_6 phase due to high availability of moisture, and C_3AH_6 phases readily react with sulfates in the exposure solution to form ettringite [108,111], as shown in Equation 8 (ii). However, a reduction in the amount of ettringite between 5 and 10 weeks of exposure can also be observed —this is because the cracking caused by the initially formed ettringite resulted in more of exposure solution to penetrate into the sample, lowering the pH of the system, which led to the decomposition of the ettringite.

Unlike the CAC1 system, the converted CAC1 system degraded entirely with 100% loss in strength even at 5 weeks of exposure. The converted CAC1 system had more porosity and a significantly higher amount of C_3AH_6 compared to the regular CAC1 system, as shown in Fig. 68. These two factors resulted in significant formation of ettringite with exposure — which led to cracking and later complete degradation of the system, as shown in Fig. 61.

CAC2 mixtures exhibited a slight increase in strength even after 20 weeks of exposure — showing significant better performance compared to the CAC1 mixtures. This is because the CAC2 cement has a significantly lower amount of $C_{12}A_7$ phase compared to CAC1, which led to upon hydration a higher amount of CAH_{10} phase compared to the C_2AH_8 phase as shown in TGA and XRD plots of CAC2 mixture in Fig. 69. So, the process of conversion to C_3AH_6 will be significantly lower in CAC2 mixtures, which results in better

resistance of the binder in forming ettringite with the sulfates from the exposure solution. Also, since the amount of water bound in CAH_{10} is higher compared to C_2AH_8 phase, the total porosity in the CAC2 system will be lower compared to CAC1 system, resulting in lower penetration of exposure solution. This can be observed in the SEM-EDS micrographs of CAC2 system in Fig. 70. The amount of sulfates present in the center of the cement paste cube is significantly low compared to the CAC1 system. Visual observation of the CAC2 paste cubes after 20 weeks of exposure (Fig. 60) showed no signs of cracking but some surface spalling — likely due to the formation of ettringite and later its decomposition near the surface of the cube. Because of the observed surface spalling, a damage rating of 1 was assigned to the CAC2 mixtures at the end of the 20-week exposure period.

But just like the converted CAC1 system, the converted CAC2 system degraded entirely with 100% loss in strength at 10 weeks of exposure. The converted CAC2 system also had more porosity and a significantly higher amount of C_3AH_6 compared to the normal CAC2 system, as shown in Fig. 71. Visual observation of the converted paste cubes at 10 weeks of exposure (Fig. 61) showed less surface softening but heaving cracking due to expansion because of significant formation of ettringite with exposure – so a damage rating of 4 was assigned to the converted CAC2 mixtures.

CACT mixtures lost more than 20% of the strength, similar to the OPC mixtures, after 20 weeks of exposure. However, surface softening or spalling is significantly low (Fig. 63) compared to that of OPC. The strength reduction at lower exposure ages (5 and 10 weeks) is also minimal compared to OPC. XRD and TGA (Fig. 72) of CACT paste mixtures also show an only slight reduction in ettringite, portlandite, and hemicarboaluminate peaks. SEM-EDS micrographs in Fig. 73 shows that there is heavy leaching of calcium in the

outer layer (for about 800 μm). This, along with the decomposition of ettringite (Equation 9 [i]), diffusion of Na ions from exposure solution (Equation 9 [ii]), and the continued hydration of unhydrated C_3S and C_2S present in the top layer (Equation 9 [iii]) resulted in formation of dense (C,N)-A-S-H (Equation 9 [iv]). The formation of (C,N)-A-S-H type phase is also confirmed by the TGA (Fig. 72 [iv]) of CACT mixtures performed on the outer 500 μm layer after 20 weeks of exposure. Also, the matrix next to this top layer (shown in the left half of Fig. 73 [iii]) is similar to the unaltered matrix in the center of the cement paste cube (Fig. 73 [i]) — which implies the dense outer layer formed in the CACT paste mixture is preventing further penetration of exposure solution, contributing to the superior resistance of CACT mixtures. Since the visual surface damage was significantly low in these mixtures, a damage rating of 0 was assigned to them throughout the exposure period.

Equation 9

$$\text{Ettringite} \rightarrow 3\text{CH} + 3\text{C}\bar{\text{S}}\text{H}_x + \text{AH}_3 + (26 - 3x)\text{H} \quad \text{(i)}$$

$$\text{C}_2\text{S} + x\text{H} \rightarrow \text{C-S-H} + \text{yCH} \quad \text{(ii)}$$

$$\text{Na}_2\text{SO}_4 \rightarrow 2\text{Na}^+ + \text{SO}_4^{2-} \quad \text{(iii)}$$

$$\text{C-S-H} + \text{AH}_3 + \text{Na}^+ \rightarrow \text{(C,N)-A-S-H} + \text{CH} \quad \text{(iv)}$$

$$\text{CH} + \text{SO}_4^{2-} \rightarrow \text{CaSO}_4 + \text{H} \quad \text{(v)}$$

CSA1 paste mixtures lost about 30% of their strength after just 2 weeks of exposure but showed some strengthening thereafter. The loss in strength after 20 weeks of exposure is less than 20%. However, the XRD and TGA of CSA1 paste mixtures (Fig. 74) show a significant reduction in ettringite content with exposure — with higher reduction at 20 weeks of exposure. The SEM-EDS micrographs (Fig. 75 [ii]) show the formation of porous

matrix in the outer 500 μm of CSA1 paste mixture after 20 weeks of exposure. This porous layer is primarily composed of (C,N)-A-S-H and AH_3, formed due to the decomposition of ettringite and heavy leaching of calcium and sulfates into the exposure solution (Equation 9). This could be the reason for surface softening and surface cracking observed in the CSA1 mixtures, as shown in Fig. 63. However, the inside layer at about 500 μm from the edge appears to be dense similar to the outer layer observed in CACT mixtures. This, just like the mechanism observed in CACT mixtures, prevented further penetration of exposure solution into the CSA1 matrix — as evident by the micrograph shown in Fig. 75 [iii], which is similar to the micrograph taken at the center of the cube (Fig. 75 [i]). Because of the surface spalling observed in CSA1 mixtures, a damage rating of 1 was assigned to them.

CSA2 paste mixtures lost about 10% of their strength after 2 weeks of exposure and about 20% loss in strength for the rest of the exposure period until 20 weeks. Similar to the CACT mixture, the SEM-EDS micrographs of CSA2 paste mixture (Fig. 77) show dense (C,N)-A-S-H layer of about 800 μm thick at the edge — due to the decomposition of ettringite, further hydration of C_2S, and leaching of calcium and Sulphur. This prevented further decomposition of ettringite and leaching in the inner layer of the system and prevented further penetration of the exposure solution. Also, the TGA and XRD of CSA2 paste mixtures shown in Fig. 76 at different exposure periods show only a slight reduction in the amount of ettringite with exposure. This is due to the continued hydration of unhydrated phases present in the mixture before the formation of the dense outer layer which results in increase in ettringite, and the decomposition of outer layer caused reduction in ettringite — combination of these two resulted in slight reduction of total ettringite present in the

system. Also, a damage rating of 0 was assigned to the CSA2 paste mixtures since no signs of damage were observed visually in these mixtures throughout the exposure period.

CSA2P mixture, unlike CSA2 mixture, showed a higher reduction in strength – more than 50% loss in strength after 20 weeks of exposure, with significant surface spalling and cracking (Fig. 62). The TGA and the XRD of CSA2P mixtures with exposure (Fig. 78) show a significant reduction in the ettringite phase and a significant increase in gypsum. The SEM-EDS micrographs (Fig. 79) shows dense (C,N)-A-S-H outer layer similar to CACT and CSA2 mixtures. However, a layer of gypsum is also formed just inside the outer (C,N)-A-S-H layer, as shown in Fig. 78 (iii). The presence of gypsum is also confirmed by the TGA (Fig. 78 [iv]) of CSA2P mixtures performed on the outer spalled surface after 20 weeks of exposure. The expansive stresses generated by this crystallized gypsum layer caused a significant amount of perpendicular cracks in the inside relatively undecomposed stronger matrix adjacent to the gypsum layer. This resulted in a significant thick layer of surface spalling and internal damage as observed visually in Fig. 62, and was assigned a damage rating of 4 at the end of the 20 weeks of exposure.

CSA3 mixture showed significant strength reduction during the first 2 weeks of weeks, losing about 22% of its strength — but exhibited continuous significant strength gain thereafter. The strength loss is less than 5% after 20 weeks of weeks. The XRD and TGA of CSA3 mixtures with exposure given in Fig. 80 shows some reduction in ettringite peak with exposure. The SEM-EDX micrographs given in Fig. 81 show dense (C,N)-A-S-H in the outer 500 μm layer (Fig. 81 [ii]) similar to CACT and CSA2 mixtures. However, the (C,N)-A-S-H gel formed is more calcium-rich (Fig. 81 [b]) compared to one formed in CACT, CSA1, CSA2, and CSA2P mixtures – especially in the layer approximately

between 300 to 500 μm form the edge. After about 600 μm from the edge, the inside matrix (Fig. 81 [iii]) appears to be similar in composition to the one at the center of the cube. Also, no signs of damage were observed visually (Fig. 63), and the CSA3 mixtures were assigned a damage rating of 0 throughout the exposure period.

Overall, all the ettringite based systems (except CSA2P) showed superior resistance to external sulfate attack. The defense mechanism in resisting sulfate attack is similar in all these systems, i.e., formation of (C,N)-A-S-H type gel on the exposure surface. Fig. 82 (i) shows the ternary plot of atomic moles percentage of ($Ca+Mg+Na_2$), Si, (Al+Fe) in the (C,N)-A-S-H structure present in the outer layer of CACT, CSA1, CSA2, CSA2P, and CSA3 mixtures after 20 weeks of exposure. All the ACM mixtures have similar composition of (C,N)-A-S-H gel. However, in CSA1 mixtures, (C,N)-A-S-H gel with a significant lower amount of Al and Fe is possible due to separate precipitation of the AH_3 phase (Fig. 74 [iv]). This could have been the reason for more porous outer structure in CSA1 mixtures compared to other ettringite based systems. Fig. 82 (ii) shows the percentage of Na_2 w.r.t. combination of ($Ca+Mg+Na_2$) in moles in (C,N)-A-S-H gel assuming all the sulfates are bound as Na2SO4. Whereas, Fig. 82 (iii) shows the percentage of Na_2 w.r.t. combination of ($Ca+Mg+Na_2$) in moles assuming all the sulfates are bound as CaSO4.In either case, the relative composition of Na shows its presence in (C,N)-A-S-H gel.

More research needs to performed to understand why a significant amount of gypsum is formed between this outer (C,N)-A-S-H layer and the inside matrix only in the polymer-modified CSA system. Specifically, the effects of polymer addition on the permeability of the outer (C,N)-A-S-H layer need to be understood. If polymers are making this layer

impermeable, then the pressure generated by the gypsum that is forming between this outer layer and the inner layer may not be sufficient to leach out the gypsum. This can cause accumulation of calcium sulfate over time and thereby precipitation of gypsum between this outer layer and inner matrix, which is the convergence point for the calcium leaching out from inside matrix and sulfates coming in from the exposure solution through the outer layer.

AA mixtures also lost about 22% strength within the first 2 weeks of exposure, but just like CSA3 mixtures, it exhibited continuous strengthening with increased exposure age. After about 20 weeks of exposure, the loss in strength in the AA mixture is insignificant. The strength gain is likely due to the continuous hydration from the exposure solution. The TGA and XRD of AA mixtures shown in Fig. 83 also show some reduction in ettringite peaks, but overall no significant changes are observed. The SEM-EDS micrographs for AA paste mixtures after 20 weeks of exposure are given in Fig. 84. Even though significant decalcification is observed in the outer 500 μm layer, and outer matrix looks intact and dense. This prevented further leaching of calcium even in the immediate matrix inside the outer 500 μm layer, as shown in Fig. 84 (iii). In addition to Ca, Na has also leached out (by comparing the Si/Na ratio in both Fig. 84 (a) and (b) due to the lower concentration of Na in exposure solution compared to AA system [113]. Visual observation of the AA paste cube showed no signs of damage even after 20 weeks of exposure as shown in Fig. 63, so was assigned a damage rating of 0. Overall, AA systems made with class C fly ash and activators based on lactate and citrates showed superior resistance to sodium sulfate attack similar to other alkali activated materials reported in the literature [112–119].

MPC paste mixtures lost about 15% strength within the first 2 weeks of exposure but exhibited significant strength gain thereafter. The paste mixtures gained about a 17% increase in strength after 20 weeks of exposure. However, the TGA and XRD of MPC mixtures (Fig. 85) show a significant reduction in the struvite phase with exposure. Also, the K-Struvite phase present in MPC mixtures before exposure converted to (Na,K)-struvite with exposure – due to the alkali exchange from the exposure solution. The SEM-EDS micrographs of MPC paste mixture after 20 weeks of exposure are shown in Fig. 86. The struvite phase in the outer layer (until about 500 to 1000 μm from edge) got converted to $(C,M)_4PH_x$. This is different from the $(NaMg_3(OH)_2(CO_3)_2SO_4 \cdot 6H_2O)$ phase that is formed in the MPC coating exposed to sulfates in the research performed by Jun et al. [120]. The inside matrix next to the outer layer (1000 μm from the outer edge, as shown in the left half of Fig. 86 [iii]) is relatively unaltered and looks similar to the matrix at the center of the cube (Fig. 86 [i]). Visual observation of the MPC paste cube showed no signs of damage even after 20 weeks of exposure as shown in Fig. 63, so was assigned a damage rating of 0.

Table 18 Visual damage rating for degradation due to chemical sulfate attack

Cement	w/b	Visual damage rating after exposure for		
		5 weeks	10 weeks	20 weeks
OPC	0.45	**1**	**2**	**2**
CAC1	0.45	**0**	**3**	**4**
CAC1 converted	0.45	**4**	**4**	**4**
CAC2	0.45	**0**	**0**	**1**
CAC2 converted	0.45	**0**	**4**	**4**
CACT	0.45	**0**	**0**	**0**
CSA1	0.45	**0**	**1**	**1**
CSA2	0.45	**0**	**0**	**0**
CSA2P	0.45	**1**	**3**	**4**
CSA3	0.45	**0**	**0**	**0**
AA	0.25	**0**	**0**	**0**
MPC	0.30	**0**	**0**	**0**

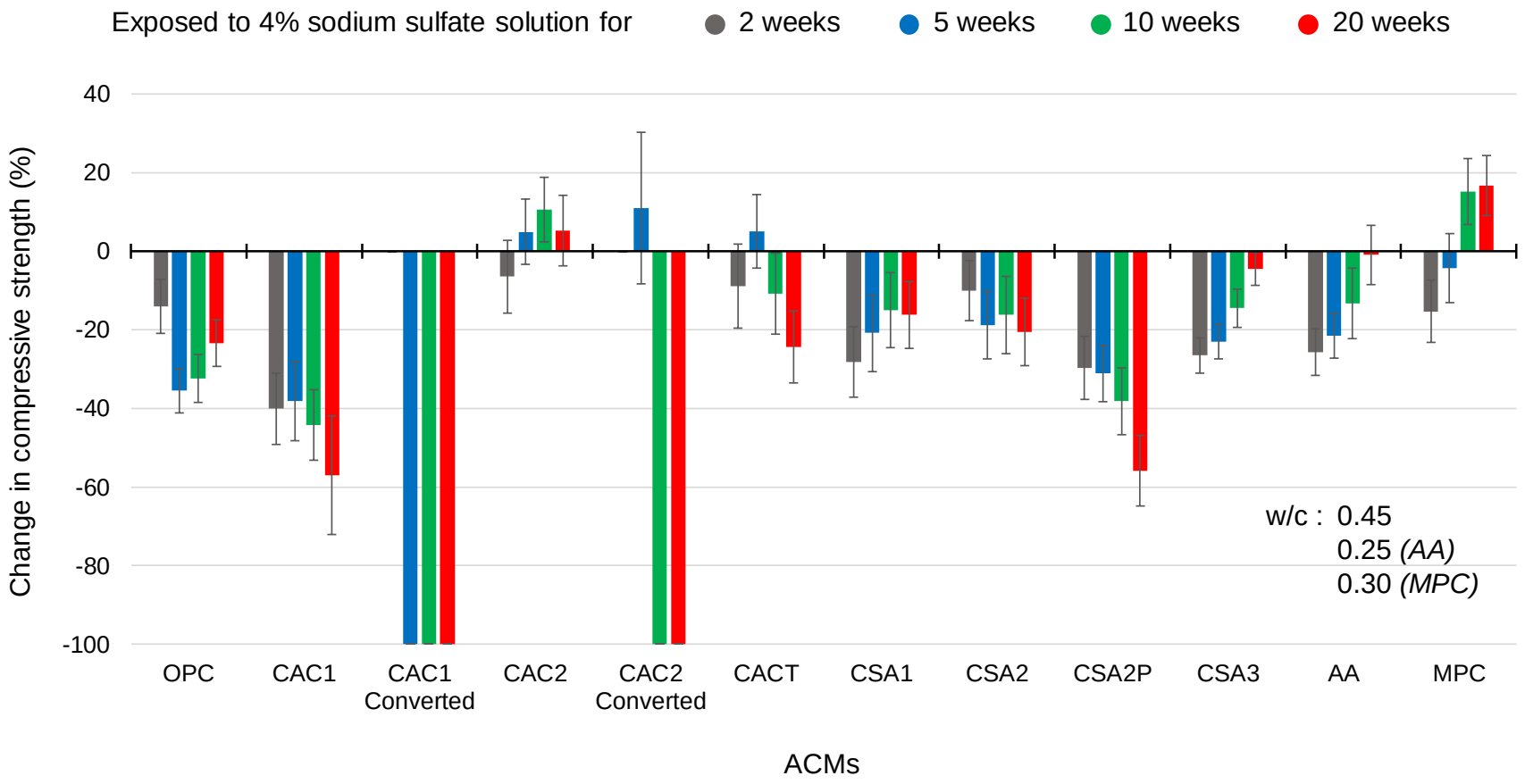

Fig. 58 The average change in compressive strength of cement paste cubes made with ACMs and OPC, exposed to a 4% (w/w) sodium sulfate solution.

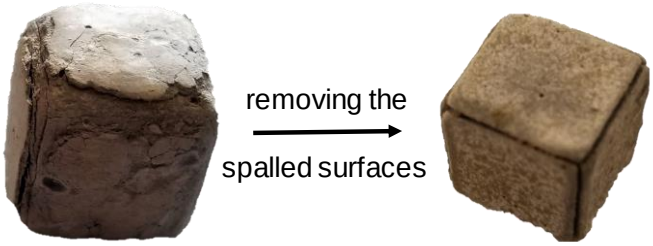

Fig. 59 OPC paste cube showing significant surface spalling after 20 weeks of exposure to sodium sulfate solution.

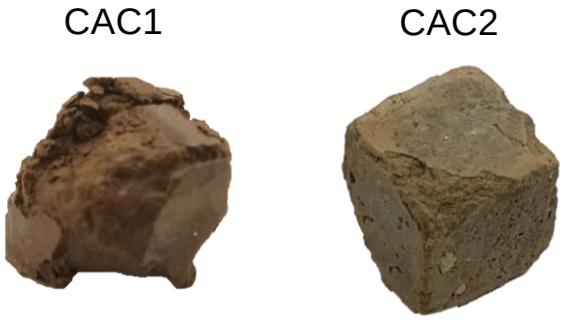

Fig. 60 CAC1 and CAC2 paste cubes after 20 weeks of exposure to sodium sulfate solution. Significant cracking and internal damage can be observed in CAC1, whereas only some surface damage can be observed in CAC2.

Fig. 61 CAC1 and CAC2 converted paste cubes showing significant expansion, cracking, and internal damage after 5 and 10 weeks of exposure to sodium sulfate solution, respectively.

Fig. 62 CSA2P paste cubes showing significant surface spalling and internal damage after 20 weeks of exposure to sodium sulfate solution.

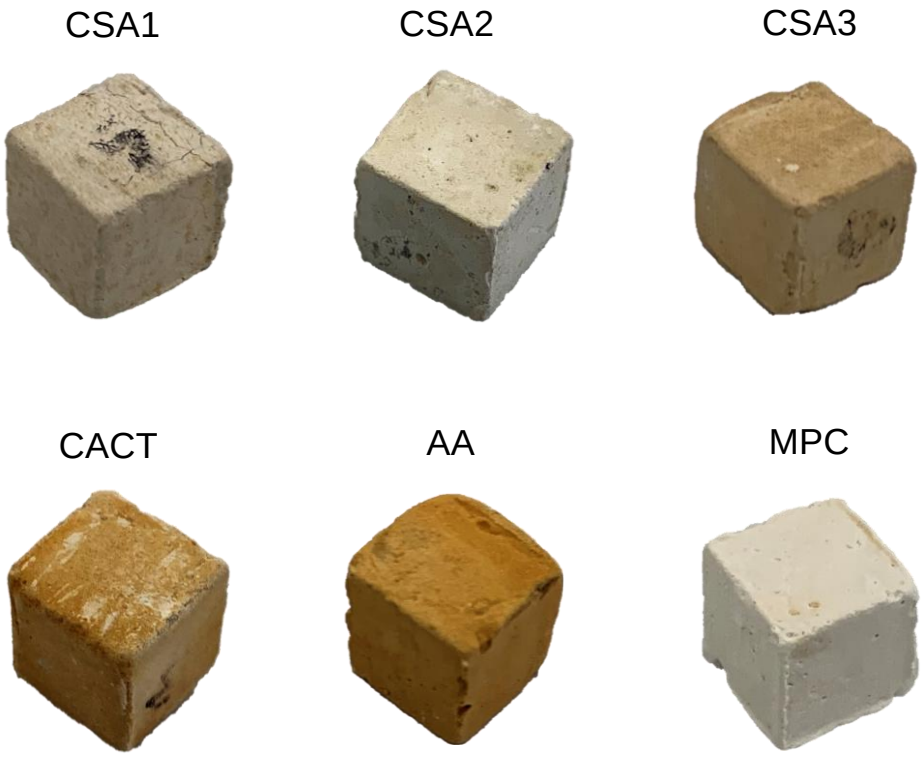

Fig. 63 CSA1, CSA2, CSA3, CACT, AA, and MPC paste cubes after 20 weeks of exposure to sodium sulfate solution. CSA2, CSA3, CACT, AA, and MPC paste cubes show little to no surface damage, whereas some surface cracking and softening can be observed in CSA1 paste cubes.

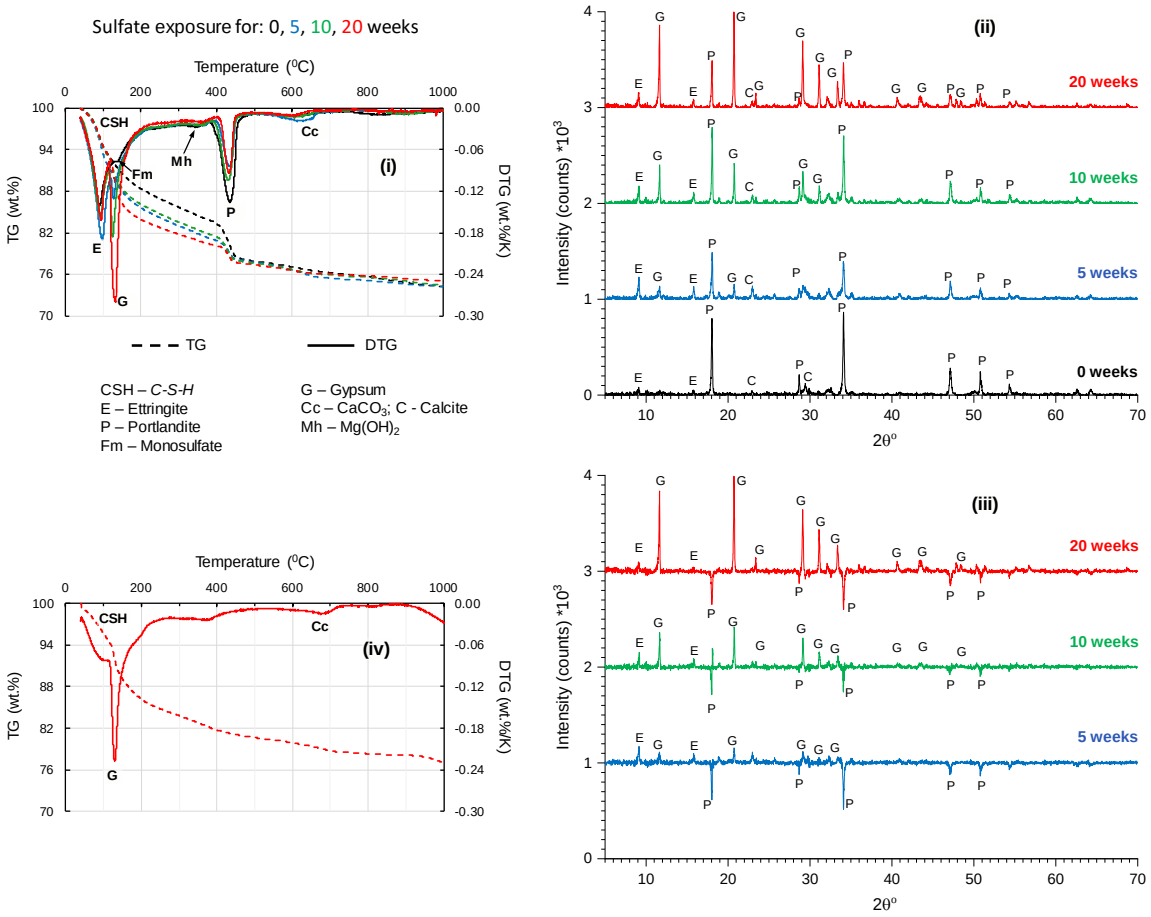

Fig. 64 (i) TG and DTG, (ii) XRD of OPC cement paste cubes exposed to 4% (w/w) sodium sulfate solution for 0, 5, 10, and 20 weeks. (iii) Shows difference in XRD peaks of OPC cement paste cubes after exposure versus without exposure. (iv) TG and DTG of the spalled surface in OPC paste cubes after 20 weeks of exposure.

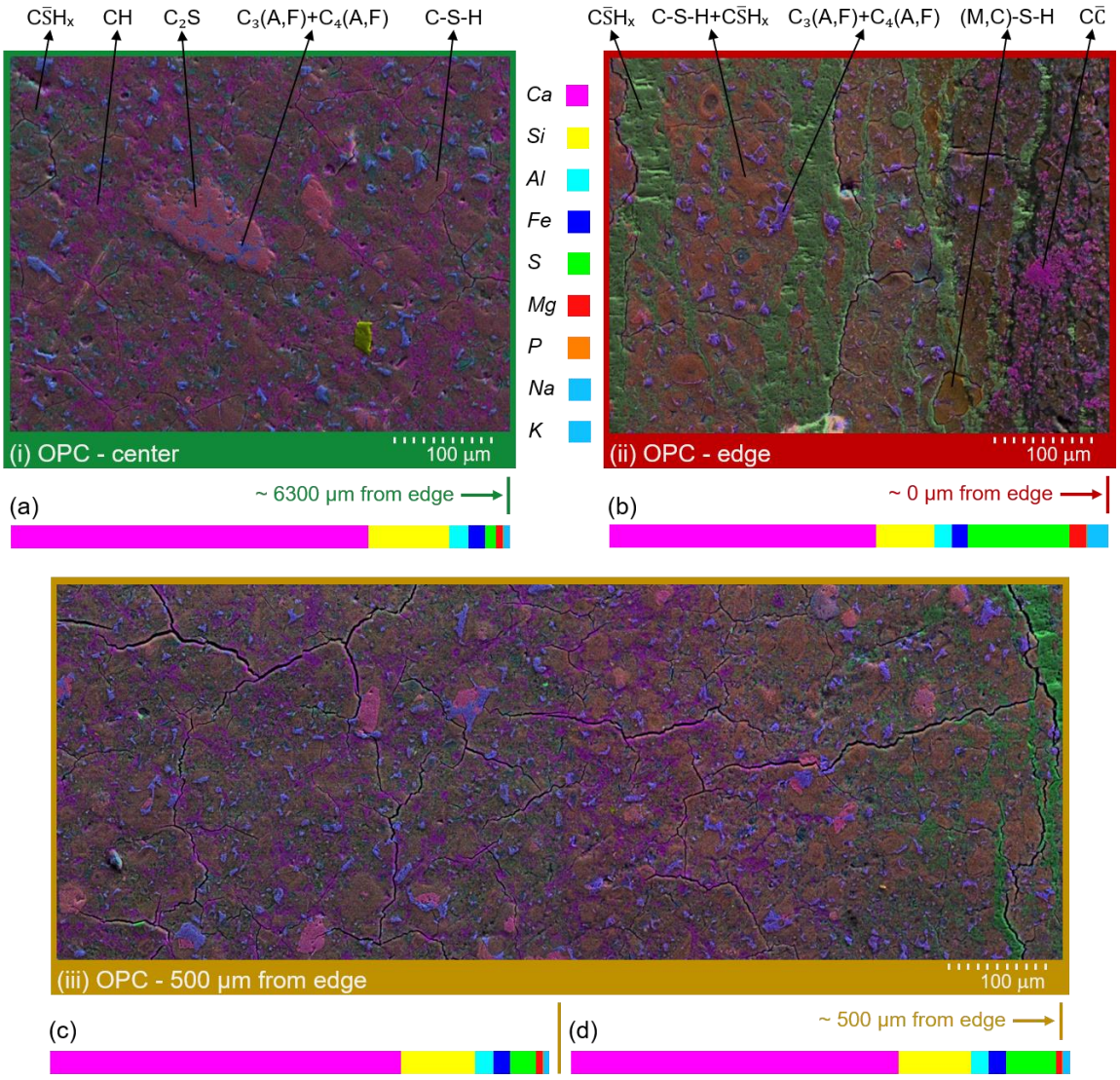

Fig. 65 SEM-EDS micrographs of OPC cement paste cube exposed to 4% (w/w) sodium sulfate solution for 20 weeks. Images were taken at approximately (i) 6300 µm, (ii) 0 µm, and (iii) 500 µm from the edge of the cube. (a), (b), (c), and (d) are normalized elemental distributions in micrograph given in (i), (ii), left half of (iii), and right half of (iii) respectively.

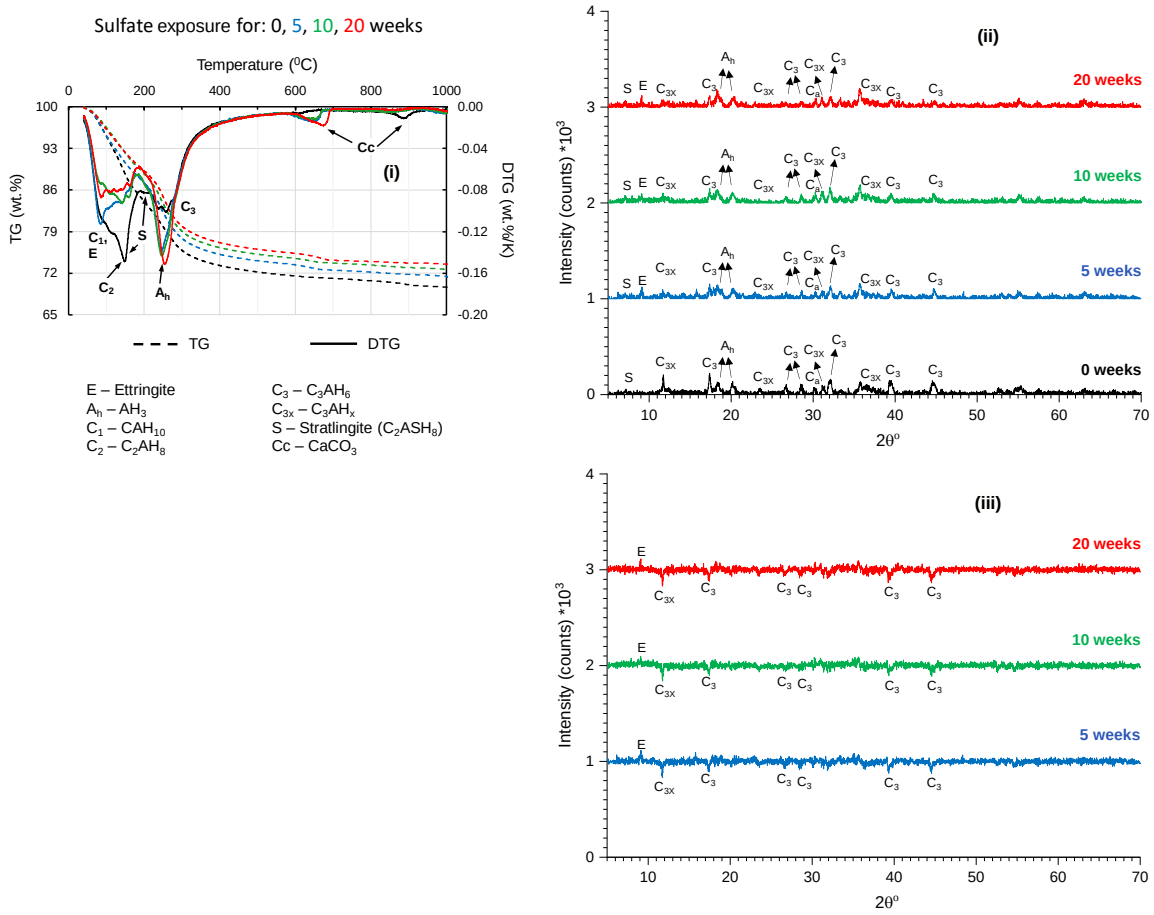

Fig. 66 (i) TG and DTG, (ii) XRD of CAC1 cement paste cubes exposed to 4% (w/w) sodium sulfate solution for 0, 5, 10, and 20 weeks. (iii) Shows difference in XRD peaks of CAC1 cement paste cubes after exposure versus without exposure.

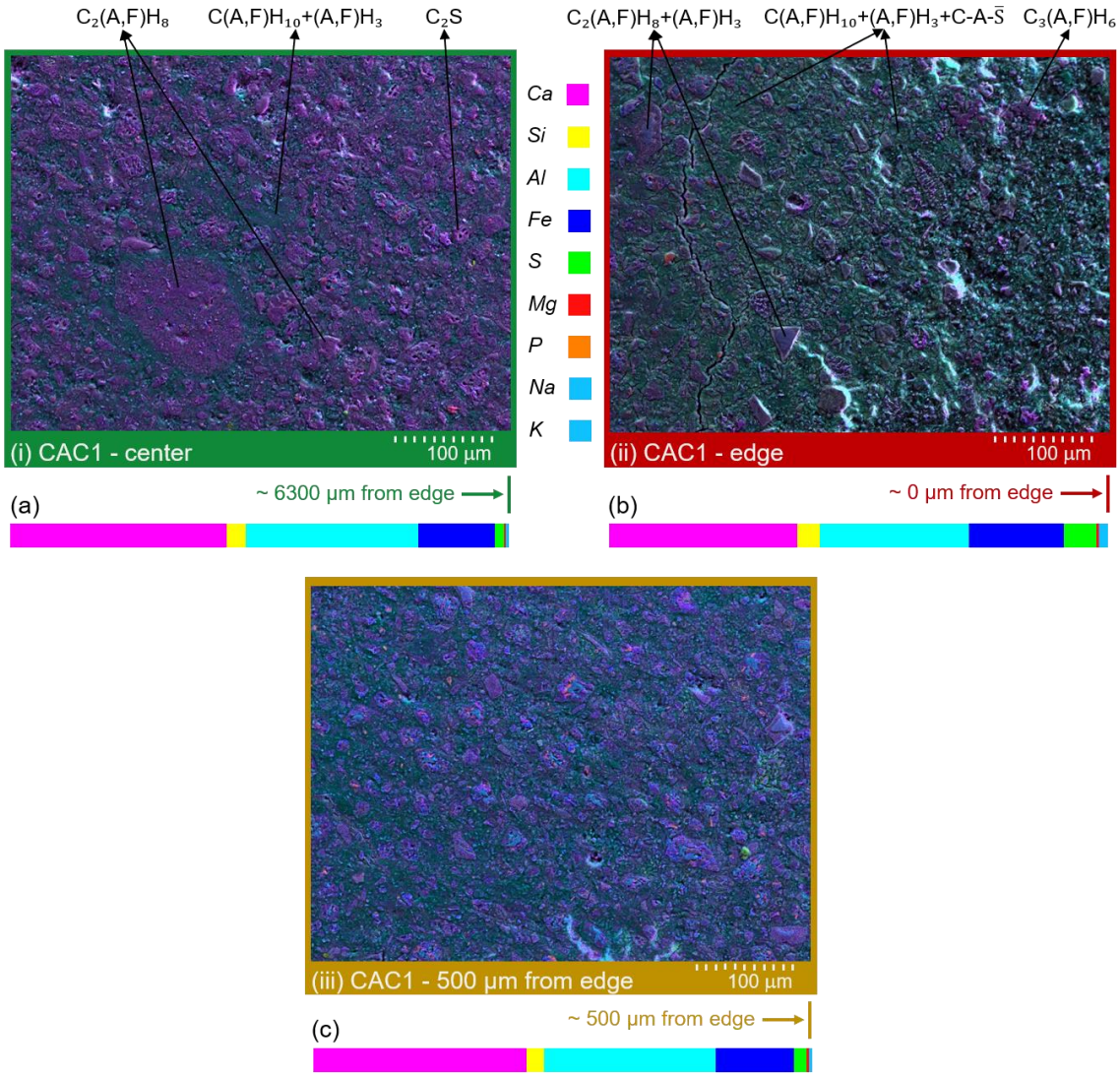

Fig. 67 SEM-EDS micrographs of CAC1 cement paste cube exposed to 4% (w/w) sodium sulfate solution for 20 weeks. Images were taken at approximately (i) 6300 µm, (ii) 0 µm, and (iii) 500 µm from the edge of the cube. (a), (b), and (c) are normalized elemental distributions in micrograph given in (i), (ii), and (iii) respectively.

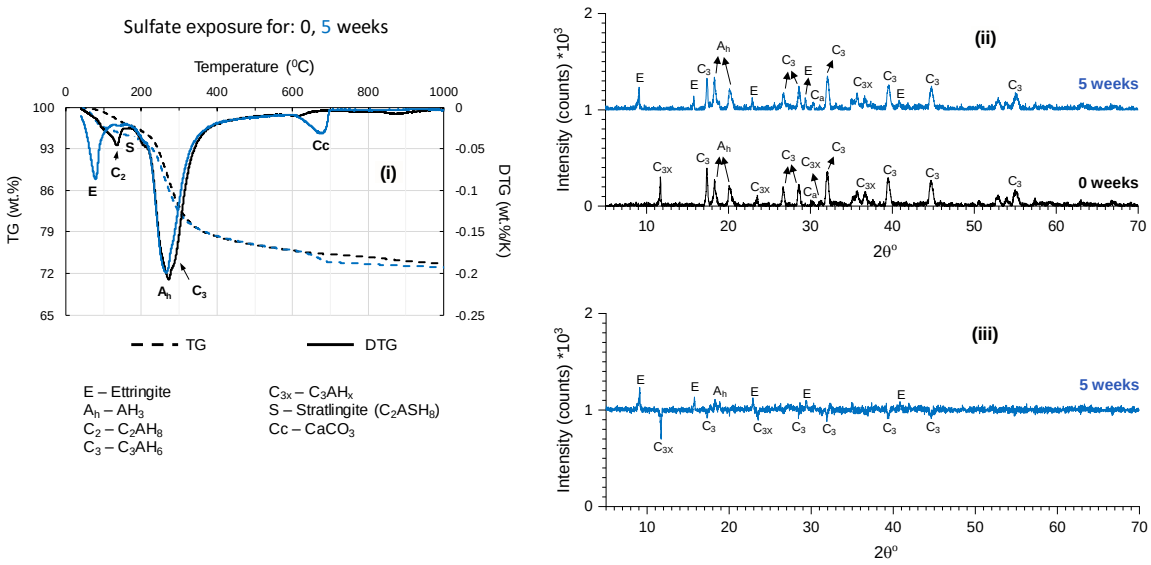

Fig. 68 (i) TG and DTG, (ii) XRD of converted CAC1 cement paste cubes exposed to 4% (w/w) sodium sulfate solution for 0 and 5 weeks. (iii) Shows difference in XRD peaks of converted CAC1 cement paste cubes after exposure versus without exposure.

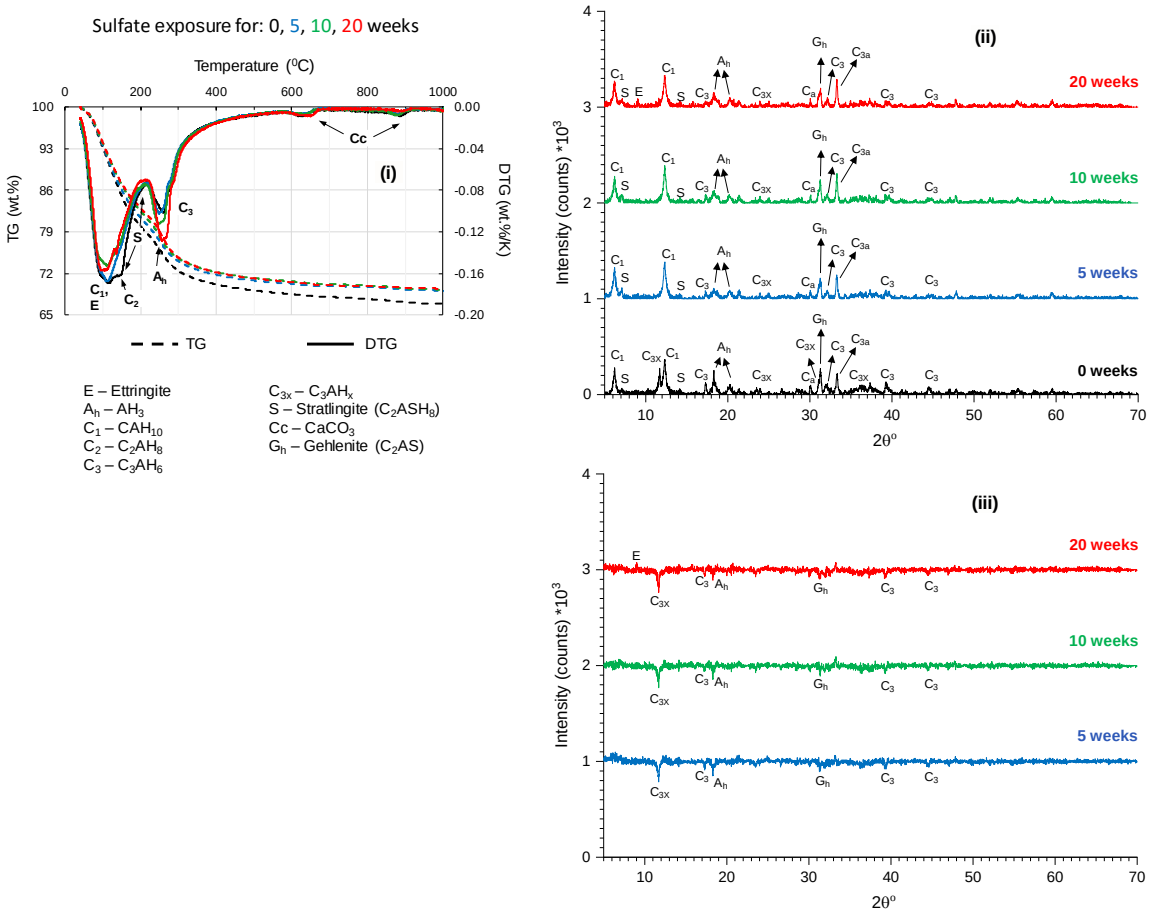

Fig. 69 (i) TG and DTG, (ii) XRD of CAC2 cement paste cubes exposed to 4% (w/w) sodium sulfate solution for 0, 5, 10, and 20 weeks. (iii) Shows difference in XRD peaks of CAC2 cement paste cubes after exposure versus without exposure.

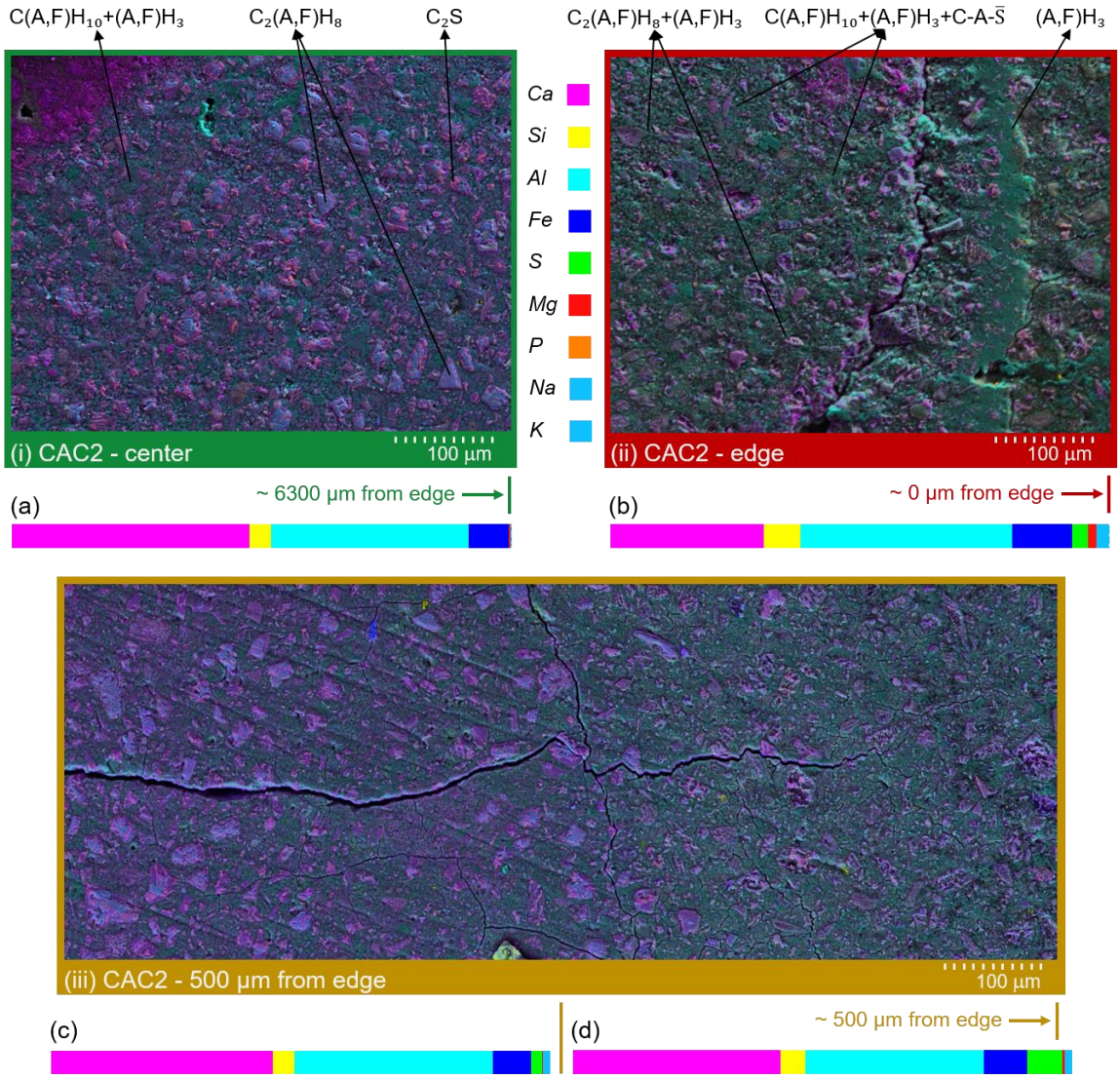

Fig. 70 SEM-EDS micrographs of CAC2 cement paste cube exposed to 4% (w/w) sodium sulfate solution for 20 weeks. Images were taken at approximately (i) 6300 µm, (ii) 0 µm, and (iii) 500 µm from the edge of the cube. (a), (b), (c), and (d) are normalized elemental distributions in micrograph given in (i), (ii), left half of (iii), and right half of (iii) respectively.

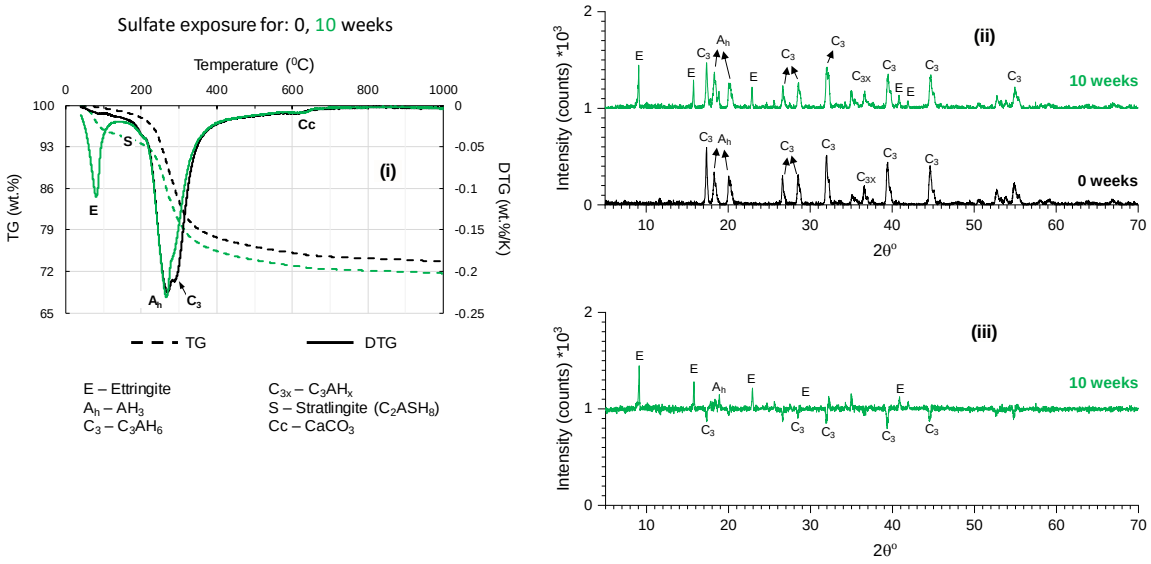

Fig. 71 (i) TG and DTG, (ii) XRD of converted CAC2 cement paste cubes exposed to 4% (w/w) sodium sulfate solution for 0 and 10 weeks. (iii) Shows difference in XRD peaks of converted CAC2 cement paste cubes after exposure versus without exposure.

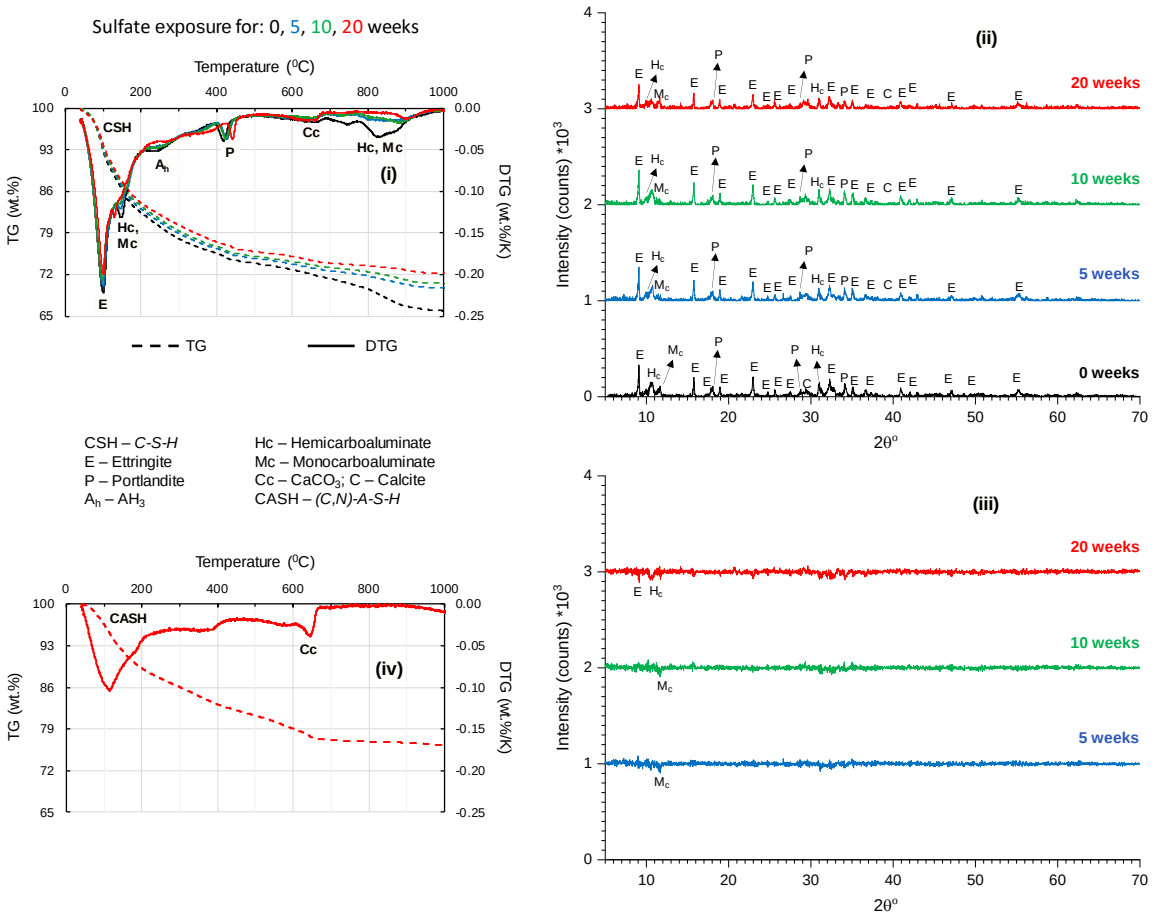

Fig. 72 (i) TG and DTG, (ii) XRD of CACT cement paste cubes exposed to 4% (w/w) sodium sulfate solution for 0, 5, 10, and 20 weeks. (iii) Shows difference in XRD peaks of CACT cement paste cubes after exposure versus without exposure. (iv) TG and DTG of CACT paste cubes on the outer 500 µm layer after 20 weeks of exposure to 4% (w/w) sodium sulfate solution.

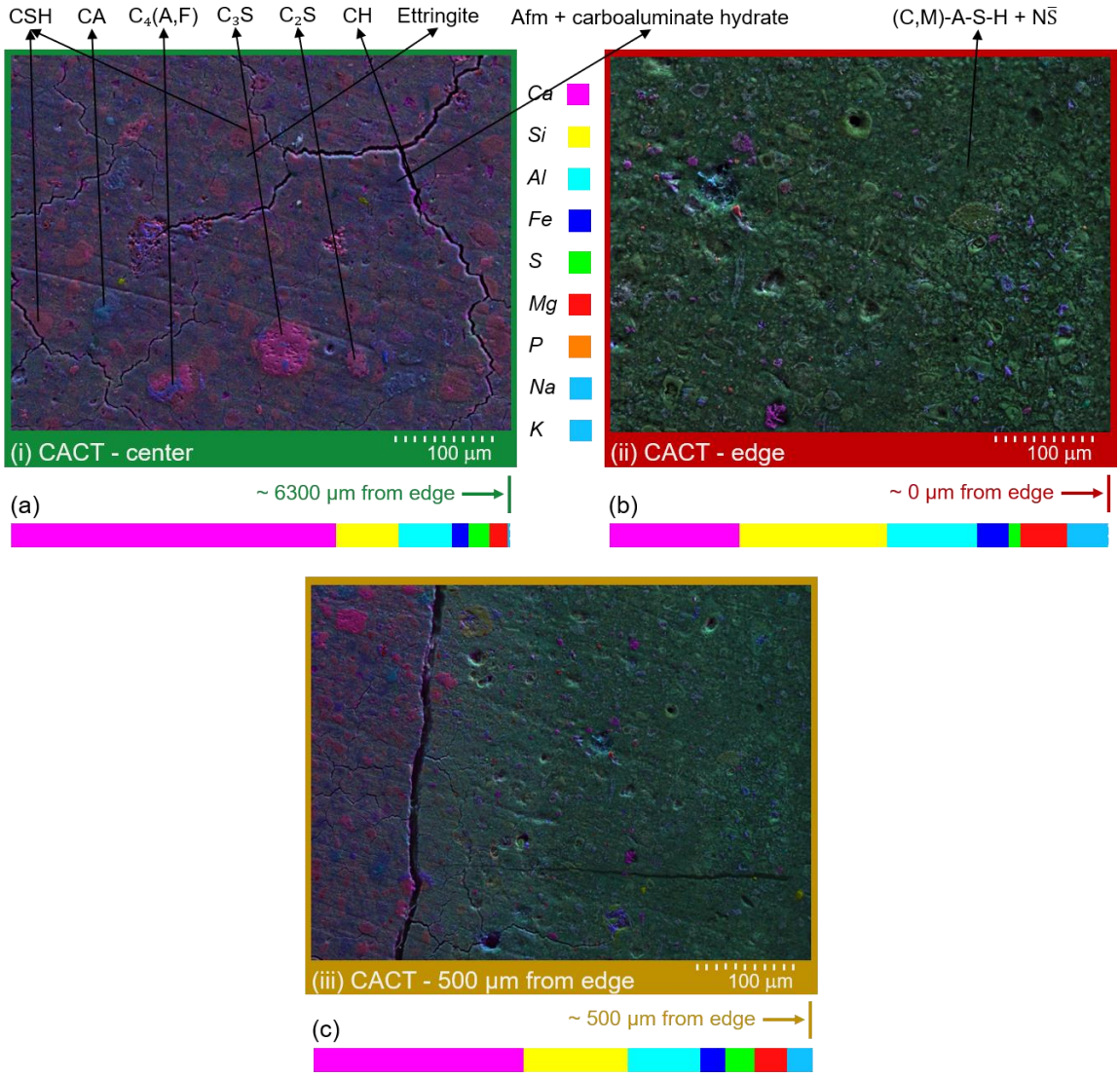

Fig. 73 SEM-EDS micrographs of CACT cement paste cube exposed to 4% (w/w) sodium sulfate solution for 20 weeks. Images were taken at approximately (i) 6300 µm, (ii) 0 µm, and (iii) 500 µm from the edge of the cube. (a), (b), and (c) are normalized elemental distributions in micrograph given in (i), (ii), and (iii) respectively.

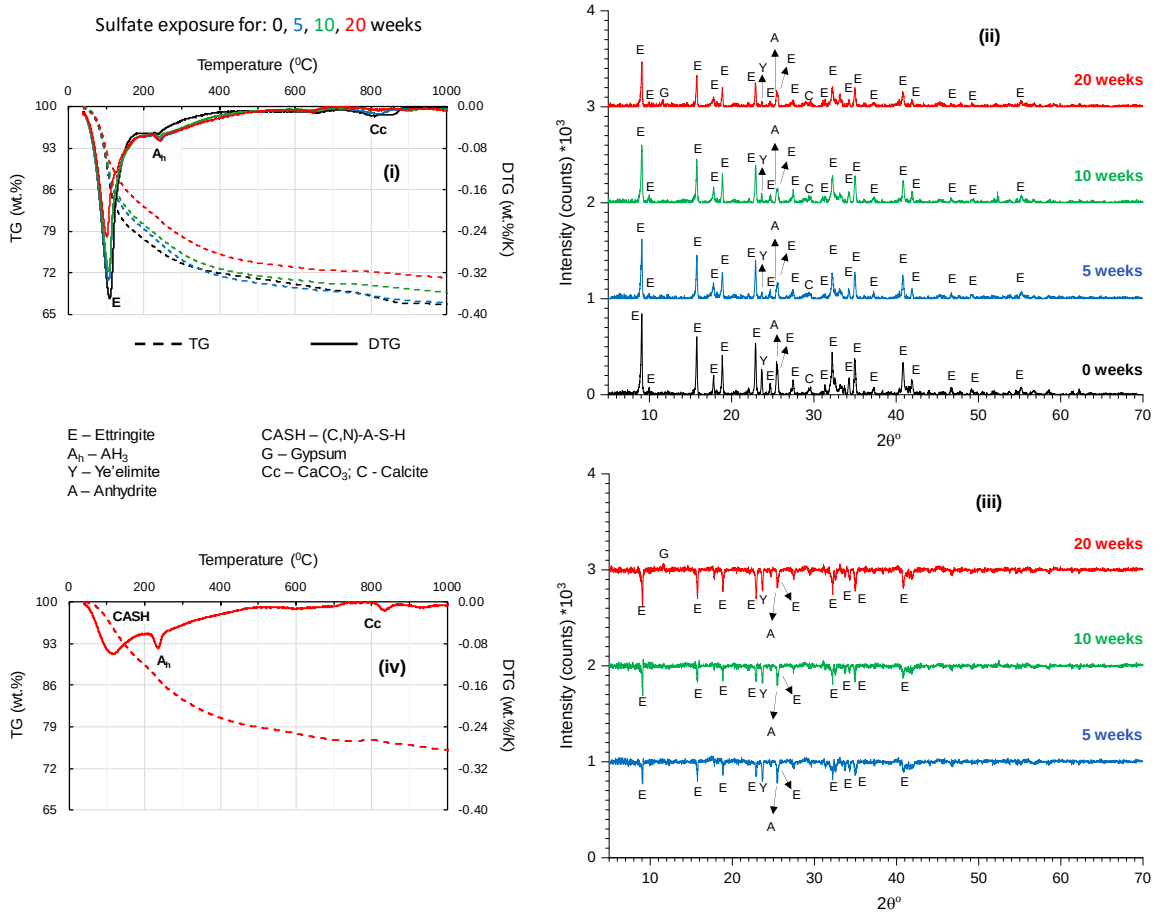

Fig. 74 (i) TG and DTG, (ii) XRD of CSA1 cement paste cubes exposed to 4% (w/w) sodium sulfate solution for 0, 5, 10, and 20 weeks. (iii) Shows difference in XRD peaks of CSA1 cement paste cubes after exposure versus without exposure. (iv) TG and DTG of CSA1 paste cubes on the outer 500 µm layer after 20 weeks of exposure to 4% (w/w) sodium sulfate solution.

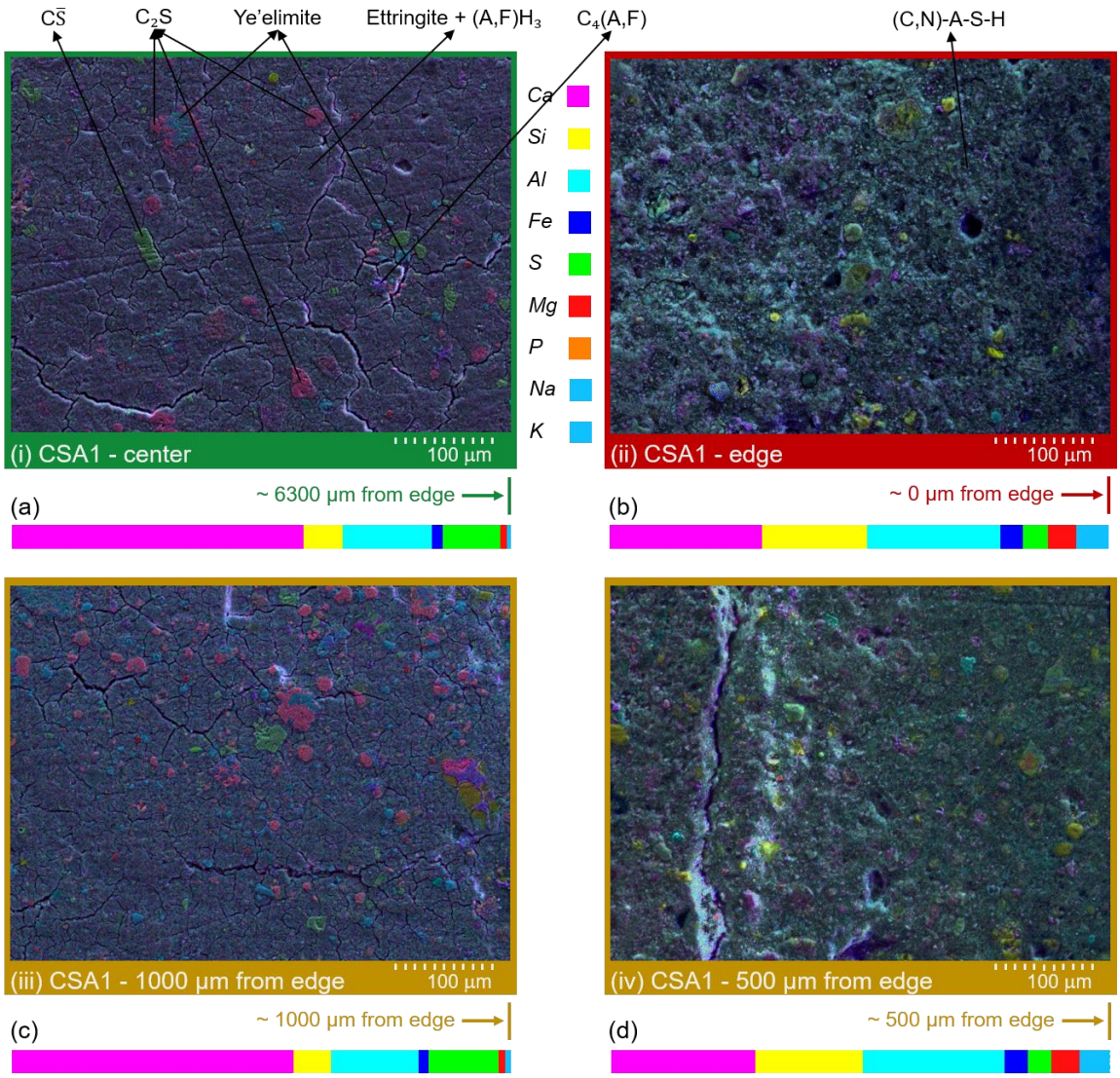

Fig. 75 SEM-EDS micrographs of CSA1 cement paste cube exposed to 4% (w/w) sodium sulfate solution for 20 weeks. Images were taken at approximately (i) 6300 µm, (ii) 0 µm, (iii) 500 µm, and (iv) 1000 µm from the edge of the cube. (a), (b), (c), and (d) are normalized elemental distributions in micrograph given in (i), (ii), (iii), and (iv) respectively.

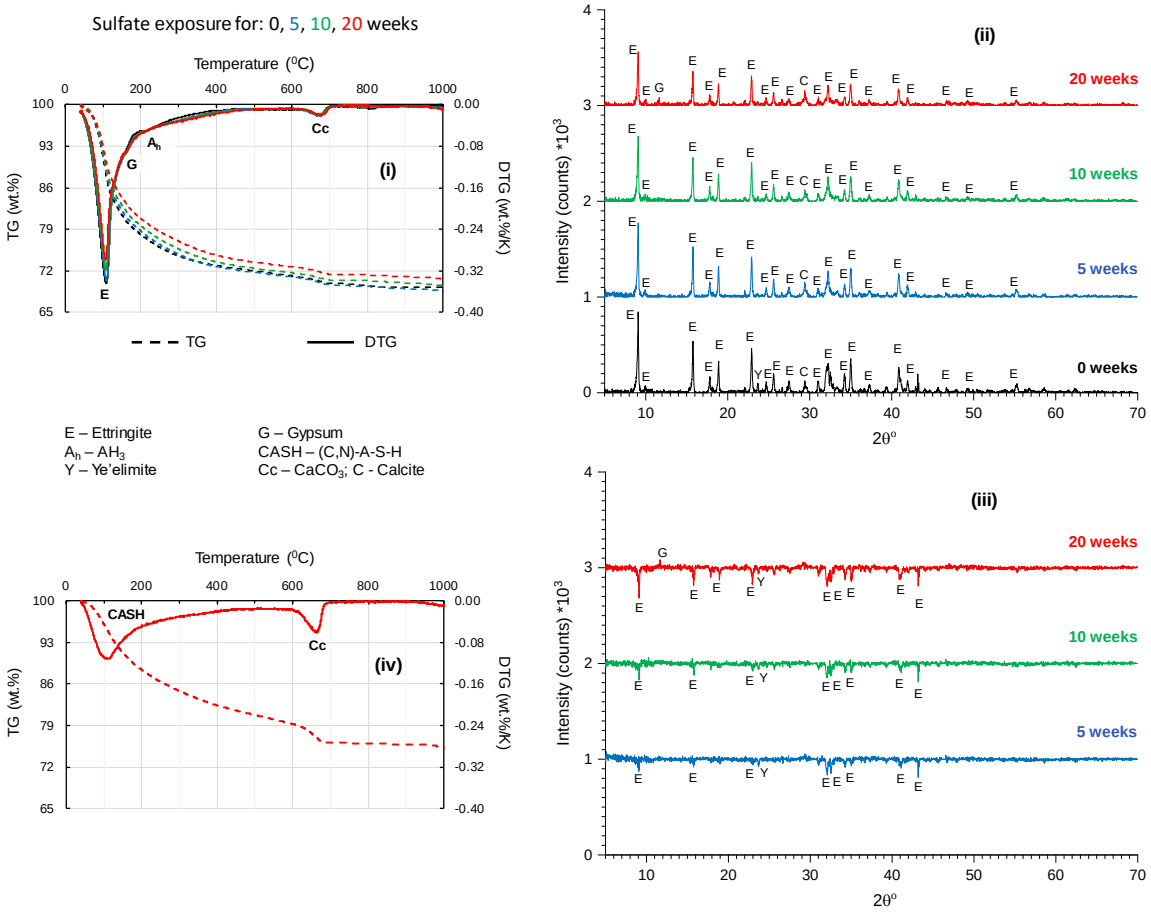

Fig. 76 (i) TG and DTG, (ii) XRD of CSA2 cement paste cubes exposed to 4% (w/w) sodium sulfate solution for 0, 5, 10, and 20 weeks. (iii) Shows difference in XRD peaks of CSA2 cement paste cubes after exposure versus without exposure. (iv) TG and DTG of CSA2 paste cubes on the outer 500 µm layer after 20 weeks of exposure to 4% (w/w) sodium sulfate solution.

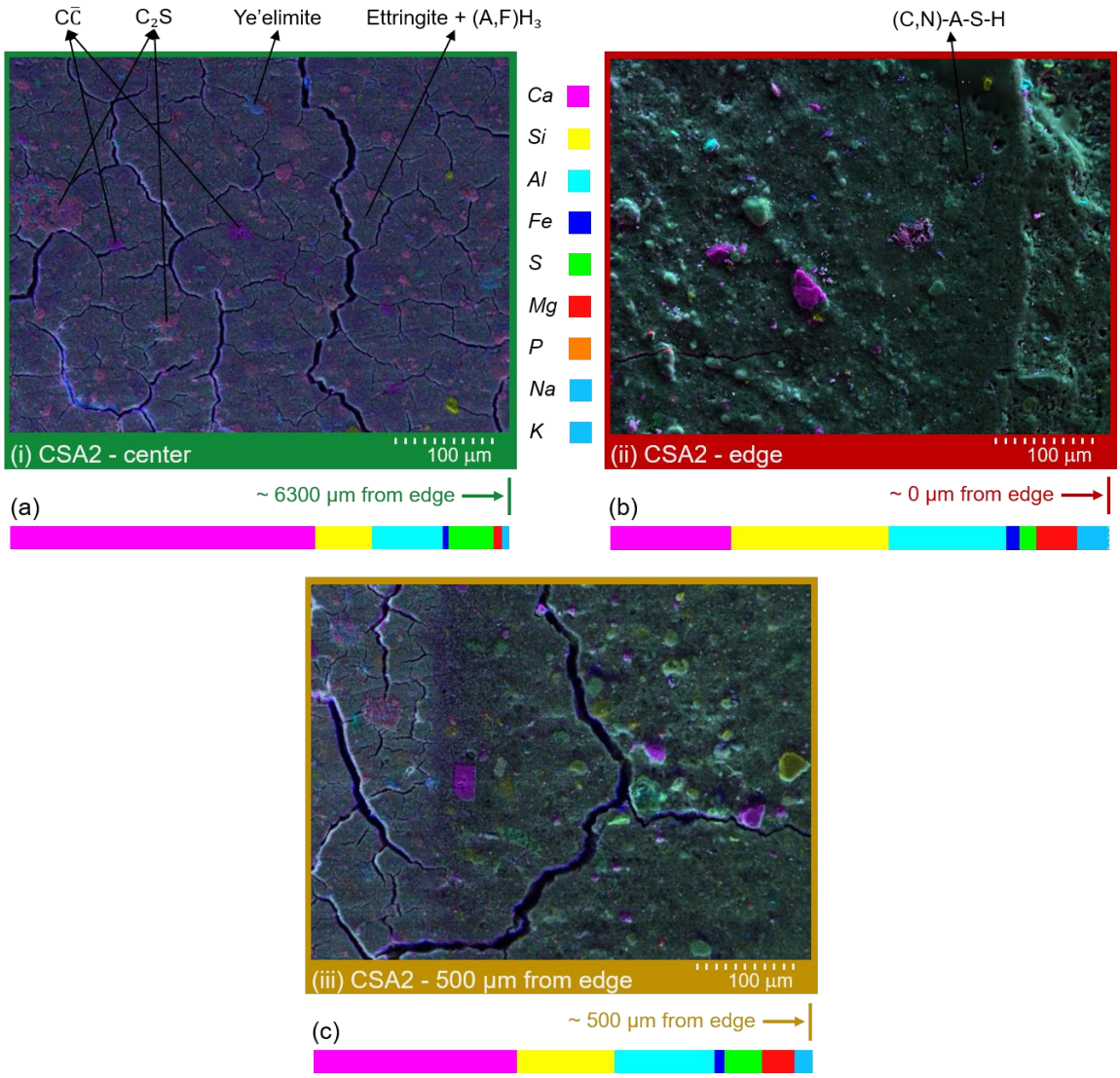

Fig. 77 SEM-EDS micrographs of CSA2 cement paste cube exposed to 4% (w/w) sodium sulfate solution for 20 weeks. Images were taken at approximately (i) 6300 µm, (ii) 0 µm, and (iii) 500 µm from the edge of the cube. (a), (b), and (c) are normalized elemental distributions in micrograph given in (i), (ii), and (iii) respectively.

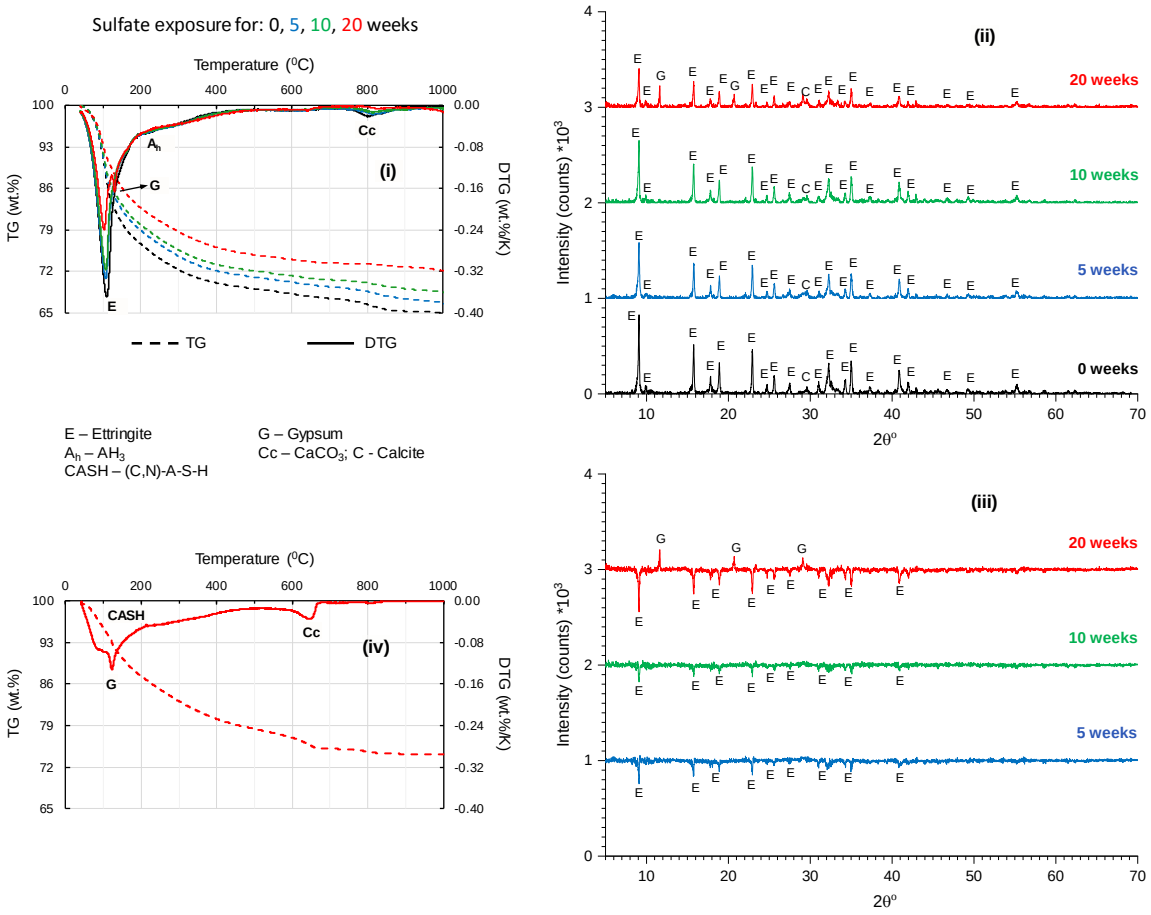

Fig. 78 (i) TG and DTG, (ii) XRD of CSA2P cement paste cubes exposed to 4% (w/w) sodium sulfate solution for 0, 5, 10, and 20 weeks. (iii) Shows difference in XRD peaks of CSA2P cement paste cubes after exposure versus without exposure. (iv) TG and DTG of the outer spalled surface in CSA2P paste cubes after 20 weeks of exposure.

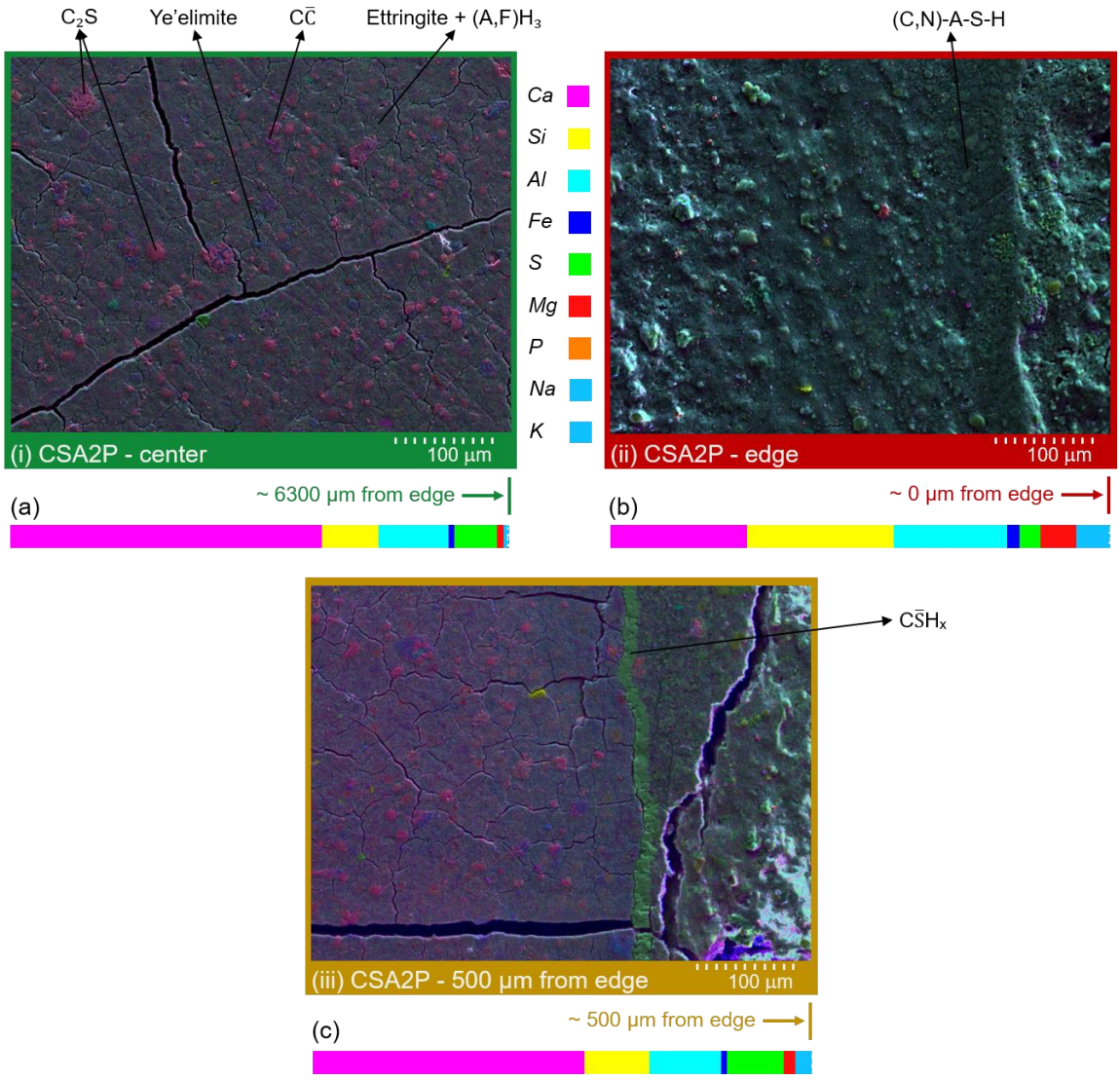

Fig. 79 SEM-EDS micrographs of CSA2P cement paste cube exposed to 4% (w/w) sodium sulfate solution for 20 weeks. Images were taken at approximately (i) 6300 µm, (ii) 0 µm, and (iii) 500 µm from the edge of the cube. (a), (b), and (c) are normalized elemental distributions in micrograph given in (i), (ii), and (iii) respectively.

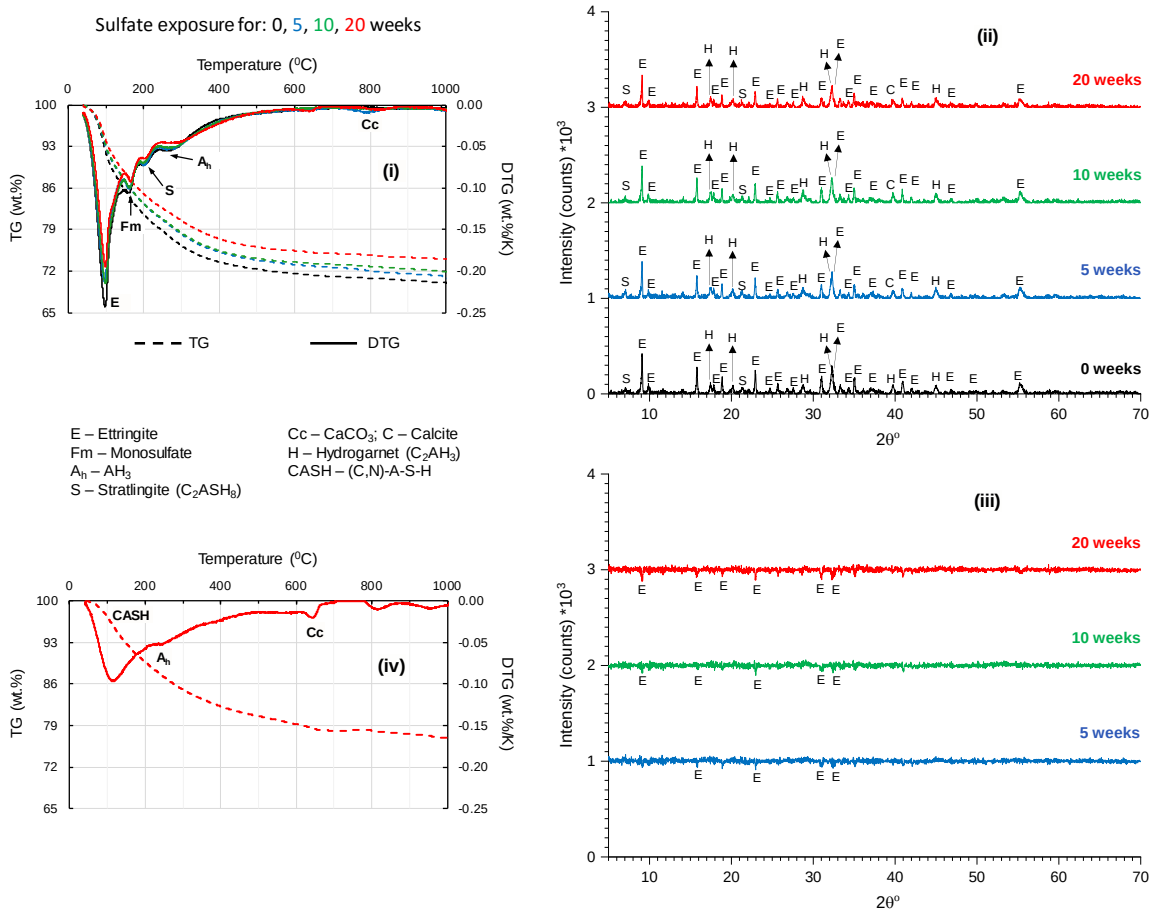

Fig. 80 (i) TG and DTG, (ii) XRD of CSA3 cement paste cubes exposed to 4% (w/w) sodium sulfate solution for 0, 5, 10, and 20 weeks. (iii) Shows difference in XRD peaks of CSA3 cement paste cubes after exposure versus without exposure. (iv) TG and DTG of CSA3 paste cubes on the outer 500 µm layer after 20 weeks of exposure to 4% (w/w) sodium sulfate solution.

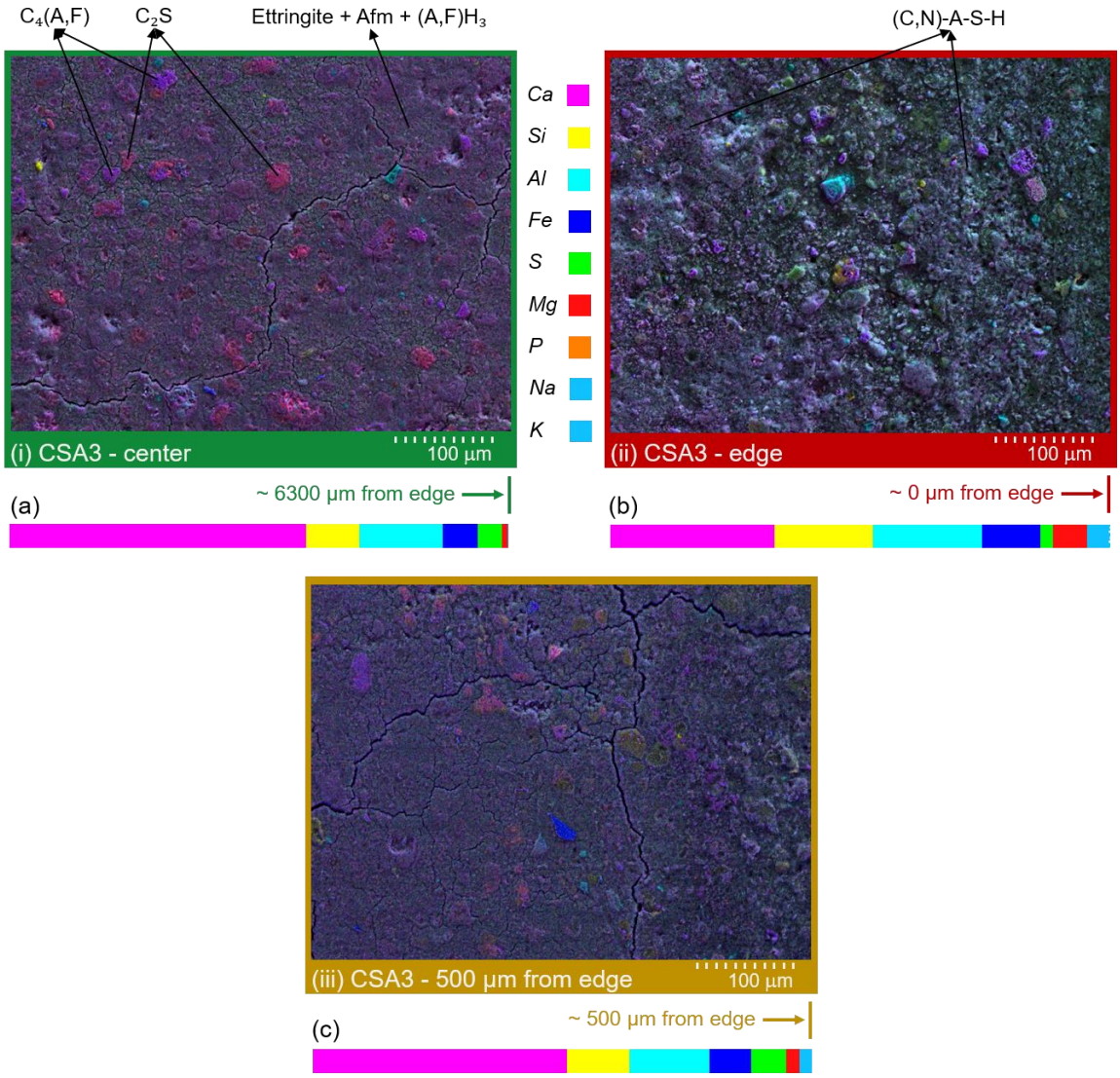

Fig. 81 SEM-EDS micrographs of CSA3 cement paste cube exposed to 4% (w/w) sodium sulfate solution for 20 weeks. Images were taken at approximately (i) 6300 µm, (ii) 0 µm, and (iii) 500 µm from the edge of the cube. (a), (b), and (c) are normalized elemental distributions in micrograph given in (i), (ii), and (iii) respectively.

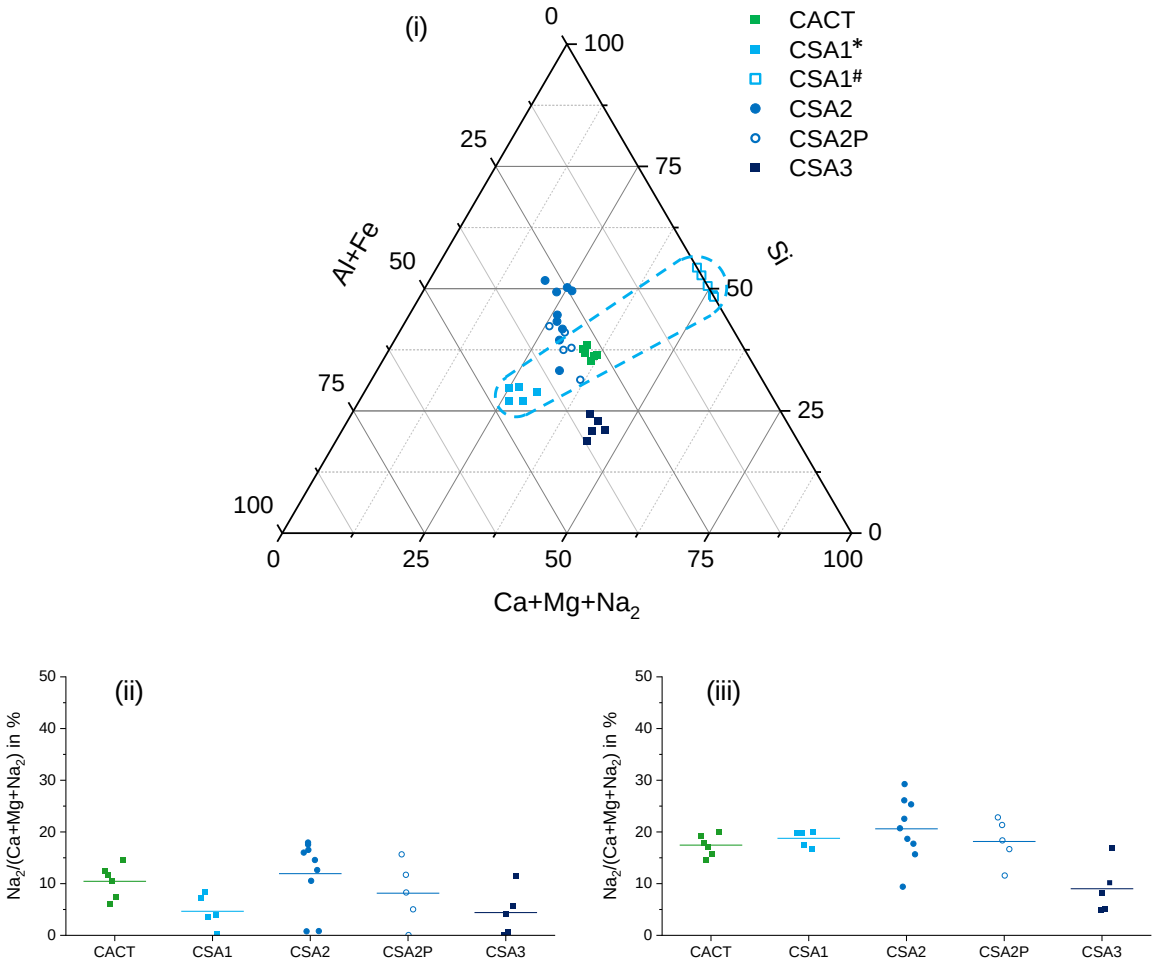

Fig. 82 (i) Ternary plot of atomic moles percentage of ($Ca+Mg+Na_2$), Si, (Al+Fe) in the C-N-A-S-H structure present in the outer layer of CACT, CSA1, CSA2, CSA2P, and CSA3 mixtures after 20 weeks of exposure. (ii) Percentage of Na_2 w.r.t. combination of ($Ca+Mg+Na_2$) in moles assuming all the sulfates are bound as Na_2SO_4. (iii) Percentage of Na_2 w.r.t. combination of ($Ca+Mg+Na_2$) in moles assuming all the sulfates are bound as $CaSO_4$. Note: For CSA1 mixtures, AH_3 phase also precipitated in addition to C-N-A-S-H. Since it is difficult to separate out those two phases in SEM-EDs, a possible range of composition of C-N-A-S-H is provided (dotted region in [i]) for CSA1 mixtures. *Assuming all the (Al+Fe) is present in C-N-A-S-H phase instead of in AH_3 phase. #Assuming all the (Al+Fe) is present in AH_3 phase instead of in C-N-A-S-H phase.

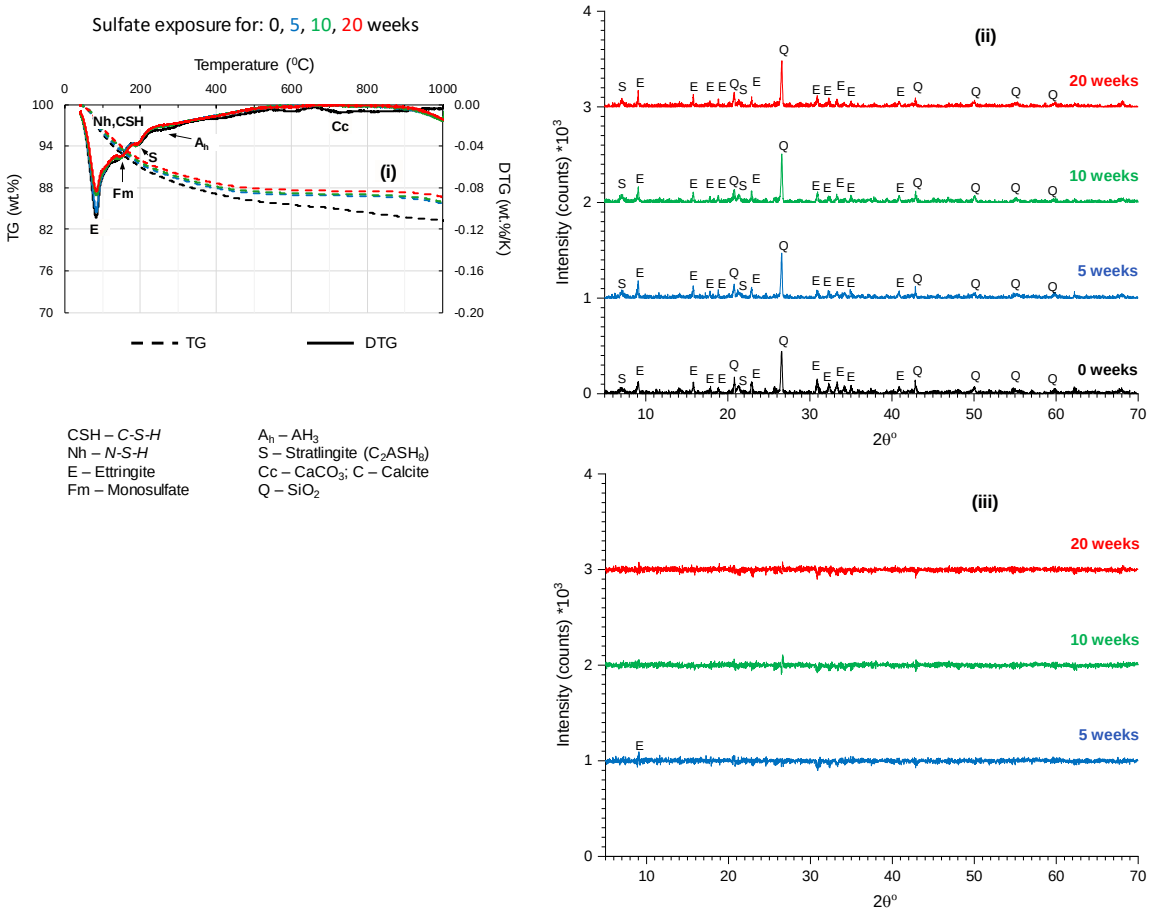

Fig. 83 (i) TG and DTG, (ii) XRD of AA paste cubes exposed to 4% (w/w) sodium sulfate solution for 0, 5, 10, and 20 weeks. (iii) Shows difference in XRD peaks of AA paste cubes after exposure versus without exposure.

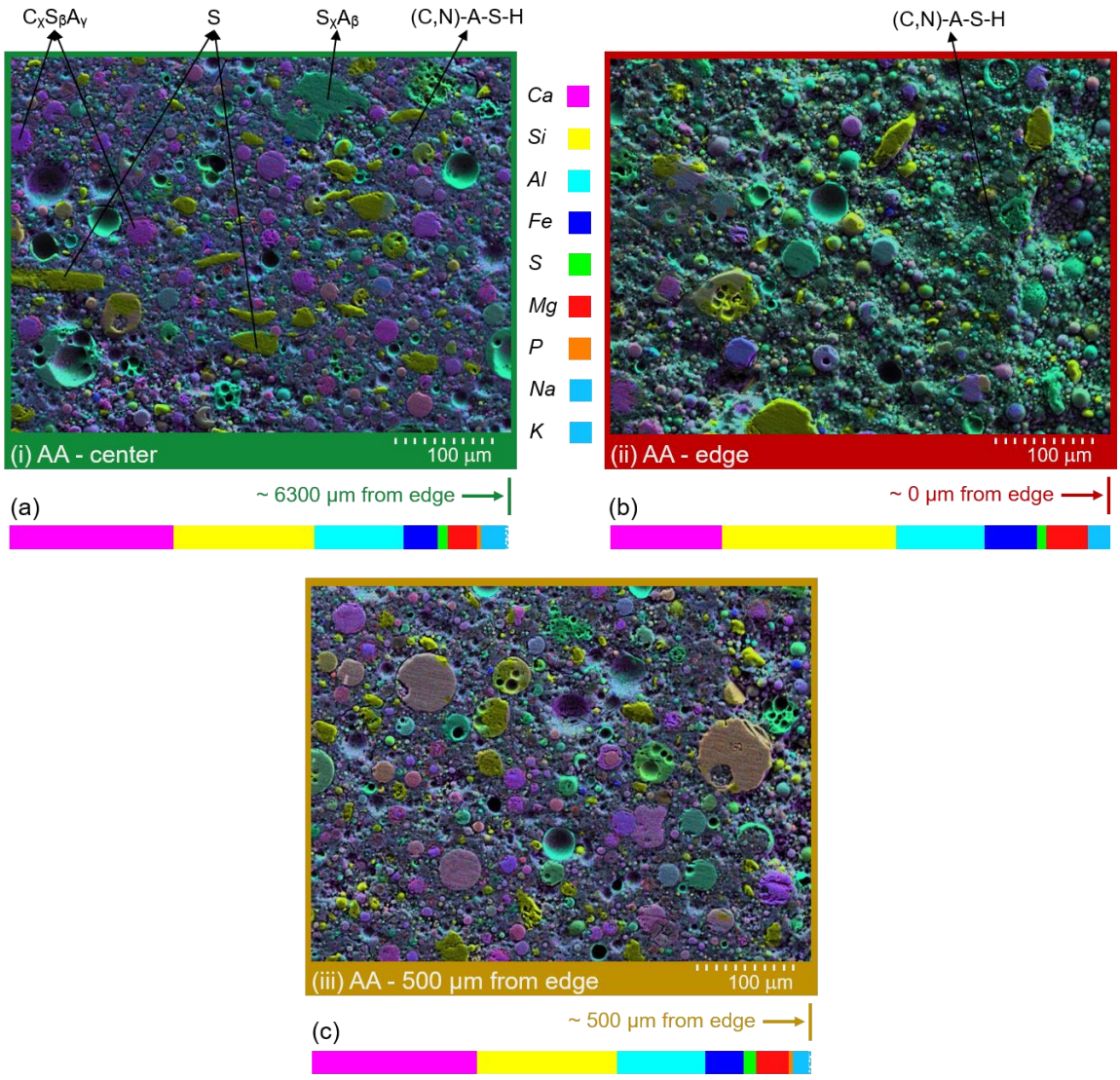

Fig. 84 SEM-EDS micrographs of AA cement paste cube exposed to 4% (w/w) sodium sulfate solution for 20 weeks. Images were taken at approximately (i) 6300 µm, (ii) 0 µm, and (iii) 500 µm from the edge of the cube. (a), (b), and (c) are normalized elemental distributions in micrograph given in (i), (ii), and (iii) respectively.

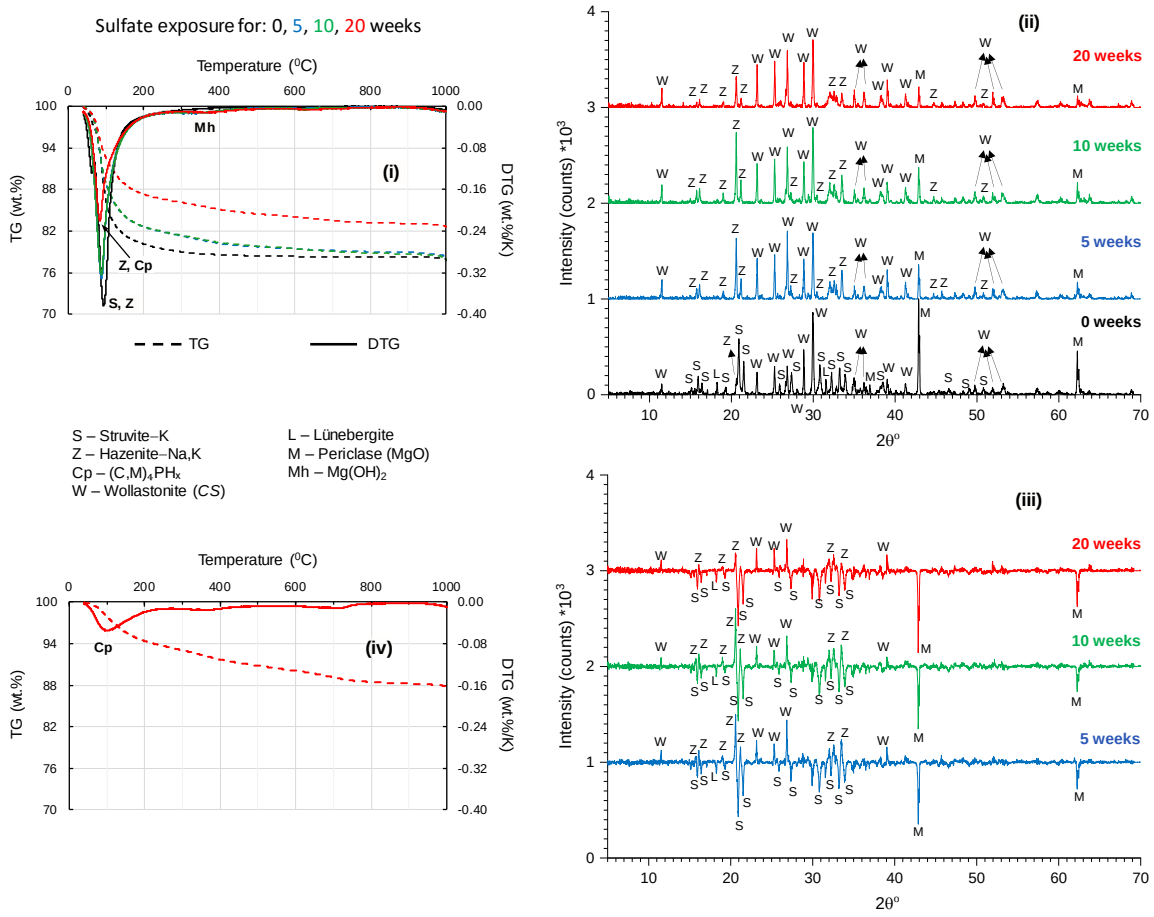

Fig. 85 (i) TG and DTG, (ii) XRD of MPC cement paste cubes exposed to 4% (w/w) sodium sulfate solution for 0, 5, 10, and 20 weeks. (iii) Shows difference in XRD peaks of MPC cement paste cubes after exposure versus without exposure. (iv) TG and DTG of MPC paste cubes on the outer 500 µm layer after 20 weeks of exposure to 4% (w/w) sodium sulfate solution.

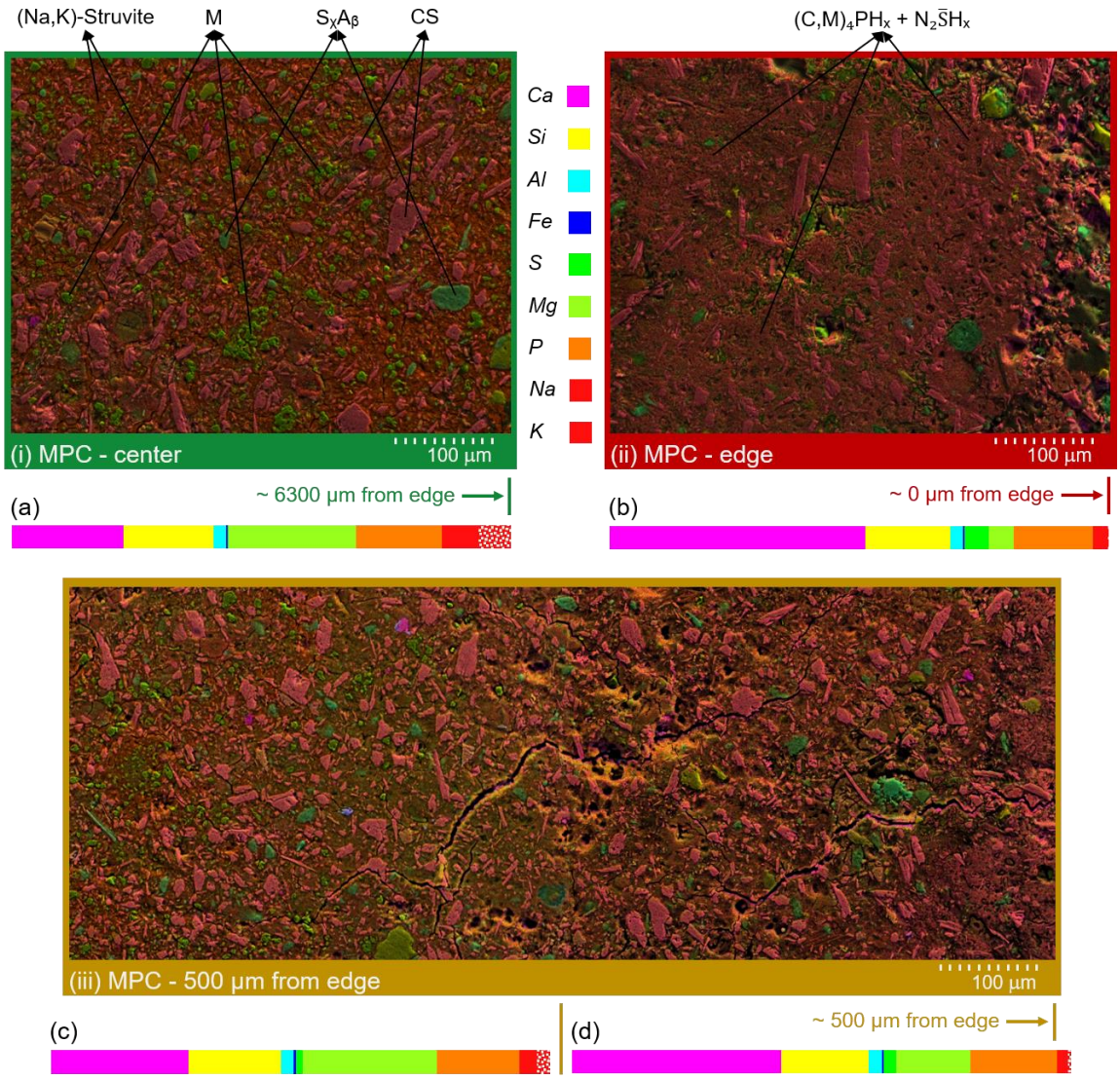

Fig. 86 SEM-EDS micrographs of MPC cement paste cube exposed to 4% (w/w) sodium sulfate solution for 20 weeks. Images were taken at approximately (i) 6300 µm, (ii) 0 µm, and (iii) 500 µm from the edge of the cube. (a), (b), (c), and (d) are normalized elemental distributions in micrograph given in (i), (ii), left half of (iii), and right half of (iii) respectively.

10.4 Conclusions and Recommendations

The accelerated sulfate exposure tests at constant pH, along with complementary characterization by TGA, XRD, and SEM-EDS performed in this study were intended to understand the chemical sulfate mechanisms in OPC and ACM mixtures, and evaluate the

performance of commercially available ACM systems in resisting chemical sulfate exposure compared to OPC systems, and has led to the following conclusions.

- Crystallization of gypsum is the primary damage mechanism observed in all the mixtures that showed significant spalling and cracking (except CAC1 and CAC2) when the mixtures are subjected to constant pH sulfate exposure.

- Even though a significant amount of gypsum formed and crystallized in the outer exposed layer of OPC mixtures, it did not result in cracking of the whole matrix – since the outer layer was already weekend due to the decalcification of C-S-H, so expansive stresses generated by gypsum crystallization resulted in significant spalling of outer layer rather than cracking in the inner matrix.

- A dense outer layer composed of C-N-A-S-H is formed in all the CSA and CACT mixtures with exposure to sodium sulfate. This layer reduced the permeability of sodium sulfate into the inner matrix. However, in the CSA2P mixture, a layer of gypsum is formed between this dense outer layer and the inner matrix. Since the outer layer is dense compared to the decalcified C-S-H layer in the OPC mixtures, the expansive stresses generated by the crystallization of gypsum in CSA2P mixtures resulted in significant cracking of the inner matrix. Further research is needed to understand the cause for the formation of this gypsum only in the polymer-modified CSA mixtures (i.e., CSA2P).

- The CAC mixtures having a lower amount of C_3AH_6 phase performed significantly better compared to the mixtures containing the C_3AH_6 phase. So, conversion in CAC mixtures can lead to significant degradation with sulfate exposure due to the

formation of ettringite from the C_3AH_6 phase. CACs with a lower amount of $C_{12}A7$ phase and produced at lower w/b can drastically improve the sulfate resistance.

- In AA mixtures, no significant degradation is observed even though some decalcification of the outer layer is observed. Whereas in MPC mixtures, exposure to sodium sulfate solution resulted in significant leaching of Mg from the outer layer and partial alkali replacement in the K-Struvite phase. However, no significant degradation in microstructure or compressive strength is observed.

Overall, CSA3, AA, MPC, and CAC2 (before conversion) mixtures exhibited superior resistance to chemical sulfate attack, followed by CACT, CSA2, and CSA1 mixtures compared to that of OPC. CAC1 and CSA2P, followed by both the converted CAC1 and CAC2 systems, exhibited the least resistance to chemical sulfate attack. Even though OPC showed strengthening at later exposure ages, the exposure resulted in significant spalling of the outer surfaces.

11 RESISTANCE TO ALKALI EXPOSURE

11.1 Introduction

Two durability mechanisms associated with alkali exposure are examined in the chapter: (1) alkali degradation of binders and (2) resistance to damage by the alkali-silica reaction. First, some ACMs are known to exhibit poor alkali resistance [133–138], which can limit their suitability for use as a replacement to portland cement concrete, as an over the cement-treated base, or as a whitetopping or adjacent to any portland cement concrete, where high pH runoff is likely to occur. Calcium aluminate hydrates are known to undergo alkali hydrolysis, which leads to the decomposition of aluminate hydrates to alkali aluminate and calcium hydroxide [134–136]. The mixtures made with calcium sulfoaluminate hydrates are also found to decompose to thernadite (Na_2SO_4) or mirabilite ($Na_2SO_4 \cdot 10H_2O$) when exposed to the high alkaline environment (pH $\geq$ 14) [138]. Magnesium phosphate mixtures containing struvite phase are also not resistant to high alkaline exposure due to the low stability of struvite phase [133]. However, the stability of K-struvite phase is not known and needs to be verified. Portland cement mixtures are also known to degrade at high alkali exposure levels and temperatures [139,140]. To rapidly assess alkali resistance, OPC and ACM mortars, cast with non-reactive aggregates, are tested in the accelerated mortar bar test (AMBT) by ASTM C1260.

Alkali-silica reaction (ASR) in one of the primary durability issues in portland cement concrete mixtures (OPC). For the damaging reaction to occur due to ASR, the following four conditions are required: (1) sufficient quantity of reactive silica either within the fine or coarse aggregate, (2) sufficient concentration of hydroxyl ions (pH) in the system, (3)

sufficient concentration of alkali (primarily from cements or sometimes can be from external exposure), and (4) sufficient moisture (primarily from exterior exposure) [141,142]. A sufficient concentration of hydroxy ions is required to facilitate the dissolution of silica. Calcium ions also play an essential role in the expansion of alkali-silica gel. Calcium promotes alkali recycling and promotes further reaction by regenerating alkalis. The formation of calcium-rich ASR gels is also necessary to cause expansion as they are known to be highly viscous and form semi-permeable membrane around the reactive aggregate particles [141,143–148]. CAC and CSA cement mixtures have low alkalinity and pH compared to OPC mixtures [5] and also lower calcium hydroxide content (section 4.2.1), which could lead to lower ASR damage in these CAC and CSA mixtures compared to OPC mixtures. To date, no ASR tests were performed on CAC mixtures to validate their effectiveness in resisting ASR. Extensive research has been performed to understand the ASR in alkali-activated materials [149–154], all of which showed the superior performance of these materials in resisting ASR compared to OPC mixtures. However, no research has been done to understand the ASR in activated aluminosilicates that are primarily activated by lactates and citrates (for example, the AA mixtures investigated in this thesis). MPC formulations were also not investigated extensively till now to understand the ASR in these mixtures, especially in MPC formulation containing significant amounts of potassium.

To understand the performance of ACM mixtures resisting ASR-induced expansion and cracking when exposed to a high pH environment, the AMBT test was performed on these binders in combination with reactive aggregate. In addition to the AMBT tests, the modified Concrete Prism Test (CPT) by ASTM C1293 was also performed to assess their

resistance to ASR when exposed to high humidity rather than an external high pH environment. Because some of the ACM formulations (AA and MPC) examined in this chapter have a high amount of alkalis (Table 2), it will be essential to assess the potential for ASR-induced expansion and cracking. CPT is selected because it is the only current standardized test method where the assessment can be done without inducing significant leaching, which is problematic in other standard ASR tests.

However, leaching can still be an issue, particularly in systems with less tortuous network [155–157]. So, a complementary cylinder mortar test (CMT) was also performed to minimize leaching. This complementary cylinder mortar test is adopted from the concrete cylinder test (CCT) [158–160]. CCT test was developed to overcome the leaching issues and long testing duration with the CPT test. However, in the trial CCT tests performed on ACMs, significant leaching was still observed on the water ponded surface (especially in CACT and MPC mixtures). To further minimize the leaching issues and to further accelerate the testing duration, a modified cylinder mortar test was designed and performed as complementary to the CPT test. More details about this modified cylinder test are provided in section 11.2.2.

To allow for true comparison among the binders, the alkali content of the concretes will not be "boosted" in the CPT, and the cylinder mortar test evaluation [161]. Instead, portland cement concrete prisms cast with and without SCM (class C Fly ash at high replacement level), suitable for mitigation of expansion of the reactive aggregate, will serve as lower and upper bounds for performance.

11.2 Methods

11.2.1 ASTM 1260 length expansion test

Mortar bars of dimensions 11.25 × 1 × 1 inches were prepared with potentially reactive and nonreactive aggregates. The mixture proportions for the cement mortars are shown in Table 19. Crushed metapelite green schist aggregate (Vulcan Materials Company, Gold Hill, North Carolina) with gradation conforming to ASTM 1260 standard was used as a reactive aggregate , whereas Georgia DOT approved crushed granitic river sand (Lambert Sand and Gravel, Shorter, Alabama) with gradation also conforming to ASTM 1260 standard was used as a potentially nonreactive aggregate. The composition of the metapelite green schist aggregate is shown in Table 20. Mortar samples were prepared and cured according to ASTM 1260 test method and exposed to 1N sodium hydroxide solution at 80 ºC for 120 days, with expansions measured at different intervals.

Table 19 Cement mortar mixture proportions.

Cement	w/b	Admixtures/ activators (by weight of cement)	Cement (g)	Water (g)	Sand (g)
OPC	0.47	–	100	47	225
CAC2	0.47	–	100	47	225
CACT	0.47	citric acid – 1.5%	100	47	225
CSA1	0.47	citric acid – 2.0%	100	47	225
CSA2	0.47	citric acid – 0.5%	100	47	225
CSA2P	0.47	citric acid – 0.5%	100	47	225
CSA3	0.47	citric acid – 0.75%	100	47	225
AA	0.30	activator 1 - 2.47%, activator 2 - 2.21%	100	30	225
MPC	0.30	boric acid – 14%	100	30	225

Table 20 Phase composition* of the metapelite green schist reactive aggregate.

Phase	Amount (%)
Muscovite	39
Clinochlore	31
Quartz	18
Albite	9
Calcite	1
Orthoclase	1
Cristobalite	1

*Source: Robert Moser, U.S. Army Engineer Research and Development Center, Vicksburg, MS.

11.2.2 Mortar cylinder test

Cylinder mortar samples of height 60 mm and diameter 27 mm are prepared with reactive aggregate according to the mixture proportions given in Table 19. Crushed metapelite green schist aggregate (Vulcan Materials Company, Gold Hill, North Carolina) was used as a reactive fine aggregate. Using the reactive aggregate as fine aggregate instead of coarse aggregate (in CCT) can accelerate the ASR due to the increased surface are of aggregate. The gradation of the fine aggregate follows the ASTM 1260 standard. Three samples were cast for each of the mixture proportions in polypropylene centrifuge tubes with the inside sidewall covered with wick lining, as shown in Fig. 87. The wick extends from the bottom of the centrifuge tube to the top end of the water reservoir to transport the moisture to the sample. In order to minimize the water draw from mortar mixtures by the wick lining during curing, the wick lining was pre-saturated at 100% RH environment prior to casting the samples. After casting, the samples were cured for 1 day in sealed condition, and later

the top surface of the cylinder is coated with epoxy of medium-to-high viscosity to prevent leaching, and also to force the water from the top reservoir to only enter the sample from the sides. The samples were further cured in the airtight condition until 7 days of hydration time. Later the samples were placed in an airtight container with deionized and deaerated water reservoir on the bottom of the container, as shown in Fig. 88. The top reservoir on each of the samples is also filled with deionized and deaerated water, and the samples were exposed to 100% RH environment at 60 ºC for 384 days. Initial length measurements were made with the length comparator after 12 hours of exposure to 100% RH and 60 ºC, with subsequent measurements made at 3, 7, 14, 28, 42, 56, 84, 165, and 384 days of exposure.

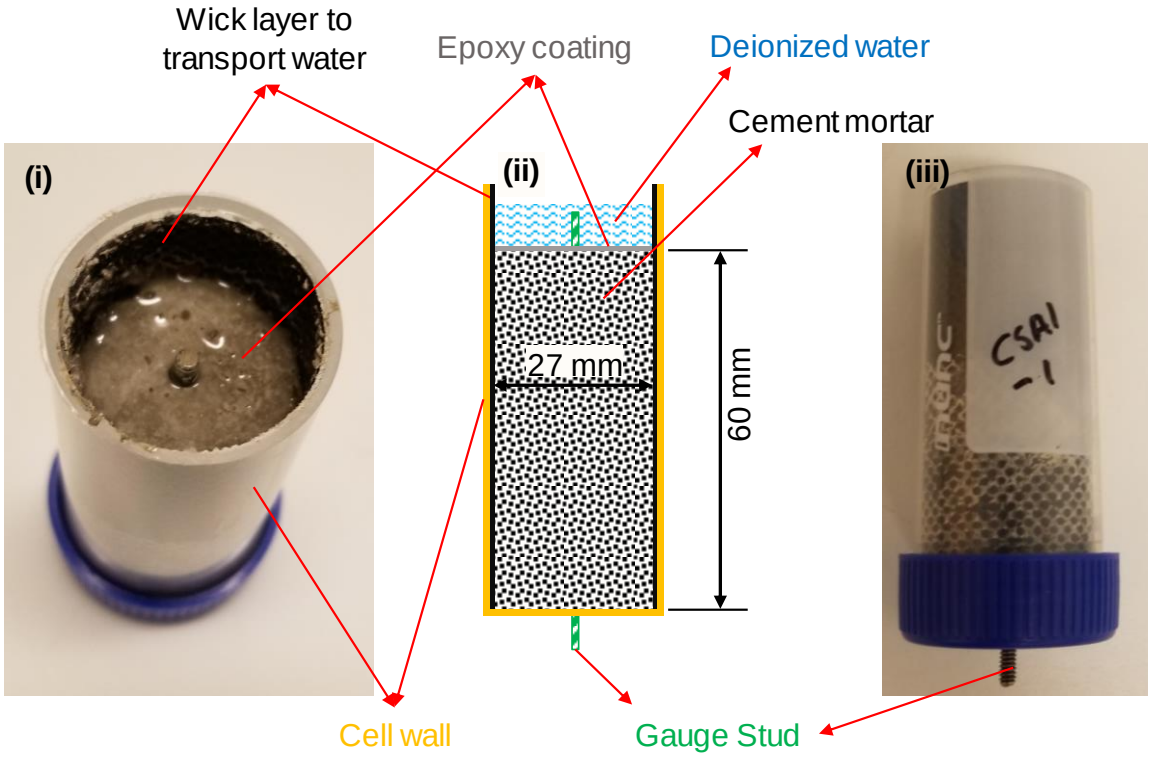

Fig. 87 (i) and (iii) Photo of a cylinder mortar sample showing wick and gauge studs. (ii) Sketch of the cylinder mortar sample used for testing the resistance of binder towards ASR reaction.

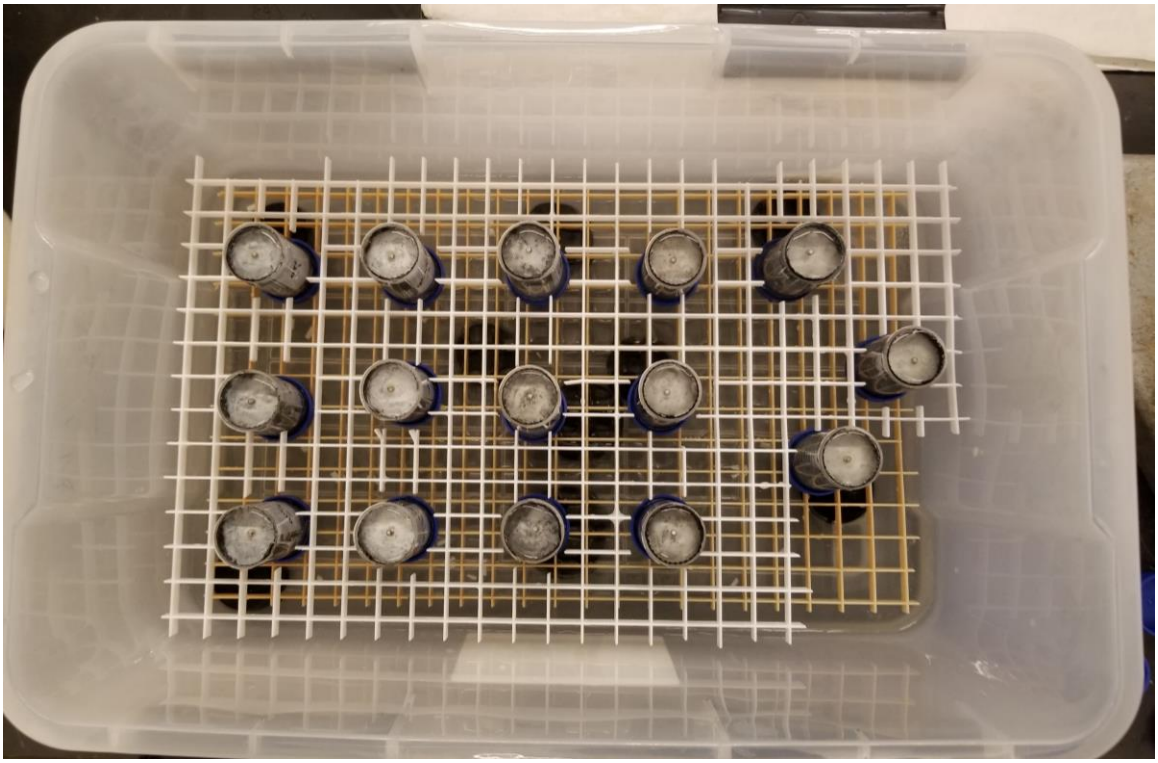

Fig. 88 Water ponded cylinder mortar samples placed in a container.

11.2.3 Modified ASTM 1293 length expansion test

Concrete prisms of dimensions 11.25 × 3 × 3 inches were cast with potentially reactive coarse aggregate and potentially nonreactive fine aggregate according to the mixture proportions given in Table 21. Crushed metapelite green schist aggregate (Vulcan Materials Company, Gold Hill, North Carolina) was used as a coarse aggregate, whereas Georgia DOT approved crushed granitic river sand (Lambert Sand and Gravel, Shorter, Alabama) with gradation conforming to ASTM C33 specification was used as a fine aggregate. The gradation of the coarse aggregate meets the requirements of ASTM 1293. The fine aggregate had an expansion less than 0.1% at 14 days when tested according to the ASTM C1260 test (section 11.3.1). All the concrete prisms were demolded after 1 day and cured in sealed condition for 56 days at 23 ºC. Later, the samples were placed in a

sealed cylindrical container with a water reservoir on the bottom and placed in 38 ºC storage environment for the remaining duration of the test. The height difference between the top surface of the water in the reservoir and the bottom surface of the samples is maintained at 15 mm. The inside sidewall of the container is covered with wick (shown in Fig. 89) that extends from the bottom to top of the container to uniformly distribute moisture inside the container. Initial length measurements were made with comparator after 1 day of exposure to 100% RH at 38 ºC, with subsequent measurements at 3, 6, 9, 12, 18 and 24 months of exposure.

Table 21 Concrete mixture proportions.

Cement	w/b	Admixtures/ activators (by weight of cement)	Cement (kg/m^3)	Water (kg/m^3)	Sand (kg/m^3)	#67 aggregate (kg/m^3)
OPC	0.45	HRWR1 – 2.0 ml/kg	454	210	574	1120
OPC + Flyash	0.45	HRWR1 – 1.2 ml/kg	227 (OPC) + 227 (Class C Fly ash)	210	541	1120
CAC2	0.45	–	454	211	563	1120
CACT	0.45	citric acid – 1.5%, HRWR1 – 2.0 ml/kg	454	210	544	1120
CSA1	0.45	citric acid – 2.0% HRWR1 – 2.0 ml/kg	454	211	526	1120
CSA2	0.45	citric acid – 0.5%	454	211	537	1120
CSA2P	0.45	citric acid – 0.5%	454	211	537	1120
CSA3	0.45	citric acid – 0.75%	454	211	561	1120
AA	0.25	activator 1 - 2.27%, activator 2 – 1.78%	488	129	684	1120
MPC	0.25	boric acid – 14%	533	211	520	1120

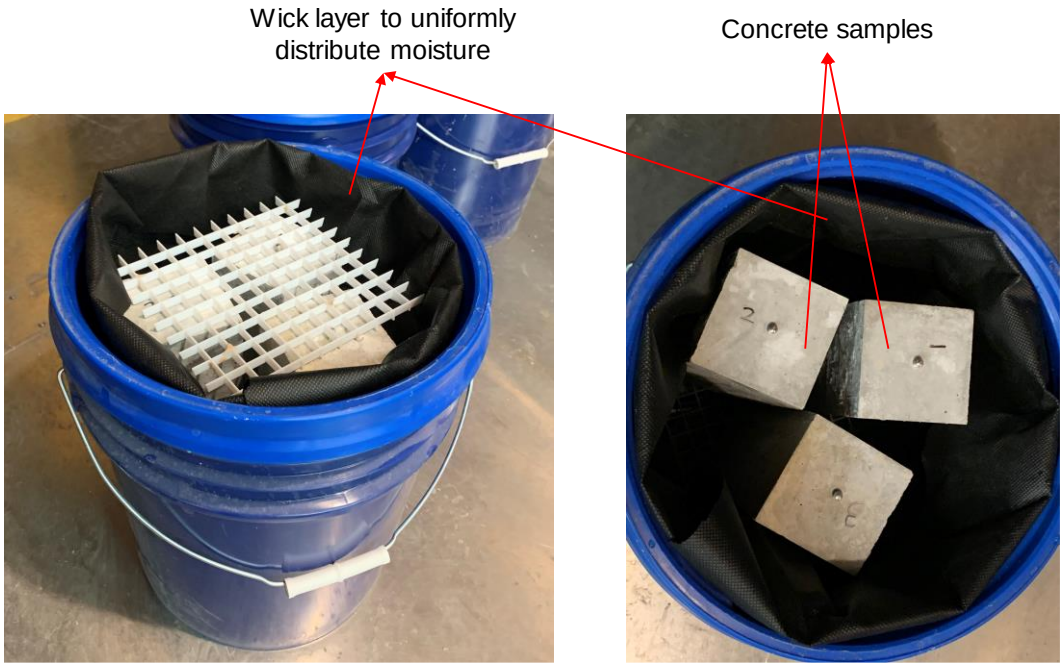

Fig. 89 ASTM 1293 concrete samples placed in an airtight container. Note: the 4th sample is removed from testing at the end of the 2-year exposure period.

11.2.4 Pore solution pH measurement

Pore solution pH measurements were made on cement paste samples made with same w/b and set modifier dosages used in Table 21 using ex-situ leaching cold water extraction method [82,83,162]. Cement paste cubes of dimension 12.7 mm were prepared according to mixture proportions shown in Table 22, and cured for 56 days at 23 ºC and 100% RH. After curing, the paste cubes were crushed and quickly ground to particle size less than 74 µm. Approximately 10 g of the ground sample is taken and mixed with 10 ml of deionized and deaerated water, and stirred vigorously and continuously at 25 ºC under a constant stream of Nitrogen (N_2) gas for 5 min. Immediately after stirring, the mixed suspension is filtered through a 0.45 µm nylon hydrophilic membrane filter. The pH was measured on the extracted solution using a pH electrode.

Table 22 Cement paste mixture proportions.

Cement	w/b	Set modifier/ activators (by weight of cement)
OPC	0.45	–
CAC1	0.45	–
CAC2	0.45	–
CACT	0.45	Citric acid – 1.5%
CSA1	0.45	Citric acid – 2.0%
CSA2	0.45	Citric acid – 0.5%
CSA2P	0.45	Citric acid – 0.5%
AA	0.25	Activator 1 - 2.27%, Activator 2 – 1.78%
MPC	0.25	Boric acid – 14%

11.3 Results and Discussion

11.3.1 ASTM 1260 length expansion test (AMBT)

The length expansions of ACM and OPC cement mortar bars made with potentially non-reactive aggregate are shown in Fig. 90. All the ACM mixtures except MPC had similar or lower expansions compared to OPC after 120 days of exposure – with length expansions less than 0.15%. AA, CAC2, CSA1, and CSA3 showed the lowest expansions (or highest resistance to alkali) compared to that of CACT, CSA2, CSA2P, and OPC. CACT and CSA2 mixtures have a similar expansion, whereas CSA2P had lower expansion compared to CSA2. OPC started to expand at significantly higher rates after 28 days of exposure, with the expansion at 120 days exceeding 0.6%. MPC mortar bars showed the least resistance to alkali exposure compared to OPC and other ACM mixtures, with expansion higher than 0.3% even at 14 days of exposure, and the mortars showed significant disintegration after just 28 days of exposure as shown in Fig. 91.

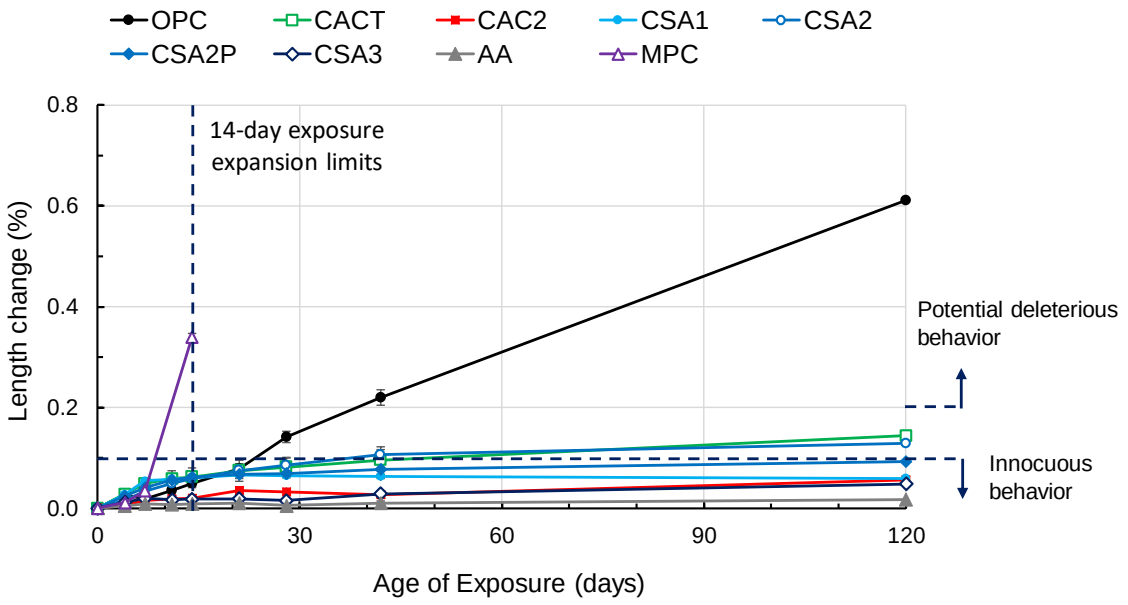

Fig. 90 Length expansion of ACM and OPC mortar mixes made with potentially non-reactive sand and exposed to NaOH solution at 80±1 °C. Mortar bars made with MPC disintegrated after 14 days of exposure. Note: The expansion limits shown here are for 14-day expansion.

Fig. 91 MPC mortars made with potentially non-reactive sand and exposed to NaOH solution at 80±1 ° for 28 days.

Fig. 92 shows the length expansions of ACM and OPC mortar mixtures made with reactive aggregate and exposed to 1M NaOH solution for 120 days. The petrographic examination on the cross-section of mortar bars stained with uranyl acetate and observed under short-wave UV after 120 days of exposure are shown in Fig. 93 to Fig. 102.

OPC mortar bars expanded by about 0.3% after 14 days of exposure and continued to expand to about 0.75% after 120 days of exposure. Fig. 93 shows the images taken on the cross-section of OPC mortar samples stained with uranyl acetate. The images show the presence of alkali throughout the cross-section of the mortar bar and thick layer of ASR gel around the aggregates. The total expansion seen in these OPC mortars is likely due to the combination of expansive stresses generated by the ASR gel and the alkali attack on the binder.

CACT mortar bars showed a significantly higher rate of expansion at an early age compared to OPC mortar bars, with about 0.4% expansion after 14 days of exposure. The rate of expansion after 120 days of exposure was lower than OPC, with total expansion of about 0.55% at the end of the 120-day exposure period. Petrographic examination on the cross-section of the CACT mortar bars (Fig. 94) shows the presence of a relatively higher amount of loosely bound alkalis near the edge compared to the center – whereas a thick layer of ASR gel can be observed around the aggregates throughout the cross-section.

CAC2 mortar mixtures expanded by about 0.1% after 7 days of exposure but did not expand further throughout the 120-day exposure period – even though the petrographic images taken on the cross-section (Fig. 95) show a thick layer of ASR gel around the aggregate throughout the section. The higher exposure temperature accelerated the process of conversion in these CAC2 mortar bars resulting in higher porosity. The expansive stresses generated by the ASR gels combined with the higher porosity caused the gel to leach out, as shown in Fig. 96.

Similar to CAC2 mixtures, the CSA1 mortar bars also expanded by about 0.1% after 14 days of exposure and did not expand further throughout the rest of the exposure period. The petrographic images on the cross-section of CSA1 mortar bars in Fig. 97 shows the significant low presence of ASR gel around the reactive aggregates. The faster hydration kinetics and lower sorption rates in the CSA1 mortar mixtures, as discussed in chapters 4 and 9, might have significantly reduced the permeation of exposure solution into the mortar bars, leading to a lower amount of ASR gel and lower expansion.

Both CSA2 and CSA2P mixtures expanded at higher rates during the initial exposure period but had lower expansion compared to OPC mixtures. The total expansion at the end of the 120–day exposure period is about 0.6 and 0.5% in CSA2 and CSA2P mixtures, respectively. CSA2P showed moderate improvement in ASR resistance compared to CSA2 mixtures. Both the CSA2 and CSA2P mixtures have higher sorption rates and lower formation factor compared to CSA1 mixtures at w/c ratios between 0.45 and 0.485 – which contributed to higher ASR ion these CSA mixtures compared to CSA1. The petrographic observation on the cross-section of these mortar bars (Fig. 98 and Fig. 99) also show a higher presence of ASR gel around and through the reactive aggregate, corroborating the length expansions.

Similar to CAC2 and CSA1 mortar mixtures, the CSA3 mortar bars also had significant lower expansions, with a 120-day expansion of about 0.1%. The petrographic examination on the CSA3 mortar bars (Fig. 100) also shows the significant low amount of ASR gel around the aggregates throughout the cross-section.

AA mortar bars had the least expansion compared to all other ACMs and OPC mixtures. The total expansion at the end of the 120-day exposure period is about 0.02%. The petrographic examinations on the cross-section shown in Fig. 101 reveal the effectiveness of AA mortar bars in resisting the permeation of alkalis into the system, and no ASR gel is present around the aggregate (except near the edges where there is a significant presence of alkali in the system).

In contrast, MPC mortar bars showed the least resistance with the mortar bars disintegrating after 60 days of exposure. The alkali attack on the MPC binder might be the reason for the higher expansion and the disintegration of mortar bars. The petrographic examination on the cross-section of the MPC mortars (Fig. 102) also shows the significant presence of alkalis in the paste.

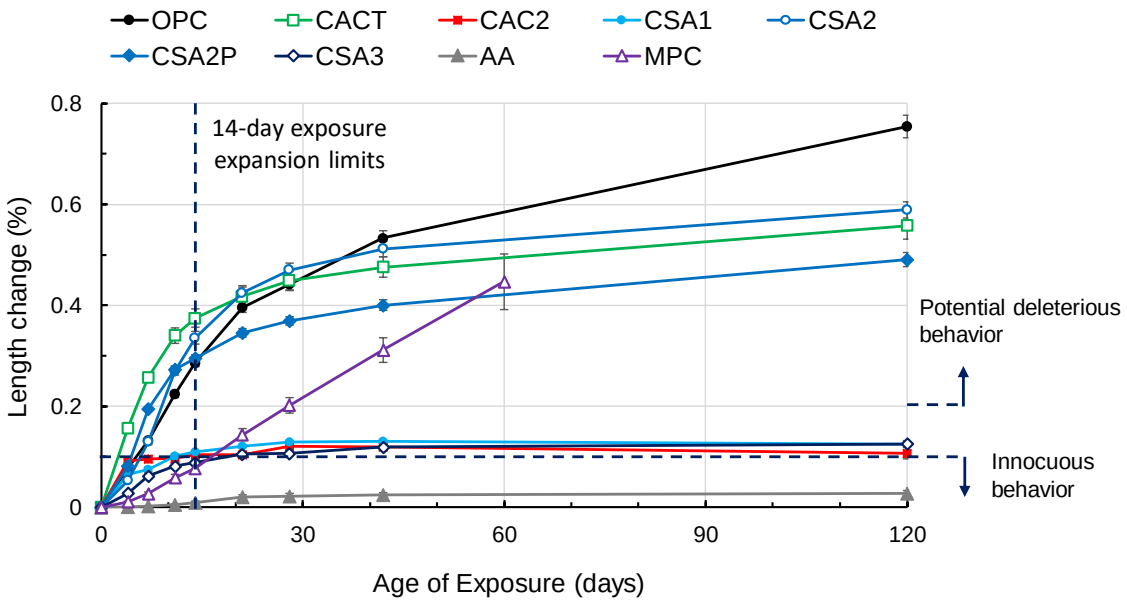

Fig. 92 Length expansion of ACM and OPC mortar mixes made with potentially reactive sand and exposed to NaOH solution at 80±1 ºC. Mortar bars made with MPC disintegrated after 60 days of exposure.

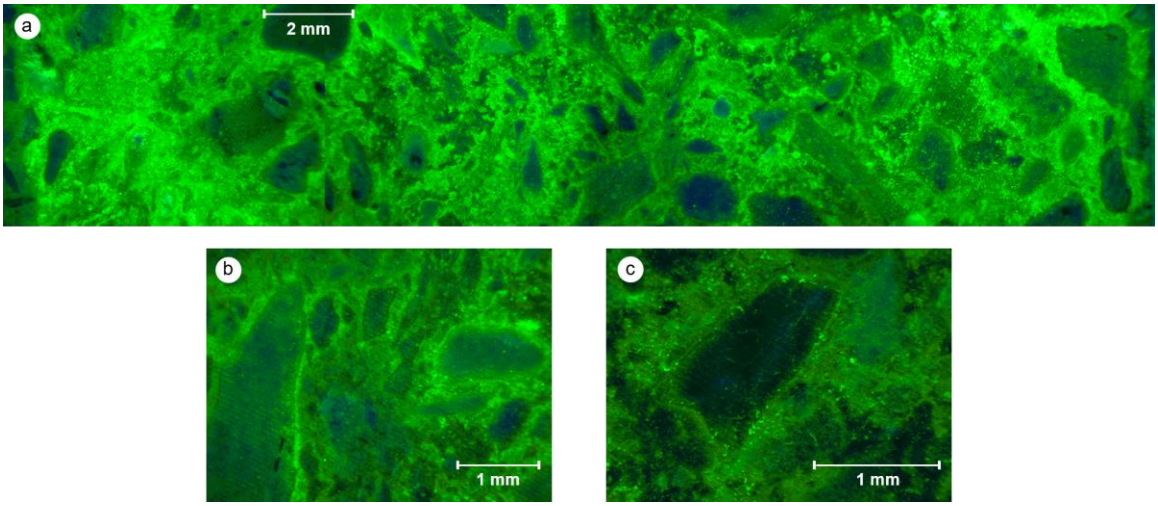

Fig. 93 Images taken on the cross-section of OPC mortar sample made with potentially reactive aggregate, subjected to ASTM 1260 exposure conditions for 120 days, stained with uranyl acetate and observed under short-wave UV.

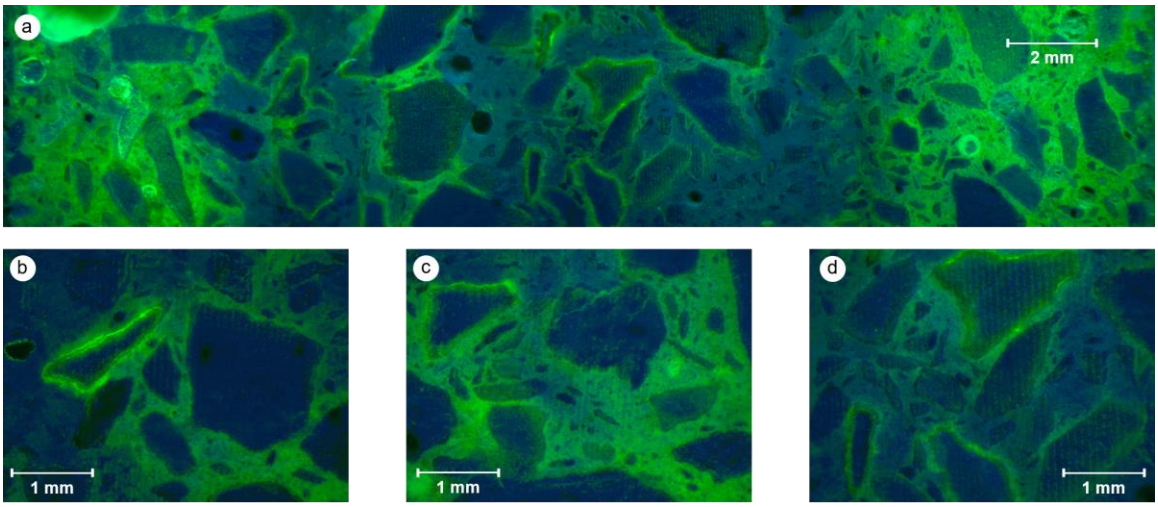

Fig. 94 Images taken on the cross-section of CACT mortar sample made with potentially reactive aggregate, subjected to ASTM 1260 exposure conditions for 120 days, stained with uranyl acetate and observed under short-wave UV.

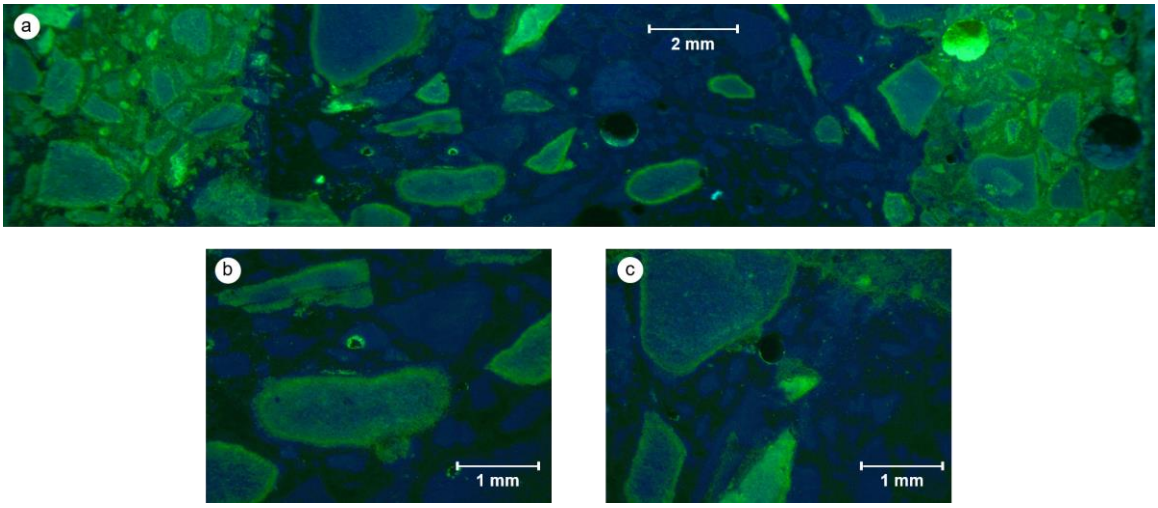

Fig. 95 Images taken on the cross-section of CAC2 mortar sample made with potentially reactive aggregate, subjected to ASTM 1260 exposure conditions for 120 days, stained with uranyl acetate and observed under short-wave UV.

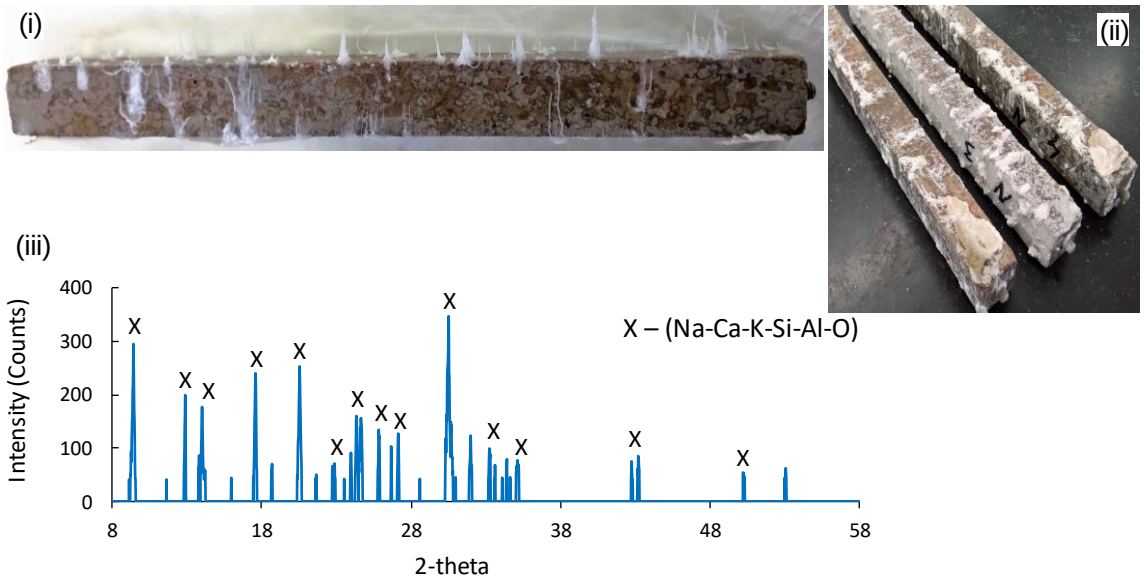

Fig. 96 (i) and (ii) Showing white product precipitating outwards on the surface of the CAC2 mortar sample made with potentially reactive aggregate subjected to ASTM 1260 exposure conditions for 120 days. (iii) XRD of the white precipitate shown in (i) and (ii).

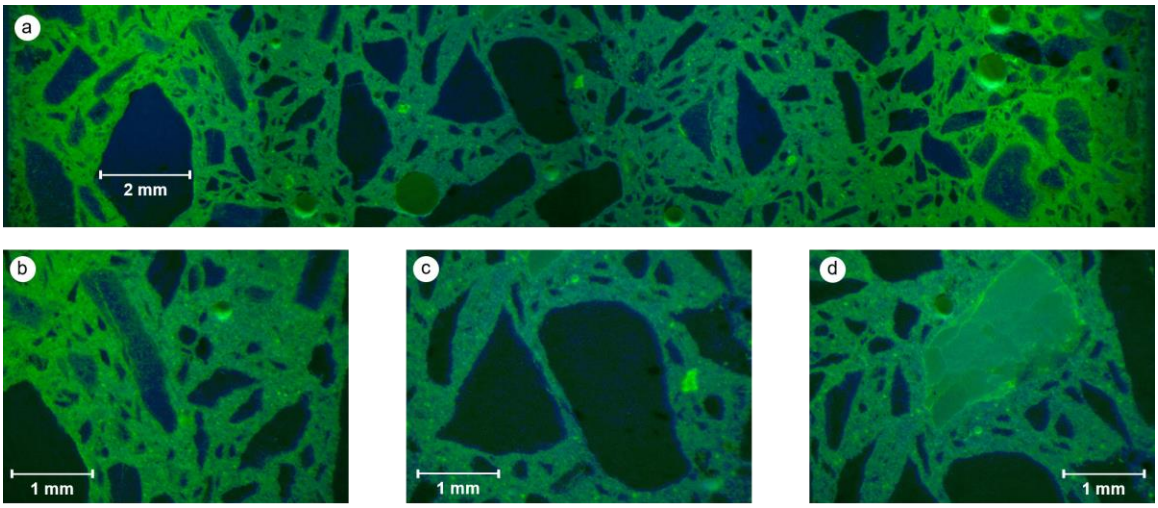

Fig. 97 Images taken on the cross-section of CSA1 mortar sample made with potentially reactive aggregate, subjected to ASTM 1260 exposure conditions for 120 days, stained with uranyl acetate and observed under short-wave UV.

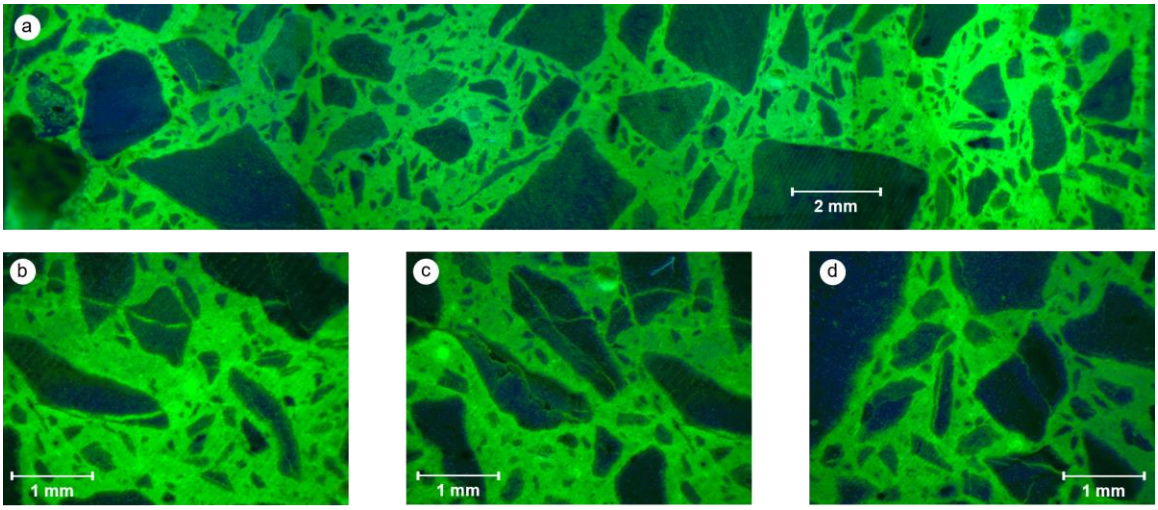

Fig. 98 Images taken on the cross-section of CSA2 mortar sample made with potentially reactive aggregate, subjected to ASTM 1260 exposure conditions for 120 days, stained with uranyl acetate and observed under short-wave UV.

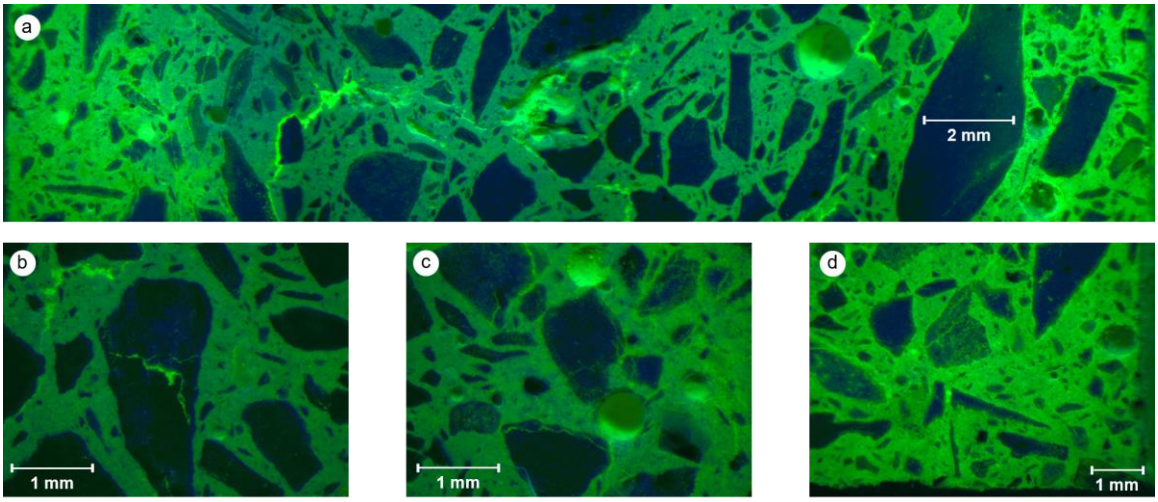

Fig. 99 Images taken on the cross-section of CSA2P mortar sample made with potentially reactive aggregate, subjected to ASTM 1260 exposure conditions for 120 days, stained with uranyl acetate and observed under short-wave UV.

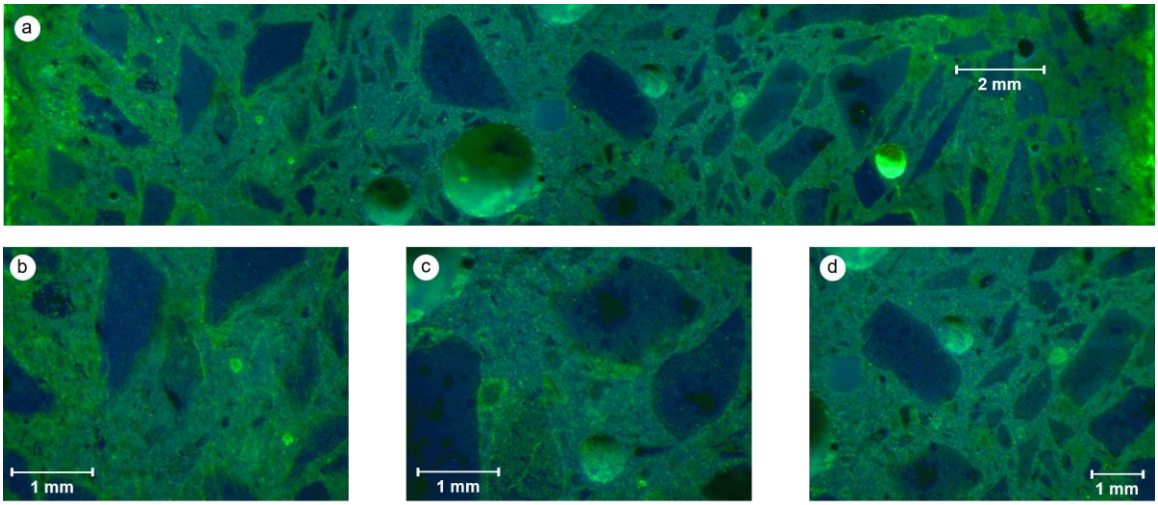

Fig. 100 Images taken on the cross-section of CSA3 mortar sample made with potentially reactive aggregate, subjected to ASTM 1260 exposure conditions for 120 days, stained with uranyl acetate and observed under short-wave UV.

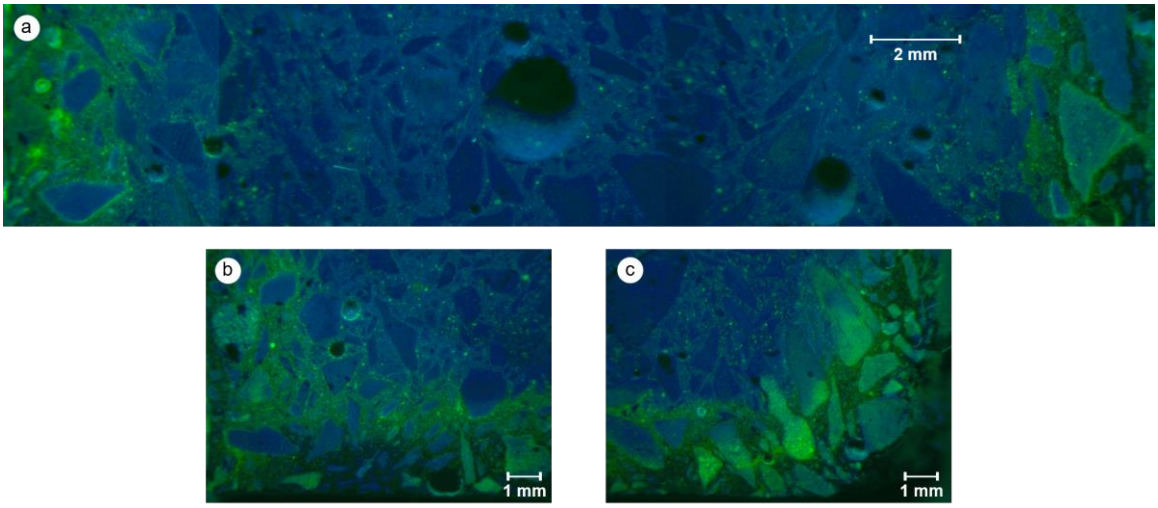

Fig. 101 Images taken on the cross-section of AA mortar sample made with potentially reactive aggregate, subjected to ASTM 1260 exposure conditions for 120 days, stained with uranyl acetate and observed under short-wave UV.

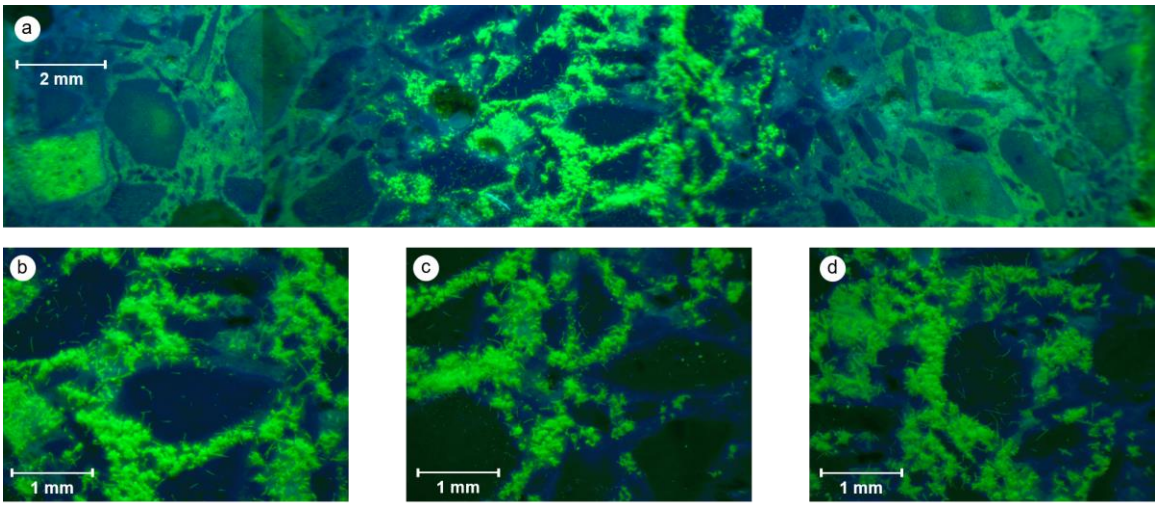

Fig. 102 Images taken on the cross-section of MPC mortar sample made with potentially reactive aggregate, subjected to ASTM 1260 exposure conditions for 60 days, stained with uranyl acetate and observed under short-wave UV.

11.3.2 Modified ASTM 1293 length expansion test

Fig. 103 shows the length expansions of ACM and OPC concrete mixtures made with reactive coarse aggregate and exposed to 100% RH at 38 ºC for 24 months. OPC concrete

mixtures expanded by about 0.2% after 2 years of exposure to 38 ºC and 100% RH. Fig. 108 shows the images taken on the cross-section of OPC mortar samples stained with uranyl acetate. The images show the presence of a significant amount of ASR gel around and through the reactive aggregates corroborating the length expansions.

The concrete mixtures (OPC+Flyash) made with a blend of 50% OPC and 50% class C fly ash showed significant improvement over plain OPC mixtures as expected. The total length expansion in the OPC+Flyash system is less about 0.08% at the end of the 2-year exposure period. Fig. 109 shows the petrographic examination on the cross of the OPC+Flyash concrete bars. The images show the presence of some ASR gel around the aggregates, but it is significantly lower when compared to that of the plain OPC system.

CACT concrete bars showed a significantly higher rate of expansion at an early age compared to OPC mixtures, with about 0.2% expansion after 9 months of exposure, even though the amount of alkalis present in CACT cement is similar to OPC as shown in Fig. 104. The pH of the CACT mixtures is also slightly lower compared to OPC mixtures, as shown in Fig. 105. However, the rate of expansion between 9 and 24 months of exposure was significantly lower compared to OPC. The total expansion at the end of the 2-year exposure period is about 0.23% and is higher than OPC. The higher rate of expansion in the CACT system at the early exposure period is likely due to the lower tortuous network in CACT systems compared to OPC as shown in Fig. 107 [163,164]. CACT mixtures also have portlandite in them, as shown in Fig. 106, however, it is significantly lower compared to OPC mixtures. Even though several researchers reported that presence of calcium produces more viscous gel and contributes to alkali recycling [68,70–75], which would imply increase in expansion with increase in calcium content, Powers and Steinour [165]

reported that low concentration of portlandite formed more expansive ASR gel compared to higher concentration of portlandite. This would imply a pessimum effect exists linking the ratio of Ca/Si to ASR gel expansion. Leemann et al. [147] showed the existence of this pessimum effect linking the Ca/Si ratio to the water-binding capacity of ASR gel. So even though CACT mixtures have lower portlandite content, the amount that is present in the system might have been close to the optimum Ca/Si ratio required to produce ASR gel with higher water-binding capacity compared to OPC mixtures. More research needs to be performed to identify the optimum Ca/Si ratio in these systems. Petrographic examination on the cross-section of the CACT concrete bars (Fig. 110) shows the presence of a significant amount of thick layer of ASR gel around the aggregates.

CAC2 mortar mixtures expanded by only about 0.04% after 15 months of exposure and had a slight reduction in expansion thereafter, which could be either due to conversion or leaching [156], or both. Also, images taken on the cross-section (Fig. 111) does not show any presence of ASR gel in the system. CAC2 mixtures have significantly lower pH compared to OPC and CACT mixtures (Fig. 105). The amount of alkalis present in the CAC2 system is significantly low compared to OPC and other ACMs (Fig. 104 and Table 2). Also, CAC2 mixtures have significantly lower (below the detectable limit in TGA) compared to OPC and CACT mixtures Fig. 106. All these three reasons could have contributed to such low expansion in these CAC2 mixtures.

Similar to CAC2 mixtures, the CSA1 concrete samples also showed significantly low expansions, with only about 0.02% expansion at the end of the 2-year exposure period. The petrographic examination on the cross-section of CSA1 concrete bars in Fig. 112 does not show any presence of ASR gel around the reactive aggregates. The relatively low amount

of alkalis (Fig. 104), portlandite content (Fig. 106), lower pH (Fig. 105), and the higher tortuous network in the CSA1 mixture (Fig. 107) contributed to the resistance of this system against ASR. Even though the pH in CSA1 mixtures is higher than CAC2 mixtures, the CSA1 mixtures have significantly higher tortuous network compared to CACA2 mixtures, so lower ASR expansions even compared to CAC2 mixtures.

Both CSA2 and CSA2P mixtures also exhibited significantly lower expansions compared to OPC and CACT systems, but higher expansions compared to the CAC2 and CSA1 mixtures. The total expansion at the end of the 120–day exposure period is about 0.07 and 0.06% in CSA2 and CSA2P mixtures, respectively, which is slightly lower when compared to the OPC+Flyash system. Because of the polymer modification, the CSA2P showed moderate improvement in ASR resistance compared to CSA2 mixtures. Since the amount of alkalis present in the CSA2 and CSA2P system is lower than OPC, and due to the absence of portlandite in these systems, the total length expansions were lower, even though both these systems have a less tortuous network when compared to OPC. Since these CSA2 and CSA2P systems have higher pH compared to CAC2 and CSA1 mixtures, their expansions were slightly higher compared to them. The petrographic observation on the cross-section of these concrete bars (Fig. 113 and Fig. 114) shows the presence of ASR gel around and through the reactive aggregate, but it is significantly lower when compared to OPC and CACT systems.

CSA3 concrete bars also had significantly lower expansions, with about 0.04% at the end of the 2-year exposure. However, the length expansions were higher when compared to CAC2 and CSA1 mixtures. The petrographic examination on the CSA3 concrete bars (Fig. 115) shows the presence of ASR gel inside the aggregates, but it is significantly low when

compared to that of OPC and CACT mixtures. The lower amount of alkalis present in the CSA3 cement compared to OPC and CACT, and the absence of portlandite in these CSA3 mixtures are likely the contributing factor for the lower amount of ASR, even though the CSA3 mixtures have less tortuous network compared to the OPC system as shown in Fig. 107. The pH in these CSA3 mixtures is also lower compared to OPC and CACT mixtures. Even though the pH and the amount of alkalis are significantly higher compared to CAC2 mixtures, the expansions in CSA3 mixtures are similar to CAC2 mixtures. This could likely be due to the better tortuous network in the CSA3 mixtures compared to the CAC2 mixtures.

AA mortar bars had the least expansion compared to all other ACMs and OPC mixtures. The total expansion at the end of the 2-year exposure period is about 0.003%. The petrographic examinations on the cross-section shown in Fig. 116 does not show any presence of ASR gel in the system, corroborating the length expansions. Even though the AA precursor, class C fly ash, has a higher amount of alkalis present in it, they must have been bounded in the hydration product as N-A-S-H and C-N-A-H gel [153], as discussed in chapter 4. Also, the AA system has a higher tortuous network when compared to OPC and other ACMs (except CSA1), lower pH, and doesn't have portlandite in them, all of which contributed to its effectiveness in resisting ASR.

Similar to CACT mixtures, MPC concrete bars also showed a significantly higher rate of expansion at an early age compared to OPC mixtures, with about 0.22% expansion after 9 months of exposure. The MPC system had a significantly lower tortuous network and higher amount of alkalis in the binder. However, the petrographic examination on the cross-section of the MPC mortars (Fig. 117) does not show any presence of ASR gel around or

through the aggregates. Either the ASR gels that are formed might have dispersed into the pore network (due to the absence of Ca from portlandite in the system), or the expansion observed in this MPC system is due to the reaction of the binder itself with water from exposure.

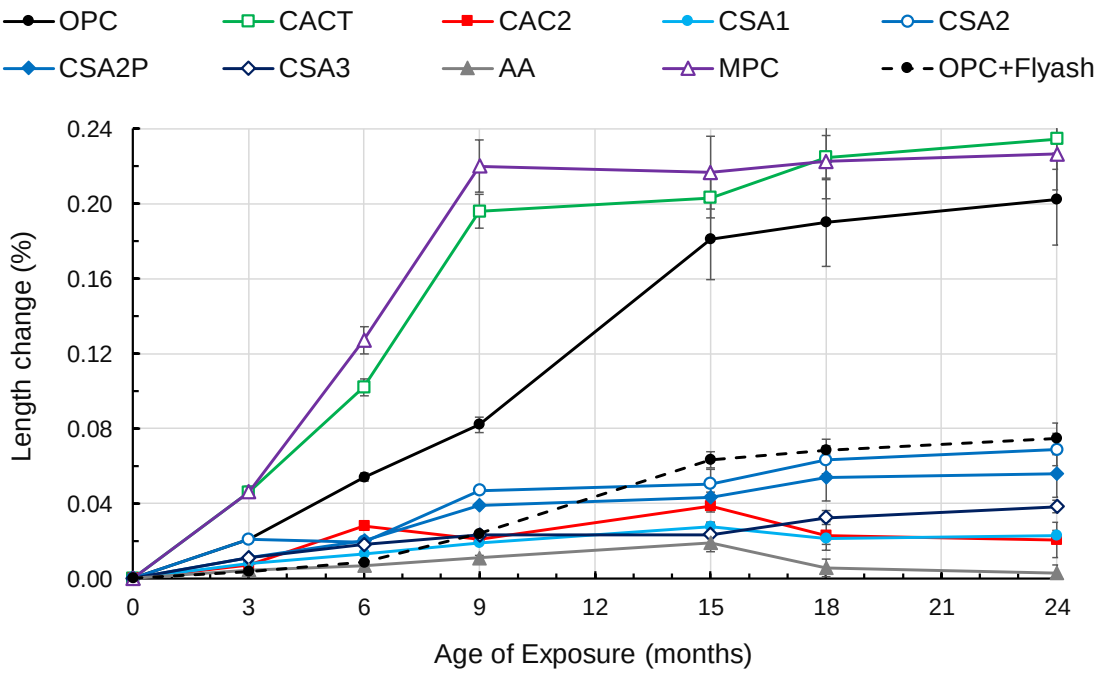

Fig. 103 Length expansion of ACM and OPC concrete mixtures made with reactive coarse aggregate and exposed to 100% RH at 38±1 ºC.

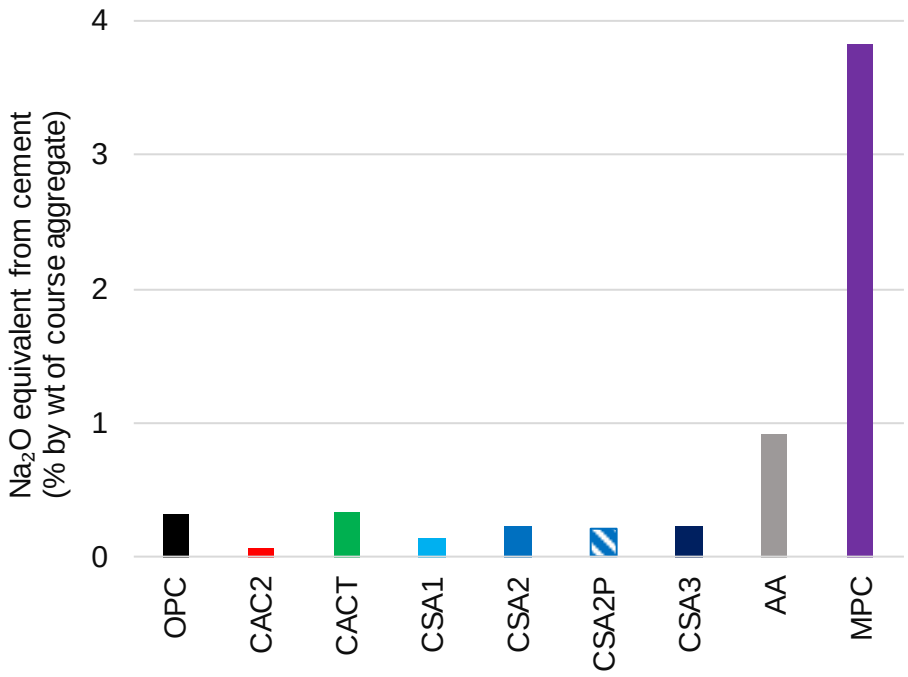

Fig. 104 Amount of alkali (Na_2O equivalent) present in ACM concrete mixtures compared to that of OPC. Note: The amount of alkalis is determined based on the alkali content of the cement. This may not relate to the amount of free alkalis present in the pore solution of the concrete.

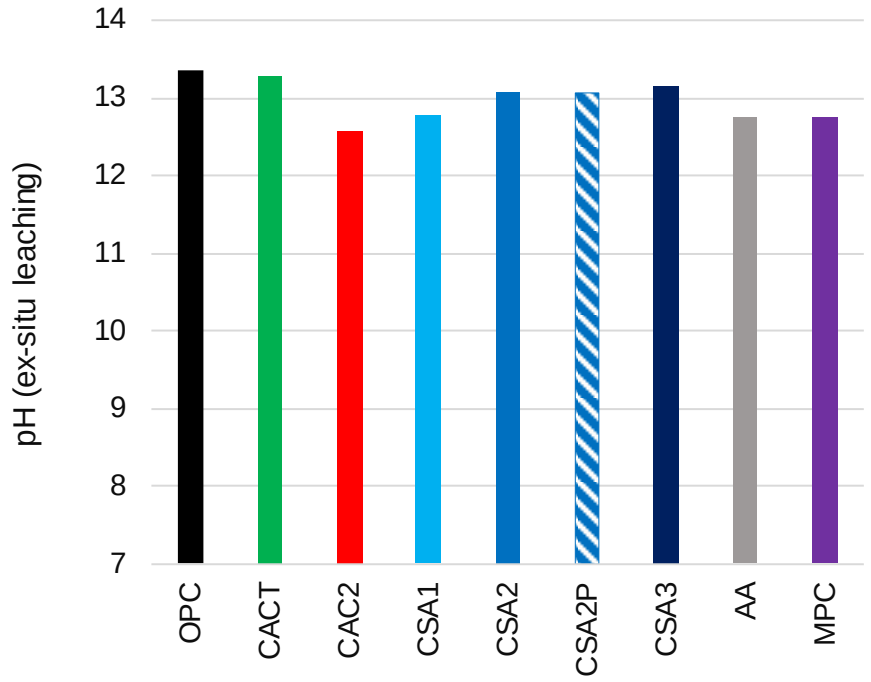

Fig. 105 pH in ACM and OPC paste mixtures at 0.45 w/b (AA and MPC at 0.25 w/b).

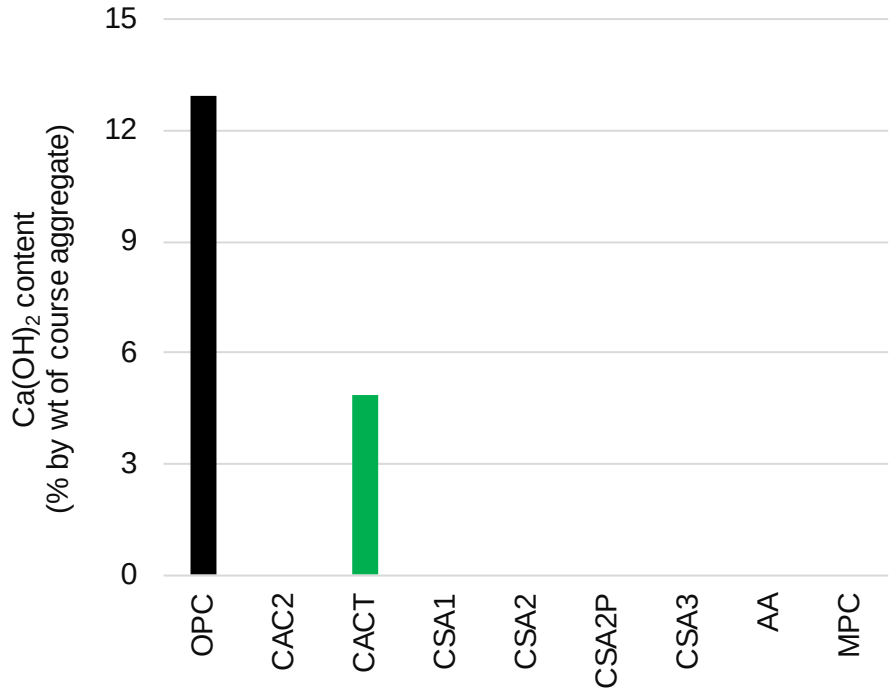

Fig. 106 $Ca(OH)_2$ content in ACM and OPC paste mixtures at 0.45 w/b (AA and MPC at 0.25 w/b).

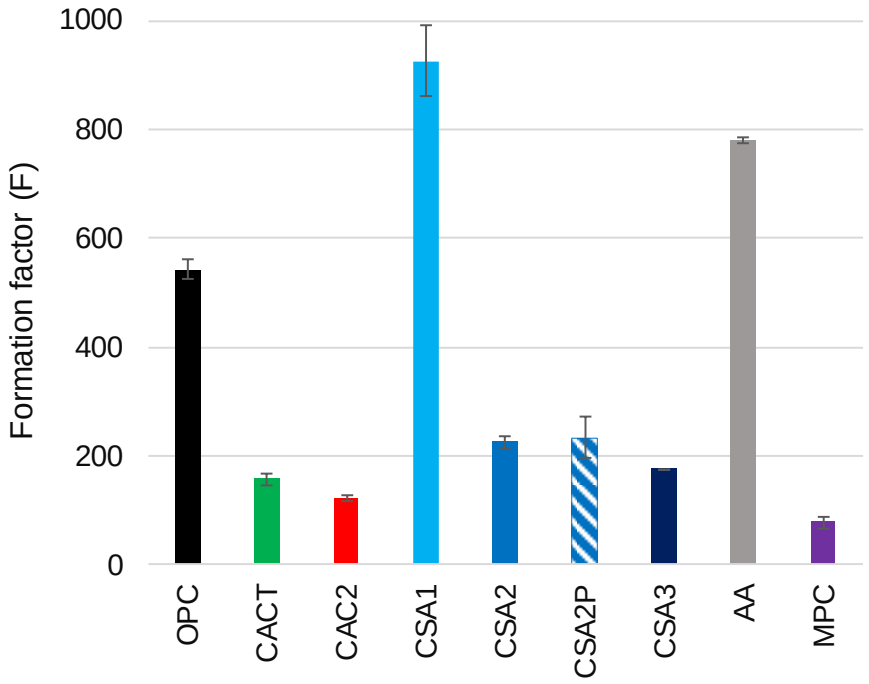

Fig. 107 Formation factor in ACM and OPC mortar mixtures at 0.45 w/b (AA and MPC at 0.25 w/b). Recreated from Fig. 53.

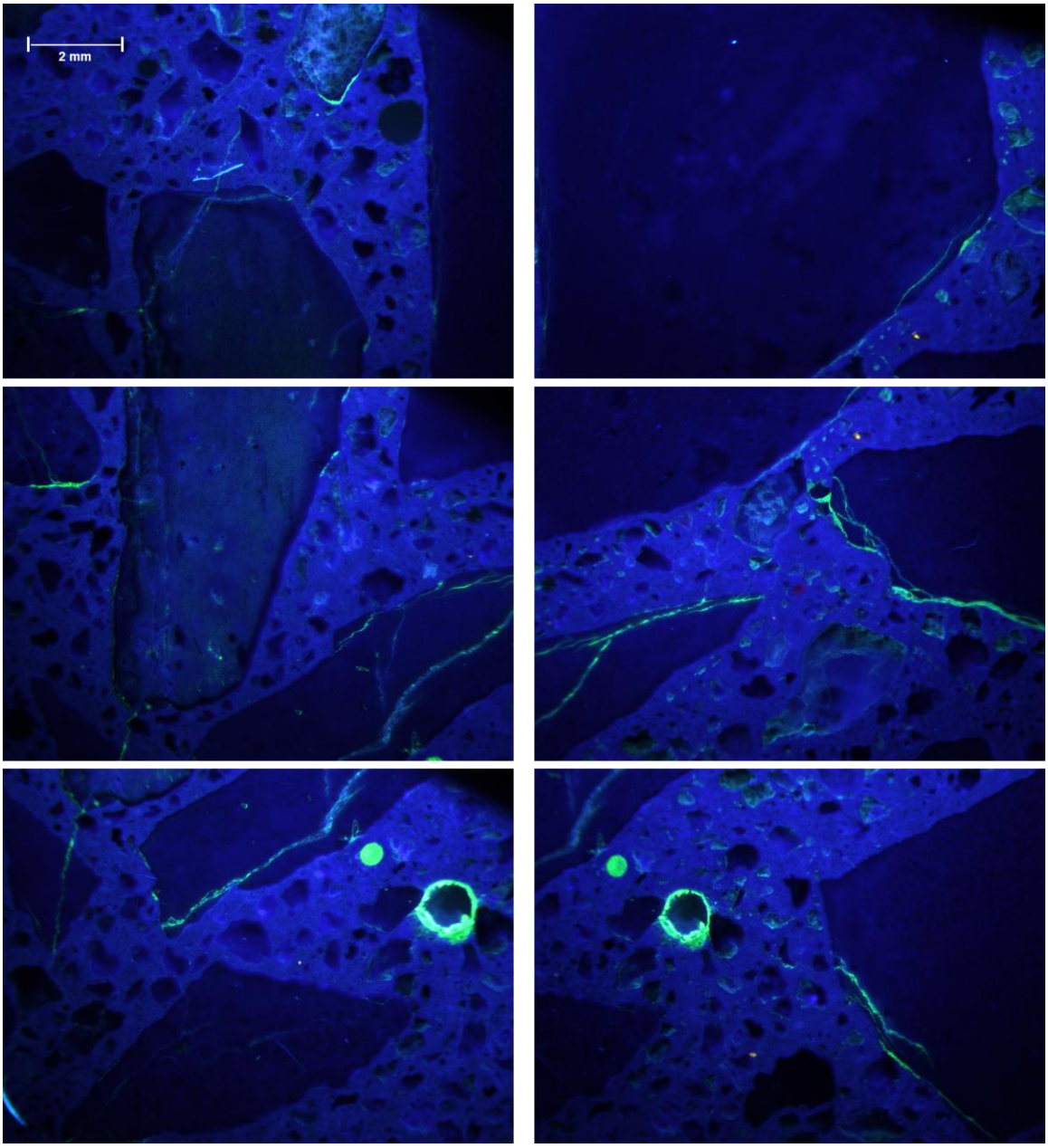

Fig. 108 Images taken on the cross-section of OPC concrete sample subjected to ASTM 1293 exposure conditions for 2 years, stained with uranyl acetate and observed under short wavelength UV.

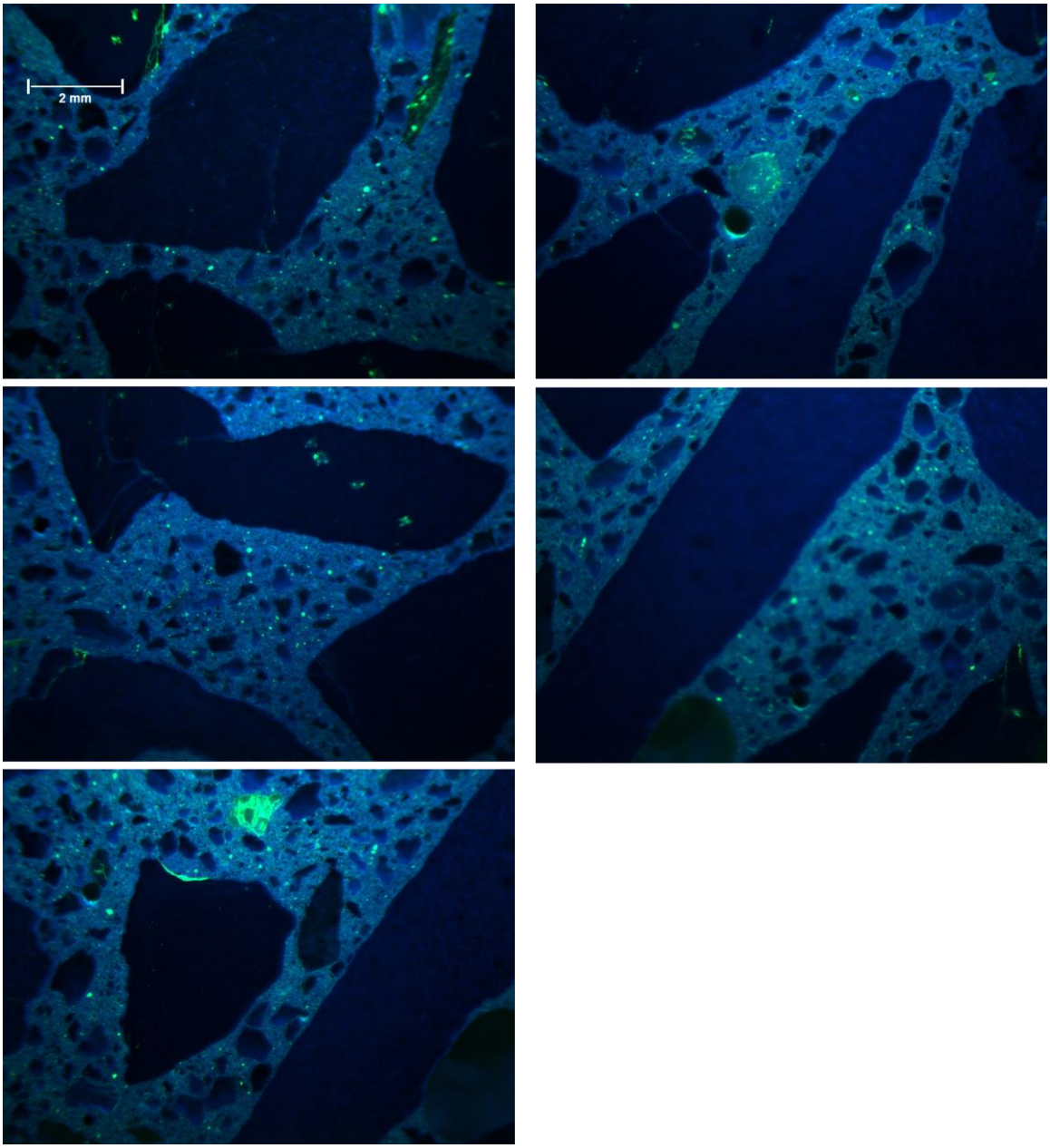

Fig. 109 Images taken on the cross-section of OPC+Flyash concrete sample subjected to ASTM 1293 exposure conditions for 2 years, stained with uranyl acetate and observed under short wavelength UV.

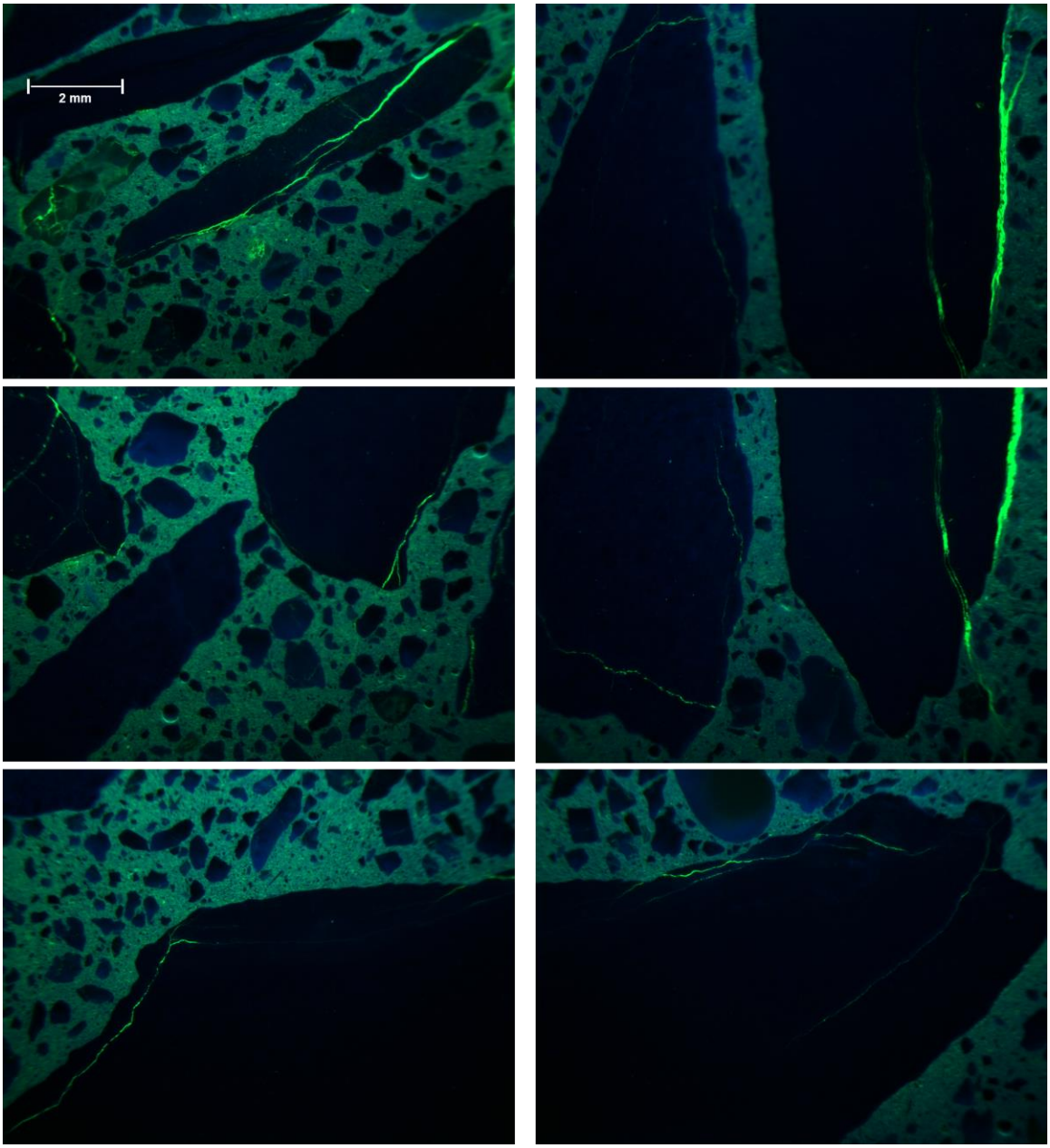

Fig. 110 Images taken on the cross-section of CACT concrete sample subjected to ASTM 1293 exposure conditions for 2 years, stained with uranyl acetate, and observed under short wavelength UV.

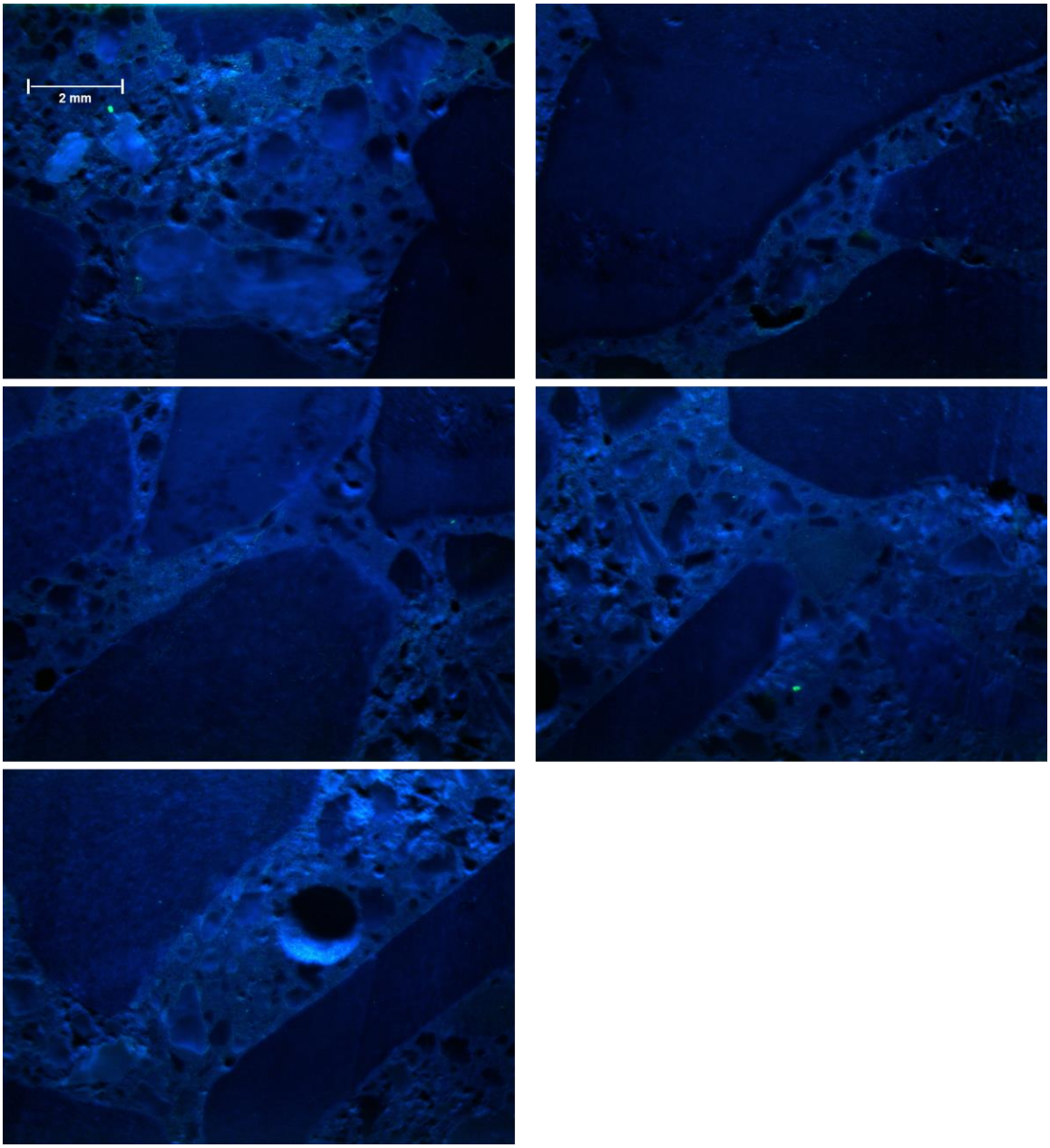

Fig. 111 Images taken on the cross-section of CAC2 concrete sample subjected to ASTM 1293 exposure conditions for 2 years, stained with uranyl acetate and observed under short wavelength UV.

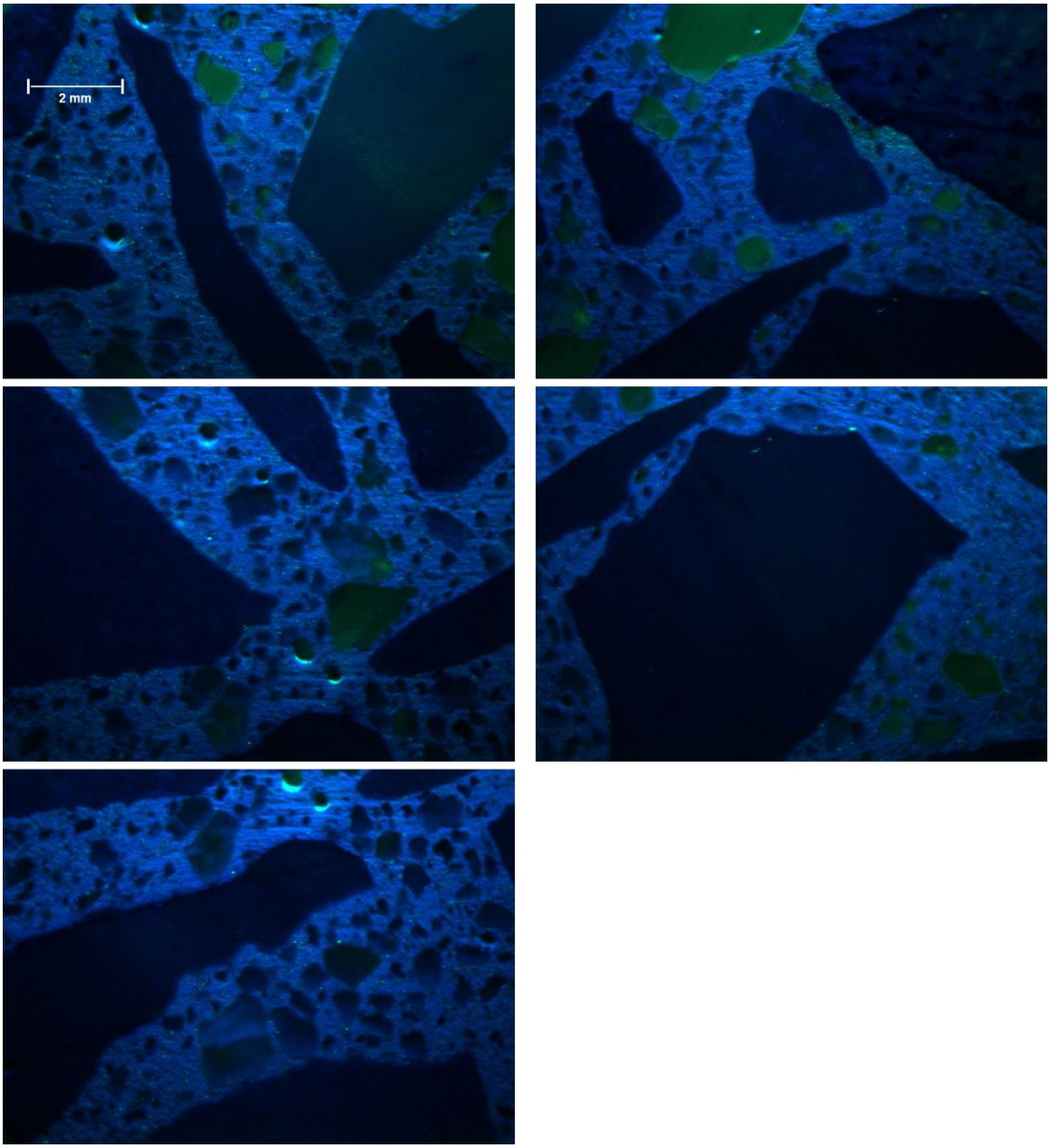

Fig. 112 Images taken on the cross-section of CSA1 concrete sample subjected to ASTM 1293 exposure conditions for 2 years, stained with uranyl acetate and observed under short wavelength UV.

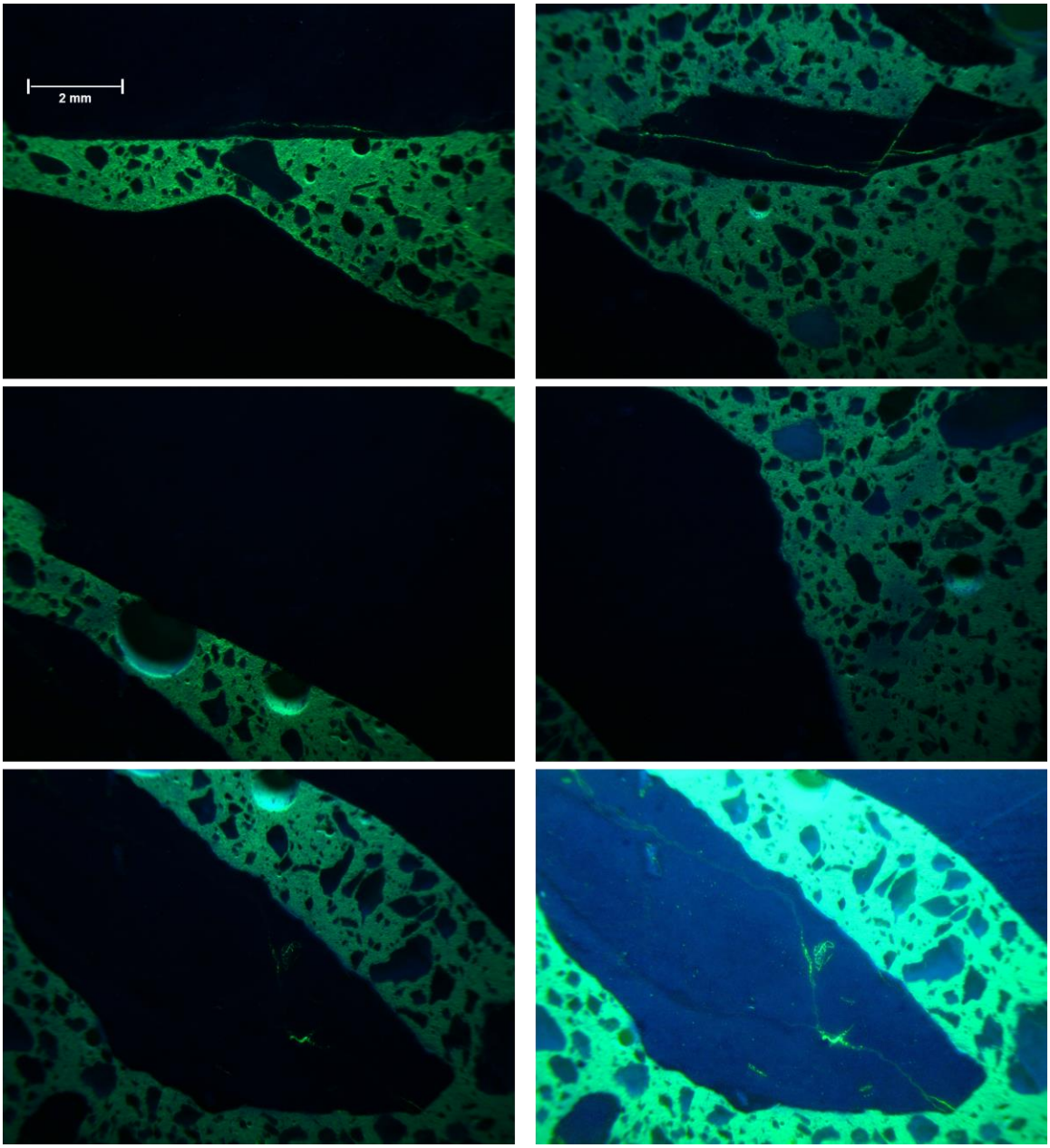

Fig. 113 Images taken on the cross-section of CSA2 concrete sample subjected to ASTM 1293 exposure conditions for 2 years, stained with uranyl acetate and observed under short wavelength UV.

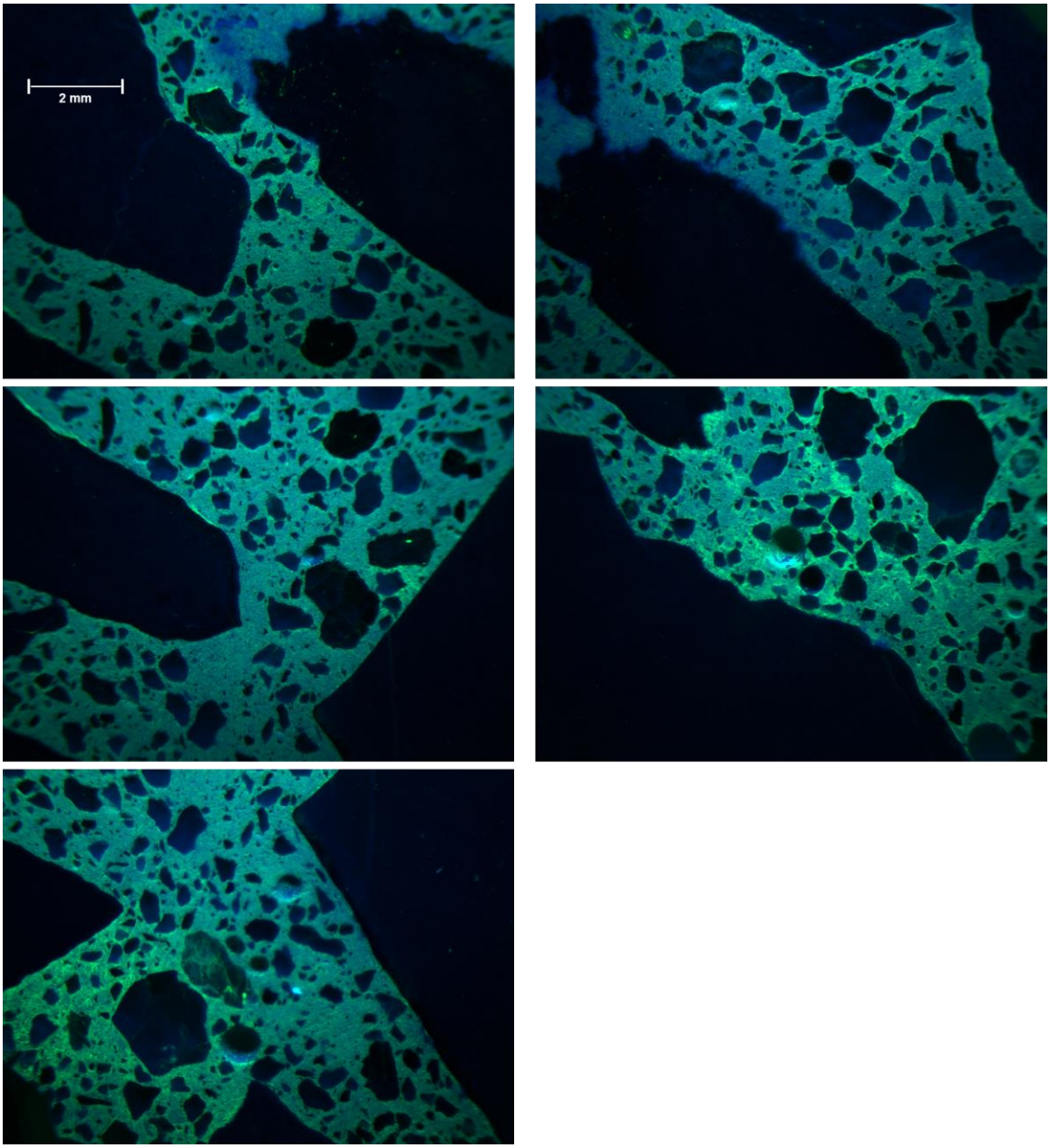

Fig. 114 Images taken on the cross-section of CSA2P concrete sample subjected to ASTM 1293 exposure conditions for 2 years, stained with uranyl acetate and observed under short wavelength UV.

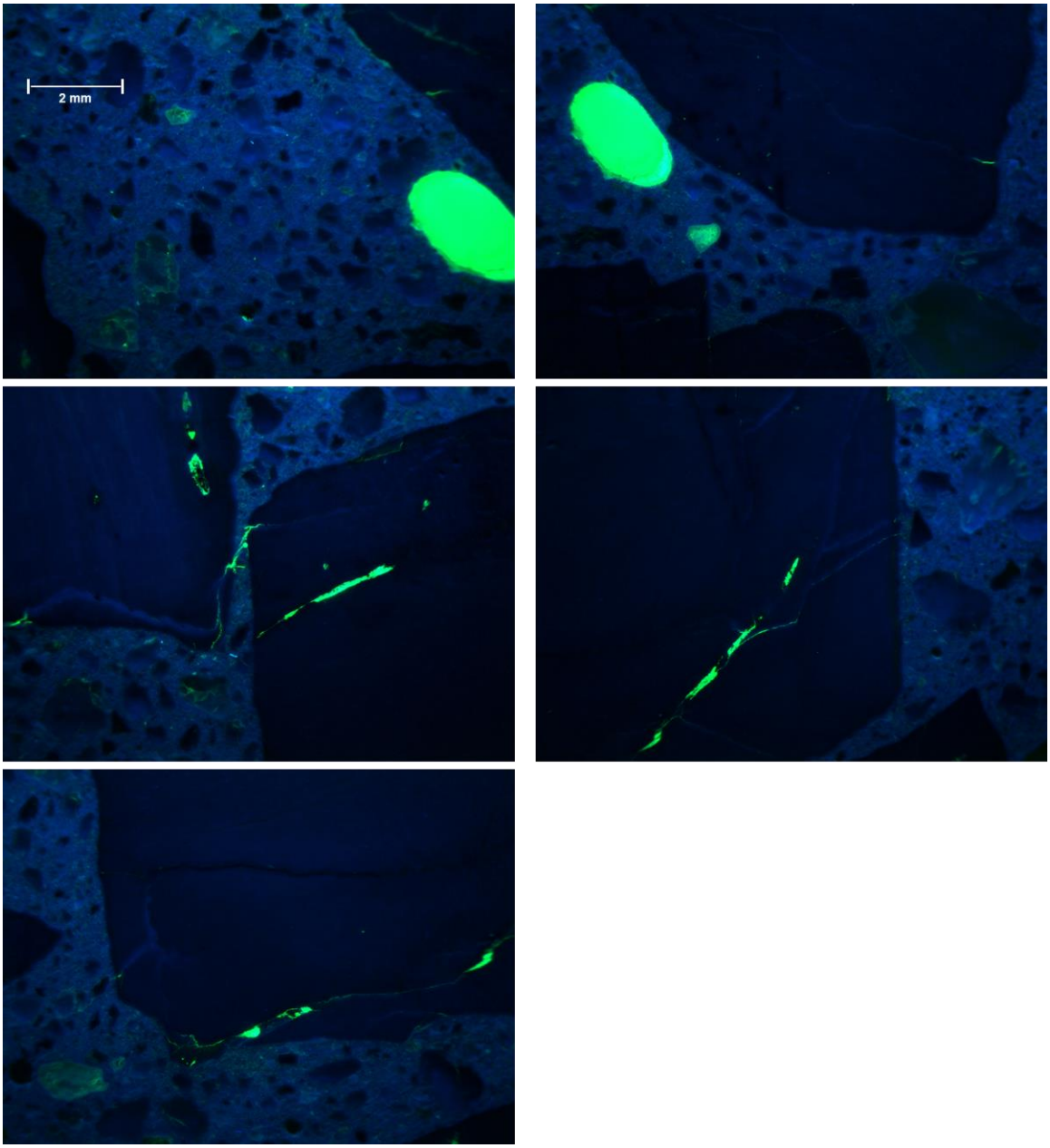

Fig. 115 Images taken on the cross-section of CSA3 concrete sample subjected to ASTM 1293 exposure conditions for 2 years, stained with uranyl acetate and observed under short wavelength UV.

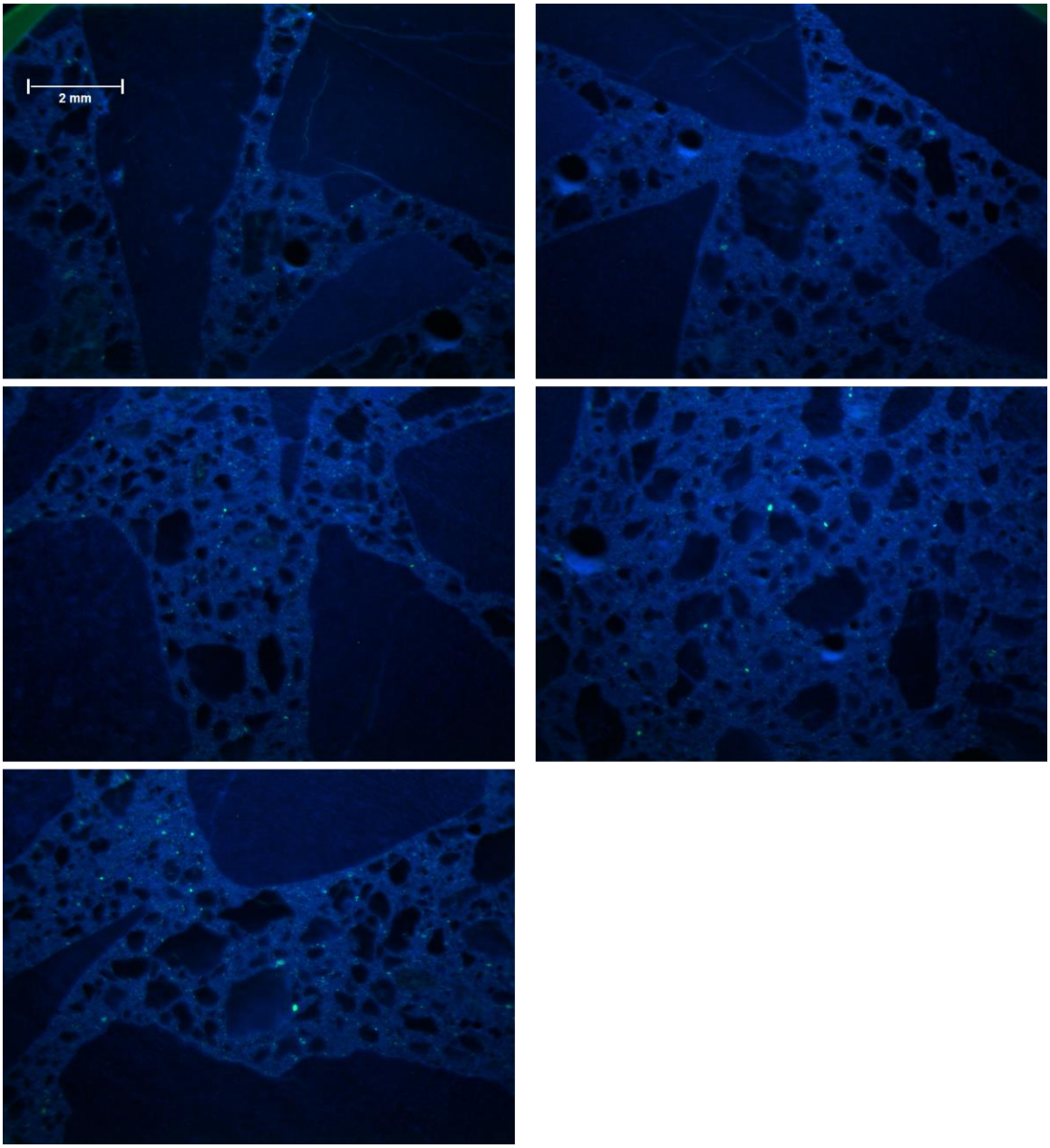

Fig. 116 Images taken on the cross-section of AA concrete sample subjected to ASTM 1293 exposure conditions for 2 years, stained with uranyl acetate and observed under short wavelength UV.

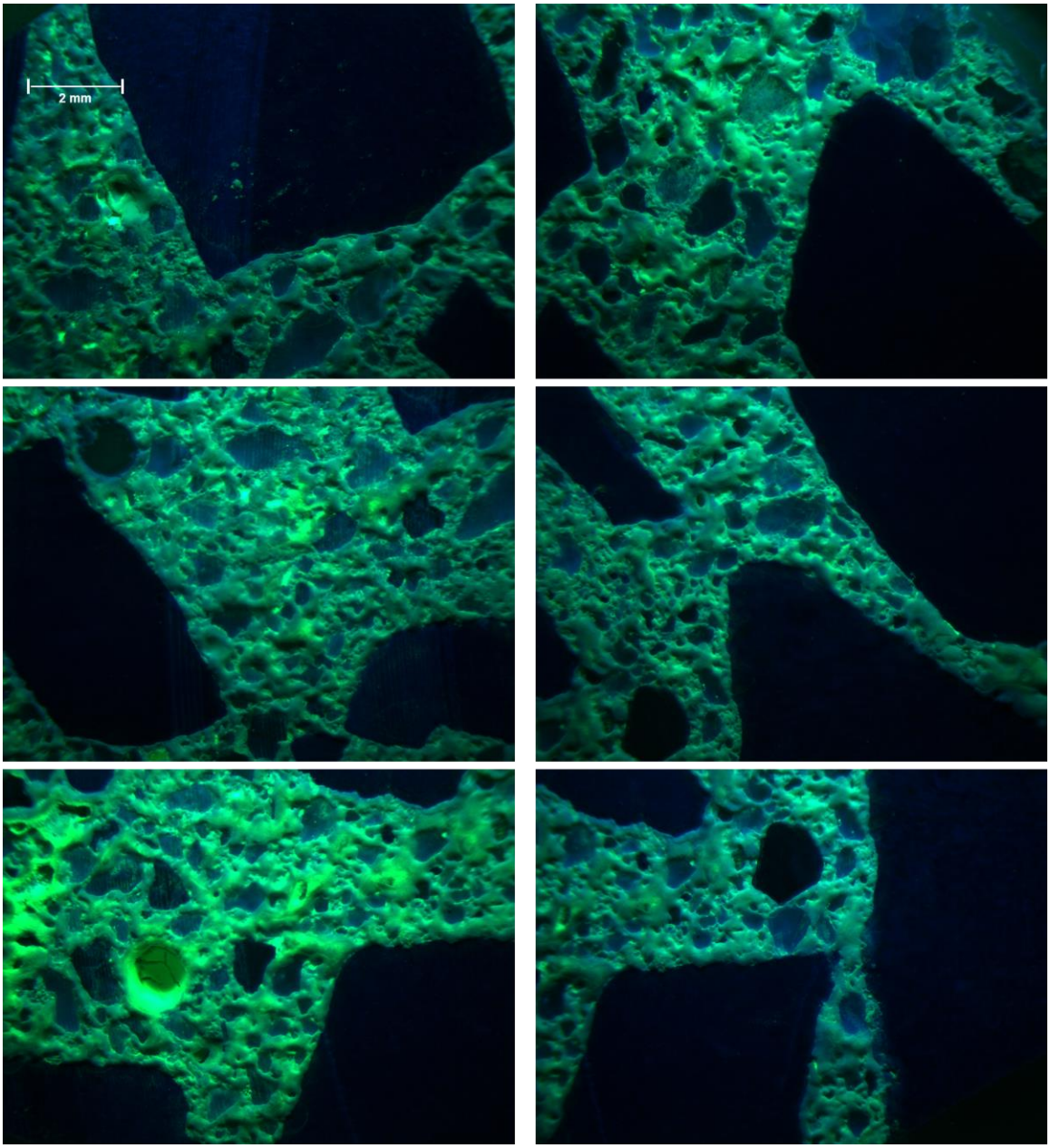

Fig. 117 Images taken on the cross-section of MPC concrete sample subjected to ASTM 1293 exposure conditions for 2 years, stained with uranyl acetate and observed under short wavelength UV.

11.3.3 Mortar cylinder test

The length expansions of the ACM and OPC mortar mixtures made with reactive aggregate from the mortar cylinder test are shown in Fig. 118. Similar to length expansions in the

modified ASTM 1293 test, OPC, CACT, and MPC had significantly higher expansions compared to other ACM mixtures. AA and CSA1 mixtures exhibited lower expansions with expansions even lower than OPC+Flyash mixture. CSA2P had similar expansion to OPC+Flyash mixture. Whereas, both CSA2 and CSA3 exhibited slightly higher expansions compared to OPC+Flyash mixture. Both the CSA2 and CSA3 mixtures had a significant lower formation factor (i.e., higher permeability). So, leaching of the gel in the ASTM 1293 test could be the reason for slightly lower expansions observed in these mixtures in ASTM 1293 test compared to the cylinder test. CAC2 mixtures showed significant shrinkage with exposure – likely due to conversion, which got accelerated with exposure to high temperature and humidity.

Overall, the alkali content and the portlandite content led to higher expansions in ASR compared to the permeability and pH of the system. All the ACM mixtures (CAC2, CSA1, CSA2, CSA2P, and CSA3) with lower alkali content and portlandite content showed significant lower expansions compared to OPC, CACT, and MPC mixtures. Even though AA mixtures had significantly higher alkali content in the precursor material, its expansions were least of all the mixtures investigated in this chapter. This is due to the alkali binding in the hydration products of these AA mixtures. This mechanism has also been reported in the literature [149–154] for alkali-activated materials, and it is shown in this chapter that this mechanism is valid for activated aluminosilicates (without alkali activator) as well. Even though MPC mixtures do not have portlandite (or significant source of Ca) in them, their expansions were very similar to OPC and CACT mixtures. More research needs to be performed to understand if the Mg ions present in the MPC systems recycle alkali in ASR gel similar to Ca ions in OPC mixtures and if this can lead

to significant ASR expansion. However, in some of the studies performed with alkali-carbonate reaction, the Mg-silicate gels are reported as less expansive compared to the ASR gel [166–168].

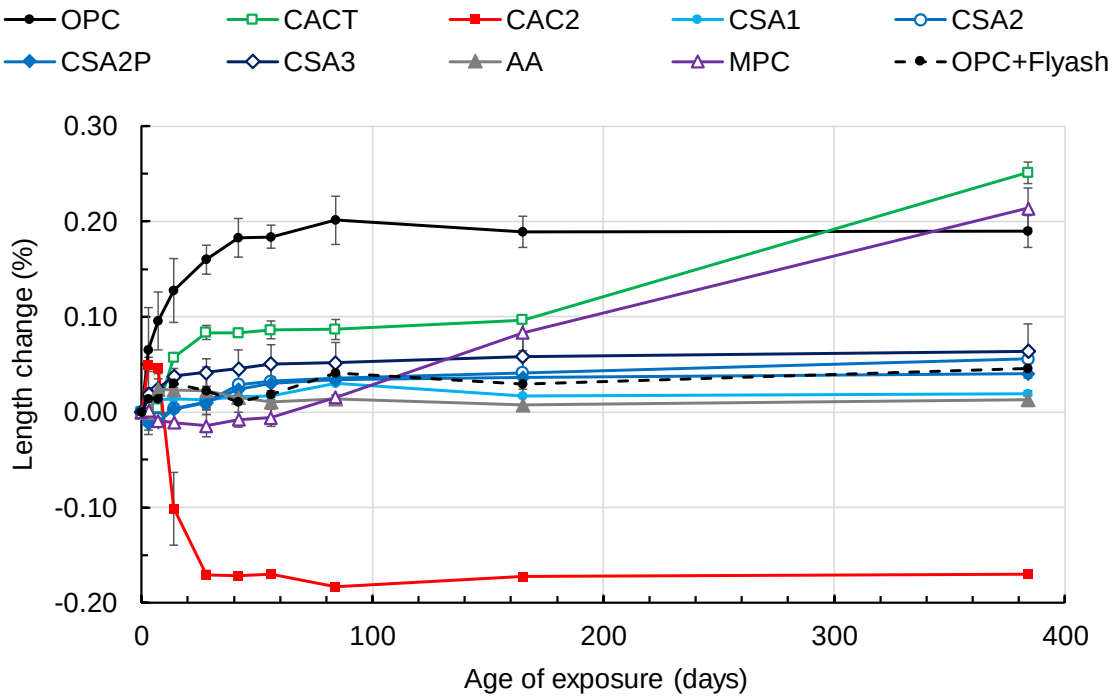

Fig. 118 Length expansion of ACM and OPC mortar mixtures made with reactive fine aggregate and exposed to 100% RH at 60±1 °C.

11.4 Conclusions and Recommendations

Based on the evaluation of the OPC and ACM mixtures with 4 test methods and with the complementary petrographic examinations, the following conclusions are made:

- All the ACM binders except MPC showed significantly higher resistance to expansion with alkali exposure compared to OPC. AA, followed by CAC2, CSA1,

and CSA3, showed the highest resistance to expansion to alkali exposure compared to others. MPC had the least resistance to alkali exposure.

- OPC, CACT, CSA2, CSA2P, and MPC showed the least performance with resisting the ASR of embedded reactive aggregates when exposed to a high pH environment. CSA2P only showed moderate improvement in ASR resistance compared to CSA2 mixtures. AA followed by CSA1 and CSA3 showed the highest resistance towards ASR even when exposed to a high pH environment for an extended duration of 120 days of exposure.

- AA, followed by CAC2 and CSA1, showed the highest resistance towards ASR of embedded reactive aggregates when exposed to 100% RH even with an extended duration of 2 years of exposure. CSA3, followed by CSA2P and CSA2, also showed similar or higher resistance even when compared to OPC+Flyash mixture. OPC, CACT, and MPC showed the least resistance of all.

- The mixtures having lower permeability, lower alkali content, and no portlandite content showed superior resistance to ASR, followed by mixtures with low alkali content, no portlandite content, but higher permeability. The mixture that had significantly lower permeability, but higher alkali and portlandite content resulted in significant expansion similar to the mixtures with both high permeability, high alkali content, and high portlandite content. So having even small amounts of portlandite in the ACM systems can still lead to significant expansions similar to OPC mixtures. So blends of OPC and ACM mixtures are not recommended for applications that need high ASR resistance.

- Even though AA mixtures had high alkali loading from fly ash, the expansions were still significantly lower. This could be because alkalis are bound tightly to the hydration as N-A-S-H and C-N-A-S-H gel in these mixtures.

Overall, both AA and CSA1 mixtures show superior performance towards both alkali exposure and in resisting ASR-induced cracking of embedded reactive aggregates, followed by CSA3 mixtures.

12 ACCELERATED CARBONATION

Carbonation resistance is a vital durability parameter as it is often associated with corrosion of steel reinforcement embedded in concrete and shrinkage. Many of these ACMs have different cement chemistry, which leads to different hydration products, and in turn, can affect the carbonation mechanisms.

12.1 Background

12.1.1 Carbonation in portland cements (OPC)

The calcium hydroxide (portlandite), along with the oxides of sodium and potassium are mainly responsible for the alkalinity of portland cement systems. Concrete alkalinity helps to maintain the steel reinforcement in a passive state limiting corrosion rate. Carbonation, which occurs when CO_2 in the presence of moisture reacts with the calcium-bearing phases in concrete to form calcium carbonate ($CaCO_3$), causes a reduction in the pH of the pore solution and sometimes dissociation of the strength-giving hydration products. $CaCO_3$ formed from the carbonation of portlandite usually precipitates in the concrete pores. The typical reaction mechanism of carbonation in the traditional OPC system is shown in Equation 10 (i, ii). Carbonation reduces pH of the concrete in the carbonated zone due to the reduction in the soluble portlandite phase and formation of insoluble CaCO3, as well as potentially acidic H_2CO_3 [169].

Equation 10

$$\mathrm{CH} + \mathrm{CO_2} \rightarrow \mathrm{CaCO_3} + \mathrm{H} \quad \text{(i)}$$

$$CO_2 + 2H \rightarrow H_2CO_3 \quad \text{(ii)}$$

12.1.2 Carbonation in calcium sulfo-aluminate cement (CSA)

CSA cements have either low or no C_3S phase present in them, and if any CSH is formed, it is from the hydration of C_2S reaction. So, the amount of portlandite formed is low compared to traditional portland cement systems. Also, the portlandite can be consumed back in the reaction forming just the ettringite. Since the amount of portlandite present in the CSA system is significantly lower than the traditional portland systems, the carbonation mechanisms in CSA systems can be considerably different. The ettringite phase decomposes significantly due to carbonation in CSA systems (Equation 11) causing a reduction in the strength of the matrix. With ettringite being the main hydration product and strength-giving component (rather than CSH), the long-term stability and the added rapid rate of carbonation is a concern for many researchers [105,106]. However, an accelerated carbonation study performed in the laboratory (at 20% CO_2 and 70% RH) showed no significant difference in the carbonation depths between CSA and portland cement concrete mixtures [14,170]. Even though several carbonation studies were performed on CSA systems, the effect of accelerated carbonation exposure level compared to natural carbonation level is not known.

Equation 11

$$\text{Ettringite} + CO_2 \rightarrow 3CaCO_3 + 3C\bar{S}H_x + AH_3 + 29(H - x)$$

12.1.3 Carbonation in calcium aluminate cement (CAC)

Like CSA cement, in general, the CAC does not contain the C_3S phase. If C_2S is present, all the CSH is formed from its reaction, resulting in low amounts of portlandite in the hydrated matrix; thus lower pH in the system and different carbonation mechanisms compared to the traditional portland cement. The possible mechanisms of carbonation in CAC is given in reaction (i) and (ii) of Equation 12. The occurrence of either of the reaction greatly depends on the ease of water evaporation or diffusion to other sources [171]. Thermodynamically, reaction (i) (Equation 12) is favored, as the higher liberation of water from reaction (ii) (Equation 12) can inhibit the carbonation reaction. The dissolution of the CAH_{10} phase buffers the pore solution, and with carbonation of this phase, it can result in significant reduction in the pH of the system [171,172]. Similar to CSA systems, the effect of accelerated carbonation exposure level compared to natural carbonation level is not researched to date.

Equation 12

$$CO_2 + CAH_{10} \rightarrow CaCO_3 + 2AH_3 + 7H \quad \text{(i)}$$
$$CO_2 + 4CAH_{10} \rightarrow C_4AcH_{11} + 6AH_3 + 25H \quad \text{(ii)}$$

12.1.4 Carbonation in activated aluminosilicate binder (AA)

The carbonation mechanisms in AA systems greatly depend on the type of precursor and composition of the activator solution. In general, carbonation in AA systems involves the decomposition of C-S-H phase to $CaCO_3$ and calcium silicate, and carbonation of NaOH to sodium carbonate, sodium bicarbonate and their hydrates [173–177]. In alkali-activated systems, any CO_2 exposure level above 1% in accelerated carbonation seems to be

significantly underestimating the service life compared to natural carbonation level [173]. However, little is known about the effects of accelerated carbonation is activated aluminosilicates with non-alkaline activators.

12.1.5 Carbonation in magnesium phosphate cements (MPC)

To date, no testing has been performed to understand the susceptibility of MPC systems to carbonation, especially the effects of carbonation on the struvite phase is not known. The MPC system investigated in the chapter has significant amount of alkalis in the binder (Table 2) and lower pH compared to OPC system (Fig. 105). So, it is important to understand the effects of carbonation on the binder composition and on the passivation of embedded reinforcements.

12.2 Research significance

Understanding the long-term durability performance, such as carbonation resistance of the ACM systems, is essential in designing 'green' alternatives to traditional portland cements for intended service lives. Even though prior research exists in understanding the carbonation mechanisms/ reactions of the ACMs, further research is required to better understand its effects on the microstructure, porosity, and pH of these systems. This chapter verifies and provides new insights into the carbonation mechanisms in commercially available CSA, CAC, AA, and MPC cements and evaluates the implications of carbonation on phase composition, porosity, and pH in these systems against one traditional OPC system.

12.3 Methods

A standard ASTM 20-30 test sand from Humboldt Mfg. Co. conforming to ASTM C778 specification was used in making all mortar mixtures. Crushed granitic gneiss coarse aggregates from Vulcan Materials Company (Lithia Springs, Georgia) conforming to ASTM C33 #67 gradation, and river sand from the Lambert Sand and Gravel Plant (Shorter, Alabama) with gradation conforming to ASTM C33 specification were used in making all concrete mixtures.

Cement paste samples were used to test for microstructure, compressive strength, and carbonation depth. Cement paste samples with embedded rebar were used for open circuit potential measurements. Cement mortar and concrete samples were used to test for water sorption and carbonation front, respectively. The cement paste mixtures (shown in Table 23) were mixed in a high shear mixer according to ASTM C1738-14 at w/c of 0.45 (0.25 for AA). The set modifier/ activator dosages were chosen so that the corresponding concrete mixes had a workable window of at least 60 min. All the mortar mixes (Table 24) were mixed in Hobart mixer at w/b of 0.45 (AA at 0.25 w/b), and sand/binder of 2.75. The sand content was adjusted to account for the differences in the specific gravity of all the ACMs compared to OPC, to have the same volume of binder in all the mortar mixes. The water dosage was also adjusted to account for the sand absorption. The concrete mixes were machine mixed according to ASTM C192-14 at w/b of 0.4 (AA at 0.2055 w/b as per manufacturer recommendations). The detailed concrete mixture proportions are shown in Table 25. The admixture/ activator dosages were chosen so that the concrete had a slump of at least 3 inches after 60 minutes of addition of water.

Table 23 Cement paste mixture proportions.

Cement	w/b	Set modifier/ activators (by weight of cement)
OPC	0.45	–
CAC1	0.45	–
CAC2	0.45	–
CACT	0.45	Citric acid – 1.5%
CSA1	0.45	Citric acid – 2.0%
CSA2	0.45	Citric acid – 0.5%
CSA2P	0.45	Citric acid – 0.5%
AA	0.25	Activator 1 - 2.47%, Activator 2 - 2.21%
MPC	0.30	Boric acid – 14%

Table 24 Cement mortar mixture proportions.

Cement	w/b	Admixtures (by weight of cement)	Cement (g)	Water (g)	Sand (g)
OPC	0.45	-	100	45	275
CAC2	0.45	-	100	45	273
CACT	0.45	Citric acid – 1.5%	100	45	271
CSA1	0.45	Citric acid – 2.0%	100	45	268
CSA2	0.45	Citric acid – 0.5%	100	45	268
CSA2P	0.45	Citric acid – 0.5%	100	45	268
CSA3	0.45	Citric acid – 0.5%	100	45	268
AA	0.25	Activator 1 - 2.47%, Activator 2 - 2.21%	100	25	259
MPC	0.30	Boric acid – 14%	100	30	259

Table 25 Concrete mixture proportions.

Cement	w/b	Admixtures/ activators (by weight of cement)	Cement (kg/m^3)	Water (kg/m^3)	Sand (kg/m^3)	#67 aggregate (kg/m^3)
OPC	0.40	HRWR1 - 3.5 ml/kg	454	189	703	1056
CAC2	0.40	HRWR2 - 1.6 ml/kg	454	189	693	1056
CACT	0.40	citric acid – 1.5%, HRWR1 - 3.5 ml/kg	454	189	674	1056
CSA1	0.40	citric acid - 2%, HRWR1 – 3.0 ml/kg	454	189	656	1056
CSA2	0.40	citric acid – 0.5%, HRWR1 - 0.5 ml/kg	454	189	656	1056
AA	0.205	activator 1 - 2.27%, activator 2 – 1.78%	488	109	811	1056

12.3.1 Microstructure Analysis

Microstructure analysis was carried out on powdered cement paste samples, both carbonated and uncarbonated. Cement paste cubes of dimension 12.7 mm were prepared according to mixture proportions shown in Table 23, and cured for 56 days at 23 ºC and 100% RH. After curing, some of the samples were exposed to 7% CO_2 at 55% Rh and

30 ºC for 56 days (carbonated), and the other samples were stored in an airtight container for the same period (uncarbonated).

Prior to testing microstructure, the paste samples, both carbonated and uncarbonated, were ground and sieved to a particle size less than 300 microns, and the free water was removed using solvent exchange procedure [42]. 5 g of powdered sample was mixed in 50 ml of isopropyl alcohol, and the suspension rests for 15 min. Then, the suspension is filtered using Büchner funnel and a vacuum pump for 5 min, and later, it is washed with 10 ml of diethylene ether for 1 min, during which the vacuum pump is turned off. The resulting suspension is again filtered under vacuum for five more minutes, or until the suspension is dry, whichever is longer. The dried sample is sealed in a small sealed plastic bag and stored in an airtight container.

12.3.1.1 Thermogravimetric Analysis (TGA)

A Hitachi simultaneous thermogravimetric analyzer STA7300 was used to carry out the thermogravimetric measurements. After solvent exchange, the sample is further ground to particle size less than 74 microns. Approximately 20 mg of the ground sample is taken in an open 70 µl platinum crucible and further dried in TG at 25 ºC under a constant stream of Nitrogen (N_2) gas for 15 min, or until the constant mass, whichever is longer. Later the temperature is increased to 40 ºC and held constant for 5 min. Then, the sample was heated from 40 to 1000 ºC, at a rate of 10 ºC/min, and the data is recorded at a rate of 120 data points per minute. During measurement, N_2 was used as a protective gas with a flow rate of 100 Cc/min.

12.3.1.2 X-ray Diffraction (XRD)

A PANalytical Empyrean diffractometer with Bragg–Brentano HD X-ray mirror and goniometer radius of 240 mm was used for data collection. The sample was incident with CuKα X-rays generated using Empyrean Cu LFF HR X-ray tube at 45 kV and 40 mA operating conditions. Soller slits of 0.04 rad and the fixed Mask, anti-scatter, and divergence slits of 4 mm, 1 º, and ¼ º were used in the incident beam path. In the diffracted beam path, a fixed anti-scatter slit of 7.5 mm and soller slits of 0.04 rad were used. A PIXcel3D-Medipix3 1x1 area detector with an active length of 3.347 º was used for data acquisition. Data was collected over an angular range of 5 º to 70 º with a step size and counting time of 0.013 º and 16.32 s, respectively, resulting in a total measurement time of less than 7 min.

The powdered samples with particle dimension less than 149 microns were backloaded into the sample holder with an opening diameter of 17 mm. Phase identification was carried out using PANalytical X' Pert High Score plus v4.5 using PDF-4+ 2018 material identification database by International Center for Diffraction Data.

12.3.2 Water Sorption

The initial and secondary water sorptivity rate was determined on cement mortar discs, averaged from two test specimens. The cylinders are cast according to mix proportions given in Table 24 and cured at 23 ºC and 100% RH for 28 days. Then they are cut into discs of 76 mm in diameter and thickness of 38 mm using a wet tile saw. Later, the mortar discs were further cured for an additional 90 days at 55% RH, and epoxy coated on all sides except one end of the flat surface. After the epoxy coat dried, the uncoated side of the sample was exposed to water with 1 to 2 mm of the sample immersed. The uptake of water

is measured by weighing the specimens at intervals of 30 min, 60 min, every hour until 6 hours to determine initial sorption rate; and once a day up to 7 days to determine secondary sorption rate. The sorption rate ($mm/s^{0.5}$) is measured using the slope of the line that is the best fit to water absorption plotted against the square root of time ($s^{0.5}$).

After measuring the sorptivity rates on uncarbonated samples, they were vacuum dried for 4 hours and stored at 55% RH and 23 ºC for an additional 28 days. Then the mortar discs are carbonated by exposing them to 7% CO_2 at 55% RH and 30 ºC for 56 days, and the sorptivity measurements were carried out once again to determine the initial and secondary sorption rates in the carbonated samples.

12.3.3 Compressive strength

Cement paste cubes of dimension 12.7 mm were used to test for their strength under compression. The cubes were prepared according to the mixture proportions shown in Table 23 and cured for 56 days at 23 ºC and 100% RH. After curing, some of the samples were exposed to either 1% or 7% CO_2 at 55% Rh and 30 ºC for 56 days (carbonated). Compressive strength was measured on 8 replicas before the exposure and after 56 days of exposure to either 1% or 7% CO_2.

12.3.4 Carbonation depth and passivation of embedded steel in paste mixtures

The schematic of the test specimen used for measuring open circuit potential is shown in Fig. 119. The test specimen consists of a grade 40 - ASTM A615 rebar of diameter 9.5 mm (number 3 size) and length 140 mm . The rebar is coated with epoxy at the ends (20 mm at the bottom and 70 mm at the top), leaving 50 mm uncoated in the middle. The prepared

rebar specimen is embedded in the cementitious paste with a cover depth of 8.5 mm. Whereas cylinder specimens of diameter 26.5 mm and height 90 mm without embedded rebar were used for measuring carbonation depth. All the test specimens with and without embedded rebar are cast according to the mixture proportions shown in Table 23 and cured for 56 days at 23 ºC and 100% RH. Later half of the specimens (3 for each mixture) with embedded rebar were cured for further 90 days at 30 ºC and 55% RH in a container purged with N_2 gas. The other half of the specimens with embedded rebar were exposed to 1% CO_2 at 30 ºC and 55% RH for 90 days. The specimens without embedded rebar were exposed to 1% CO2 at 30 ºC and 55% RH for 0, 7, 30, 60, and 90 days. At the end of each exposure, the samples were cut using diamond saw and sprayed with a commercially available 'rainbow indicator' (sourced from Germann Instruments) on the cut surface. Carbonation depth was determined by calculating the area of the carbonated region based on the color change with the rainbow indicator. Also, based on the color profile achieved with the rainbow indicator, the pH levels were estimated in both carbonated and uncarbonated regions.

Open circuit potential (OCP) measurements were made on both carbonated and uncarbonated specimens to assess the change in embedded rebar passivation with carbonation. A silver chloride electrode filled with saturated potassium chloride solution (Ag/AgCl/Sat. KCl) was used as a reference electrode. The standard potential of this electrode is +0.197 mV with respect to standard hydrogen electrode at 23 ºC. A potentiostat with a dc-potential resolution of 0.1 mV and accuracy of 0.2% is used for mearing the OCP.

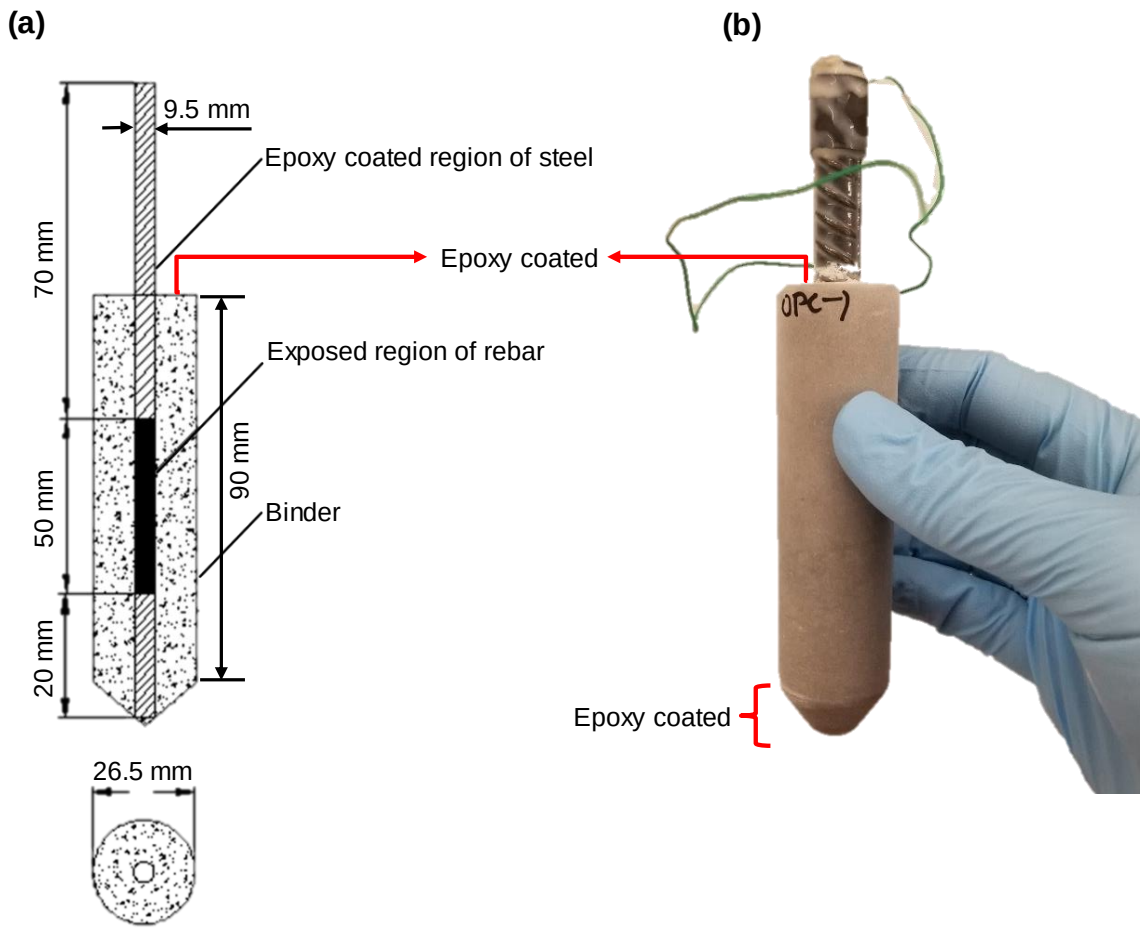

Fig. 119 (a) Sketch and (b) photo of the test specimen used for determining the open circuit potential of embedded rebar.

12.3.5 Carbonation front in concrete mixtures

Concrete cylinders of 152 mm diameter and 305 mm height were cast according to mixture proportions shown in Table 25 and cured for 28 days at 23 ºC and 100% RH. Then they were cut into two pieces using a wet tile saw, resulting in cylinders with dimensions 152 mm diameter and 150 mm height. The samples were further cured for an additional 28 days at 23 ºC and 55% RH.

After the curing regime, the concrete samples were exposed to 7% CO_2 at 30 ºC and 55% RH for 0, 3, 7, 14, 21, 28, 42, 56, and 84 days. At the end of the exposure, the samples

were split into two halves along the major axis and sprayed with a 1% phenolphthalein indicator on the split surface of one half, and with a commercially available 'rainbow indicator' (sourced from Germann Instruments) on the other half. The carbonation front was determined by averaging the carbonation depths measured based on the color change with the phenolphthalein and rainbow indicator, with five measurements taken on each side of the curved surface. Also, based on the color profile achieved with the rainbow indicator, the pH levels were estimated in both carbonated and uncarbonated regions.

12.4 Results and Discussion

12.4.1 Effects of carbonation on microstructure

The TGA results and XRD peaks of all OPC, CACT, CAC2, CSA2, and AA paste mixtures, both carbonated and uncarbonated, are shown in Fig. 120 to Fig. 131. Fig. 132 shows the bound CO_2 levels in OPC and ACM mixtures at different exposure levels.

In OPC mixture, with carbonation, there is a reduction in the DTG peaks of portlandite, ettringite, and monosulfate phases, suggesting carbonation of not only the portlandite phase but also ettringite and monosulfate phases. However, even after exposure to 15% CO_2, there is still a significant amount of portlandite present, which can maintain the pH in the system. The TGA data shows the monosulfate phase has completely disintegrated with 7% and 15% CO_2 level. The bound CO_2 levels at 0.04% and 1% exposure is about 4.7 and 5.7%, respectively. However, with an increase in exposure level to 7% and 15%, the bound CO_2 level increased by about 3 folds to about 15.3% and 15.8%, respectively. This suggests that 1% accelerated exposure is similar to the atmospheric level, whereas both the 7% and 15% exposure are very aggressive. The XRD plot of carbonated cement paste shows

$CaCO_3$ with two polymorphs, calcite, and vaterite – with vaterite being the dominant polymorph at 7 and 15% CO_2 exposure. Vaterite is usually formed with the carbonation of the CSH phase. It is metastable at room temperature and can readily recrystallize to calcite polymorph when exposed to water.

Unlike OPC mixtures, the CAC1 mixture has no portlandite present in the system, and the carbonation resulted in the significant decomposition of primarily C_2AH_8 phase along with C_3AH_6 phase to $CaCO_3$ (Aragonite and Vaterite) and AH_3 (Gibbsite), suggesting carbonation mechanism similar to reaction (i) in Equation 12. At exposure levels greater than 0.04%, the carbonation involved the decomposition of C_2AH_8 and C_3AH_6 into CAH_{10} along with $CaCO_3$ and AH_3, as proposed in Equation 13. The reaction mechanisms shown in Equation 13 do not involve the liberation of free water, which can thermodynamically favor the carbonation process [171]. The bound CO_2 in CAC1 mixtures at 0.04%, 1%, 7%, and 15% exposure levels in about 5.7%, 15.4%, 13.9%, and 11.5%, respectively. This suggests that the accelerated exposure levels even at 1% and higher are aggressive in CAC1 system. Interestingly, the extent of carbonation is higher at 1% exposure compared to 7% and 15% exposure levels – which is expected if the carbonation involves the formation of CAH_{10} phase along with the $CaCO_3$ phase. Since CAH_{10}, C_2AH_8, and C_3AH_6 are the main strength-giving hydration products, which also buffers the pore solution, decomposition of these phases due to carbonation in the CAC1 system can result in significant reduction of both the mechanical properties of the matrix and also the pH of the pore solution. No change is observed in the amount of C_3AH_6 phase present in the matrix with carbonation, suggesting that carbonation of the C_3AH_6 phase is less favorable compared to the CAH_{10} phase.

Equation 13

$$6CO_2+5C_2AH_8 \rightarrow 4CAH_{10} + 6CaCO_3+AH_3 \quad \text{(i)}$$
$$12CO_2+5C_3AH_6 \rightarrow 3CAH_{10} + 12CaCO_3+2AH_3 \quad \text{(ii)}$$

In the converted CAC1 system, similar to the normal CAC1 system, the carbonation at 7% exposure level involved the complete decomposition of C_2AH_8 along with significant decomposition of C_3AH_6 phases to CAH_{10}, $CaCO_3$, and AH_3 phases.

In CAC2 mixtures, the carbonation resulted in the significant decomposition of CAH_{10}, C_2AH_8, and C_3AH_6 phase to CaCO3 (Aragonite and Vaterite) and AH_3. The carbonation mechanism is more similar to Equation 12 (i) at lower exposure levels and similar to Equation 13 at higher exposure levels. The bound CO_2 in CAC2 mixtures at 0.04%, 1%, 7%, and 15% exposure levels is about 13.4%, 9%, 8%, and 9.7%, respectively. This suggests that the atmospheric exposure level (0.04%) is aggressive compared to the exposure at 1% and higher. So, the accelerated carbonation in CAC2 mixtures will underestimate the level of carbonation. Since CAH_{10}, C_2AH_8, and C_3AH_6 are the main strength-giving hydration products, which also buffers the pore solution, decomposition of these phases due to carbonation in the CAC2 system can result in a significant reduction of both the mechanical properties of the matrix and also the pH of the pore solution.

In the converted CAC2 system, similar to the converted CAC1 system, the carbonation at both 1% and 7% exposure level involved the decomposition of C_3AH_6 phases to CAH_{10}, $CaCO_3$, and AH_3 phases. However, the amount of $CaCO_3$ formed is significantly low when compared to the converted CAC1 system. The converted CAC1 system has a significantly

high amount of C_2AH_8 phase compared to the converted CAC2 system. Also, the bound CO_2 levels in both the converted systems are lower than their respective normal systems, as shown in Fig. 133. This suggests that the carbonation of C_3AH_6 phase is less favorable compared to the CAH_{10} and the C_2AH_8 phases – likely due to the difference in their thermodynamic stability.

The carbonation in the CACT mixtures resulted in significant decomposition of ettringite, portlandite, monocarboaluminate, and hemicarboaluminate phases – with a significant reduction in both the monocarboaluminate and hemicarboaluminate even with 0.04% CO_2 exposure level. There is a gradual reduction in both ettringite and portlandite phases up to 7% CO_2, with both these phases along with monocarboaluminate and hemicarboaluminate, completely disappeared with further increase in CO_2 exposure level to 15%. The bound CO_2 levels in CACT mixtures are about 8.7%, 9.7%, and 13% with 0.04%, 1%, and 7% CO_2 exposure levels, respectively. However, with a further increase in exposure level to 15%, the bound CO_2 level increased to about 23% – which suggests the 15% CO_2 is aggressive compared to other exposure levels investigated. With ettringite being one of the main strength-giving phases in CACT mixture, carbonation can result in significant reduction in mechanical properties, especially at 15% CO_2 exposure level.

In CSA1 mixtures, the carbonation involved the decomposition of ettringite to $CaCO_3$ (as calcite and aragonite), anhydrite, hemihydrate, and AH_3 – according to the reaction mechanism shown in Equation 11. The decomposition of ettringite is gradual and in small quantity until the 1% exposure level. Thereafter, at 7% and 15% exposure level, the ettringite phase decomposed completely. The bound CO2 levels at 0.04%, 1%, 7%, and 15% exposure levels is about 5%, 6.8%, 15.4%, and 12.1%, respectively. This suggests,

similar to OPC mixtures, the 1% accelerated exposure is similar to the atmospheric level exposure – whereas both the 7% and 15% exposures are very aggressive. Since ettringite is the main hydration product and the primary strength contributing phase in CSA1 mixtures, the carbonation can result in a significant reduction in mechanical properties, especially at both 7% and 15% exposure levels, within the exposure levels tested.

Similar to the CSA1 mixtures, the carbonation in CSA2 and CSA2P mixtures involved the decomposition of ettringite to $CaCO_3$ (as calcite and aragonite), anhydrite, hemihydrate, and AH_3. At a 15% exposure level, gypsum is also formed is these mixtures in addition to anhydrite and hemihydrate. The decomposition of ettringite in CSA2 mixtures is gradual and in small quantity until the 1% exposure level. Thereafter, at 7% and 15% exposure level, the ettringite phase decomposed completely. Whereas, in CSA2P mixtures, a significant amount of ettringite is still present even at 7% exposure level – likely due to the polymer modification in CSA2P mixtures, which reduced the permeability of CO_2 into the matrix. The bound CO2 levels in CSA2 mixtures at 0.04%, 1%, 7%, and 15% exposure levels is about 5.4%, 11%, 18.8%, and 17%, respectively. Whereas in CSA2P mixtures, it is about 5.3%, 7%, 15%, and 17.1%, respectively. This suggests, similar to OPC and CSA1 mixtures, the 1% accelerated exposure in CSA2P mixtures is similar to the atmospheric level exposure, whereas both the 7% and 15% exposures are very aggressive. Whereas, in CSA2 mixtures, even the 1% exposure level in aggressive, but not as significant as the 7% and 15% exposure levels. Also, similar to CSA1 mixtures, since the ettringite is the main strength-giving phase, the carbonation in both the CSA2 and CSA2P mixtures can result in a significant reduction in mechanical properties, especially at higher exposure levels.

In CSA3 mixtures, the carbonation involved the decomposition of ettringite, stratlingite, monosulfate, and hydrogarnet phases into $CaCO_3$ (as calcite and aragonite), AH_3, and hemihydrate. The aragonite polymorph of CaCO3 only appeared at exposure levels 1% and higher. Ettringite decomposed significantly at 1% exposure, and it completely disappeared at 7% and 15% exposure levels. Stratlingite, monosulfate, and hydrogarnet phases also got decomposed completely at both 7% and 15% exposure levels – whereas it is significantly low at atmospheric and 1% exposure levels. The bound CO2 levels at 0.04%, 1%, 7%, and 15% exposure levels is about 3.4%, 9.7%, 17.3%, and 15.5%, respectively. This suggests, the 1% exposure level is also aggressive in CSA3 mixtures similar to CSA2 mixtures, but not as significant as compared to both the 7% and 15% exposure levels.

In AA mixtures, at atmospheric exposure level, the decomposition of ettringite, monosulfate, and the stratlingite phases is minimal. Whereas at exposure levels greater than atmospheric level, the ettringite phase completely disappeared, and a significant reduction in both the monosulfate and the stratlingite phase can also be observed. However, unlike the CSA and CACT mixtures, ettringite is not the dominant strength-giving phase in the AA matrix. (Na-A-S-H) and (C-S-H) are dominant strength contributing phases in this AA system, and no significant reduction is observed in those two phases with carbonation. This suggests the reduction in strength in this AA system might be significantly lower when compared to the other three ACM mixtures discussed earlier. But the pore solution pH might drop considerably due to the carbonation of alkalis (NaOH) into alkali carbonates ($Na\text{-}CO_2$) – DTG peak at around 400 ºC. The carbonation of alkalis is only observed at 1% and higher exposure levels. So, the accelerated exposure conditions

in AA mixtures might be not representative of the natural carbonation process, especially when considering its effects on the pH of the system [173].

MPC mixtures are relatively inert to carbonation when compared to other ACM and OPC mixtures. At exposure levels greater than 1%, some decomposition of struvite phase is observed, but it is not significant. At 15% exposure level, a small quantity of $MgCO_3$ is formed – likely from the carbonation of $Mg(OH)_2$ phase.

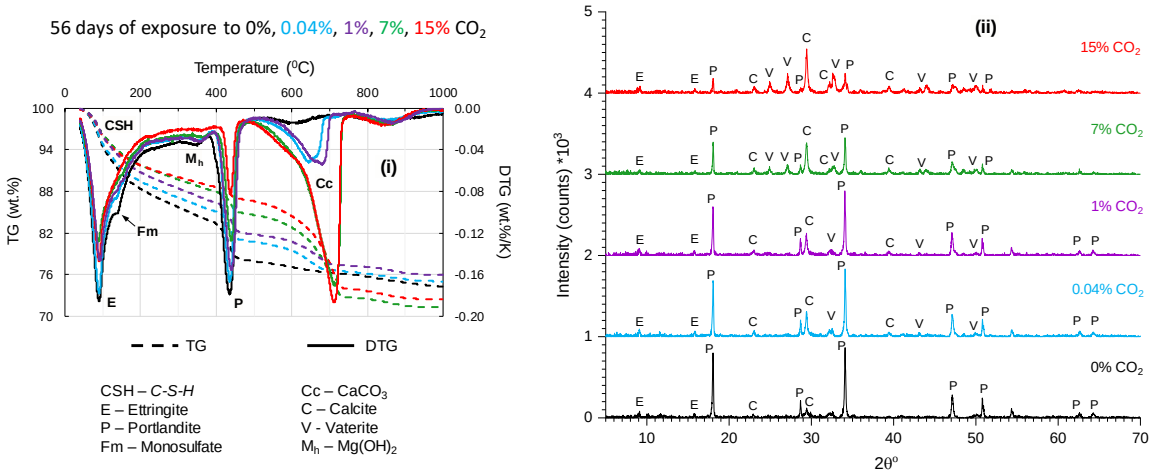

Fig. 120 (i) TG and DTG, (ii) XRD of OPC cement paste cubes after 56 days of exposure to 0%, 0.04%, 1%, 7%, and 15% CO_2.

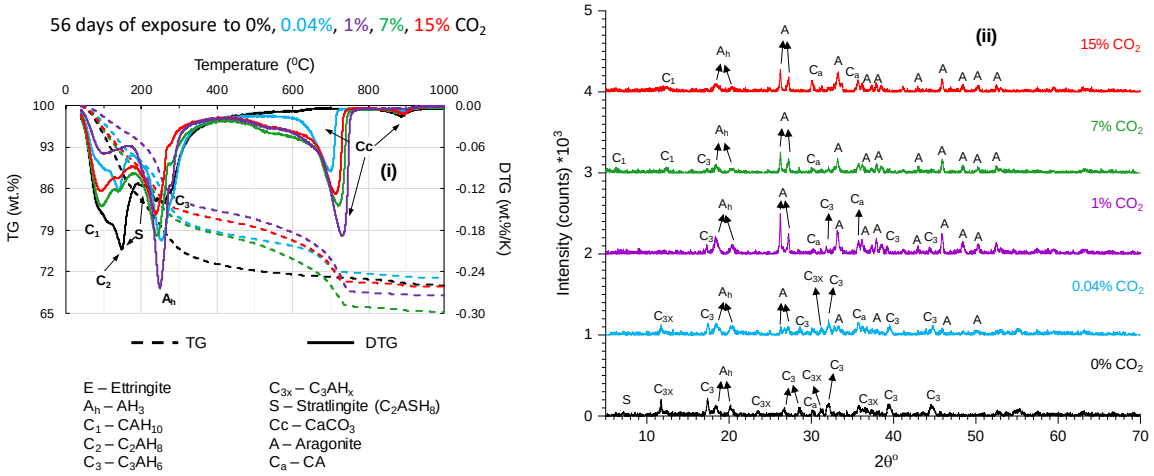

Fig. 121 (i) TG and DTG, (ii) XRD of CAC1 cement paste cubes after 56 days of exposure to 0%, 0.04%, 1%, 7%, and 15% CO_2.

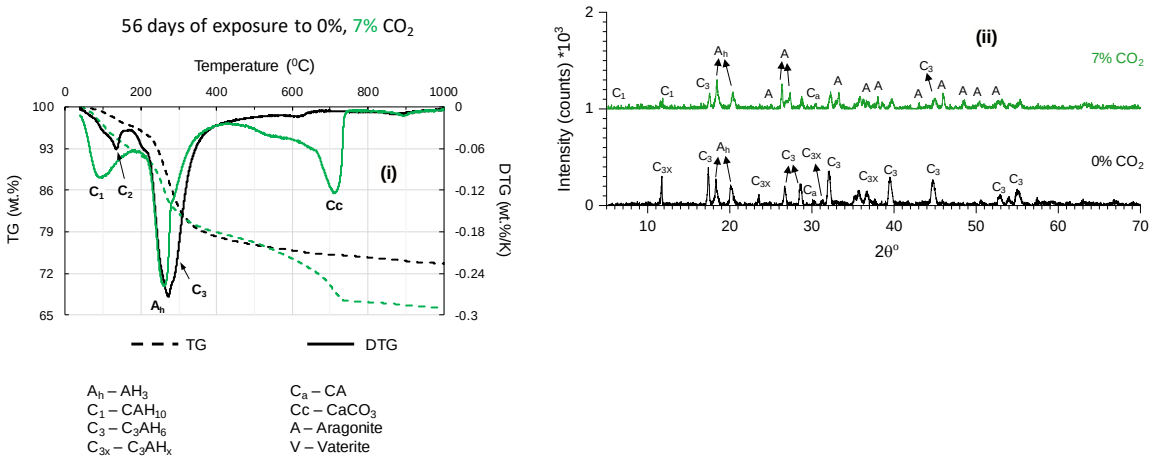

Fig. 122 (i) TG and DTG, (ii) XRD of converted CAC1 cement paste cubes after 56 days of exposure to 0%, 0.04%, 1%, 7%, and 15% CO_2.

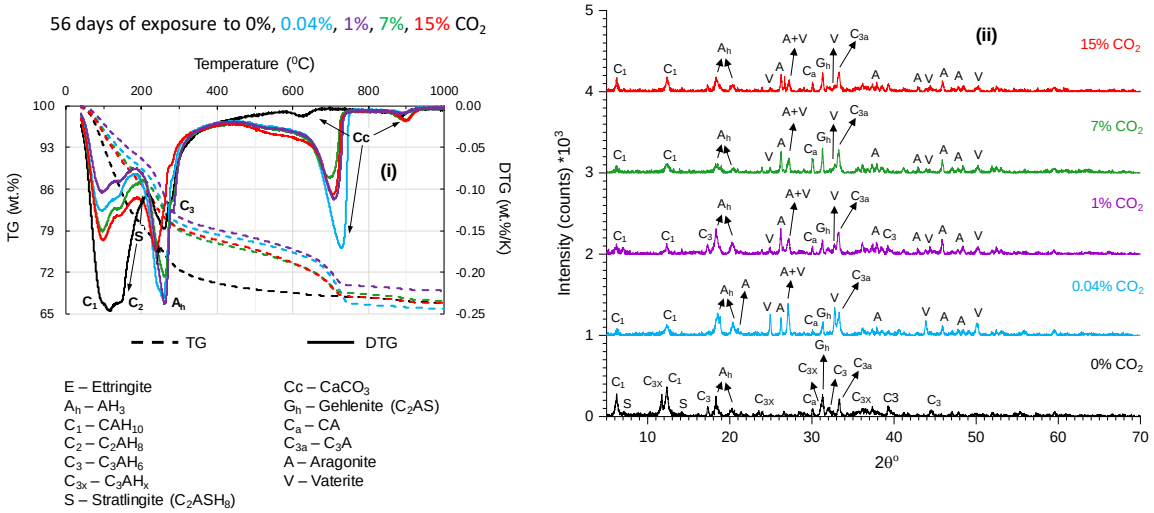

Fig. 123 (i) TG and DTG, (ii) XRD of CAC2 cement paste cubes after 56 days of exposure to 0%, 0.04%, 1%, 7%, and 15% CO_2.

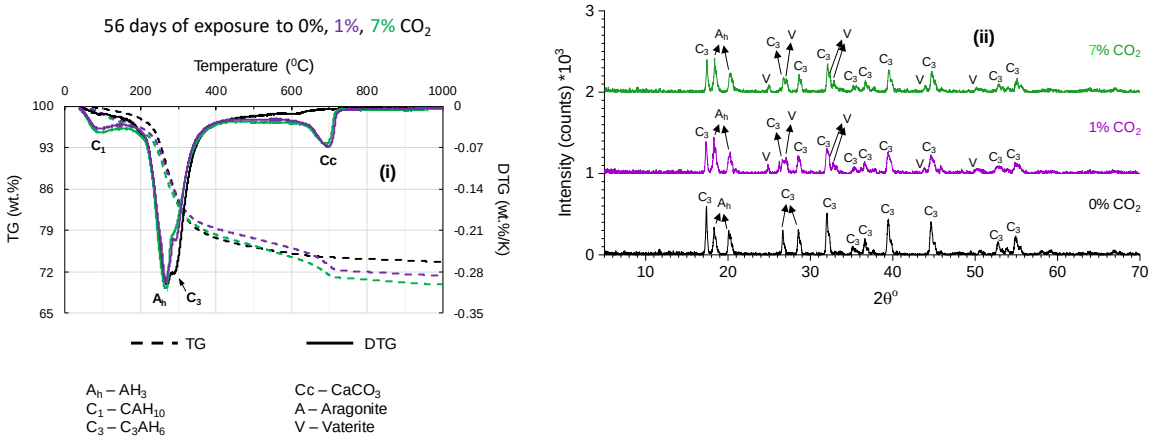

Fig. 124 (i) TG and DTG, (ii) XRD of converted CAC2 cement paste cubes after 56 days of exposure to 0%, 0.04%, 1%, 7%, and 15% CO_2.

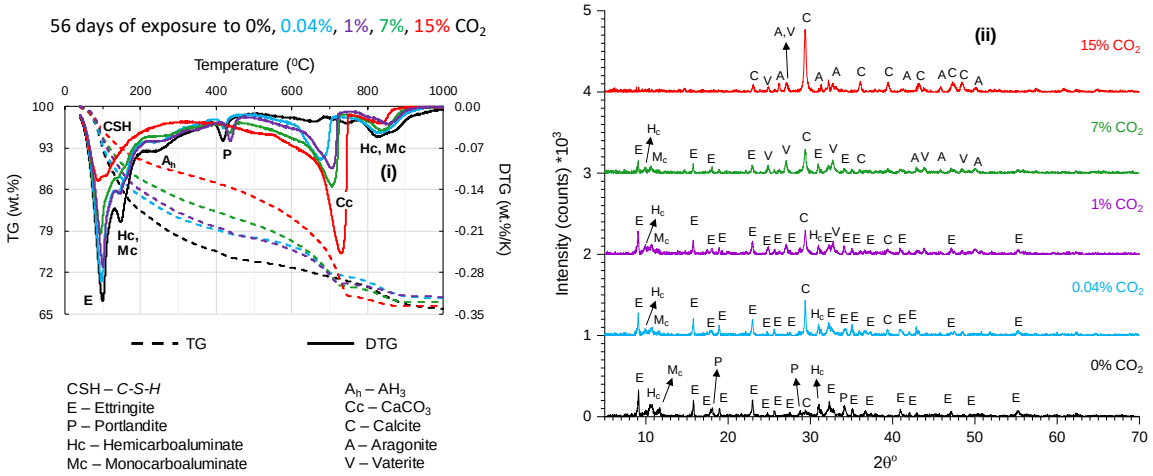

Fig. 125 (i) TG and DTG, (ii) XRD of CACT cement paste cubes after 56 days of exposure to 0%, 0.04%, 1%, 7%, and 15% CO_2.

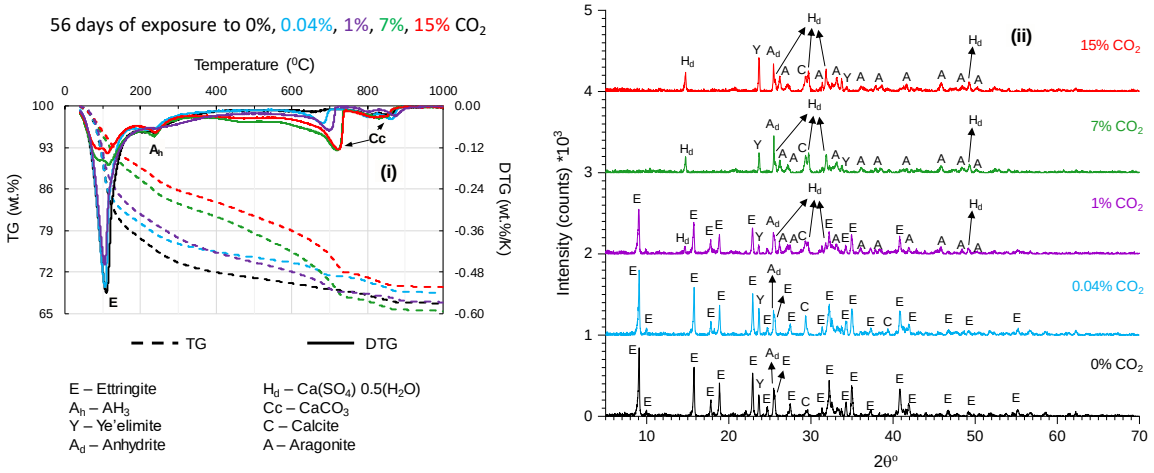

Fig. 126 (i) TG and DTG, (ii) XRD of CSA1 cement paste cubes after 56 days of exposure to 0%, 0.04%, 1%, 7%, and 15% CO_2.

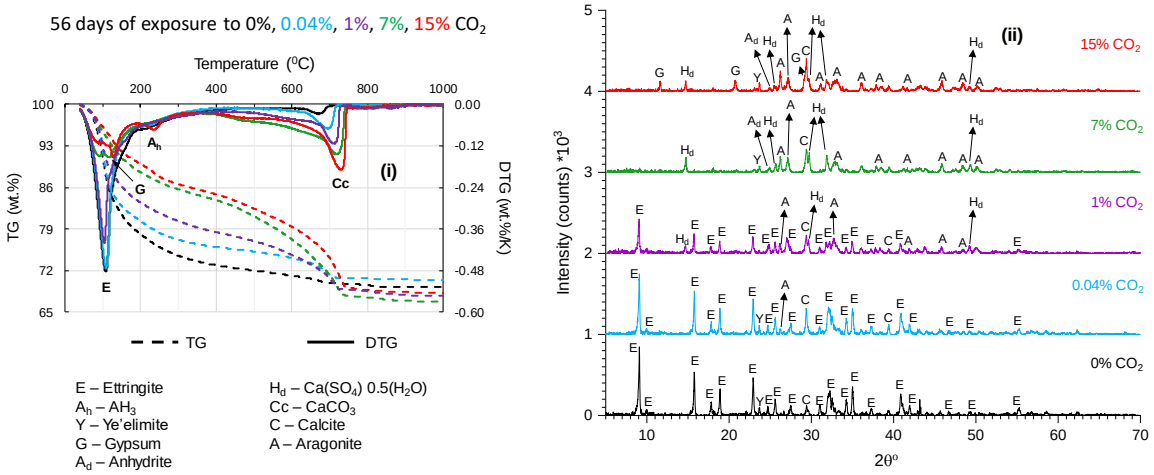

Fig. 127 (i) TG and DTG, (ii) XRD of CSA2 cement paste cubes after 56 days of exposure to 0%, 0.04%, 1%, 7%, and 15% CO_2.

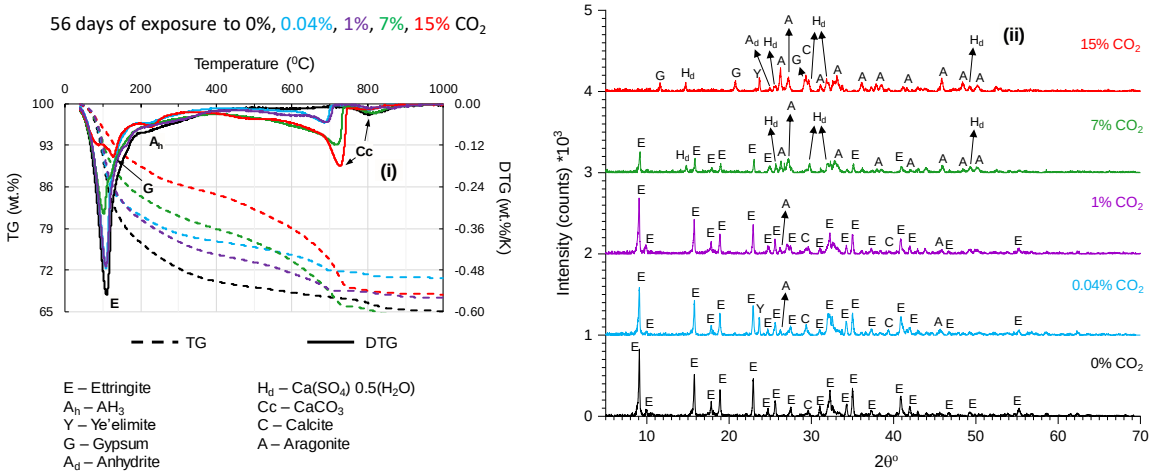

Fig. 128 (i) TG and DTG, (ii) XRD of CSA2P cement paste cubes after 56 days of exposure to 0%, 0.04%, 1%, 7%, and 15% CO_2.

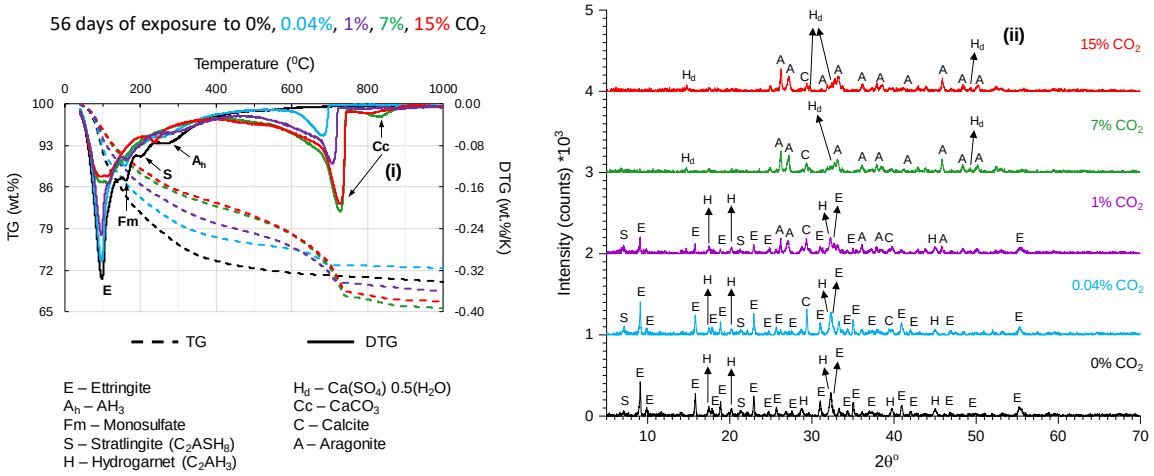

Fig. 129 (i) TG and DTG, (ii) XRD of CSA3 cement paste cubes after 56 days of exposure to 0%, 0.04%, 1%, 7%, and 15% CO_2.

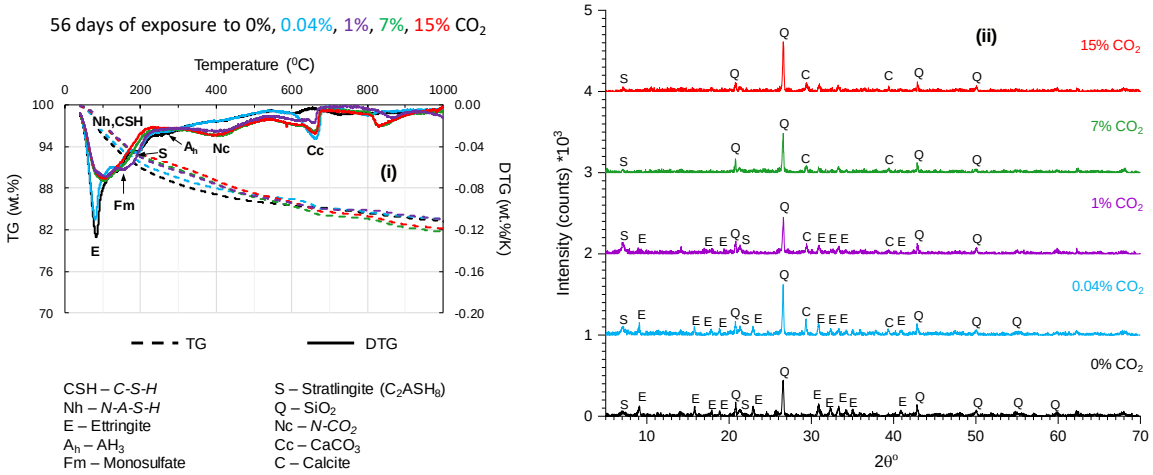

Fig. 130 (i) TG and DTG, (ii) XRD of AA cement paste cubes after 56 days of exposure to 0%, 0.04%, 1%, 7%, and 15% CO_2.

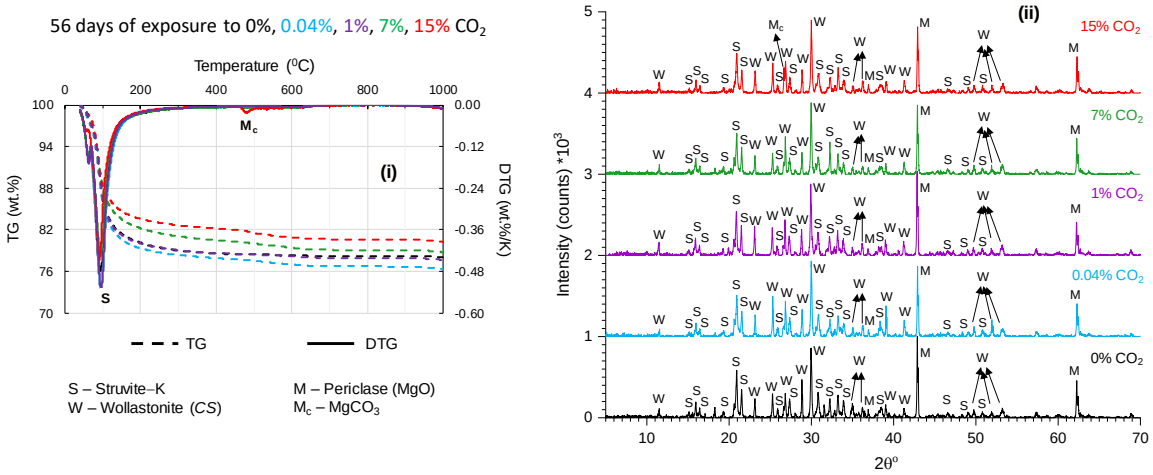

Fig. 131 (i) TG and DTG, (ii) XRD of MPC cement paste cubes after 56 days of exposure to 0%, 0.04%, 1%, 7%, and 15% CO_2.

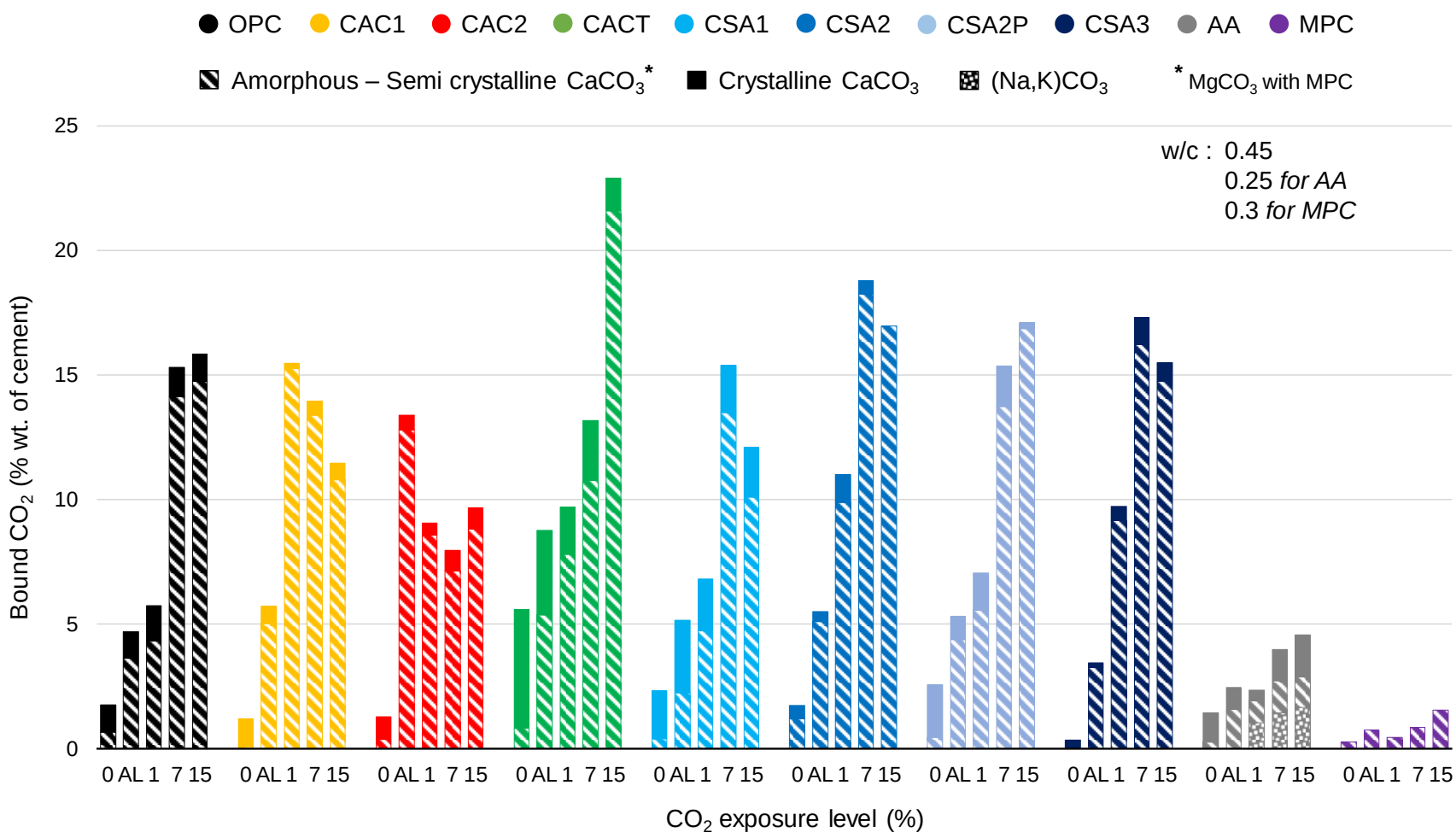

Fig. 132 Bound CO_2 levels in cement paste made with OPC and ACMs exposed to 0%, AL (0.04%), 1, 7, and 15% CO_2 for 56 days.

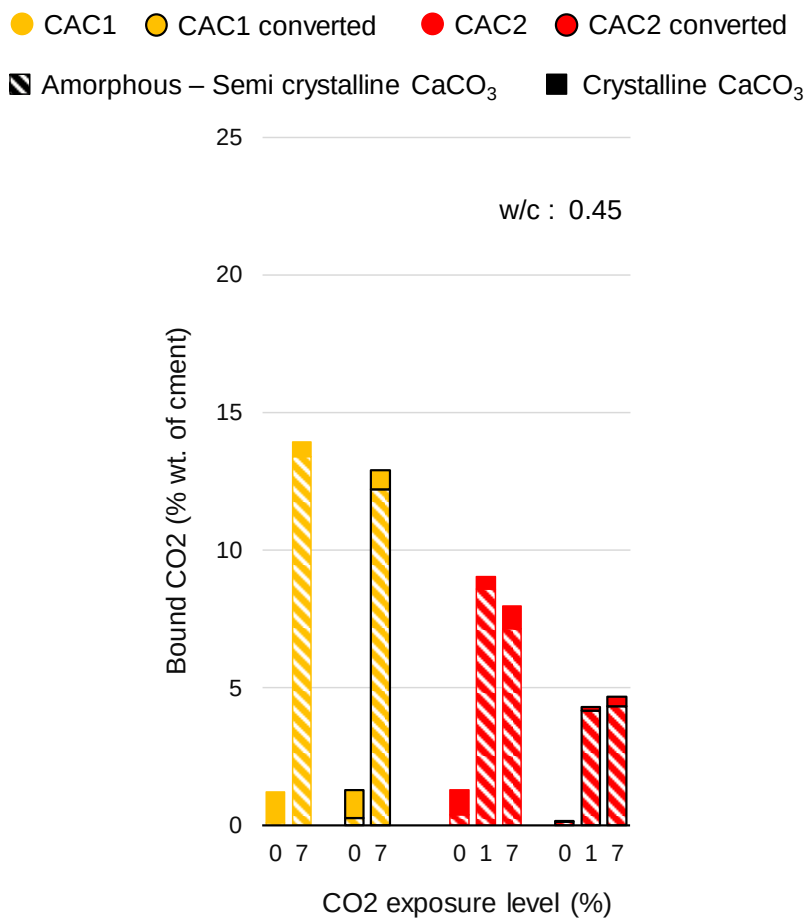

Fig. 133 Bound CO_2 levels in cement paste made with CAC1 and CAC2 mixtures, both converted and unconverted, exposed to 0%, 1%, and 7% CO_2.

12.4.2 Effect of carbonation on water sorption

Fig. 134 shows the initial and secondary sorption rates of both carbonated and uncarbonated cement mortars made with OPC and ACM mixtures. Significant reduction in initial sorption rate with carbonation in OPC and CAC2 mortars suggests precipitation of $CaCO_3$ in the capillary pores. Whereas an increase in secondary sorption rate with carbonation might be due to the significant decomposition of hydration products, thereby increasing gel porosity or porosity in the interfacial transition zone (ITZ). This may be attributed to the initial dissolution of portlandite and CAH_{10} phases, followed by

carbonation of these phases in pore water and, eventually, precipitation of the carbonated products (mainly $CaCO_3$). But further study is required to verify this mechanism.

However, with CACT, CSA1, CSA2, and CSA3 mixtures, the decrease in initial water sorption and an increase in secondary sorption with carbonation is not significant compared to OPC and CAC2 mixtures. This could be due to the filling of carbonated products within the gel, or ITZ pores since ettringite is the dominant phase that carbonated in these mixtures, and these phases do not readily dissolve in pore water unlike the CH and CAH_{10} phases present in OPC and CAC2 mixtures respectively. The same reason, including the precipitation of alkalis in the pore water to alkali carbonates, could also be attributed to the slight increase in initial sorption and decrease in secondary sorption observed in AA mixtures. In MPC mixtures, the precipitation of $MgCO_3$ from the carbonation of $Mg(OH)_2$ might be the reason for the reduction in the initial sorption rate.

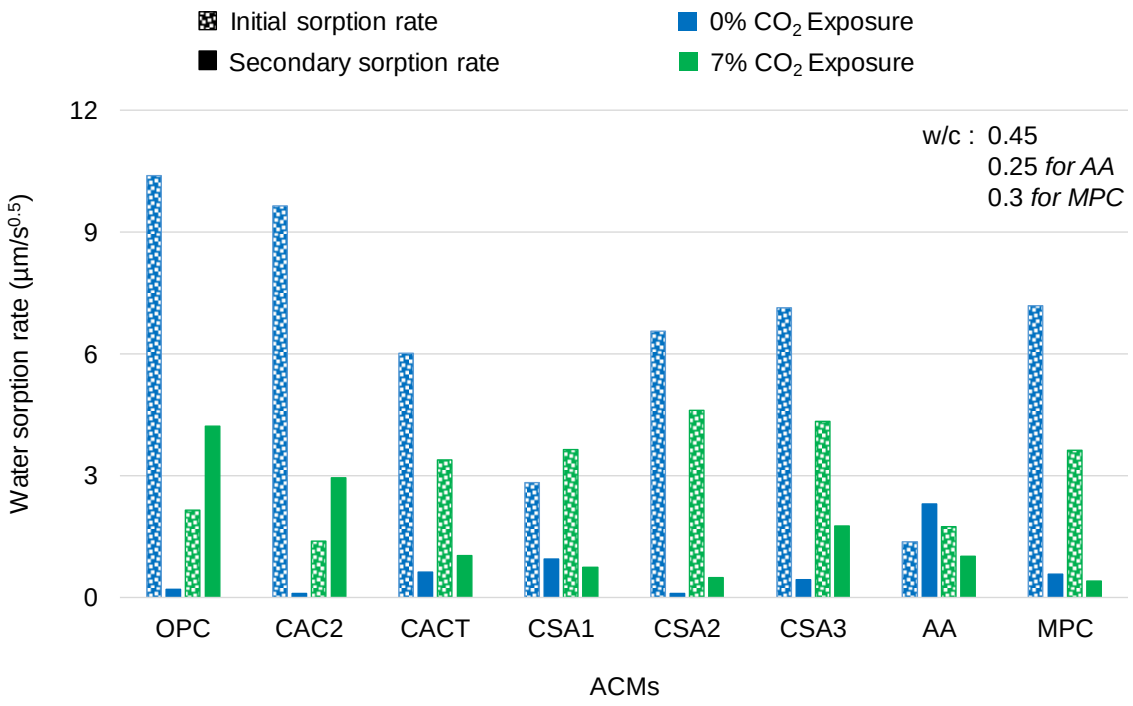

Fig. 134 Initial and secondary sorption rate of cement mortar samples made with OPC and ACMs, exposed to 0% and 7% CO_2.

12.4.3 Effects of carbonation on compressive strength

Fig. 135 shows the changes in compressive strength with carbonation in OPC and ACM mixtures at 1% and 7% exposure levels. Out of all the mixtures tested, only CAC1 and CAC2 showed a significant reduction in strength. However, the converted CAC1 and CAC2 systems (Fig. 136) showed significant improvement in strength – likely due to the pore filling due to the precipitation of $CaCO_3$ and the formation of low dense CAH_{10} phase. The increase in mechanical strength in CAC systems containing hexagonal hydrates (i.e., C_3AH_6 phase) is also reported in the literature [178]. OPC mixtures showed significant improvement in strength due to the conversion of calcium hydroxide to $CaCO_3$ precipitate. Similarly, AA mixtures also had a significant increase in strength – likely due to the precipitation of alkalis in pore solution to alkali carbonates. The change in strength in CACT, CSA1, CSA2, CSA2P is insignificant considering the error bars – even though

carbonation in these mixtures results in decomposition of their main strength-giving phases. This could be due to the combination of other factors, such as pore-filling due to the precipitation of carbonate and sulfate phases, continued hydration of unreacted cement due to the release of water with carbonation, that can play a role in strength contribution. Overall, in all the ACM and OPC mixtures (except the unconverted CACs), carbonation involves in either increase in mechanical properties or no change in mechanical properties.

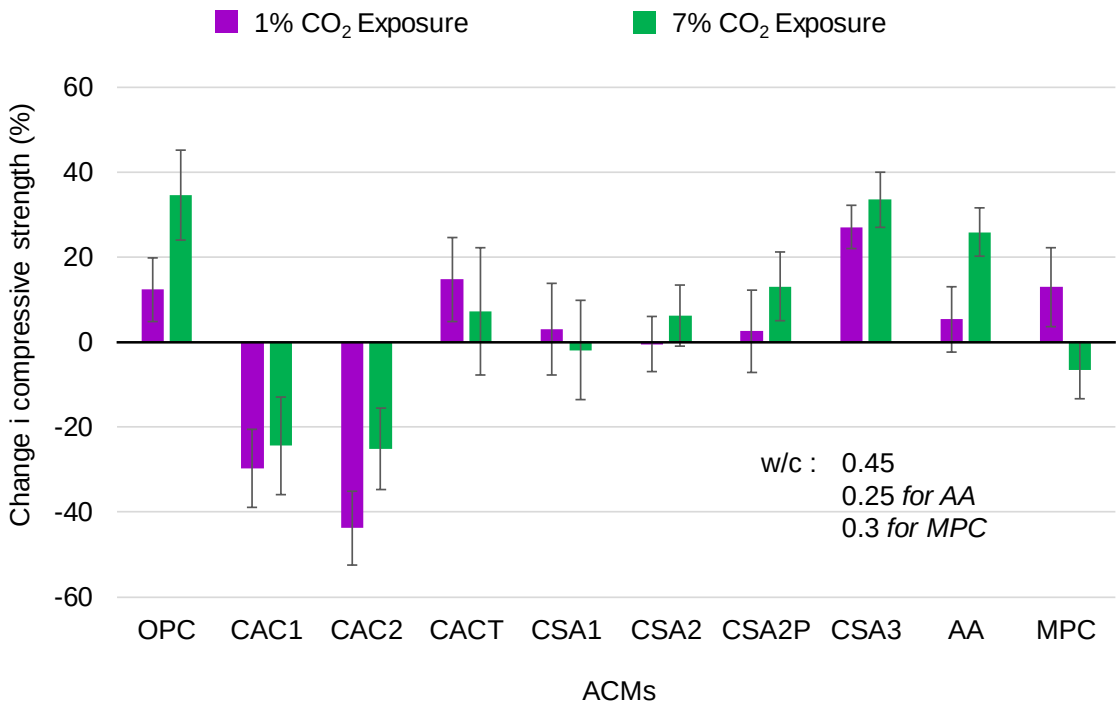

Fig. 135 Change in compressive strength in OPC and ACM mixtures after 56 days of carbonation at 1% and 7% CO_2 exposure.

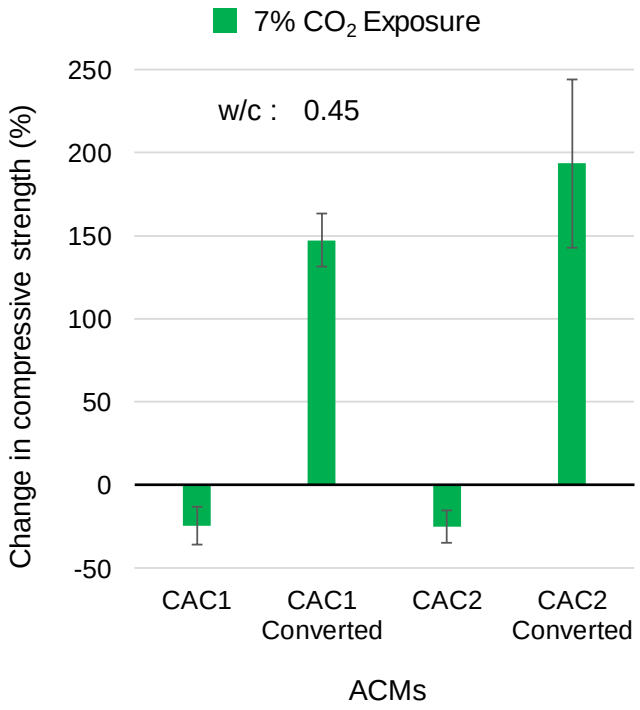

Fig. 136 Change in compressive strength in CAC1 and CAC2 mixtures, both converted and unconverted, after 56 days of carbonation at 7% CO2 exposure.

12.4.4 Carbonation front and pH estimates

Fig. 137 shows the pictures of the cut surface of OPC and ACM mixtures exposed to 1% CO_2 for 0, 7, 30, 60, and 90 days, and sprayed with the rainbow indicator at the end of each exposure period. The area of carbonation front at exposure ages of 0, 7, 30, 60, and 90 days measured based on the color change with the rainbow indicator are shown in Fig. 138. The pH levels in both carbonated and uncarbonated regions were estimated based on the color change with the rainbow indicator and are shown in Table 26.

The pH in the uncarbonated region of OPC and CACT mixtures was higher than 13, and it is between 11 to 13 in CAC1, CAC2, CAC2 converted, AA, and MPC mixtures. In CSA1, CSA2, CSA2P, and CSA3, the pH varied between 11-13 to greater than 13. With carbonation, the pH levels dropped to 11-13 in OPC, and it dropped to 9-11 in CACT,

CSA2, and CSA2P mixtures. Whereas the pH dropped to less than 9 in CAC1, CAC2 converted, CSA1, CSA3, and AA mixtures, and it is about 9 in CAC2 mixtures. The pH remained between 11-13 in MPC mixtures, even after 84 days of carbonation.

All the CAC (CAC1, CAC2, CAC2 converted) and CSA (CSA1, CSA2, CSA2P, CSA3) mixtures carbonated significantly compared to other mixtures. After 90 days of exposure, the area of carbonation front in those mixtures is higher than 90%. CAC2 carbonated at a significantly low rate compared to CAC1 initially, but later carbonated to higher rates. CSA2P showed a slight improvement in resisting carbonation compared to CSA2 – likely due to reduction in permeability in CSA2P with polymer addition. The total area of carbonated region in AA mixtures is about 77% after 90 days of exposure, and it is about 72% in CACT mixtures. However, AA mixtures carbonated at higher rates initially compared to CACT mixtures. In OPC mixtures, the area of carbonation front after 90 days of exposure is about 42%. However, the pH is the carbonated region is still higher than 11 in OPC mixtures compared to ACM mixtures (except MPC). OPC mixtures have higher amounts of portlandite phase in the system, and as observed in the carbonation of paste samples in the previous section, a significant amount of portlandite phase can still be present even after exposure to higher CO_2 levels, that can buffer the pore solution. MPC mixtures did not show any carbonation based on pH observed with the rainbow indicator. Overall, MPC mixtures performed the best in resisting carbonation compared to other ACM and OPC mixtures. CACT and AA mixtures are the next best performers in resisting carbonation compared to other ACM mixtures – However, they still carbonated significantly compared to OPC mixtures.

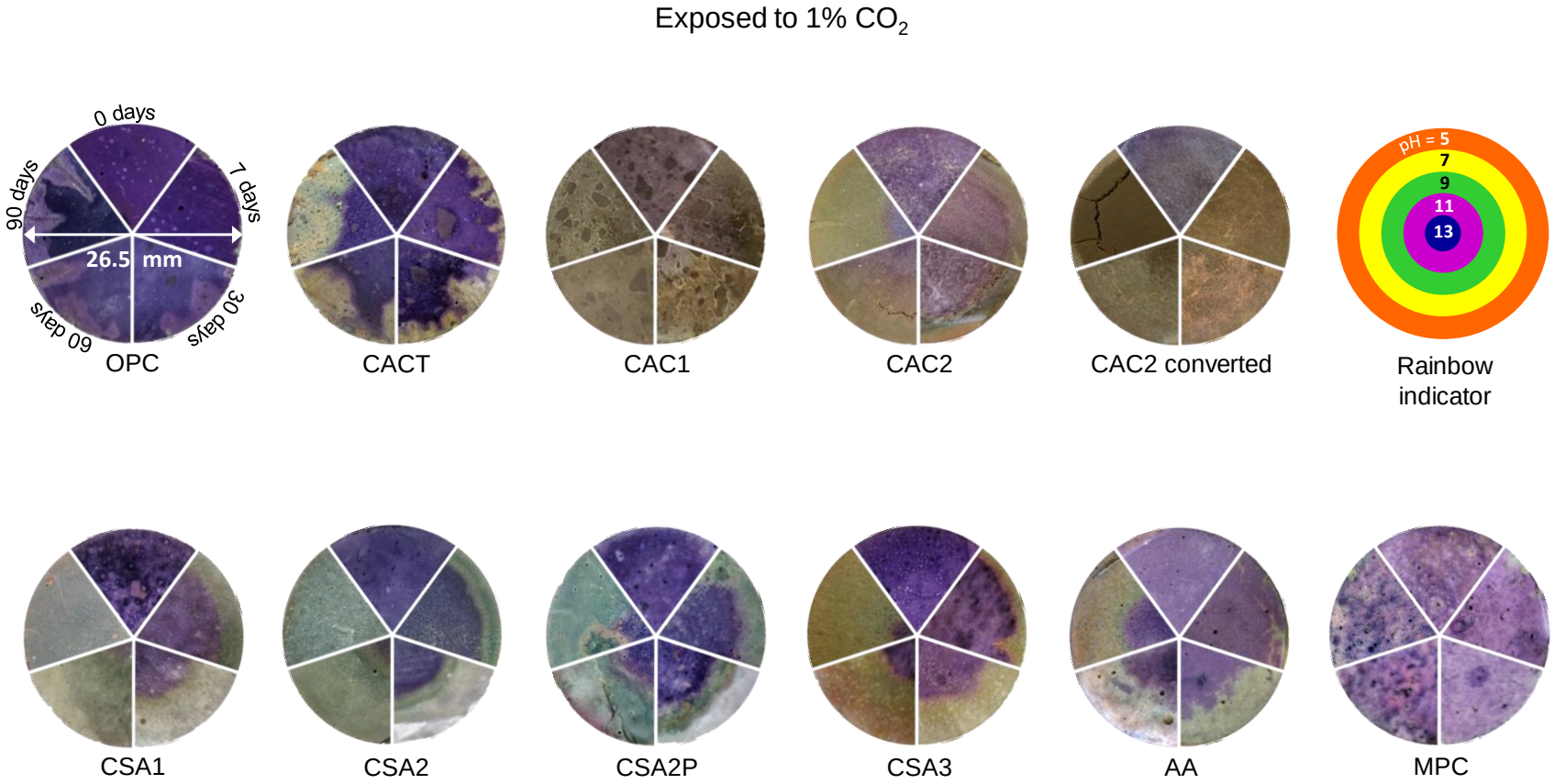

Fig. 137 Cement paste samples made with OPC and ACMs, after exposure to 1% CO2 for 0, 7, 30, 60, and 90 days, and sprayed with a rainbow indicator on the cut surface.

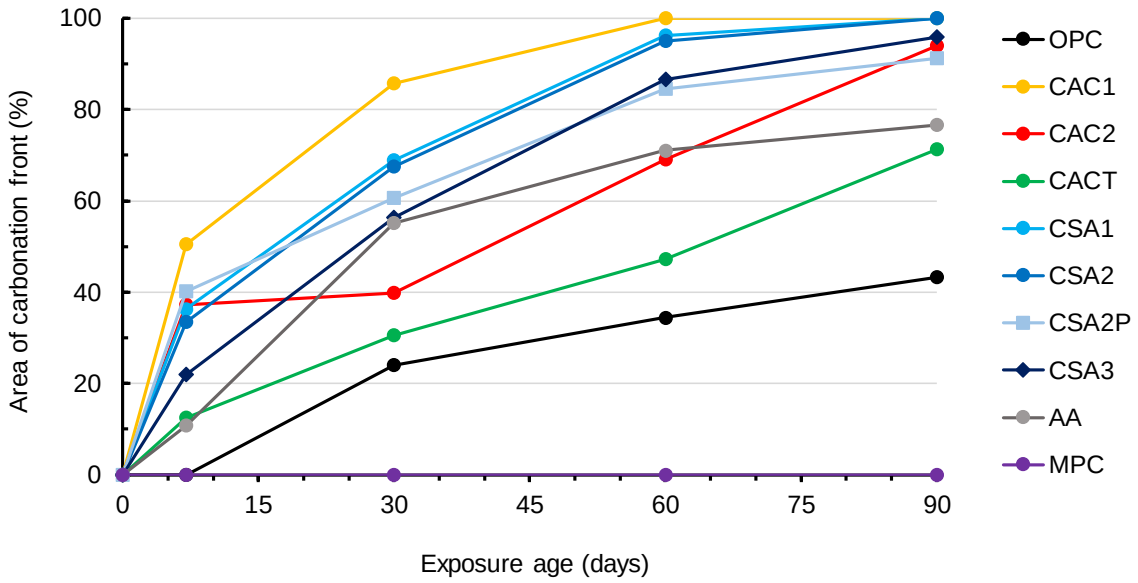

Fig. 138 Carbonation front in cement paste samples made with OPC and ACMs, exposed to 1% CO2, at different exposure ages (0, 7, 30, 60, and 90 days).

Table 26 pH levels based on visual observation in both carbonated and uncarbonated regions of cement paste samples made with OPC and ACMs, exposed to 1% CO_2 for 90 days and sprayed with rainbow indicator.

Binder	Uncarbonated pH	Carbonated pH
OPC	> 13	11 - 13
CAC1	11 - 13	< 9
CAC2	11 - 13	~ 9
CAC2 converted	11 - 13	< 9
CACT	> 13	9 - 11
CSA1	> 11	< 9
CSA2	> 11	9 - 11
CSA2P	> 11	9 - 11
CSA3	> 11	< 9
AA	11 - 13	< 9
MPC	11 - 13	11 - 13

12.4.5 Effect of carbonation on the passivation of embedded steel

Fig. 139 shows the open circuit potential (OCP) of embedded steel in uncarbonated and carbonated ACM and OPC mixtures. Fig. 140 shows the difference in OCP of embedded steel between carbonated and uncarbonated mixtures. Both the CSA1 and CSA2 mixtures had a significant reduction in their open circuit potential with carbonation compared to other ACM and OPC mixtures. Even though CAC1, CAC2, and CAC2 mixtures carbonated significantly, the change (reduction) in the OCP values of their embedded steel is similar or significantly lower compared to all the CSA and AA mixtures. This could be likely due to the significant increase in AH_3 or CAH_{10} composition with carbonation, which can help in repassivation of steel due to their OH^- ion buffering capacity [179]. CACT mixtures also had a lower reduction in OCP values, likely due to their higher pH in the uncarbonated region and to slightly lower carbonation front compared to other ACM

mixtures (except MPC). No change is observed in the OCP value of the steels embedded MPC mixtures with carbonation, suggesting superior resistance of these mixtures in resisting carbonation and thereby protecting the embedded steels from depassivation.

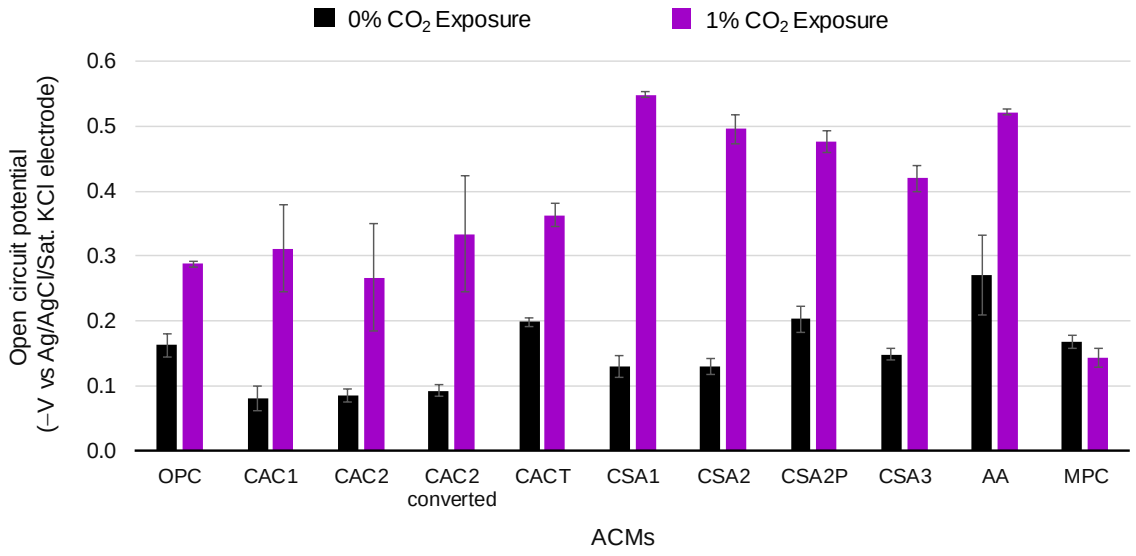

Fig. 139 Open circuit potential of embedded steel in carbonated and uncarbonated paste mixtures. The mixtures are carbonated by exposing to 1% CO_2 for 90 days.

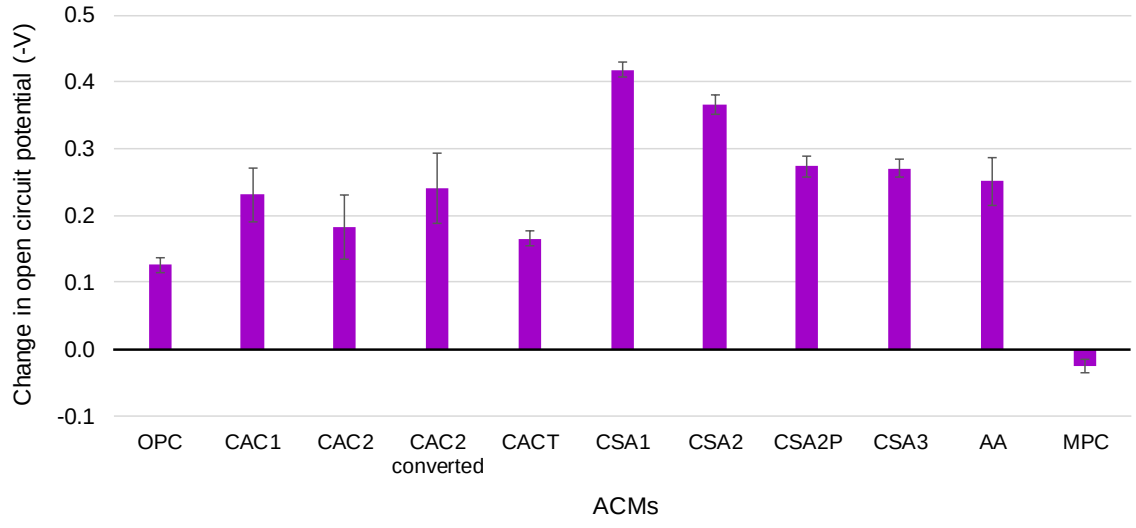

Fig. 140 Change in open circuit potential of embedded steel in paste mixtures after exposure to 1% CO_2 for 90 days.

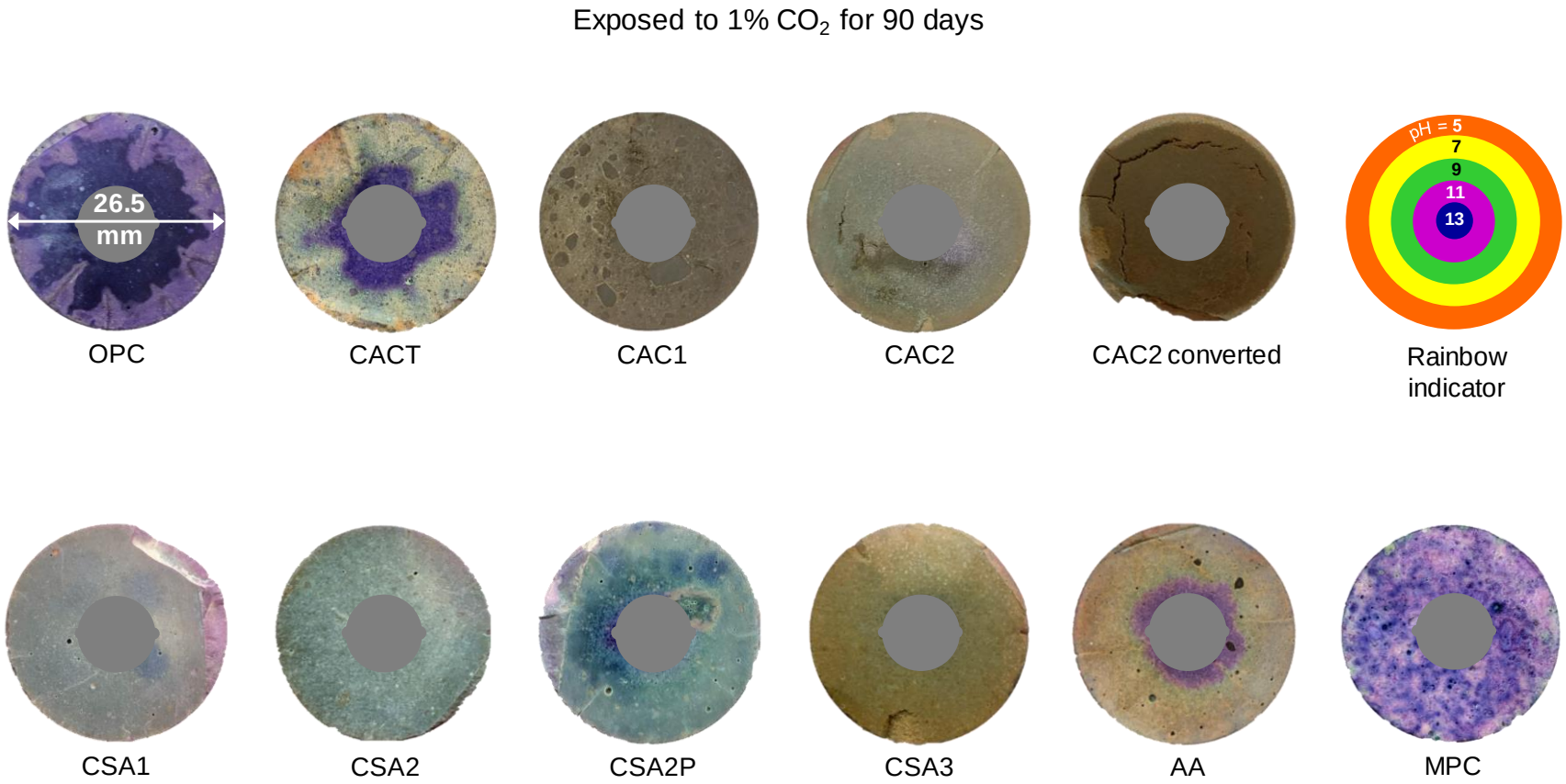

Fig. 141 Cement paste samples made with OPC and ACMs, after exposure to 1% CO2 for 90 days, and sprayed with a rainbow indicator on the cut surface.

12.4.6 Carbonation rate and pH estimates in concrete mixtures exposed to 7% CO_2

Fig. 142 and Fig. 143 shows the pictures of the split surface of OPC and ACM concrete cylinders exposed to 7% CO_2 for 84 days and sprayed with phenolphthalein and rainbow indicator, respectively. The mean carbonation front at exposure ages of 0, 3, 7, 14, 21, 28, 42, 56, and 84 days and carbonation rates in in/yr$^{0.5}$ were measured based on the color change with the phenolphthalein and rainbow indicator, and are shown in Fig. 144. The pH levels in both carbonated and uncarbonated regions were estimated based on the color change with the rainbow indicator and are shown in Table 27. A distinctive two regions can be observed in all the ACM mixtures, the outer carbonated layer, and the inner uncarbonated layer. Whereas OPC mixtures had a total three distinctive regions with carbonation. The outer layer has pH between 9 to 11, the middle layer between 11 to 13, and the inner layer greater than 13. So, in Fig. 144 and Table 27, for the OPC mixtures, denoted as 'OPC (pH <11)', the carbonation front is calculated based on the outer layer alone. Whereas for the OPC mixtures denoted with 'OPC (pH 11-13)', the carbonation front is calculated based on the combination of the outer and the middle layer.

The pH in the uncarbonated region of OPC, CACT, CSA2, and AA concrete mixtures was higher than 13, between 11 to 13 in CSA1 mixtures, and it is between 9 to 11 in CAC2 mixtures – which suggests that even the pre-carbonation environment in CAC2 systems may be detrimental to embedded steel passivation. With carbonation, the pH levels dropped to 9-11 in both the 'OPC (pH <11)', CACT, and CSA2 mixtures and to less than 9 in the CAC2, CSA1, and AA mixtures. Also, the carbonation rate in the CACT mixture is similar to that of 'OPC (pH <11)' mixtures and at least 4 folds higher in CAC2, CSA1, CSA2, and AA mixtures. If the carbonation rate for OPC mixtures is calculated based on the

combination of both the outer and the middle layer, the carbonation rate in OPC mixtures is significantly higher than CACT mixtures and is similar to other ACM mixtures.

OPC mixtures have higher amounts of portlandite phase in the system, and as observed in the carbonation of paste samples in the previous section, a significant amount of portlandite phase can still be present even after exposure to higher CO_2 levels, that can buffer the pore solution. So, the carbonation front measured using phenolphthalein and rainbow indicators may not be representative of the actual depth of CO_2 ingress in the system. However, since the passivation of embedded steel reinforcement in concrete systems is dependent on the pH of the system at the interface rather than the CO_2 ingress depth levels, the carbonation rate measured here (with assuming the outer layer alone as the carbonated layer in OPC) can provide reasonable estimates of relative performance of these ACM mixtures compared to OPC mixture in resisting depassivation of reinforcement.

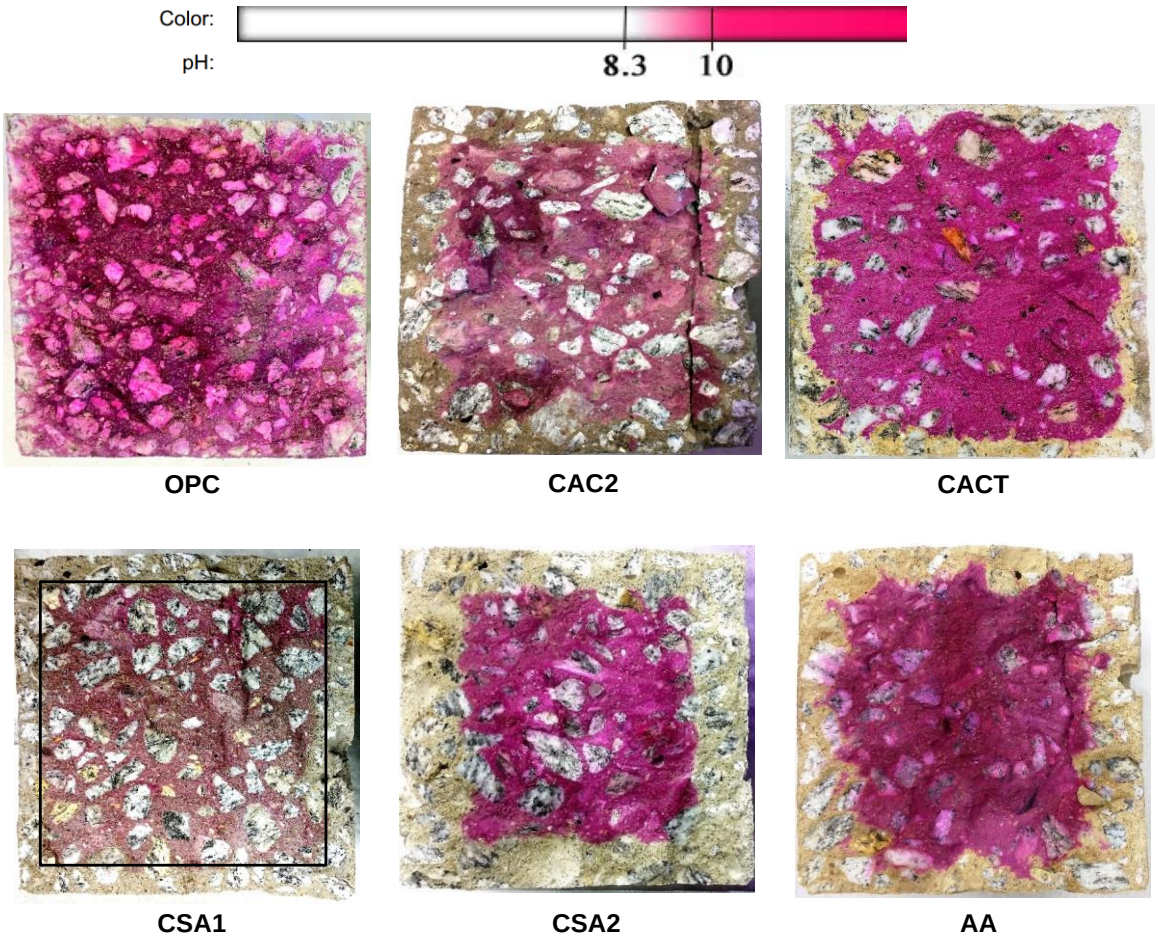

Fig. 142 Concrete samples after exposure to 7% CO_2 for 84 days and sprayed with phenolphthalein indicator on the split surface.

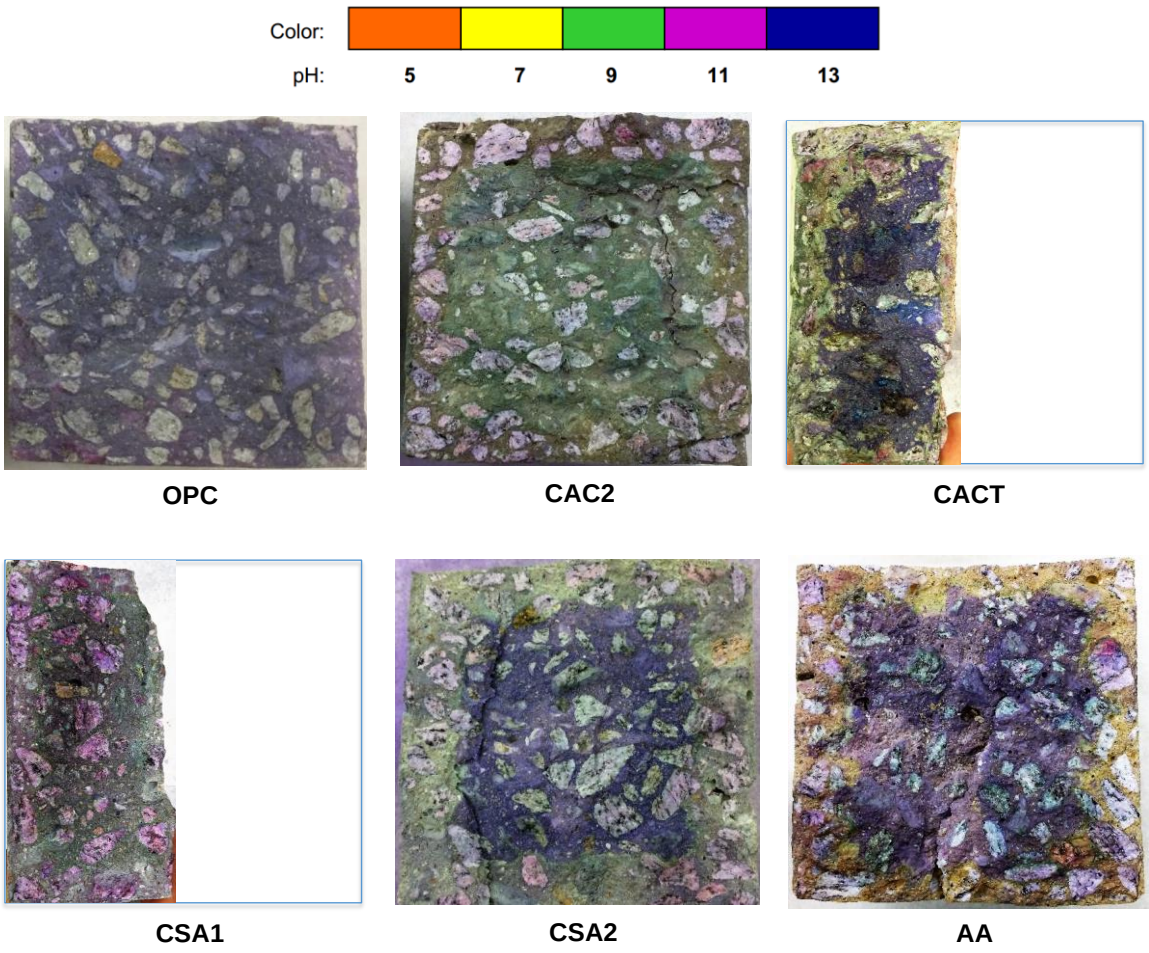

Fig. 143 Concrete samples after exposure to 7% CO_2 for 84 days and sprayed with a rainbow indicator on the split surface.

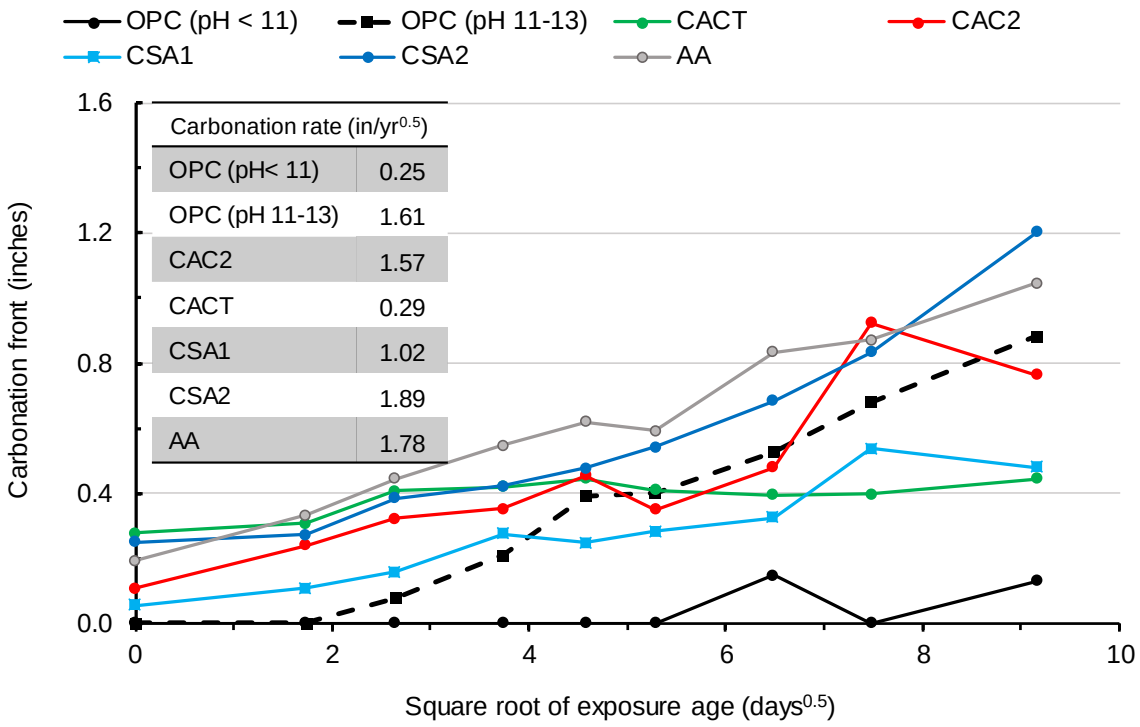

Fig. 144 Carbonation front of concrete samples made with OPC and ACMs, exposed to 7% CO_2, at different exposure ages.

Table 27 pH levels based on visual observation in both carbonated and uncarbonated regions of concrete samples made with OPC and ACMs, exposed to 7% CO_2 for 84 days and sprayed with rainbow indicator.

Binder	Uncarbonated pH	Carbonated pH
OPC (pH <11)	> 13	9 - 11
OPC (pH 11-13)	> 13	11 - 13
CAC2	9 - 11	< 9
CACT	> 13	9 - 11
CSA1	11 -13	< 9
CSA2	> 13	9 - 11
AA	> 13	< 9

12.5 Conclusion and Recommendations

The accelerated carbonation tests, along with complementary characterization by TGA and XRD, water sorptivity, and strength measurements performed in this study, were intended to understand the carbonation mechanisms and evaluate the performance of commercially available ACM systems in resisting carbonation compared to OPC systems and has led to the following conclusions.

- Out of the accelerated CO_2 exposure levels tested in this chapter, both 7% and 15% exposure levels were found to be aggressive in OPC, CAC1, CACT, CSA1, CSA2, CSA2P, and AA mixtures. Whereas, all the 1%, 7%, and 15% exposure levels underestimated the carbonation compared to the atmospheric levels in CAC2 mixtures. Even the 1% exposure level seemed to be aggressive in both CSA2 and CSA3 mixtures. In AA mixtures, the 1% accelerated exposure also resulted in significant carbonation of alkalis in the pore solution, which is not observed with carbonation at atmospheric levels.
- Carbonation in CAC1, CAC2, CACT, CSA1, CSA2, CSA2P, and CSA3 systems can result in significant decomposition of main hydration products, whereas, no significant decomposition of main hydration products is observed in OPC, AA, and MPC systems.
- The variation in the bound CO_2 levels with cement type is due to the differences in the carbonation nature of their hydration products and may not necessarily relate to the extent of carbonation.
- Carbonation in OPC and CAC2 mortar mixtures resulted in a significant reduction in capillary porosity, followed by CACT, CSA2, CSA3, and MPC mixtures at a 7%

exposure level, whereas, no significant change is observed in CSA1 and AA mixtures.

- Carbonation resulted in significant strength loss in both CAC1 and CAC2 systems. Whereas, it contributed to strength in both their converted systems. OPC, CSA3, and AA mixtures experienced increase in strength with carbonation – likely due to precipitation of carbonates in their pores, whereas no significant change in strength with carbonation is observed in other ACM mixtures.
- All the CAC and CSA mixtures carbonated to significantly higher depths at 1% carbonation exposure. AA and CACT mixtures also carbonated to higher depths compared to OPC mixtures but were significantly lower compared to other ACM mixtures (except MPC). MPC mixtures showed the highest resistance to carbonation with zero carbonation depth even after exposure to 90 days at a 1% accelerated condition.
- The pH levels in the carbonated region of OPC and MPC mixtures is between 11 to 13. Whereas in CACT, CSA2, and CSA2P concrete mixtures, the pH dropped to between 9 to 11. In the other ACM mixtures, the pH dropped to even below 9 – which may result in significant destabilization of the passive layer in steel reinforcements.
- The steels embedded in both the CSA1 and CSA2 mixtures experienced the most depassivation compared to the steel in other ACM mixtures. The change in passivation state of embedded steel in the other ACM mixtures (except MPC) is also higher compared to OPC mixtures. The steels embedded in MPC mixtures showed no significant change in the passivation state.

- CAC2, CSA2, and AA concrete mixtures carbonated at a much faster rate (at least 6 times) compared to OPC concrete mixture when exposed to 7% CO_2. CSA1 mixtures carbonated at 4 times faster compared to OPC mixtures. CACT carbonated at a rate similar to OPC mixture. However, it experienced significant pre-carbonation even compared to all other ACM mixtures. Whereas, no pre-carbonation is observed in OPC mixtures.

13 CONCLUSIONS AND RECOMMENDATIONS

13.1 Conclusions

In this thesis, nine commercially available ACMs of different binder chemistry were examined for their suitability as alternatives to portland cement for transportation infrastructure construction. A multi-scale approach was used to design concrete mixtures with these commercial ACMs to meet both the prescriptive requirements and the performance targets. The multi-approach involved (i) using multiple material characterization techniques to understand how these commercially blends hydrate, and (ii) changing their fresh properties to meet the prescriptive requirements without adversely affecting their long-term material properties to meet the performance targets. New test methods and protocols also involving multi-scale material characterization were proposed and were used to gauge the long-term performance of these ACMs against a wide range of exposure conditions. These new test methods were designed, relying as much as possible on existing test methods for traditional portland systems, to facilitate the rapid adoption of the ACM formulations. From this multi-scale investigation of commercial alternative cementitious materials, the following conclusions were made. Table 28 provides a summary of the performance of these ACM formulations in aspects investigated in this thesis.

13.1.1 Constructability and Hardened properties

- By using commercially available set modifiers and plasticizers, successful concrete mixtures were designed with all the ACM mixtures (except MPC and CAC1) that had a concrete slump of at least 3 inches at the end of 60-minute hydration period.

- While the citric acid addition in CSA3 mixtures and the boric acid addition in MPC mixtures successfully retarded the mixtures initially, its retardation effects continued even until about 10 days of hydration, where the total heat of hydration with retarder dosage is about 7 to 10% lower compared to the mixtures without retarder dosage.

- The addition of plasticizer (admix1) did not significantly affect the hydration in the cement pastes made with OPC, CACT, CSA1, and CSA2.
- No retardation in heat evolution is observed during the initial 24 hours of hydration in CSA3 mixtures with the addition of admix1. However, significant retardation is observed in the hydration between 1 and 6 days of hydration time. This lead to a significant slower strength development in these mixtures. The significant presence of iron in this binder could be the reason for incompatibility with the current admixtures. So, a better combination of set modifier and plasticizer needs to be identified and/or developed, to reduce the retardation at later ages in the CSA3 mixtures.
- CAC1 requires identification and/or development of appropriate plasticizing admixtures to enhance workability in concrete. With the admixtures recommended

by the CAC1 cement producer, a workable mix with at least 3 inches of slump at 60 min could not be achieved.

- Also, an extended set time necessary for conventional concrete mixing could not be achieved with the MPC cements. In addition, expansion during hydration and leaching can be problematic in some applications.

- CAC2, CSA1, CSA2, CSA3, and AA mixtures showed significant lower autogenous shrinkage compared to OPC and other ACM mixtures, whereas, both the CSA3 and MPC mixtures exhibited significant expansion. CACT and CSA2P mixtures exhibited significant shrinkage compared to other ACM mixtures but were similar to that of OPC mixtures.

- CACT, CAC2, CSA1, CSA2, and AA mixtures along with the OPC mixtures met the 7-days and the 28-day compressive strength requirements, whereas only OPC, CACT, CAC2, CSA1, and CSA2 mixtures met the 28-day flexural strength requirement. CSA3 mixtures did not meet both the 7-day compressive strength and 28-day MOR requirements.

13.1.2 Influence of w/b on permeability in ACM mixtures

A new test method is proposed for measuring formation factor and interconnectivity in OPC and ACM mixtures and is described in detail in section 9.1.2. This method can be effective, especially in highly resistant systems where pore water extraction is not reliable. Water sorptivity, total porosity, and formation factor measurements were performed at a range of w/b to evaluate the performance of commercially available ACMs and their

sensitivity towards w/b in resisting ingress of foreign substances. Analyzed together, this series of tests has led to the following conclusions:

- The influence of w/b on sorptivity (as influenced by porosity and pore structure) varied with different binder systems, with CACT being the most sensitive to variations in w/b of all. At w/b less than or equal to 0.485, the CACT mixtures exhibited higher differences in initial sorption rates with changes in w/b compared to OPC and other ACM mixtures investigated.
- To design mixtures with similar or lower sorption compared to OPC at 0.40, the w/b in all the ACM mixtures (except CSA2P) should be less than 0.40. The CSA2P mixture at 0.4 w/b has significantly lower sorption compared to that of OPC. In the AA mixture, the w/b should be further lower than 0.233 and 0.30. Whereas in MPC it should be lower than 0.30.
- Overall, CSA1 and AA mixtures had either lower or similar interconnectivity of pore structure compared to the OPC mixtures. CSA2P mixtures also had significantly lower interconnectivity, but only at w/b of 0.40. CSA2 mixtures had higher interconnectivity compared to OPC mixtures, but not significantly higher. Whereas CACT, CAC2, CSA3, and MPC mixtures have significantly higher interconnectivity compared to the OPC and the other ACM mixtures.
- A linear relationship exists between formation factor in log-log scale for all the OPC and ACM mixtures except CAC2 mixtures. In both CSA3 and AA mixtures, a bilinear relation is observed in the w/b examined in this chapter. Using these relationships, the formation factor (thereby permeability) can be estimated based on the total porosity measurements.

13.1.3 Resistance to chemical sulfate attack

The accelerated sulfate exposure tests at constant pH, along with complementary characterization by TGA, XRD, and SEM-EDS performed in this thesis were used to understand the chemical sulfate mechanisms in OPC and ACM mixtures, and evaluate the performance of commercially available ACM systems in resisting chemical sulfate exposure compared to OPC systems, and has led to the following conclusions.

- Crystallization of gypsum is the primary damage mechanism observed in all the mixtures that showed significant spalling and cracking (except CAC1 and CAC2) when the mixtures are subjected to constant pH sulfate exposure. In CAC mixtures, the formation of ettringite is the primary damage mechanism.

- Surface spalling (rather than cracking) is the main damage mechanisms observed in OPC mixtures due to the decalcification of C-S-H and crystallization of gypsum.

- A dense outer layer composed of C-N-M-A-S-H is formed in all the CSA and CACT mixtures with exposure to sodium sulfate. This layer reduced the permeability of sodium sulfate into the inner matrix. However, in the CSA2P mixture, a layer of gypsum is formed between this dense outer layer and the inner matrix and resulted in significant cracking of the inner matrix. Further research is needed to understand the cause for the formation of this gypsum only in the polymer-modified CSA mixtures (i.e., CSA2P).

- Both the converted CAC mixtures degraded significantly with sulfate exposure due to the formation of ettringite from the C_3AH_6 phase. However, the CAC mixtures

having a lower amount of C_3AH_6 (i.e., pre-conversion) phase performed significantly better.

- In AA and MPC mixtures, no significant degradation in microstructure or compressive strength is observed.

Overall, CSA3, AA, MPC, and CAC2 (before conversion) mixtures exhibited superior resistance to chemical sulfate attack, followed by CACT, CSA2, and CSA1 mixtures compared to that of OPC. CAC1 and CSA2P, followed by both the converted CAC1 and CAC2 systems, exhibited the least resistance to chemical sulfate attack. Even though OPC showed strengthening at later exposure ages, the exposure resulted in significant spalling of the outer surfaces. So compressive strength alone may not be a reliable indicator in assessing damage to sulfate exposure.

13.1.4 Resistance to Alkali exposure

A 120-day long exposure test adapted from ASTM 1260 test procedure was proposed and is used to assess the resistance of ACM binders towards alkali exposure relative to OPC mixtures. All the ACM binders except MPC showed significantly higher resistance to alkali exposure compared to OPC. AA, followed by CAC2, CSA1, and CSA3, showed the highest resistance to alkali exposure compared to others. MPC had the least resistance to alkali exposure.

13.1.5 Resistance to Alkali-silica reaction (ASR)

A modified Concrete Prism Test (CPT) by ASTM C1293 was performed to assess the performance of ACM mixtures containing reactive aggregates in resisting ASR relative to

OPC mixtures when exposed to high humidity. To allow for true comparison among the binders, the alkali content of the concrete mixtures is not "boosted." Instead, the test duration was extended to 2 years, and the OPC concrete prisms cast with and without SCM, suitable for mitigation of expansion of the reactive aggregate, served as lower and upper bounds for performance. Since leaching can still be an issue, even in the modified CPT test, a complementary cylinder mortar test was also performed where leaching is minimized – and the relative expansions from this cylinder tests were compared to the CPT tests. In addition, a 120-day long exposure test adapted from ASTM 1260 test procedure was proposed and is used to assess the performance, relative to OPC mixtures, of ACM mortar mixtures containing reactive aggregate in resisting ASR, when exposed to high pH environment. These three series of tests, along with complementary petrographic examinations has led to the following conclusions:

- AA, followed by CAC2 and CSA1, showed the highest resistance towards ASR of embedded reactive aggregates when exposed to 100% RH even with an extended duration of 2 years of exposure. CSA3, followed by CSA2P and CSA2, also showed similar or higher resistance even when compared to OPC+Flyash mixture. OPC, CACT, and MPC showed the least resistance of all.

- The mixtures having lower permeability, lower alkali content, and no portlandite content showed superior resistance to ASR, followed by mixtures with low alkali content, no portlandite content, but higher permeability. The mixture that had significantly lower permeability, but higher alkali and portlandite content resulted in significant expansion similar to the mixtures with both high permeability, high alkali content, and high portlandite content. So having even small amounts of

portlandite in the ACM systems can still lead to significant expansions similar to OPC mixtures. So blends of OPC and ACM mixtures are not recommended for applications that need high ASR resistance.

- When exposed to high pH environment, CSA2 and CSA2P mixtures along with OPC, CACT, CAC2, and MPC showed the least performance with resisting the ASR of embedded reactive aggregates. CSA2P only showed moderate improvement in ASR resistance compared to CSA2 mixtures. AA followed by CSA1 and CSA3 showed the highest resistance towards ASR even when exposed to a high pH environment for an extended duration of 120 days of exposure.

- Even though AA mixtures had high alkali loading from fly ash, the expansions were still significantly lower. This could be because alkalis are bound tightly to the hydration as N-A-S-H and C-N-A-S-H gel in these mixtures.

13.1.6 Resistance to carbonation

The accelerated carbonation tests, along with complementary characterization by TGA and XRD, water sorptivity, and strength measurements performed in this study, were used to understand the carbonation mechanisms and evaluate the performance of commercially available ACM systems in resisting carbonation compared to OPC systems and has led to the following conclusions.

- Both 7% and 15% exposure levels were found to be aggressive in all the OPC and ACM mixtures (except CAC2 and MPC mixtures). In CSA2, CSA3, and AA mixtures, the 1% exposure level also seemed to be aggressive. In AA mixtures, the

1% accelerated exposure also resulted in significant carbonation of alkalis in the pore solution, which is not observed with carbonation at atmospheric levels. Whereas, all the 1%, 7%, and 15% accelerated exposure levels underestimated the carbonation compared to the atmospheric levels in CAC2 mixtures. MPC mixtures did not show any significant carbonation at all the CO_2 exposure levels tested.

- The variation in the bound CO_2 levels with cement type is due to the differences in the carbonation nature of their hydration products and may not necessarily relate to the extent of carbonation.
- Carbonation in CAC1, CAC2, CACT, CSA1, CSA2, CSA2P, and CSA3 systems can result in significant decomposition of main hydration products, whereas, no significant decomposition of main hydration products is observed in OPC, AA, and MPC systems. Carbonation resulted in significant strength loss in both CAC1 and CAC2 systems. Whereas, it contributed to strength in both their converted systems. OPC, CSA3, and AA mixtures experienced increase in strength with carbonation – likely due to precipitation of carbonates in their pores, whereas no significant change in strength with carbonation is observed in other ACM mixtures.
- Carbonation in OPC and CAC2 mortar mixtures resulted in a significant reduction in capillary porosity, followed by CACT, CSA2, CSA3, and MPC mixtures, whereas, no significant change is observed in CSA1 and AA mixtures.
- All the CAC and CSA mixtures carbonated to significant higher depths at 1% carbonation exposure. AA and CACT mixtures also carbonated to higher depths compared to OPC mixtures but were significantly lower compared to other ACM mixtures (except MPC). MPC mixtures showed the highest resistance to

carbonation with zero carbonation depth even after exposure to 90 days at a 1% accelerated condition.

- The pH levels in the carbonated region of OPC and MPC mixtures is between 11 to 13. Whereas in CACT, CSA2, and CSA2P concrete mixtures, the pH dropped to between 9 to 11. In the other ACM mixtures, the pH dropped to even below 9 – which may result in significant destabilization of the passive layer in steel reinforcements.
- The steels embedded in both the CSA1 and CSA2 mixtures experienced the most depassivation compared to the steel in other ACM mixtures. The change in passivation state of embedded steel in the other ACM mixtures (except MPC) is also higher compared to OPC mixtures. The steels embedded in MPC mixtures showed no significant change in the passivation state.

MPC mixtures showed the best performance in resisting carbonation even compared to OPC mixtures. CACT is the next ACM that performed better when compared to other ACMs, but not better when compared to OPC.

Even though this study allowed to conclude that, unlike the traditional OPC system, carbonation in these ACM systems (except MPC) systems resulted in higher carbonation rates and more significant reduction in pH, the author emphasizes the need for further research to better understand the effects of carbonation on steel passivation and chloride threshold levels in the ACM systems.

Table 28 Summary of the performance of ACM mixtures relative to OPC mixtures.

	OPC	CAC1	CAC2	CACT	CSA1	CSA2	CSA2P	CSA3	AA	MPC
Constructability	✓	×	✓	✓	✓	✓	✓	✓	✓	×
Compressive strength	✓	NT	✓[3]	✓	✓	✓	✓[1]	✓[2]	✓	NT
Flexural stregth	✓	NT	✓[3]	✓	✓	✓	✓[1]	×	×	NT
Autogenous shrinkage[R]	–	NT	✓	✓	✓	✓	✓	✓	✓	✓
Alkali resistance[R]	×	NT	✓	✓	✓	✓	✓	✓	✓	×
ASR resistance[R]	×	NT	✓[4]	×	✓	✓[2,4]	✓[2,4]	✓[2]	✓	×
Chemical sulfate resistance[R]	×	×	✓[3]	✓	✓	✓	×	✓	✓	✓
Carbonation[R]	✓	×	×	✓[2]	×	×	×	×	×	✓

✓ – acceptable performance; × – not acceptable performance; NT – Not tested.

[R]Performance was gauged relative to OPC mixtures. [1]Not tested, but performance is expected to be similar to CSA2 mixtures.

[2]Should be used with caution since these mixtures barely met the performance requirements.

[3]Concerns about conversion can limit the advancement of these mixtures and require additional investigation.

[4]These mixtures did not show acceptable performance when exposed to a high pH environment.

13.2 Recommendations for adoption

For this investigation, some ACM types and sources were found to be unsuitable for transportation infrastructure construction for a variety of reasons:

Two CACs showed potential for use in transportation applications, but further technology development is necessary prior to their implementation:

- For CAC2 concrete, depending on the application, identification, and/or development of appropriate accelerating admixtures may be necessary. At w/c of 0.40 initial and final set were 2-3x that of OPC. Also, CAC2, once converted, showed poor sulfate resistance. The cracking after conversion is also a concern for local chloride ingress and needs to be investigated in more detail. CAC2 mixtures exhibited significant resistance to alkali exposure. However, CAC2 mixtures containing reactive aggregate can be detrimental in a structure where alkali runoff is likely to occur.

For all CACs, an adjustment of design methodology to account for strength loss, increased permeability, and increased propensity for cracking due to conversion and carbonation is mandatory. This is viewed as a critical impediment for broader use of CACs in transportation infrastructure construction at this time and one that needs more investigation.

Of the remaining ACMs examined, CACT, CSA2, CSA2P, and AA are each potentially deployable, using lessons learned from this research effort. All these materials showed

satisfactory workability, set time, and strength development with a w/c of 0.40 (or w/c = 0.205 for AA).

- AA showed improvements in shrinkage, sulfate resistance, and ASR resistance relative to OPC but unsatisfactory performance in corrosion, scaling, and ion penetration. It is recommended to be used in dry environments that are not expected to receive freeze/thaw cycles. However, care must be taken in this evaluation as this is a large class of materials that may change as the raw materials are varied. Also, the usage of fibers as reinforcement in these mixtures is recommended to improve their flexural capacity.
- CACT showed similar shrinkage and ASR performance to OPC but showed much better performance in resistance to expansion by sulfate attack. This would make this material useful in locations where it will be frequently subjected to sulfate exposure (add reference to the final report).
- CSA1 and CSA2 showed significant improvement in shrinkage, sulfate resistance, and ASR performance. This makes these materials good choices to suppress ASR, minimize drying shrinkage, reduce the risk of sulfate-induced damage. The CSA2P material showed significant improvements in reducing permeability compared to CSA2 mixtures. The CSA2P material with the right mixture proportions can be the most versatile material investigated.

One area of concern for all ACMs investigated was carbonation. Before these ACMs can be recommended to be used in structures with low amounts of cover such as bridge decks or substructure elements, the rate of carbonation and the subsequent corrosion from carbonation must be better understood. However, these materials can be used immediately

in structures with large amounts of cover, such as pavements and structures that do not contain reinforcing steel, such as overlays or patches. Another option would be to combine the use of these materials with corrosion-resistant rebar technologies such as galvanizing or fiberglass-reinforced polymer rebars. These combinations of innovative materials could lead to game-changing materials that could provide long-term durability of infrastructure concrete.

Furthermore, it should be noted that the best performing materials in this project (CACT and CSA2P) were a blend of different materials. It appears that these blends show great promise as the combination of the materials can address the weakness of the single components. Similar examples can be seen in OPC using fly ash, slag, and silica fume. It would greatly benefit these materials if they could be investigated with a wider array of material combinations, as this could further improve the performance of these ACMs.

From this guidance for the lab-scale investigation and guidance for the ACM selection and mixture design for use in transportation infrastructure, primarily in the aspects investigated in this thesis, are provided.

In addition, expansion during hydration and leaching can be problematic in some applications. Several different MPC formulations, from three producers, were examined. Despite exploring a range of admixture types and dosages, along with variations in mixture proportions, none of the MPCs examined could achieve the necessary workability, set time, and strength requirements to make them suitable for large-scale pavement or bridge deck construction. In the future, if extended set in MPC is possible – either through the advent of new admixtures or new cement formulations – it is recommended that additional MPC

concrete studies should be performed. In particular, MPC concrete could be useful for applications requiring high heat resistance and chemical resistance (e.g., to oils, acids).

13.3 Recommendations for future research

- Since the primary goal of this research is to facilitate the adoption of ACM mixtures, the already available commercial admixtures that were designed for portland systems were adopted for the ACM mixtures. Even though successful concrete mixtures were developed with most of the ACM formulation investigated in this thesis, it would be much more effective when admixtures that are developed and/or optimized for these specific binder chemistries were used. So, there is a dire need for the development of admixtures for ACM systems, especially for CAC, CSA (with high iron content), and MPC formulations.

- A single higher w/b was used in all the durability exposure tests. Even though this provided a conservative estimate of the performance of the ACM mixtures relative to OPC, it is important to understand how these ACM mixtures respond to the aggressive exposures at lower w/b. Especially in CSA belite mixtures where the chemical makeup of the hydrated phases can vary based on the w/b.

- More durability tests need to be performed to understand how these ACM mixtures perform when exposed to a combination of multiple aggressive exposures. Such as in coastal structures, where a combination of sulfate attack, chloride attack, carbonation, and physical salt attack are possible. Additional chemical sulfate attack based on magnesium sulfate exposure solution needs to be performed to

understand the impact of Mg ions on the ability of ACM systems to resist sulfate attack.

- Additional durability tests including microstructural characterization tests need to be performed to better understand the effect of alkali exposure on binder integrity and mechanical properties of OPC and ACM systems.

- The new test method that is proposed in this thesis for measuring formation factor is ACM mixtures need to be validated and verified with other permeability/diffusion tests.

APPENDIX A. ERROR ANALYSIS

In this chapter, error analysis was performed for a normal setting binder and a faster setting binder to understand the measurement errors in the heat of hydration from isothermal calorimetry tests and bound water from thermogravimetric analysis (TGA) tests. From this, recommendations were provided for the standard errors that can be used in the earlier chapters in this thesis for each of these types of measurements performed on the same instrument by the same person.

A.1 Materials and Methods

Table 29 Oxide composition of ACMs compared to OPC.

Oxide	SiO_2	Al_2O_3	Fe_2O_3	CaO	MgO	SO_3	Other	LOI
PC*	21.82	3.56	4.28	66.24	0.21	1.61	0.29	1.99
CSAC#	12.97	20.61	1.74	43.94	1.1	15.97	1.82	1.85

*Determined using phase composition. Source: Andrew chaffin, Lehigh Cement Company LLC.
#Source: Robert Moser, U.S. Army Engineer Research and Development Center, Vicksburg, MS.

A.1.1 Isothermal calorimetry

Isothermal calorimetry was performed on cement pastes mixed in a high shear mixer and planetary mixer (ASTM C305-14) to understand the effects of mixing action on variation in hydration kinetics across multiple mixtures. The mix proportions for cement pastes are given in Table 30. The dosages of set modifiers/activators were chosen such that the corresponding concrete mixtures had a working time of at least 1 hour (refer to section 5 and 7 for more details). Immediately after mixing, approximately 5g of paste mixtures are loaded into HDPE ampules of volume 20 ml, and then loaded into an isothermal

calorimeter (8 channel TAM Air by Thermometric) at 23 ºC. The heat evolution of the sample was measured at a rate of 6 data points per minute.

A.1.2 Thermogravimetric Analysis (TGA)

A Hitachi simultaneous thermogravimetric analyzer STA7300 was used to carry out the thermogravimetric measurements. TGA was carried out on powdered cement paste samples prepared according to mixture proportions shown in Table 4 and cured at 23 ºC in sealed bags. Prior to performing TGA, the paste samples were ground and sieved to a particle size of less than 300 microns, and the free water was removed using a solvent exchange procedure [42]. 5 g of powdered sample was mixed in 50 ml of isopropyl alcohol, and the suspension rests for 15 min. Then, the suspension is filtered using Büchner funnel and a vacuum pump for 5 min, and later, it is washed with 10 ml of diethylene ether for 1 min, during which the vacuum pump is turned off. The resulting suspension is again filtered under vacuum for five more minutes, or until the suspension is dry, whichever is longer.

The dried sample is further ground and approximately 20 mg of the sample with the particle size less than 74 microns is taken in an open 70 μl platinum crucible and dried in TG at 25 ºC under a constant stream of Nitrogen (N_2) gas for 15 min, or until the constant mass, whichever is longer. Later the temperature is increased to 40 ºC and held constant for 5 min. Then, the sample is heated from 40 to 1000 ºC, at a rate of 10 ºC/min, and the data is recorded at a rate of 120 data points per minute. During measurement, N_2 is used as a protective gas with a flow rate of 100 mL/min.

Table 30 Cement paste mixture proportions.

Cement	w/b	Set modifier/ activators (by weight of cement)
PC	0.40	–
CSAC	0.40	Citric acid – 2.0%

A.2 Results and Discussion

A.2.1 Error analysis in isothermal calorimetry measurements

Fig. 145 (i) and (iii) shows the heat evolution and heat of hydration of six replicate separately prepared PC paste batches, mixed in a planetary mixer and a high shear mixer, respectively. Fig. 145 (ii) and (iv) shows the heat evolution and heat of hydration of two PC paste mixtures from the same batch, mixed in a planetary mixer and a high shear mixer, respectively. Fig. 146 provides the coefficient of variation in the heat of hydration with hydration time in PC mixtures across different samples within the same batch and different batch, mixed in either planetary mixer or high shear mixer. In PC mixtures, the coefficient of variation in the heat of hydration is higher across different mixtures mixed in higher shear mixer compared to the planetary mixer. This could be due to the high mixing action provided by the high shear mixer that could break the cement particles into pieces. However, after about 15 hours of hydration (less than twice the duration of the main hydration peak), the coefficient of variation is less than 2%. For the mixtures mixed in a planetary mixer, the coefficient of variation across different batches dropped to less than 2% in about 8 hours.

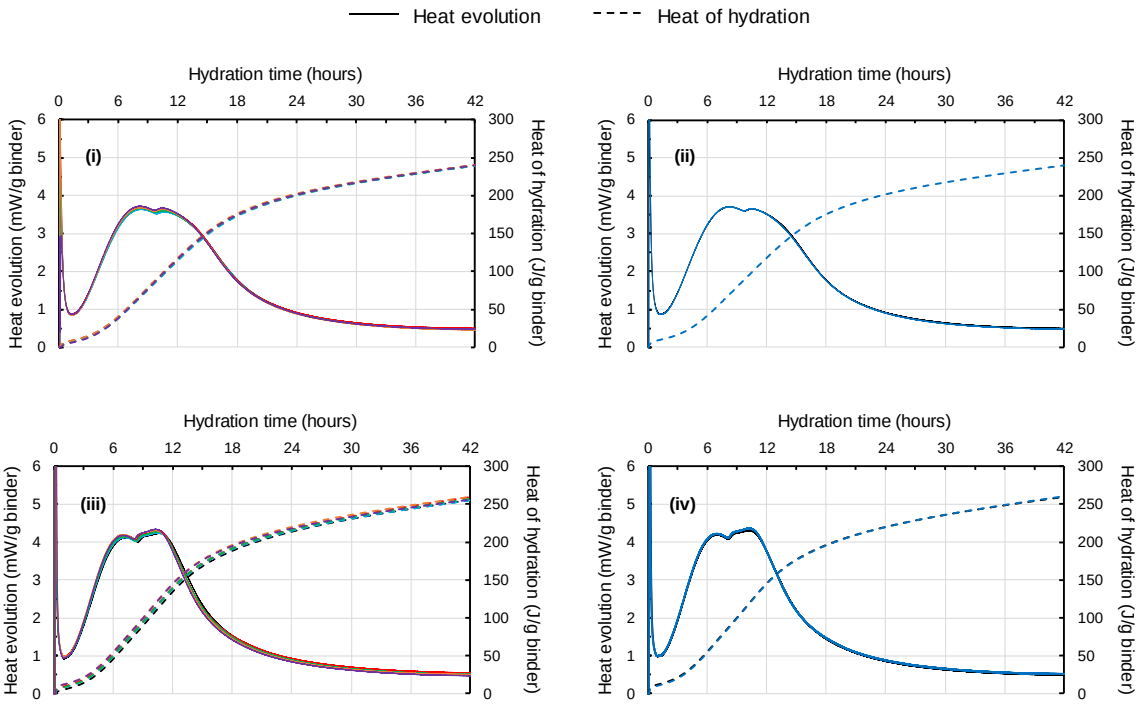

Fig. 145 Heat evolution and heat of hydration in PC mixtures mixed in (i) planetary mixer for six different samples across different batches, (ii) planetary mixer for two different samples within same batch, (ii) high shear mixer for six different samples across different batches, and (iv) high shear mixer for 2 different samples within same batch.

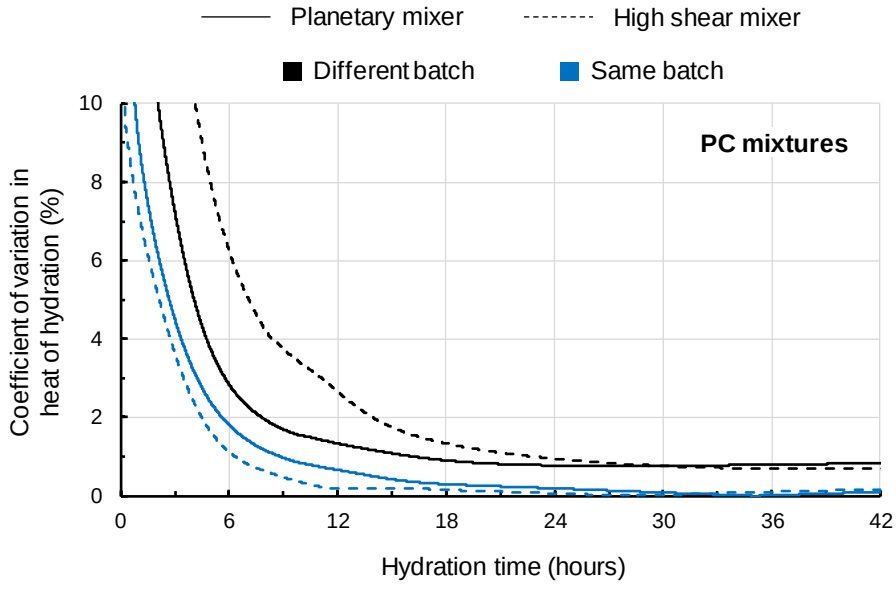

Fig. 146 Coefficient of variation in heat of hydration with hydration time in PC mixtures across different samples within same batch and different batch, mixed in either planetary mixer or high shear mixer.

Fig. 147 (i) and (iii) shows the heat evolution and heat of hydration of six replicate separately prepared CSAC paste batches, mixed in a planetary mixer and a high shear mixer, respectively. Fig. 147 (ii) and (iv) shows the heat evolution and heat of hydration of two CSAC paste mixtures from the same batch, mixed in a planetary mixer and a high shear mixer, respectively. Fig. 147 provides the coefficient of variation in the heat of hydration with hydration time in CSAC mixtures across different samples within the same batch and different batch, mixed in either planetary mixer or high shear mixer. In CSAC mixtures, similar to PC mixtures, the coefficient of variation in the heat of hydration is higher across different mixtures mixed in higher shear mixer compared to the planetary mixer. However, after about 4 hours of hydration (less than twice the duration of the main hydration peak), the coefficient of variation is less than 2% for both the mixtures mixed in high shear and planetary mixer. For the mixtures mixed the planetary mixer, the coefficient of variation continued to increase after the occurrence of the main hydration peak. But it is still lower than 2% even after 42 hours of hydration.

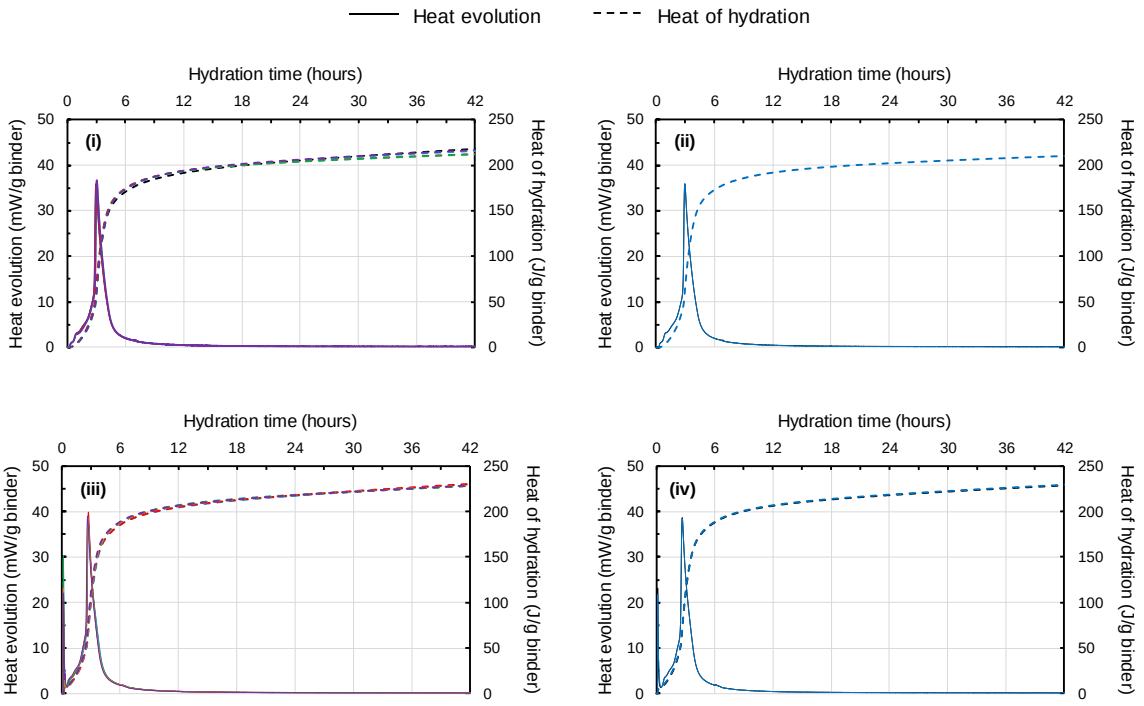

Fig. 147 Heat evolution and heat of hydration in CSAC mixtures mixed in (i) planetary mixer for six different samples across different batches, (ii) planetary mixer for two different samples within same batch, (ii) high shear mixer for six different samples across different batches, and (iv) high shear mixer for 2 different samples within same batch.

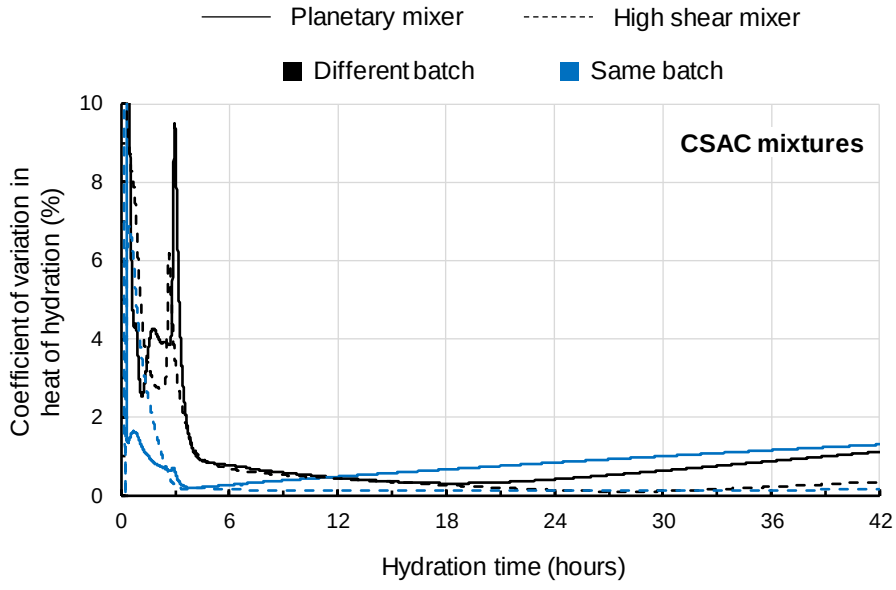

Fig. 148 Coefficient of variation in the heat of hydration with hydration time in CSAC mixtures across different samples within the same batch and different batch, mixed in either planetary mixer or high shear mixer.

Table 31 shows in range in time to reach maximum hydration peak for PC and CSAC mixtures mixed in planetary and high shear mixers of 6 replicate samples across different mixing batches. ASTM C 1679-14 standard only requires calorimetry measurements to be performed on two specimens from one batch if the range in time to reach maximum hydration peak is greater than 60 minutes in OPC mixtures for six replicate separately-prepared specimens. For an OPC mixture that takes about 632 minutes to reach maximum hydration peak, the range limit specified by the standard is about 10% with respect to the average time to reach the main hydration peak. However, for both the PC and CSAC mixtures mixed in either planetary or high shear mixer, the range in time to reach maximum hydration peak is less than 4.1% - which is well below the ASTM specified limit.

Table 31 Repeatability of the isothermal calorimetry measurements with mixing procedures.

Cement	w/b	Mixer	Average time to reach the maximum of hydration peak (min)	Range in time to reach the maximum of hydration peak	
				(min)	(%)
PC	0.40	Planetary	632	11	1.7
		High shear	625	21	3.4
CSAC	0.40	Planetary	180	7	4.1
		High shear	162	6	3.6

Table 32 Time to reach thermal equilibrium.

Cement	w/b	Mixer	Estimated time to reach thermal equilibrium (i.e. elapsed hydration time when the range of the thermal power falls below 0.2 mW/g cement)
PC	0.40	Planetary	23 min
		High shear	30 min
CSAC	0.40	Planetary	21 min
		High shear	27 min

A.2.2 Error analysis in TGA measurements

Fig. 149 shows the comparison between TG and DTG of two PC mixtures mixed in high shear mixer across different mixing batches at both 9 hours and 28 days of hydration. Fig. 150 shows the comparison between TG and DTG of two CSAC mixtures mixed in high shear mixer across different mixing batches at both 6 hours and 28 days of hydration. Table 33 shows the coefficient of variation in the bound water between two replicates from mixing batches for both PC and CSAC mixtures at an early age and later ages of hydration. The coefficient of variation in the bound water is less than 1% for both the PC and CSAC mixtures at an early age and as well as later age of hydration. Also, with hydration, the coefficient of variation reduced for both these mixtures.

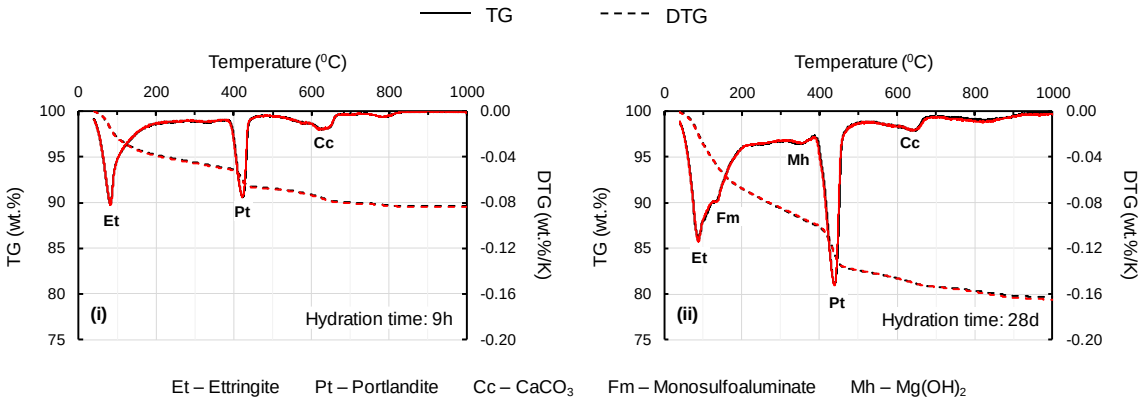

Fig. 149 TG and DTG of PC mixtures mixed in high shear mixer of two samples across different batches at (i) 9 hours and (ii) 28 days of hydration.

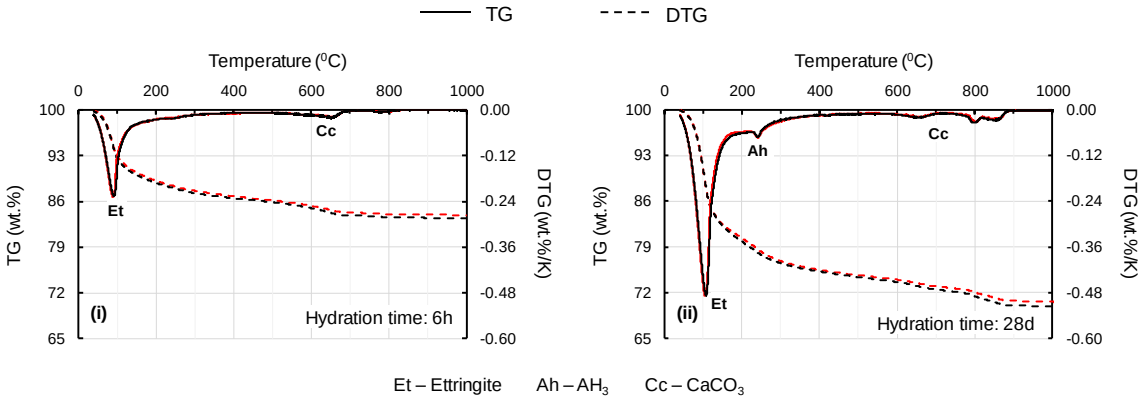

Fig. 150 TG and DTG of CSAC mixtures mixed in high shear mixer of two samples across different batches at (i) 6 hours and (ii) 28 days of hydration.

Table 33 Coefficient of variation in bound water in PC and CSAC mixtures.

Cement	Hydration time	Coefficient of variation in bound water (%)
PC	9 hours	0.49
	28 days	0.03
CSAC	6 hours	0.96
	28 days	0.66

A.3 Conclusions

- The range in time to reach maximum hydration peak across six replicate separately-prepared specimens is significantly less than 10% with respect to the average time to reach the main hydration peak (or 60 minutes for OPC mixtures specified by the ASTM C 1679-14) for both the normal setting mixture (for example PC mixtures) and faster setting mixture (for example CSAC) mixed either in a planetary or a high shear mixer. So, isothermal calorimetry measurements performed on just one sample from a single mixing batch meets the current ASTM C 1679 standard.

- The coefficient of variation in the heat of hydration is less than 2% even before twice the time required to reach the main hydration peak in both the normal setting mixture (for example, PC mixtures) and a faster setting mixture (for example CSAC) mixed either in a planetary or a high shear mixer. So, on a conservative side, a standard error of 2% can be used for total heat of hydration measurements for hydration times greater than twice the time required to reach the maximum hydration peak.

- The coefficient of variation in the bound water is less than 1% for both the normal setting mixture (for example, PC mixtures) and faster setting mixture (for example, CSAC) mixed in high shear mixer at both early age and as well as later age of hydration. Also, with hydration, the coefficient of variation reduced for both these mixtures. So, a standard error of 1% can be used for bound water measurements in TGA.

REFERENCES

[1] L. Burris, K.E. Kurtis, T. Morton, Novel Alternative Cementitious Materials for Development of the Next Generation of Sustainable Transportation Infrastructure, 2015. https://www.fhwa.dot.gov/publications/research/ear/16017/index.cfm (accessed February 14, 2019).

[2] P. Alapati, L.E. Burris, K.E. Kurtis, T. Ley, N. Berke, R. Moser, Novel Alternative Cement Binders for Highway Structures and Pavements, 2020. Forthcoming.

[3] Dan Lockney, High-Heat Cement Gives Ashes New Life, Spinoff NASA Technol. Transf. Progr. (2017). https://spinoff.nasa.gov/Spinoff2017/ip_10.html (accessed March 27, 2019).

[4] K.L. Scrivener, J.-L.L. Cabiron, R. Letourneux, High-performance concretes from calcium aluminate cements, Cem. Concr. Res. 29 (1999) 1215–1223. doi:10.1016/S0008-8846(99)00103-9.

[5] M.C.G. Juenger, F. Winnefeld, J.L. Provis, J.H. Ideker, Advances in alternative cementitious binders, Cem. Concr. Res. 41 (2011) 1232–1243. doi:10.1016/J.CEMCONRES.2010.11.012.

[6] K.E. Kurtis, K. Shomglin, P.J.M. Monteiro, J. Harvey, J. Roesler, ACCELERATED TEST FOR MEASURING SULFATE RESISTANCE OF CALCIUM SULFOALUMINATE,CALCIUM ALUMINATE, AND PORTLAND CEMENTS, J. Mater. Civ. Eng. 13 (2001) 1–20.

[7] S. Zhutovsky, R. Douglas Hooton, Accelerated testing of cementitious materials for resistance to physical sulfate attack, Constr. Build. Mater. 145 (2017) 98–106. doi:10.1016/j.conbuildmat.2017.03.239.

[8] S. Zhutovsky, R. Douglas Hooton, Experimental study on physical sulfate salt attack, Mater. Struct. Constr. 50 (2017) 1–10. doi:10.1617/s11527-016-0936-z.

[9] J.L. Provis, Alkali-activated materials, Cem. Concr. Res. 114 (2017) 40–48. doi:10.1016/J.CEMCONRES.2017.02.009.

[10] A.K.K. Suryavanshi, J.D.D. Scantlebury, S.B.B. Lyon, Mechanism of Friedel's salt formation in cements rich in tri-calcium aluminate, Cem. Concr. Res. 26 (1996) 717–727. doi:10.1016/S0008-8846(96)85009-5.

[11] U.. A. Birnin-Yauri, F.. P. Glasser, Friedel's salt, Ca2Al(OH)6(Cl,OH)·2H2O: Its solid solutions and their role in chloride binding, Cem. Concr. Res. 28 (1998) 1713–1723. doi:10.1016/S0008-8846(98)00162-8.

[12] L. Tang, L.O. Nilsson, Chloride binding capacity and binding isotherms of OPC pastes and mortars, Cem.Concr.Res. 23 (1993) 247–253.

[13] Q. Yuan, C. Shi, G. De Schutter, K. Audenaert, D. Deng, Chloride binding of cement-based materials subjected to external chloride environment – A review, Constr. Build. Mater. 23 (2009) 1–13.

doi:10.1016/J.CONBUILDMAT.2008.02.004.

[14] H. Geng, P. Duan, W. Chen, Z. Shui, Carbonation of sulphoaluminate cement with layered double hydroxides, J. Wuhan Univ. Technol. Sci. Ed. 29 (2014) 97–101. doi:10.1007/s11595-014-0874-y.

[15] F. Winnefeld, S. Barlag, Calorimetric and thermogravimetric study on the influence of calcium sulfate on the hydration of ye'elimite, J. Therm. Anal. Calorim. 101 (2010) 949–957. doi:10.1007/s10973-009-0582-6.

[16] F.P. Glasser, L. Zhang, High-performance cement matrices based on calcium sulfoaluminate-belite compositions, Cem. Concr. Res. 31 (2001) 1881–1886. doi:10.1016/S0008-8846(01)00649-4.

[17] Q. Zhou, N.B. Milestone, M. Hayes, An alternative to Portland Cement for waste encapsulation-The calcium sulfoaluminate cement system, J. Hazard. Mater. 136 (2006) 120–129. doi:10.1016/j.jhazmat.2005.11.038.

[18] T.. J. Chotard, M.. P. Boncoeur-Martel, A. Smith, J.. P. Dupuy, C. Gault, Application of X-ray computed tomography to characterise the early hydration of calcium aluminate cement, Cem. Concr. Compos. 25 (2003) 145–152. doi:10.1016/S0958-9465(01)00063-4.

[19] X. Cong, R. james Kirkpatrick, Hydration of Calcium Aluminate Cements: A solid-state Al NMR study, J. Am. Ceram. Soc. 76 (1993) 409–416. doi:10.1017/CBO9781107415324.004.

[20] T. Gaztanaga, S. Goñi, A. Guerrero, Accelerated carbonation of Friedel's salt in calcium aluminate cement paste, Cem. Concr. Res. 33 (2003) 21–26.

[21] S. Goñi, M.T. Gaztañaga, J.L. Sagrera, M.S. Hernández, The influence of NaCl on the reactivity of high alumina cement in water: Pore-solution and solid phase characterization, J. Mater. Res. 9 (1994) 1533–1539. doi:10.1557/JMR.1994.1533.

[22] S. Goñi, C. Andrade, C.L. Page, Corrosion behavior of steel in high alumina cement mortar samples: Effect of chloride, Cem. Concr. Res. 21 (1991) 635–646. doi:10.1016/0008-8846(91)90114-W.

[23] D. Torrens-Martin, L. Fernandez-Carrasco, Long-term hydration and mechanical behaviour of portland cement, calcium aluminate cement and calcium sulfate blends, in: Proc. Int. Conf. Calcium Aluminates, Avignon, France, 2014: pp. 242–249.

[24] S. Lamberet, Durability of ternary binders based on portland cement, calcium aluminate cement and calcium sulfate, Ecole Polytechnique Federale de Lausanne, 2005.

[25] L. Pelletier, F. Winnefeld, B. Lothenbach, The ternary system Portland cement-calcium sulphoaluminate clinker-anhydrite: Hydration mechanism and mortar properties, Cem. Concr. Compos. 32 (2010) 497–507. doi:10.1016/j.cemconcomp.2010.03.010.

[26] M. Ben Haha, G. Le Saout, F. Winnefeld, B. Lothenbach, Influence of activator type on hydration kinetics, hydrate assemblage and microstructural development of alkali activated blast-furnace slags, Cem. Concr. Res. 41 (2011) 301–310.

doi:10.1016/J.CEMCONRES.2010.11.016.

[27] R.J. Myers, S.A. Bernal, R. San Nicolas, J.L. Provis, Generalized Structural Description of Calcium–Sodium Aluminosilicate Hydrate Gels: The Cross-Linked Substituted Tobermorite Model, Langmuir. 29 (2013) 5294–5306. doi:10.1021/la4000473.

[28] S.-D. Wang, X.-C. Pu, K.L. Scrivener, P.L. Pratt, Alkali-activated slag cement and concrete: a review of properties and problems, Adv. Cem. Res. 7 (1995) 93–102. doi:10.1680/adcr.1995.7.27.93.

[29] S.A. Walling, J.L. Provis, Magnesia-Based Cements: A Journey of 150 Years, and Cements for the Future?, Chem. Rev. 116 (2016) 4170–4204. doi:10.1021/acs.chemrev.5b00463.

[30] S.S. Seehra, S. Gupta, S. Kumar, Rapid setting magnesium phosphate cement for quick repair of concrete pavements — characterisation and durability aspects, Cem. Concr. Res. 23 (1993) 254–266. doi:10.1016/0008-8846(93)90090-V.

[31] Y. Li, B. Chen, Factors that affect the properties of magnesium phosphate cement, Constr. Build. Mater. 47 (2013) 977–983. doi:10.1016/j.conbuildmat.2013.05.103.

[32] B. Xu, H. Ma, Z. Li, Influence of magnesia-to-phosphate molar ratio on microstructures, mechanical properties and thermal conductivity of magnesium potassium phosphate cement paste with large water-to-solid ratio, Cem. Concr. Res. 68 (2015) 1–9. doi:10.1016/j.cemconres.2014.10.019.

[33] J. Bensted, Special Cements, in: Lea's Chem. Cem. Concr., Elsevier Ltd., 2003: pp. 783–840. doi:10.1016/B978-075066256-7/50026-6.

[34] P.T. Durdziński, C.F. Dunant, M. Ben Haha, K.L. Scrivener, A new quantification method based on SEM-EDS to assess fly ash composition and study the reaction of its individual components in hydrating cement paste, Cem. Concr. Res. 73 (2015) 111–122. doi:10.1016/J.CEMCONRES.2015.02.008.

[35] M. Gallardo-Heredia, R.X. Magallanes-Rivera, J.M. Almanza-Robles, U. Avila-López, J.S. Luna-Álvarez, Effect of citric acid on calcium sulfoaluminate cements synthesised from industrial wastes at low temperature, Adv. Cem. Res. 32 (2020) 125–136. doi:10.1680/jadcr.18.00019.

[36] L.E. Burris, K.E. Kurtis, Influence of set retarding admixtures on calcium sulfoaluminate cement hydration and property development, Cem. Concr. Res. 104 (2018) 105–113. doi:10.1016/J.CEMCONRES.2017.11.005.

[37] F. Winnefeld, K. Stefanie, Influence of citric acid on the hydration kinetics of calcium sulfoaluminate cement, in: 1st Int. Conf. Sulphoaluminate Cem. Mater. Eng. Technol., Wuhan, China, 2013: pp. 288–308.

[38] Y. Hu, W. Li, S. Ma, X. Shen, Influence of borax and citric acid on the hydration of calcium sulfoaluminate cement, Chem. Pap. 71 (2017) 1909–1919. doi:10.1007/s11696-017-0185-9.

[39] D. V. Ribeiro, G.R. Paula, M.R. Morelli, Effect of boric acid content on the properties of magnesium phosphate cement, Constr. Build. Mater. 214 (2019) 557–

564. doi:10.1016/j.conbuildmat.2019.04.113.

[40] D.A. Hall, R. Stevens, B. El-Jazairi, The effect of retarders on the microstructure and mechanical properties of magnesia-phosphate cement mortar, Cem. Concr. Res. 31 (2001) 455–465.

[41] Y. Li, J. Sun, J. Li, T. Shi, Effects of fly ash, retarder and calcination of magnesia on properties of magnesia–phosphate cement, Adv. Cem. Res. 27 (2015) 373–380. doi:10.1680/adcr.14.00029.

[42] J. Zhang, G.W. Scherer, Comparison of methods for arresting hydration of cement, Cem. Concr. Res. 41 (2011) 1024–1036. doi:10.1016/J.CEMCONRES.2011.06.003.

[43] J. Bensted, Hydration of Portland Cement, in: Adv. Cem. Technol., Elsevier, 1983: pp. 307–347. doi:10.1016/B978-0-08-028670-9.50015-6.

[44] K.L. Scrivener, P. Juilland, P.J.M. Monteiro, Advances in understanding hydration of Portland cement, Cem. Concr. Res. 78 (2015) 38–56. doi:10.1016/j.cemconres.2015.05.025.

[45] R.H. Bogue, W. Lerch, Hydration of Portland Cement Compounds, n.d. https://pubs.acs.org/sharingguidelines (accessed May 7, 2020).

[46] L. Zhang, F.P. Glasser, Investigation of the microstructure and carbonation of CSA-based concretes removed from service, Cem. Concr. Res. 35 (2005) 2252–2260. doi:10.1016/j.cemconres.2004.08.007.

[47] M.C.G. Juenger, F. Winnefeld, J.L. Provis, J.H. Ideker, Advances in alternative cementitious binders, Cem. Concr. Res. 41 (2011) 1232–1243. doi:10.1016/j.cemconres.2010.11.012.

[48] L.E. Burris, P. Alapati, R.D. Moser, M.T. Ley, N. Berke, K.E. Kurtis, Alternative cementitious materials: Challenges and opportunities, in: Am. Concr. Institute, ACI Spec. Publ., 2015.

[49] K. Quilln, Performance of belite-sulfoaluminate cements, Cem. Concr. Res. 31 (2001) 1341–1349. doi:10.1016/S0008-8846(01)00543-9.

[50] T. Sugama, Citric acid as a set retarder for calcium aluminate phosphate cements, Adv. Cem. Res. 18 (2006) 47–57. doi:10.1680/adcr.2006.18.2.47.

[51] N.B. Singh, A.K. Singh, S. Prabha Singh, Effect of citric acid on the hydration of portland cement, Cem. Concr. Res. 16 (1986) 911–920. doi:10.1016/0008-8846(86)90015-3.

[52] D. Wyrzykowski, J. Czupryniak, T. Ossowski, L. Chmurzyński, Thermodynamic interactions of the alkaline earth metal ions with citric acid, J. Therm. Anal. Calorim. 102 (2010) 149–154. doi:10.1007/s10973-010-0970-y.

[53] G. Möschner, B. Lothenbach, R. Figi, R. Kretzschmar, Influence of citric acid on the hydration of Portland cement, Cem. Concr. Res. 39 (2009) 275–282. doi:10.1016/j.cemconres.2009.01.005.

[54] V.S. Ramachandran, M.S. Lowery, Conduction calorimetric investigation of the

effect of retarders on the hydration of Portland cement, Thermochim. Acta. 195 (1992) 373–387. doi:10.1016/0040-6031(92)80081-7.

[55] N.B. Singh, A.K. Singh, S.P. Singh, Hydration Study of the System Ca3Al2O6-CaSO4 . 2H2O-Ca(OH)2-H2O with and without Citric Acid, J. Am. Ceram. Soc. 73 (1990) 3063–3068. doi:10.1111/j.1151-2916.1990.tb06717.x.

[56] A.M. Cody, H. Lee, R.D. Cody, P.G. Spry, The effects of chemical environment on the nucleation, growth, and stability of ettringite [Ca3Al(OH)6]2(SO 4)3·26H2O, Cem. Concr. Res. 34 (2004) 869–881. doi:10.1016/j.cemconres.2003.10.023.

[57] W. Schwarz, Novel cement matrices by accelerated hydration of the ferrite phase in portland cement via chemical activation: kinetics and cementitious properties, Adv. Cem. Based Mater. 2 (1995) 189–200. doi:10.1016/1065-7355(95)90003-9.

[58] H. Lahalle, C.C.D. Coumes, A. Mesbah, D. Lambertin, C. Cannes, S. Delpech, S. Gauffinet, Investigation of magnesium phosphate cement hydration in diluted suspension and its retardation by boric acid, Cem. Concr. Res. 87 (2016) 77–86. doi:10.1016/j.cemconres.2016.04.010.

[59] Q. Yang, X. Wu, Factors influencing properties of phosphate cement-based binder for rapid repair of concrete, Cem. Concr. Res. 29 (1999) 389–396. doi:10.1016/S0008-8846(98)00230-0.

[60] F. Winnefeld, Interaction of superplasticizers with calcium sulfoaluminate cements, in: Tenth Int. Conf. Superplast. Other Chem. Admixtures Concr., Prague, Czech Republic, 2012: pp. 21–36. https://www.researchgate.net/publication/311766463_Interaction_of_superplasticizers_with_calcium_sulfoaluminate_cements.

[61] N. Sun, W. Chang, L. Wang, J. Zhang, M. Pei, Effects of the chemical structure of polycarboxy-ether superplasticizer on its performance in sulphoaluminate cement, J. Dispers. Sci. Technol. 32 (2011) 795–798. doi:10.1080/01932691.2010.488132.

[62] X. Yuan, W. Chen, M. Yang, Effect of superplasticizers on the early age hydration of sulfoaluminate cement, J. Wuhan Univ. Technol. Mater. Sci. Ed. 29 (2014) 757–762. doi:10.1007/s11595-014-0992-6.

[63] T. Su, X. Kong, H. Tian, D. Wang, Effects of comb-like PCE and linear copolymers on workability and early hydration of a calcium sulfoaluminate belite cement, Cem. Concr. Res. 123 (2019) 105801. doi:10.1016/j.cemconres.2019.105801.

[64] B. Ma, M. Ma, X. Shen, X. Li, X. Wu, Compatibility between a polycarboxylate superplasticizer and the belite-rich sulfoaluminate cement: Setting time and the hydration properties, Constr. Build. Mater. 51 (2014) 47–54. doi:10.1016/j.conbuildmat.2013.10.028.

[65] P. Wedding, D. Kantro, Influence of Water-Reducing Admixtures on Properties of Cement Paste—A Miniature Slump Test, Cem. Concr. Aggregates. 2 (1980) 95. doi:10.1520/CCA10190J.

[66] F. Collins, J. Lambert, W.H. Duan, The influences of admixtures on the dispersion, workability, and strength of carbon nanotube-OPC paste mixtures, Cem. Concr.

Compos. 34 (2012) 201–207. doi:10.1016/j.cemconcomp.2011.09.013.

[67] M. Vahdani, I. Mehdipour, S. Yousefi, Rheological Properties and Stability of Self Effect of Viscosity Modifying Admixtures on the Rheological Properties and Stability of Self, (2010).

[68] K.H. Khayat, a. Yahia, Effect of welan gum-high-range water reducer combinations on rheology of cement grout, ACI Mater. J. 94 (1997) 365–372.

[69] N. Tregger, L. Ferrara, S.P. Shah, Identifying viscosity of cement paste from mini-slump-flow test, ACI Mater. J. 105 (2008) 558–566.

[70] C. Jolicoeur, T.C. To, É. Benoît, R. Hill, Z. Zhang, M. Pagé, Fly Ash-Carbon Effects on Concrete Air Entrainment : Fundamental Studies on their Origin and Chemical Mitigation, World Coal Ash Conf. (2009) 1–23.

[71] D. Kantro, Influence of Water-Reducing Admixtures on Properties of Cement Paste—A Miniature Slump Test, Cem. Concr. Aggregates. 2 (1980) 95–102. doi:10.1520/CCA10190J.

[72] T. Hanson, EVALUATION OF THE MINI SLUMP CONE TEST Iowa Department Of Transportation, Ames, IOWA, 2000.

[73] E. John, R. Gettu, Effect of temperature on flow properties of superplasticized cement paste, ACI Mater. J. 111 (2014) 67–76. doi:10.14359/51686447.

[74] M. Palacios, F. Puertas, Effect of superplasticizer and shrinkage-reducing admixtures on alkali-activated slag pastes and mortars, Cem. Concr. Res. 35 (2005) 1358–1367. doi:10.1016/j.cemconres.2004.10.014.

[75] K. Kovler, S. Zhutovsky, Overview and Future Trends of Shrinkage Research, Mater. Struct. 39 (2006) 827–847. doi:10.1617/s11527-006-9114-z.

[76] L.E. Burris, P. Alapati, K.E. Kurtis, A. Hajibabaee, M.T. Ley, Understanding Shrinkage in Alternative Binder Systems, in: ACI Conv., ACI, Anaheim, 2017.

[77] W.J. Weiss, T.J. Barrett, C. Qiao, H. Todak, Toward a Specification for Transport Properties of Concrete Based on the Formation Factor of a Sealed Specimen, Adv. Civ. Eng. Mater. 5 (2016) 179–194. doi:10.1520/ACEM20160004.

[78] M.K. Moradllo, C. Qiao, B. Isgor, S. Reese, W.J. Weiss, Relating formation factor of concrete to water absorption, ACI Mater. J. 115 (2018) 887–898. doi:10.14359/51706844.

[79] V. Jafari Azad, A.R. Erbektas, C. Qiao, O.B. Isgor, W.J. Weiss, Relating the Formation Factor and Chloride Binding Parameters to the Apparent Chloride Diffusion Coefficient of Concrete, J. Mater. Civ. Eng. 31 (2019) 04018392. doi:10.1061/(ASCE)MT.1943-5533.0002615.

[80] W. Jason Weiss, R.P. Spragg, O. Burkan Isgor, M. Tyler Ley, T. Van Dam, Toward performance specifications for concrete: Linking resistivity, RCPT and diffusion predictions using the formation factor for use in specifications, in: High Tech Concr. Where Technol. Eng. Meet - Proc. 2017 Fib Symp., Springer International Publishing, 2017: pp. 2057–2065. doi:10.1007/978-3-319-59471-2_235.

[81] D.P. Bentz, A virtual rapid chloride permeability test, Cem. Concr. Compos. 29 (2007) 723–731. doi:10.1016/j.cemconcomp.2007.06.006.

[82] G. Plusquellec, M. Geiker, J. Duchesne, J. Lindgård, K. De Weerdt, Review of methods to determine the pH and the free alkali content of the pore solution in concrete, in: 15th Int. Conf. Alkali-Aggregate React., At São Paulo, BRAZIL, 2016. https://www.researchgate.net/publication/314503454_Review_of_methods_to_determine_the_pH_and_the_free_alkali_content_of_the_pore_solution_in_concrete.

[83] G. Plusquellec, M.R. Geiker, J. Lindgård, J. Duchesne, B. Fournier, K. De Weerdt, Determination of the pH and the free alkali metal content in the pore solution of concrete: Review and experimental comparison, Cem. Concr. Res. 96 (2017) 13–26. doi:10.1016/j.cemconres.2017.03.002.

[84] A. Behnood, K. Van Tittelboom, N. De Belie, Methods for measuring pH in concrete: A review, Constr. Build. Mater. 105 (2016) 176–188. doi:10.1016/j.conbuildmat.2015.12.032.

[85] W.C. Lyons, G.S. Plisga, Chapter 5 – Reservoir Engineering, Elsevier, 2016. doi:10.1016/B978-0-12-383846-9.00005-9.

[86] J.A. Tallmadge, Flow of fluids through porous materials, John Wiley & Sons, Ltd, 1962. doi:10.1002/aic.690080102.

[87] K.. Snyder, X. Feng, B.. Keen, T.. Mason, Estimating the electrical conductivity of cement paste pore solutions from OH−, K+ and Na+ concentrations, Cem. Concr. Res. 33 (2003) 793–798. doi:10.1016/S0008-8846(02)01068-2.

[88] G.E. Archie, The Electrical Resistivity Log as an Aid in Determining Some Reservoir Characteristics, Trans. AIME. 146 (1942) 54–62. doi:10.2118/942054-G.

[89] E.R. Atkins Jr., G.H. Smith, The Significance of Particle Shape in Formation Resistivity Factor-Porosity Relationships, J. Pet. Technol. 13 (1961) 285–291. doi:10.2118/1560-G-PA.

[90] H. Sallehi, P. Ghods, O.B. Isgor, Formation factor of fresh cementitious pastes, Cem. Concr. Compos. 91 (2018) 174–188. doi:10.1016/j.cemconcomp.2018.05.011.

[91] Y.-Y. Kim, K.-M. Lee, J.-W. Bang, S.-J. Kwon, Effect of W/C Ratio on Durability and Porosity in Cement Mortar with Constant Cement Amount, Adv. Mater. Sci. Eng. 2014 (2014) 1–11. doi:10.1155/2014/273460.

[92] K.H. Obla, C.L. Lobo, H. Kim, Tests and Criteria for Concrete Resistant to Chloride Ion Penetration, ACI Mater. J. 113 (2016) 621–631. doi:10.14359/51689107.

[93] P. Hewlett, M. Liska, Lea's chemistry of cement and concrete, Butterworth-Heinemann, 2019.

[94] W.C. Hansen, The chemistry of sulphate-resisting Portland cements, Perform. Concr. Resist. Concr. to Sulphate Other Environ. Cond. (1968) 18–55.

[95] D.M. Roy, Mechanisms of Cement Paste Degradation due to Chemical and Physical Factor, 8th Int. Cong. Chem. Cem. 1 (1986) 362–380.

[96] P.J. Tikalsky, D. Roy, B. Scheetz, T. Krize, Redefining cement characteristics for sulfate-resistant Portland cement, Cem. Concr. Res. 32 (2002) 1239–1246. doi:10.1016/S0008-8846(02)00767-6.

[97] Rasheeduzzafar, O.S.B. Al-Amoudi, S.N. Abduljauwad, M. Maslehuddin, Magnesium-sodium sulfate attack in plain and blended cements, J. Mater. Civ. Eng. 6 (1994) 201–222. doi:10.1061/(ASCE)0899-1561(1994)6:2(201).

[98] E. Bescher, E.K. Rice, C. Ramseyer, S. Roswurm, Sulfate resistance of calcium sulphoaluminate cement, J. Struct. Integr. Maint. 1 (2016) 131–139. doi:10.1080/24705314.2016.1211235.

[99] B. Tan, M.U. Okoronkwo, A. Kumar, H. Ma, Durability of calcium sulfoaluminate cement concrete, J. Zhejiang Univ. A. 21 (2020) 118–128. doi:10.1631/jzus.A1900588.

[100] W. Hou, Z. Liu, F. He, J. Huang, J. zhou, Sulfate diffusion in calcium sulphoaluminate mortar, Constr. Build. Mater. 234 (2020) 117312. doi:10.1016/j.conbuildmat.2019.117312.

[101] I.A. Chen, C.W. Hargis, M.C.G. Juenger, Understanding expansion in calcium sulfoaluminate–belite cements, Cem. Concr. Res. 42 (2012) 51–60. doi:10.1016/j.cemconres.2011.07.010.

[102] A. Gabrisová, J. Havlica, S. Sahu, Stability of calcium sulphoaluminate hydrates in water solutions with various pH values, Cem. Concr. Res. 21 (1991) 1023–1027. doi:10.1016/0008-8846(91)90062-M.

[103] M. Santhanam, M.D. Cohen, J. Olek, Sulfate attack research - Whither now?, Cem. Concr. Res. 31 (2001) 845–851. doi:10.1016/S0008-8846(01)00510-5.

[104] I. Biczok, N. Blasovszky, Concrete corrosion and concrete protection, (1964).

[105] T. Grounds, H. G Midgley, D. V Novell, Carbonation of ettringite by atmospheric carbon dioxide, Thermochim. Acta. 135 (1988) 347–352. doi:10.1016/0040-6031(88)87407-0.

[106] T. Nishikawa, K. Suzuki, S. Ito, K. Sato, T. Takebe, Decomposition of synthesized ettringite by carbonation, Cem. Concr. Res. 22 (1992) 6–14. doi:10.1016/0008-8846(92)90130-N.

[107] R.J. Mangabhai, F.P. Glasser, Calcium Aluminate Cements 2001 Proceedings of the International conference on Calcium Aluminate Cements (CAC)-Mineralogy of CAC, (2001) 77–148.

[108] C.H. Fentiman, R.J. Mangabhai, K.L. Scrivener, Calcium Aluminate Cements, IHS BRE Press, 2008. https://books.google.com/books?id=PCxVPgAACAAJ.

[109] H.W. Harrison, D.C. Teychenné, Sulphate resistance of buried concrete : second interim report on long-term investigation at Northwick Park LK - https://gatech.on.worldcat.org/oclc/8670382, Dept. of the Environment, Building Research Establishment, London SE - vi, 165 pages : illustrations ; 30 cm., 1981.

[110] S.C. Bate, High Alumina Cement Concrete in Existing Building Superstructures,

Construction Research Communications Limited, 1992. https://books.google.com/books?id=cEfGPAAACAAJ.

[111] R.J. Mangabhai, Calcium Aluminate Cements: Proceedings of a Symposium dedicated to H G Midgley, London, July 1990, Taylor \& Francis, 1990. https://books.google.com/books?id=d%5C_aQQgAACAAJ.

[112] H. Ye, Z. Chen, L. Huang, Mechanism of sulfate attack on alkali-activated slag: The role of activator composition, Cem. Concr. Res. 125 (2019) 105868. doi:10.1016/j.cemconres.2019.105868.

[113] M. Komljenović, Z. Baščarević, N. Marjanović, V. Nikolić, External sulfate attack on alkali-activated slag, Constr. Build. Mater. 49 (2013) 31–39. doi:10.1016/j.conbuildmat.2013.08.013.

[114] D. Bondar, C.J. Lynsdale, N.B. Milestone, N. Hassani, Sulfate Resistance of Alkali Activated Pozzolans, Int. J. Concr. Struct. Mater. 9 (2015) 145–158. doi:10.1007/s40069-014-0093-0.

[115] I. Ismail, S.A. Bernal, J.L. Provis, S. Hamdan, J.S.J. Van Deventer, Microstructural changes in alkali activated fly ash/slag geopolymers with sulfate exposure, Mater. Struct. Constr. 46 (2013) 361–373. doi:10.1617/s11527-012-9906-2.

[116] E. Rodríguez, S. Bernal, R. Mejía De Gutiérrez, F. Puertas, Alternative concrete based on alkali-activated slag | Hormigón alternativo basado en escorias activadas alcalinamente, Mater. Constr. 58 (2008) 53–67.

[117] E. Douglas, A. Bilodeau, V.M. Malhotra, Properties and durability of alkali-activated slag concrete, Mater. J. 89 (1992) 509–516.

[118] R.O.Y. AMITAVA, S.P. J, E.H. C, Alkali Activated Class C Fly Ash Cement, 1995. https://lens.org/052-671-702-341-824.

[119] R.O.Y. AMITAVA, S.P. J, E.H. C, Alkali Activated Class C Fly Ash Cement, 1996. https://lens.org/012-381-065-265-040.

[120] L. Jun, J. Yongsheng, Z. Linglei, L. Benlin, Resistance to sulfate attack of magnesium phosphate cement-coated concrete, Constr. Build. Mater. 195 (2019) 156–164. doi:10.1016/j.conbuildmat.2018.11.071.

[121] J. Li, Y. Ji, G. Huang, L. Zhang, Microstructure Evolution of a Magnesium Phosphate Protective Layer on Concrete Structures in a Sulfate Environment, Coatings. 8 (2018) 140. doi:10.3390/coatings8040140.

[122] G.M. Idorn, Assessment of causes of cracking in concrete, Mater. Sci. Concr., IIIpp. 71 (1992).

[123] P.K. Mehta, Evaluation of Sulfate-Resisting Cements by a New Test Method, ACI J. Proc. 72 (1975). doi:10.14359/11158.

[124] M.D. Bentur, A. Cohen, Durability of Portland Cement-Silica Fume Pastes in Magnesium and Sodium Sulfate Solutions, ACI Mater. J. 85 (1988). doi:10.14359/1809.

[125] M.D. Cohen, B. Mather, Sulfate Attack on Concrete: Research Needs, ACI Mater.

J. 88 (1991). doi:10.14359/2382.

[126] P. Mehta, Sulfate attack on concrete--a critical review, Mater. Sci. Concr., IIIpp. 105 (1992).

[127] P.W. Brown, An evaluation of the sulfate resistance of cements in a controlled environment, Cem. Concr. Res. 11 (1981) 719–727. doi:10.1016/0008-8846(81)90030-2.

[128] P. Mehta, O.. Gjorv, A New Test for Sulfate Resistance of Cements, J. Test. Eval. 2 (1974) 510–515. doi:10.1520/JTE11684J.

[129] J. Skalny, J. Pierce, Sulfate attack issues, in: J. Skalny, J. Marchand (Eds.), Mater. Sci. Concr. - Sulfate Attack Mech., American Ceramic Society, Westerville, OH, 1999: pp. 49–64.

[130] J.R. Clifton, G. Frohnsdorff, C. Ferraris, Standards for Evaluating The Susceptibility of Cement-Based Materials to External Sulfate Attack, in: J. Skalny, J. Marchand (Eds.), Mater. Sci. Concr. - Sulfate Attack Mech., American Ceramic Society, Westerville, OH, 1999: pp. 337–356.

[131] I. Biczok, Concrete Corrosion Concrete Protection, Chemical Publishing Company Inc, NY, 1967.

[132] P.K. Mehta, D. Pirtz, M. Polivka, Properties of alite cements, Cem. Concr. Res. 9 (1979) 439–450. doi:10.1016/0008-8846(79)90041-3.

[133] H. Wang, M. Xue, J. Cao, Research on the Durability of Magnesium Phosphate Cement, Adv. Mater. Res. 168–170 (2011) 1864–1868. doi:10.4028/www.scientific.net/AMR.168-170.1864.

[134] E. Rengade, P. L'Hopitallier, Durand de Fontmagne, Recherches sur les cause de certains phénoménes d'alteration des bétons de ciment alumineux, Rev Mater Constr Trav Publics. 318 (1936) 52–55.

[135] E. García Alcocel, P. Garcés, S. Chinchón, General study of alkaline hydrolysis in calcium aluminate cement mortars under a broad range of experimental conditions, Cem. Concr. Res. 30 (2000) 1689–1699. doi:10.1016/S0008-8846(00)00396-3.

[136] F.M. Lea, Effect of the temperature on high alumina cement, Trans. Soc. Chem. Ind. 59 (1940) 18–21.

[137] S. Goñi, C. Andrade, J.L. Sagrera, M.S. Hernández, C. Alonso, A new insight on alkaline hydrolysis of calcium aluminate cement concrete: Part I. Fundamentals, J. Mater. Res. 11 (1996) 1748–1754. doi:DOI: 10.1557/JMR.1996.0219.

[138] M.J. Sánchez-Herrero, A. Fernández-Jiménez, A. Palomo, C4A3Š hydration in different alkaline media, Cem. Concr. Res. 46 (2013) 41–49. doi:10.1016/j.cemconres.2013.01.008.

[139] I. Jawed, J. Skalny, Alkalies in cement: A review. II. Effects of alkalies on hydration and performance of Portland cement, Cem. Concr. Res. 8 (1978) 37–51. doi:10.1016/0008-8846(78)90056-X.

[140] S. Martínez-Ramírez, A. Palomo, OPC hydration with highly alkaline solutions,

Adv. Cem. Res. - ADV CEM RES. 13 (2001) 123–129. doi:10.1680/adcr.2001.13.3.123.

[141] F. Rajabipour, E. Giannini, C. Dunant, J.H. Ideker, M.D.A. Thomas, Alkali–silica reaction: Current understanding of the reaction mechanisms and the knowledge gaps, Cem. Concr. Res. 76 (2015) 130–146. doi:10.1016/J.CEMCONRES.2015.05.024.

[142] M.D.A. Thomas, B. Fournier, K.J. Folliard, Alkali-Aggregate Reactivity (AAR) Facts Book, 2013. http://www.fhwa.dot.gov/pavement/concrete/asr/pubs/hif13019.pdf (accessed May 4, 2020).

[143] L.S. Dent Glasser, N. Kataoka, On the role of calcium in the alkali-aggregate reaction, Cem. Concr. Res. 12 (1982) 321–331. doi:10.1016/0008-8846(82)90080-1.

[144] H. Wang, J.E. Gillott, Mechanism of alkali-silica reaction and the significance of calcium hydroxide, Cem. Concr. Res. 21 (1991) 647–654. doi:10.1016/0008-8846(91)90115-X.

[145] S.A. Greenberg, The chemisorption of calcium hydroxide by silica, J. Phys. Chem. 60 (1956) 325–330. doi:10.1021/j150537a019.

[146] S. Chatterji, The role of Ca(OH)2 in the breakdown of Portland cement concrete due to alkali-silica reaction, Cem. Concr. Res. 9 (1979) 185–188. doi:10.1016/0008-8846(79)90024-3.

[147] A. Leemann, G. Le Saout, F. Winnefeld, D. Rentsch, B. Lothenbach, Alkali–Silica Reaction: the Influence of Calcium on Silica Dissolution and the Formation of Reaction Products, J. Am. Ceram. Soc. 94 (2011) 1243–1249. doi:10.1111/j.1551-2916.2010.04202.x.

[148] L.J. STRUBLE, S. DIAMOND, Swelling Properties of Synthetic Alkali Silica Gels, J. Am. Ceram. Soc. 64 (1981) 652–655. doi:10.1111/j.1151-2916.1981.tb15864.x.

[149] F. Pacheco-Torgal, Z. Abdollahnejad, A.F. Camões, M. Jamshidi, Y. Ding, Durability of alkali-activated binders: A clear advantage over Portland cement or an unproven issue?, Constr. Build. Mater. 30 (2012) 400–405. doi:10.1016/j.conbuildmat.2011.12.017.

[150] I. García-Lodeiro, A. Palomo, A. Fernández-Jiménez, Alkali-aggregate reaction in activated fly ash systems, Cem. Concr. Res. 37 (2007) 175–183. doi:10.1016/j.cemconres.2006.11.002.

[151] T. Bakharev, J.G. Sanjayan, Y.B. Cheng, Resistance of alkali-activated slag concrete to alkali-aggregate reaction, Cem. Concr. Res. 31 (2001) 331–334. doi:10.1016/S0008-8846(00)00483-X.

[152] Z. Shi, C. Shi, S. Wan, Z. Ou, Effect of alkali dosage on alkali-silica reaction in sodium hydroxide activated slag mortars, Constr. Build. Mater. 143 (2017) 16–23. doi:10.1016/j.conbuildmat.2017.03.125.

[153] T. Williamson, M.C.G. Juenger, The role of activating solution concentration on

alkali-silica reaction in alkali-activated fly ash concrete, Cem. Concr. Res. 83 (2016) 124–130. doi:10.1016/j.cemconres.2016.02.008.

[154] F. Slaty, H. Khoury, H. Rahier, J. Wastiels, Durability of alkali activated cement produced from kaolinitic clay, Appl. Clay Sci. 104 (2015) 229–237. doi:10.1016/j.clay.2014.11.037.

[155] A.K. Mukhopadhyay, K.-W. Liu, ASR TESTING: A NEW APPROACH TO AGGREGATE CLASSIFICATION AND MIX DESIGN VERIFICATION: TECHNICAL REPORT, 2014. http://tti.tamu.edu/documents/0-6656-1.pdf.

[156] M. Thomas, B. Fournier, K. Folliard, J. Ideker, M. Shehata, Test methods for evaluating preventive measures for controlling expansion due to alkali-silica reaction in concrete, Cem. Concr. Res. 36 (2006) 1842–1856. doi:10.1016/j.cemconres.2006.01.014.

[157] R.F. Blanks, H.S. Meissner, The Expansion Test as a Measure of Alkali-Aggregate Reaction, ACI J. Proc. 42 (1946). doi:10.14359/8720.

[158] J. Tanesi, T. Drimalas, K.S.T. Chopperla, M. Beyene, J.H. Ideker, H. Kim, L. Montanari, A. Ardani, Divergence between Performance in the Field and Laboratory Test Results for Alkali-Silica Reaction, Transp. Res. Rec. 0 (n.d.) 0361198120913288. doi:10.1177/0361198120913288.

[159] K. Chopperla, T. Drimalas, J. Tanesi, A. Ardani, M. Laskey, M. Thomas, K. Folliard, J. Ideker, Benchmarking the Miniature Concrete Prism Test and the Concrete Cylinder Tests to Field Exposure Blocks for Mitigation of Alkali-Silica Reaction, in: 15th Int. Congr. Chem. Cem., Prague, Czech Republic, 2019.

[160] A. Naranjo, Proposed Test Method for Determining ASR Potential: The Concrete Cylinder Test (CCT), in: Recent Adv. ASR Test Methods Underst. Mitig. Mech. Part 1, ACI spring 2012 Convention, Dallas, TX, 2012. https://www.concrete.org/portals/0/files/pdf/webinars/Naranjo.pdf.

[161] L. R Lenke, L. Javier Malvar, Alkali Silica Reaction Criteria for Accelerated Mortar Bar Tests Based on Field Performance Data, 3rd World Coal Ash, WOCA Conf. - Proc. (2009).

[162] M.C. Alonso, J.L.G. Calvo, S. Pettersson, I. Puigdomenech, M.A. Cuñado, M. Vuorio, H. Weber, H. Ueda, M. Naito, C. Walker, Y. Takeshi, C. Cau-dit-Coumes, Round Robin Test for Defining an Accurate Protocol to Measure the Pore Fluid pH of Low-pH Cementitious Materials BT - Cement-Based Materials for Nuclear Waste Storage, in: F. Bart, C. Cau-di-Coumes, F. Frizon, S. Lorente (Eds.), Springer New York, New York, NY, 2013: pp. 251–259. doi:10.1007/978-1-4614-3445-0_22.

[163] R.D. Moser, A.R. Jayapalan, V.Y. Garas, K.E. Kurtis, Assessment of binary and ternary blends of metakaolin and Class C fly ash for alkali-silica reaction mitigation in concrete, Cem. Concr. Res. 40 (2010) 1664–1672. doi:10.1016/j.cemconres.2010.08.006.

[164] A.K. Saha, M.N.N. Khan, P.K. Sarker, F.A. Shaikh, A. Pramanik, The ASR mechanism of reactive aggregates in concrete and its mitigation by fly ash: A critical

review, Constr. Build. Mater. 171 (2018) 743–758. doi:10.1016/j.conbuildmat.2018.03.183.

[165] T.C.P. and H.H. Steinour, An Interpretation of Some Published Researches on the Alkali-Aggregate Reaction Part 1-The Chemical Reactions and Mechanism of Expansion, ACI J. Proc. 51 (n.d.). doi:10.14359/11691.

[166] A. Shayan, Expansion of AAR-affected concrete under aggressive marine conditions: a look at possible effects of complex interactions, in: Marc-Andre Berube Symp. Alkali-Aggregate React. Concr. 8th CANMET/ACI Int. Conf. Recent Adv. Concr. Technol., Montreal, Canada, 2006: pp. 369–389.

[167] T. Katayama, The so-called alkali-carbonate reaction (ACR) - Its mineralogical and geochemical details, with special reference to ASR, Cem. Concr. Res. 40 (2010) 643–675. doi:10.1016/j.cemconres.2009.09.020.

[168] J. Smeltz, J. Farver, Dedolomitization and Alkali Reactions in Ohio-Sourced Dolostone Aggregates, 2017. http://www.dot.state.oh.us/Divisions/Planning/SPR/Research/reportsandplans/Reports/Final Reports/135267_FR.pdf (accessed May 5, 2020).

[169] B. Huet, V. Tasoti, I. Khalfallah, A review of Portland cement carbonation mechanisms in CO2 rich environment, Energy Procedia. 4 (2011) 5275–5282. doi:10.1016/j.egypro.2011.02.507.

[170] L. Zhang, Y.M. Wang, M.Z. Su, Control properties of sulpho- and ferro-aluminate cement with the special admixtures, in: 10th I.C.C.C. Proc., Gothenburg, Sweden, 1996.

[171] S. Goñi, M.T. Gaztañaga, a. Guerrero, Role of Cement Type on Carbonation Attack, J. Mater. Res. 17 (2002) 1834–1842. doi:10.1557/JMR.2002.0271.

[172] L. Fernández-Carrasco, D. Torréns-Martín, S. Martínez-Ramírez, Carbonation of ternary building cementing materials, Cem. Concr. Compos. 34 (2012) 1180–1186. doi:10.1016/j.cemconcomp.2012.06.016.

[173] S.A. Bernal, J.L. Provis, D.G. Brice, A. Kilcullen, P. Duxson, J.S.J. Van Deventer, Accelerated carbonation testing of alkali-activated binders significantly underestimates service life: The role of pore solution chemistry, Cem. Concr. Res. 42 (2012) 1317–1326. doi:10.1016/j.cemconres.2012.07.002.

[174] S.A. Bernal, J.L. Provis, B. Walkley, R. San Nicolas, J.D. Gehman, D.G. Brice, A.R. Kilcullen, P. Duxson, J.S.J.J. Van Deventer, Gel nanostructure in alkali-activated binders based on slag and fly ash, and effects of accelerated carbonation, Cem. Concr. Res. 53 (2013) 127–144. doi:10.1016/j.cemconres.2013.06.007.

[175] T. Bakharev, J.. Sanjayan, Y.-B. Cheng, Resistance of alkali-activated slag concrete to carbonation, Cem. Concr. Res. 31 (2001) 1277–1283. doi:10.1016/S0008-8846(01)00574-9.

[176] R. Pouhet, M. Cyr, Carbonation in the pore solution of metakaolin-based geopolymer, Cem. Concr. Res. 88 (2016) 227–235. doi:10.1016/J.CEMCONRES.2016.05.008.

[177] E. Ul Haq, S.K. Padmanabhan, A. Licciulli, In-situ carbonation of alkali activated fly ash geopolymer, Constr. Build. Mater. 66 (2014) 781–786. doi:10.1016/j.conbuildmat.2014.06.012.

[178] L. Fernández-Carrasco, F. Puertas, M.T. Blanco-Varela, T. Vázquez, Carbonatación de pastas de cemento de aluminato de calcio, Mater. Constr. 2001 (2001) 127–136. doi:10.3989/mc.2001.v51.i263-264.358.

[179] L. Wang, S. Zhan, X. Tang, Q. Xu, K. Qian, Pore Solution Chemistry of Calcium Sulfoaluminate Cement and Its Effects on Steel Passivation, Appl. Sci. 9 (2019) 1092. doi:10.3390/app9061092.